EVALUATION DES NOUVELLES TECHNIQUES D'IMAGERIE VASCULAIRE CEREBRALE POUR L'OPTIMISATION DU DIAGNOSTIC, DU TRAITEMENT ET DU SUIVI DES ANEVRISMES INTRACRANIENS OPERES

Laurent Thines

UNIVERSITÉ DROIT ET SANTÉ – LILLE II

FACULTÉ DE MÉDECINE HENRI WAREMBOURG

Année 2008 N°_ _ _ _

THÈSE D'UNIVERSITÉ

PRÉSENTÉE ET SOUTENUE PAR

LAURENT THINES

LE 9 DÉCEMBRE 2008

ÉVALUATION DES NOUVELLES TECHNIQUES D'IMAGERIE VASCULAIRE CÉRÉBRALE POUR L'OPTIMISATION DU DIAGNOSTIC, DU TRAITEMENT ET DU SUIVI DES ANÉVRISMES INTRACRANIENS OPÉRÉS

JURY :

- **Pr. Daniel Le Gars**, CHU d'Amiens, France (rapporteur)
- **Pr. Luca Regli**, University Medical Center Utrecht, Hollande (rapporteur)
- **Pr. Jean-paul Lejeune**, CHRU de Lille, France (Directeur)
- **Pr. Xavier Leclerc**, CHRU de Lille, France (Directeur)
- **Pr. M. Christopher Wallace**, University of Toronto, Canada (examinateur)
- **Pr. Boris Lubicz**, Erasme University Hospital, Belgique (examinateur)

ÉVALUATION DES NOUVELLES TECHNIQUES D'IMAGERIE VASCULAIRE CÉRÉBRALE POUR L'OPTIMISATION DU DIAGNOSTIC, DU TRAITEMENT ET DU SUIVI DES ANÉVRISMES INTRACRANIENS OPÉRÉS

SOMMAIRE

ABRÉVIATIONS

3D : tridimensionnel

ACI : artère carotide interne

ADD : anneau dural distal

ARM : angiographie par résonance magnétique

EC/IC : extracrânien / intracrânien

IRM : imagerie par résonance magnétique

HSA : hémorragie sous-arachnoïdienne

LCS : liquide cérébro-spinal

MIP : maximum intensity projection

PCA : processus clinoïde antérieur

PMP : paraclinoid MR protocol

TSE : turbo spin echo

REMERCIEMENTS

A l'issu de ce travail de Thèse, je tiens à adresser mes remerciements et ma reconnaissance :

- A ma femme Laurence, mes fils Eliot et Ethan et mes parents sans le soutien desquels je n'aurai pu mener à terme cette épreuve
- A mes maîtres et directeurs de thèse, les Pr. Lejeune et Pr. Leclerc pour leur supervision et leurs conseils précieux
- A l'ensemble des membres du jury qui me font un honneur extrême en acceptant de faire ce long déplacement pour juger ce travail
- Aux équipes de neurochirurgie et de neuroradiologie lilloises et torontoises au sein desquelles j'ai eu la chance de pouvoir développer ces travaux de recherche clinique
- A mes amis le Pr. Taschner, le Pr. Gauvrit, le Dr. Delmaire, le Dr.Dehdashti, le Dr. Agid et le Dr.Seon Kyu avec qui j'ai eu le plaisir de conduire ces études.

LISTE DES PUBLICATIONS RAPPORTÉES DANS LA THÈSE

1. MRI location of the distal dural ring plane: anatomoradiological study and application to paraclinoid carotid artery aneurysms. Thines L, Delmaire C, Le Gars D, Pruvo JP, Lejeune JP, Lehmann P, Francke JP. *Eur Radiol*. 2006 Feb;16(2):479-88.

2. MRI localization of paraclinoid carotid aneurysms. Technical note. Thines L, Delmaire C, Le Gars D, Pruvo JP, Lejeune JP, Lehmann P, Francke JP. *J Neuroradiol*. 2006 Apr;33(2):115-20.

3. Surgical views from three-dimensional digital subtraction angiography for the planning of aneurysm surgery. Thines L, Taschner C, Lejeune JP, Le Thuc V, Pruvo JP, Bourgeois P, Leclerc X. *J Neuroradiol*. 2007 Jul;34(3):205-11.

4. Treatment decision by embolization versus surgery in patients with ruptured intracranial aneurysm: accuracy of multi-detector row CT angiography compared with digital subtraction angiography. Taschner C, Thines L, Lernout M, Lejeune JP, Leclerc X. *J Neuroradiol*. 2007 Oct;34(4):243-9.

5. Usefulness of MR imaging for the assessment of nonophthalmic paraclinoid aneurysms. Thines L, Gauvrit JY, Leclerc X, Le Gars D, Delmaire C, Pruvo JP, Lejeune JP. *AJNR Am J Neuroradiol*. 2008 Jan;29(1):125-9.

6. Intrasellar rupture of a paraclinoid aneurysm with subarachnoid hemorrhage: usefulness of MR imaging in diagnosis. Ribeiro M, Howard P, Willinsky R, ter Brugge KG, Agid R, Thines L, da Costa L. *AJNR Am J Neuroradiol*. 2008 May;29(5):980-2.

7. Direct imaging of the distal dural ring and paraclinoid internal carotid artery aneurysm with high resolution T2 turbo-spin echo technique at 3.0 Tesla MRI. Thines L, Lee SK, Dedhashti A, Agid R, Willinsky RA, Wallace MC, ter Brugge KG. *Accepté par Neurosurgery (en révision)*

8. Intraoperative biplanar rotational angiography during neurovascular surgery: Technical Note. Dehdashti AR, Thines L, da Costa L, Willinsky RA, ter Brugge KG, Wallace MC, Tymianski M. *Accepté par Journal of Neurosurgery (en révision)*

9. 64-detectors computerized tomography angiography for the postoperative assessment of clipped aneurysms. Thines L, Dehdashti AR, Howard P, Wallace MC, Tymianski M, da Costa L, Willinsky RA, Lejeune JP, Agid R. *Soumis à Neurosurgery.*

10. Assessment of extracranial-intracranial bypass patency with 64-slice multi-detector computerized tomography angiography. Thines L, Agid R, Dehdashti AR, da Costa L, Wallace MC, ter Brugge KG, Tymianski M. *Soumis à Journal of Neurosurgery.*

LISTE DES COMMUNICATIONS ORALES OU AFFICHÉES

1. Distinction between intra and extracavernous paraclinoid aneurysms: usefulness of a specific MRI paraclinoid protocol versus angiography. Thines L, Lejeune JP, Bourgeois P, Gauvrit JY, Leclerc X, Pruvo JP (communication orale); *13th World Congress of Neurological Surgery*, Marrakesh, Maroc, Juin 2005.

2. Intérêt des incidences ptérionales en angiographie 3D pour la prise en charge chirurgicale des anévrismes de la circulation antérieure. L Thines, C Taschner, JP Lejeune, X Leclerc, P Bourgeois, JP Pruvo (poster); *Société de Neurochirurgie de Langue Française*, Paris, France, Nov 2005.

3. Direct Imaging of the Distal Dural Ring and Paraclinoid Internal Carotid Artery Aneurysms with High Resolution T2 Turbo-Spin Echo Technique at 3.0 Tesla MRI.

   L Thines, SK Lee, AR Dehdashti, R Agid, MC Wallace, KG Ter Brugge (poster); *American Association of Neurological Surgeons*, Chicago, USA, Avr.2008

   Lee SK, Thines L, Agid R**,** Dehdashti AR**,** Wallace MC**,** ter Brugge KG (communication orale); American Society of NeuroRadiology, New-Orleans, USA, Fév.2008

4. Assessment of extracranial-intracranial bypass patency with 64-slice multi-detector computerized tomography angiography. L Thines, AR Dehdashti, R Agid, L da Costa, MC Wallace, KG ter Brugge, M Tymianski. (communication orale); Grand Cerebrovascular Round, Barrow Neurological Institute, Phoenix, USA, Mai 2008 et

Canadian Neurological Sciences Federation 43rd Annual Congress, Victoria, Canada, Juin 2008

5. Contrôle post-opératoire des anévrismes clippés en angioscanner 64-détecteurs. Thines L, Dehdashti AR, Howard P, Wallace MC, Tymianski M, da Costa L, Willinsky RA, Lejeune JP, Agid R (communication orale); *Société de Neurochirurgie de Langue Française*, Paris, France, Nov 2008.

PRÉAMBULE

Mes études de Médecine se sont déroulées à la Faculté de Marseille et très rapidement, j'ai été fasciné par le système nerveux central, son anatomie et sa physiologie. C'est en cours de stage infirmier à la fin de ma première année de médecine, dans le service du Pr. Péragut (hôpital de la Timone), que je me suis découvert une vocation très forte pour la neurochirurgie. J'entrepris alors de nombreux stages hospitaliers assez ciblés en neurologie (Pr. Poncet), en neurochirurgie (Pr. Péragut et Pr. Grisoli), en neuroradiologie, en neurophysiologie et obtint ma Maîtrise de Sciences Biologiques et Médicales comprenant un certificat de physiologie générale et un certificat de neuroanatomie (mémoire sur les voies visuelles). Etant mieux classé dans l'inter-région nord à l'issue des résultats du concours de l'internat et après enquête personnelle, je postulais alors, sur les conseils du Pr. Péragut, pour un poste d'interne en neurochirurgie à Lille. C'est aux côtés du Pr. Lejeune, qu'au fil des années, je me découvrais une affinité forte pour la pathologie vasculaire cérébrale chirurgicale. J'admirais la beauté du geste et l'anatomie vasculaire dans les anévrismes asymptomatiques, j'étais impressionné par la difficulté technique et le challenge vital dans les anévrismes rompus ou les malformations artério-veineuses et j'appréciais le travail en équipe multidisciplinaire lié à la prise en charge complexe de la pathologie.

C'est dans l'équipe neurovasculaire lilloise que j'ai eu la chance de pouvoir développer au cours de mon internat et de mon clinicat une activité de recherche orientée vers l'exploration neuroradiologique des anévrismes intracrâniens. Je conciliais ainsi mon intérêt pour la neuroanatomie, en particulier vasculaire, la possibilité d'améliorer directement la prise en charge clinique des patients et la poursuite d'une collaboration multidisciplinaire. Mon master puis ma thèse ont eu pour but de développer un protocole

IRM permettant de préciser la localisation exacte des anévrismes paraclinoïdiens par rapport au sinus caverneux. Ce protocole est maintenant utilisé de façon courante dans nos services pour optimiser la prise en charge de ces anévrismes. Nous avons également mis en place un protocole d'angiographie tridimensionnelle (3D) permettant d'orienter les reconstructions 3D selon la vue opératoire. L'obtention de ces vues chirurgicales a été particulièrement utile pour aider les plus jeunes à développer une vision 3D de la configuration opératoire réelle et anticiper les pièges de la voie d'abord. C'est cette même technique qui été évaluée dans son application peropératoire pour le traitement chirurgical d'anévrismes complexes. Enfin l'avènement de l'angioscanner multi-détecteurs nous a donné l'opportunité de tester ses applications en remplacement de l'artériographie cérébrale invasive, à la fois à la phase diagnostique (orientation thérapeutique des patients) et également à la phase postopératoire (contrôle des anévrismes clippés, contrôle des pontages extra-intracrâniens). C'est au cours d'une mobilité d'un an pour un fellowship de chirurgie cérébrovasculaire au sein de l'équipe du Pr. Wallace au Toronto Western Hospital que j'ai eu la possibilité de mettre en place quatre de ces études.

RÉSUMÉ

Le diagnostic, le traitement chirurgical et le suivi des anévrismes intracrâniens opérés reposaient classiquement sur l'artériographie cérébrale conventionnelle. Récemment, des améliorations de la technique d'angiographie elle-même (angiographie cérébrale tridimensionnelle) ou de nouvelles méthodes d'imagerie (IRM et angioscanner cérébral) se sont développées et sont devenues assez performantes pour compléter ou parfois supplanter la technique de référence. L'objectif de ce travail a donc été d'évaluer l'apport de ces nouvelles techniques d'imagerie aux différentes étapes de la prise en charge chirurgicale des anévrismes intracrâniens.

Les progrès apportés aux appareils d'angioscanner cérébral (scanners multi-détecteurs) ont ouvert la voie du bilan initial des anévrismes rompus à un examen plus accessible, plus confortable, plus rapide et non invasif. Au cours de ce travail, nous avons étudié cette technique à la phase diagnostique et montré la possibilité grâce à celle-ci de diriger les patients de façon fiable vers le traitement chirurgical ou endovasculaire. Certains anévrismes, comme les anévrismes paraclinoïdiens, sont de part leurs rapports anatomiques plus difficiles à traiter chirurgicalement. Sélectionner dans ce groupe d'anévrismes ceux qui nécessitent potentiellement d'être exclus (anévrismes intraduraux) est donc primordial. Dans un premier temps, nous avons développé, à l'aide d'un modèle radio-anatomique dédié, un protocole d'IRM (1.5 Tesla) permettant cette analyse, puis nous avons évalué et montré l'intérêt de celui-ci dans la prise en charge d'une population de patients porteurs d'anévrismes paraclinoïdiens, et, enfin nous avons optimisé le protocole lui-même à l'aide d'une machine d'IRM utilisant un aimant plus puissant (3.0 Tesla) et offrant une résolution spatiale supérieure.

Avec les progrès du traitement endovasculaire, les anévrismes orientés vers le

traitement chirurgical sont plus fréquemment complexes. Les outils permettant d'optimiser le planning préopératoire, la décision peropératoire ou le geste thérapeutique lui-même vont permettre d'améliorer les résultats chirurgicaux. Nos travaux ont permis de potentialiser l'aide apportée dans ces domaines par l'angiographie rotationnelle tridimensionnelle. Nous avons, d'une part, mis en oeuvre un protocole permettant d'obtenir de façon semi-automatique la vue 3D de l'arbre vasculaire porteur de l'anévrisme orientée selon la disposition opératoire. D'autre part, nous avons montré l'intérêt de la réalisation d'une angiographie rotationnelle biplan peropératoire comme aide directe au geste chirurgical (contrôle proximal de l'anévrisme avec occlusion carotidienne par ballonnet ou recherche immédiate d'un reliquat).

Le contrôle post-opératoire de la qualité du traitement chirurgical est devenu également une priorité. Si l'ARM s'est progressivement imposée dans de nombreux centres comme l'examen privilégié du contrôle des anévrismes embolisés, l'angiographie conventionnelle, examen invasif, restait encore la référence pour les anévrismes traités chirurgicalement. Nos travaux ont permis d'évaluer l'intérêt et les limites de l'angioscanner cérébral 64-détecteurs pour le contrôle post-opératoire immédiat des anévrismes traités par technique de clippage standard, et pour la confirmation de la perméabilité d'un pontage extracrânien-intracrânien associé au traitement d'un anévrisme intracrânien.

En conclusion, les nouvelles techniques d'imagerie vasculaire cérébrale étudiées dans notre travail permettent d'optimiser à tous les stades la prise en charge chirurgicale des anévrismes intracrâniens. Le développement de nouveaux logiciels de post-traitement d'image (Amira®) pourrait permettre, dans un avenir proche et à partir de l'angioscanner, de simuler la taille et l'orientation à la pose du ou des clips au niveau du collet anévrismal.

SUMMARY

ASSESSMENT OF RECENT CEREBROVASCULAR IMAGING TECHNIQUES FOR THE IMPROVEMENT IN DIAGNOSIS, TREATMENT AND FOLLOW-UP OF CLIPPED INTRACRANIAL ANEURYSMS.

Diagnosis, surgical treatment and follow-up of intracranial aneurysms were usually relying on conventional cerebral angiography. Recently the angiography technique itself improved (three-dimensional angiogram) and new imaging techniques (magnetic resonance imaging and computerized tomography angiography) became sufficiently sophisticated to replace in some circumstances the gold standard. The objective of this work was to evaluate the usefulness of those new imaging techniques at each stage of the surgical management of intracranial aneurysms.

Progress in computerized tomography angiography (multi-detectors) allowed the initial assessment of ruptured intracranial aneurysms with a more accessible, faster and non invasive exam. In this work, we studied this technique at the diagnosis stage and proved its ability to reliably select patients for the surgical or the endovascular treatment. Some aneurysmal locations, as paraclinoid aneurysms, are more difficult to treat because of their anatomical relationships. In this particular group, it is mandatory to correctly identify those requiring obliteration (intradural aneurysms). We first developed a specific MR protocol (1.5 Tesla) by the mean of a radioanatomical model, then we proved its clinical interest in the management of paraclinoid aneurysms and finally we optimized the MR protocol on a 3.0 Tesla scan allowing a higher spatial resolution.

Because of the advance in the endovascular treatment, aneurysms referred to surgery are more frequently complex. Tools improving the planning, the treatment decision or the surgical technique itself will have a positive impact on the surgical results. Our work allowed to increase the benefit obtained with three-dimensional angiography in those fields. We first developed a semi-automatic protocol directly providing surgical views of the vascular tree carrying the aneurysm from 3D angiogram. Then, we demonstrated the interest of intraoperative biplanar rotational angiography during neurovascular surgery (proximal control of the aneurysm by the mean of a carotid balloon occlusion or immediate screening for aneurysm remnant).

The postoperative evaluation of the surgical obliteration quality is essential. MRA became progressively in many centres the first choice technique for the follow-up of coiled aneurysms. Conventional angiogram is the gold standard for clipped aneurysms. We demonstrated the interest and limits of 64-detectors computerized tomography angiography for the postoperative assessment of clipped aneurysms and extracranial-intracranial bypasses associated to the treatment of an intracranial aneurysm.

In conclusion, this work underlines the interest of new vascular imaging techniques for the improvement in the surgical management of intracranial aneurysms. New post-treatment softwares (Amira®) will allow in the future to simulate the surgical clipping.

I. INTRODUCTION

A. *CONTEXTE DE L'ÉTUDE ET PROBLÉMATIQUE*

Les anévrismes intracrâniens correspondent à une dilatation de la paroi artérielle qui se présente soit sous la forme d'un sac implanté par l'intermédiaire d'un collet (anévrisme sacciforme) soit sous la forme d'un élargissement global de la paroi (anévrisme fusiforme). Les circonstances de diagnostic sont variables. Le perfectionnement des techniques d'imagerie médicale, rend la découverte de lésions dites fortuites de plus en plus fréquente et la prévalence des anévrismes asymptomatiques serait de 0,4 à 6%. Mais la plupart du temps, l'anévrisme est révélé par son caractère symptomatique, le plus souvent une hémorragie par rupture anévrismale. L'hémorragie sous-arachnoïdienne par rupture d'un anévrisme intracrânien reste une pathologie très grave et malgré les progrès dans la prise en charge des patients, elle représente un quart des décès d'origine cérébrovasculaire (28;32;39;43;55;92).

Les deux objectifs du traitement des anévrismes intracrâniens sont, d'une part, l'obtention d'une exclusion la plus complète possible du sac anévrismal de la lumière artérielle et, d'autre part, la limitation des complications liées à l'hémorragie initiale ou au traitement (1). Deux options thérapeutiques s'offrent aux équipes neurovasculaires: le traitement chirurgical ou le traitement par voie endovasculaire. Initialement, le traitement de référence était la chirurgie et consistait en la pose d'un ou plusieurs clips au niveau du collet anévrismal par voie microchirurgicale (14). A partir des années 1990, les techniques de neuroradiologie interventionnelle (embolisation par microspires ou coils à détachement contrôlé) (31;58;97) se sont perfectionnées. Du fait de son efficacité et d'une morbidité inférieure, le traitement endovasculaire est actuellement

préconisé en première intention lorsqu'il est techniquement faisable et laisse espérer la possibilité d'une oblitération complète de l'anévrisme (8;55). Dans ce nouvel algorithme décisionnel, le traitement neurochirurgical est le plus souvent retenu actuellement lorsque l'embolisation est impossible ou quand le patient présente un hématome expansif associé à un anévrisme rompu. De plus, les anévrismes récusés pour le traitement endovasculaire sont souvent également des anévrismes difficiles à traiter chirurgicalement. Réduction du nombre d'interventions chirurgicales et complexité croissante des cas opérés rendent délicat la formation des jeunes neurochirurgiens, le maintien de la qualité des résultats chirurgicaux et, à moyen terme, la survie de cette sub-spécialité.

Le diagnostic, le planning et le suivi chirurgical reposent actuellement sur l'artériographie cérébrale conventionnelle, un examen invasif comportant certaines limites. Parallèlement, de nouvelles techniques d'imagerie (artériographie rotationnelle tridimensionnelle, IRM haute résolution et 3.0 Tesla, angioscanner multi-détecteurs) se sont développées, deviennent de plus en plus performantes et concurrencent dans des indications croissantes cette technique de référence. L'objectif de ce travail a donc été d'évaluer comment ces techniques d'imagerie récentes pourraient permettre d'améliorer, à ses différents stades, la prise en charge chirurgicale des anévrismes intracrâniens.

B. *PRATIQUE COURANTE ET PROBLÈMES NON RÉSOLUS*

Les objectifs du bilan d'imagerie dans le cadre de la prise en charge chirurgicale des anévrismes intracrâniens sont multiples: mettre en évidence les conséquences d'une éventuelle rupture anévrismale, rechercher les complications de cette rupture

(hydrocéphalie, vasospasme, ischémie cérébrale retardée), identifier l'origine de l'hémorragie (visualiser l'anévrisme), choisir l'option thérapeutique la mieux adaptée, planifier le déroulement du traitement, évaluer après le traitement la qualité de l'exclusion de l'anévrisme ou ses complications.

Dans notre centre, le bilan d'un anévrisme intracrânien opéré standard comportait :

- 1 artériographie préthérapeutique
- 10 dopplers transcrâniens post-thérapeutiques et, dans certains cas d'interprétation difficile, 1 doppler 3D-contraste (anévrismes rompus)
- 1 artériographie post-thérapeutique
- 1-3 scanners de contrôle précoce (anévrismes rompus)
- 1 scanner tardif
- 1 artériographie tardive si reliquat

Pour le cas particulier des anévrismes complexes (géants, calcifiés, recanalisés…), le bilan comportait en plus de l'artériographie, une IRM + ARM et/ou un doppler 3D-contraste.

La plupart des équipes neurochirurgicales utilisent, à la phase diagnostique ou lors d'un contrôle post-opératoire, l'artériographie cérébrale conventionnelle. Cet examen comporte cependant certaines limites :

- invasif même si la morbi-mortalité reste faible : point de ponction artérielle, complications thrombo-emboliques, injection d'iode
- nécessité d'un plateau technique spécifique : neuroradiologue, anesthésiste (neuroleptanalgésie), infirmier(e) anesthésiste, manipulateur de radiologie
- accessibilité difficile et durée d'examen longue
- inconfort pour le patient

- Absence de vue axiale ou de reconstruction complète de l'arbre vasculaire

De leur côté, de nouvelles techniques d'imagerie (artériographie tridimensionnelle, IRM, angioscanner) se sont perfectionnées et offrent des avantages substantiels par rapport à l'artériographie cérébrale conventionnelle:

- morbi-mortalité diminuée (angioscanner, IRM)
- durée d'examen courte et accès facile (angioscanner, IRM)
- confort du patient accru (angioscanner, IRM)
- meilleure description de l'anatomie anévrismale et des branches de voisinages
- analyse 3D par l'acquisition d'un volume vasculaire complet
- meilleure analyse des rapports de l'arbre artériel avec son environnement : structures osseuses, parenchyme cérébral, dure-mère, veines

II. DONNÉES ACQUISES

L'artériographie cérébrale digitalisée avec soustraction reste encore la méthode de référence pour le diagnostic des anévrismes intracrâniens et le planning neurochirurgical. A partir d'un point de ponction fémoral, un microcathéter est guidé jusqu'au niveau de la crosse aortique puis dans chacun des axes artériels à destinée cervico-encéphalique où est injecté un produit de contraste iodé (Visipaque 320). Des clichés radiographiques sont acquis en incidence de face, de profil et de trois-quarts selon un mode dynamique permettant d'analyser tous les temps de la vascularisation cérébrale (artériel, capillaire puis veineux). Récemment, le développement d'appareils d'angiographie offrant la possibilité d'enregistrer un grand nombre de clichés selon un mode rotationnel a permis d'obtenir des reconstructions tridimensionnelles de l'arbre vasculaire permettant une meilleure analyse de la forme, de la taille et des rapports de l'anévrisme (2;7;11;12;25;36;54;64;76;81;91).

L'angioscanner cérébral est réalisé à l'aide d'un appareil de tomodensitométrie (rayonnement X) hélicoïdal avec ou sans détecteur multi-barettes. Après injection d'un produit de contraste iodé (Omnipaque) au niveau d'une veine périphérique, celui-ci permet l'acquisition de grands volumes de coupe en un temps très réduit, ou pour un volume donné, de coupes très fines avec une meilleure résolution spatiale. Les nouveaux appareils (multi-détecteurs) permettent ainsi à la fois de mettre en évidence l'hémorragie méningée (hyperdensité spontanée des sillons et des citernes de LCS) et d'autre part d'obtenir des reconstructions tridimensionnelles des axes artériels intracrâniens. Ils permettent ainsi de confirmer le diagnostic, participent au bilan

étiologique (identification de l'anévrisme ayant saigné) et au planning thérapeutique (6;19;38;73;80).

L'Imagerie par Résonance Magnétique (IRM) permet, de façon non irradiante et non invasive, l'obtention d'images cérébrales à partir de l'analyse, dans un champ magnétique élevé, du signal de radiofréquence émis par les protons des molécules d'eau selon l'environnement tissulaire dans lequel ils se trouvent. L'amplitude du signal est codée par une échelle de gris permettant de visualiser le contraste tissulaire. L'imagerie vasculaire (angiographie par résonance magnétique ou ARM) issue de cette technique, avec ou sans injection d'un produit de contraste non iodé, permet une exploration non invasive de la circulation artérielle cérébrale (30;33;72). La définition anatomique actuelle de cette technique, inférieure à celle de l'artériographie cérébrale ou de l'angioscanner, fait qu'elle est préférentiellement réservée au dépistage des anévrismes asymptomatiques chez les sujets à risques (polykystose rénale, anévrismes familiaux) ou au suivi des anévrismes traités par embolisation (4;23;27;75).

III. OBJECTIF GÉNÉRAL DE LA THÈSE

L'objectif principal de cette thèse est d'évaluer la place des nouvelles techniques d'imagerie vasculaire cérébrale aux différentes phases de la prise en charge neurochirurgicale des anévrismes intracrâniens dans le but d'améliorer le diagnostic, le traitement et le suivi de cette pathologie.

A la phase diagnostique les buts sont de :

- Diminuer la morbi-mortalité du bilan
- Faciliter la réalisation et augmenter la rapidité des examens
- Accroître le confort du patient
- Améliorer l'analyse radiologique: acquisition du volume vasculaire complet, analyse des rapports de l'arbre artériel avec son environnement (structures osseuses et durales, parenchyme cérébral, veines)
- Sélectionner correctement les patients pour l'une ou l'autre des modalités thérapeutiques

A la phase thérapeutique les buts sont de :

- Améliorer le planning neurochirurgical préopératoire
- Améliorer le planning neurochirurgical peropératoire
- Améliorer le geste neurochirurgical

A la phase de suivi :

- Diminuer la morbi-mortalité du bilan
- Accroître le confort du patient
- Améliorer l'analyse radiologique
- Evaluer la qualité du traitement

IV. MÉTHODOLOGIE GÉNÉRALE

A. *MATÉRIELS*

Les travaux présentés dans cette thèse ont été menés au sein des services cliniques suivants : Clinique Neurochirurgicale et Service de Neuroradiologie du CHRU de Lille (France) et Division of Neurosurgery and Neuroradiology, Toronto Western Hospital, University of Toronto (Canada). La partie anatomique de l'étude sur les anévrismes paraclinoïdiens a été réalisée dans les laboratoires d'anatomie des facultés de médecine de Lille (Pr. JP Francke) et d'Amiens (Pr. D Le Gars).

Les plateaux techniques utilisés au cours de nos travaux étaient ceux mis à disposition par les services de neuroradiologie de Lille et de Toronto. Ils comportaient :

- Appareil d'angiographie rotationnelle: Allura V5000 (Philips medical system, the Netherlands), CHRU de Lille et unité d'angiographie biplan LUA ou LCN (GE Medical Systems, France), Toronto Western Hospital.
- Appareils d'angioscanner: 16-detector row scanner (Volume Zoom, Siemens, Erlangen, Germany) et Siemens Sensation 64 (2x32 détecteurs, collimation 0.6, 64 coupes / rotation, Siemens AG Medical Solutions, Germany) CHRU de Lille et scanner 64-détecteurs (Aquilion 64, Toshiba Co., Tochigi-ken, Japan), Toronto Western Hospital.
- Appareil d'IRM : Integra Achieva 1.5T (Philips medical system, the Netherlands), Siemens Vision 1.5T (Siemens AG Medical Solutions, Germany), CHRU de Lille et 3.0 Tesla MR scanner (GE, Milwakee, WI, USA), Toronto Western Hospital.

La population étudiée était sélectionnée dans la cohorte des patients suivis et pris en charge pour un ou plusieurs anévrismes intracrâniens dans l'un des deux services cliniques cités ci-dessus entre juin 2005 et juin 2008.

Les critères d'inclusion étaient les suivants : âge compris entre 18 et 65 ans, porteurs d'un ou plusieurs anévrismes intracrâniens, fonction rénale normale.

Les critères d'exclusion étaient les suivants : mineur ou âge > 65ans, femme enceinte ou allaitante, antécédents d'insuffisance rénale ou allergie à l'iode (angioscanner), refus de signer le consentement (étude prospective)

B. *MÉTHODE GÉNÉRALE*

1. Etude "Diagnostic et orientation thérapeutique des patients porteurs d'anévrismes rompus par l'angioscanner":

Problème posé : place de la technique comme méthode de diagnostic, d'orientation et de planning thérapeutique

Objectif : remplacement de l'angiographie cérébrale pour la décision thérapeutique et le planning chirurgical

Population : patients hospitalisés en neurochirurgie pour un anévrisme cérébral rompu

Etude : évaluation de la technique en remplacement de l'angiographie conventionnelle pour le diagnostic, l'orientation thérapeutique et le planning chirurgical

Méthode : angioscanner préopératoire ; comparaison avec l'angiographie conventionnelle (taille, forme, orientation, rapports vasculaires)

2. Etude "Localisation en IRM des anévrismes carotidiens paraclinoidiens":

Problème posé : localisation des anévrismes paraclinoidiens par rapport au sinus caverneux

Objectif : améliorer la décision thérapeutique

Population: patients suivis en neurochirurgie pour un ou plusieurs anévrismes paraclinoidiens asymptomatiques

Etude : développement d'un protocole d'IRM dédié à la localisation de ces anévrismes

Méthode en 3 parties : corrélations radio-anatomiques, comparaison angiographie et IRM T2 haute résolution et protocole en IRM 3 Tesla.

3. Etude "Vue chirurgicale à partir de l'angiographie tridimensionnelle":

Problème posé : obtenir des planches réorientées selon la vue opératoire à partir de l'angiographie tridimensionnelle

Objectif : améliorer le planning chirurgical pré et peropératoire

Population : patients hospitalisés en neurochirurgie pour un anévrisme cérébral rompu ou non

Etude : développement d'un protocole semi-automatisé fournissant directement la vue chirurgicale réorientée

Méthode : angiographie tridimensionnelle préopératoire, différents angles de réorientation étudiés, corrélations radio-chirurgicales

4. Etude "Angiographie rotationnelle biplan peropératoire":

Problème posé : place de la technique comme aide lors du clippage chirurgical

Objectif : améliorer la qualité ou faciliter le traitement chirurgical des anévrismes intracrâniens

Population : patients opérés en neurochirurgie pour un anévrisme intracrânien

Etude : évaluer la faisabilité et l'intérêt d'une angiographie rotationnelle biplan peropératoire

Méthode : patient opéré en salle de neuroradiologie interventionnelle avec réalisation d'une artériographie rotationnelle biplan peropératoire ou postopératoire immédiate

5. Etude " Suivi des anévrismes intracrâniens opérés en angioscanner" :

Problème posé: estimation de la qualité de l'exclusion anévrismale à la phase initiale en angioscanner

Objectif : diagnostic et suivi des reliquats anévrismaux post-opératoires par une technique non invasive

Population : patients opérés d'un ou plusieurs anévrismes rompus ou non.

Etude : évaluation des possibilités de diagnostic et de suivi des reliquats anévrismaux après chirurgie

Méthode : angioscanner postopératoire comparé à l'angiographie conventionnelle

6. Etude " Contrôle en angioscanner de la perméabilité des pontages extra-intracrâniens associés au traitement d'un anévrisme intracrânien" :

Problème posé: contrôle postopératoire de la perméabilité des pontages extra-intracrâniens

Objectif : diagnostic et suivi post-opératoire de la perméabilité des pontages extra-intracrâniens par une technique non invasive

Population : patients opérés d'un anévrisme intracrânien avec l'association d'un pontage extra-intracrânien

Etude : évaluation des possibilités de diagnostic et de suivi après chirurgie de la perméabilité des pontages extra-intracrâniens

Méthode : analyse des données de l'angioscanner postopératoire comparé à l'angiographie conventionnelle.

7. Méthodes d'analyse des paramètres mesurés:

Paramètres analysés : précision anatomique de la technique d'imagerie, apport pour la prise en charge thérapeutique et le suivi des anévrismes opérés

Analyse descriptive

Etude sensibilité-spécificité : de la technique d'imagerie (IRM, angioscanner) en comparaison à la technique de référence (angiographie conventionnelle)

C. *COLLABORATIONS*

- Equipe d'accueil EA 2691 : Pr. Leys
- Pôle de Neurochirurgie : Pr. Dhellemmes, Pr. Lejeune, Pr. Blond, Pr. Assaker, Pr. Vinchon, Dr Bourgeois (CHRU de Lille – Hôpital Roger-Salengro)
- Service de Neuroradiologie : Pr. Pruvo, Pr. Leclerc, Pr Gauvrit, Pr Taschner, Dr Delmaire, V Le Thuc, (CHRU de Lille – Hôpital Roger-Salengro)
- Service de Neurologie B : Pr. Leys, Dr Henon, Dr Lucas, Dr Cordonnier (CHRU de Lille – Hôpital Roger-Salengro)
- Service des Explorations Fonctionnelles Cardiovasculaires : Dr Deklunker, Dr Gautier, (CHRU de Lille – Hôpital Roger-Salengro)
- Division of Neurosurgery: Pr. MC Wallace (Toronto Western Hospital – Canada)
- Division of Radiology: Pr. K ter Brugge (Toronto Western Hospital – Canada)

V. RÉSULTATS DES TRAVAUX

A. *Diagnostique et orientation thérapeutique des patients porteurs d'anévrismes rompus par l'angioscanner.*

1. Résumé

Treatment decision by embolization versus surgery in patients with ruptured intracranial aneurysm: accuracy of multi-detector row CT angiography compared with digital subtraction angiography

Taschner C, Thines L, Lernout M, Lejeune JP, Leclerc X. *J Neuroradiol*. 2007 Oct;34(4):243-

Objective: The aim of this study was to determine the accuracy of multi-detector row computed tomography angiography (CTA) for the triage of patients with acutely ruptured aneurysms, and to assess how therapeutic decisions based on this method compared with digital subtraction angiography (DSA).

Methods: Twenty-seven consecutive patients with acute subarachnoid hemorrhage were included, and underwent both CTA and DSA. CTA was performed on a 16-detector row CT scanner with a 0.75-mm collimation and a 0.558-beam pitch. Two readers reviewed the CTA data, and two different readers reviewed the DSA data. Aneurysm characteristics were recorded and treatment by surgical clipping or endovascular coil embolization was proposed.

Results: A total of 24 aneurysms were identified on DSA in 21 patients. Sensitivity and specificity for CTA were 100% and 83%, respectively, on a per-aneurysm-basis. The correlation between DSA and CTA for the determination of sac and neck sizes was very good ($r = 0.92$, and $r = 0.95$, respectively, $P < 0.0001$). Sensitivity and specificity for the detection of arterial branches incorporated into the

aneurysmal sac or neck were 50% and 100%, respectively. In three aneurysms, readers judged CTA inappropriate for triage, because peri-aneurysmal branches were not properly visualized. Overall agreement between CTA and DSA regarding the therapeutic decision between surgical clipping and endovascular coil embolization in 24 aneurysms was good ($\kappa = 0.76$).

Conclusion: Multi-detector row CTA provides accurate anatomic information for aneurysm location as well as sac and neck sizes; however, the technique appears to have a low sensitivity in detecting branches incorporated into the aneurysmal sac.

2. Discussion

Cette étude corrobore les résultats d'études précédentes montrant que l'angioscanner multi-détecteurs est un outil fiable pour le diagnostic étiologique de l'hémorragie méningée (5;6;80;88;96;104). Dans notre étude, la sensibilité et la spécificité pour la détection des anévrismes intracrâniens étaient de 100% et 83,3%, respectivement en utilisant un appareil d'angioscanner 16-détecteurs.

Une méta-analyse par Chappel et col., basée sur 21 études publiées entre 1995 et 2002 et incluant 1252 patients, retrouvait une sensibilité de 93,3% et une spécificité de 87,8% pour la détection des anévrismes intracrâniens (15). Cependant, la plupart des études étaient basées sur des appareils scanner simple détecteur. Des progrès importants ont été fait depuis peu avec l'introduction des appareils d'angioscanner multi-détecteurs. Cette nouvelle technologie permet l'investigation de grands volumes avec une résolution selon l'axe des x élevée en un temps d'acquisition très court. Avec sa haute résolution spatiale et ses coupes fines, la méthode fournit un ensemble de données comportant des tailles de voxels isotropes qui améliorent la qualité des reconstructions

multiplanaires et des images en rendu 3D (16). Des études récentes, appliquant l'angioscanner multi-détecteurs, ont rapporté des taux de détection anévrismale plus importants chez des patients victimes d'hémorragie méningée. Jayaraman et col. ont obtenu une sensibilité de 90% et une spécificité de 93% en utilisant un angioscanner 4-détecteurs (41). Tipper et col. ont rapporté une sensibilité de 96,2% et une spécificité de 100% sur un angioscanner 16-détecteurs (88). Teksam et col. ont publié leur expérience avec un appareil d'angioscanner 4-détecteurs (84). Dans leur étude, ils avaient stratifié leurs résultats en fonction de catégories de taille d'anévrisme. Ils ont mis en évidence une sensibilité de détection de 84% pour les petits anévrismes (<4mm), 97% pour des anévrismes de taille moyenne (4-10mm) et 100% pour les anévrismes larges (> 10mm). L'ensemble de ces résultats plaide en faveur d'une utilisation large de l'angioscanner pour le bilan des patients victimes d'HSA en réservant l'artériographie cérébrale aux bilans négatifs ou douteux.

La caractérisation précise du plus large diamètre anévrismal, de la taille du collet, des variations du cercle artériel du cerveau, et des branches collatérales à proximité du sac anévrismal est un problème fondamental pour l'évaluation des possibilités et des risques thérapeutiques. Dans notre étude, l'angioscanner a fourni à chaque fois des informations très précises sur la morphologie de l'anévrisme. La capacité de cet examen à détecter les fines branches artérielles à proximité immédiate du collet ou en provenance du sac était restreinte pour les anévrismes situés près de la base du crâne (Fig.1). Cette limitation a été décrite précédemment et est techniquement due aux artéfacts liés à l'os dense cortical de la base du crâne (96). Pour la caractérisation non invasive des anévrismes paraclinoïdiens, l'IRM semble être l'examen le plus performant (87). Un autre facteur limitant la performance de l'angioscanner peut être l'utilisation de techniques de rendu de volume qui mettent en jeu souvent un seuil généré

automatiquement, supprimant ainsi des informations intéressantes, comme celles concernant les petits vaisseaux à proximité du collet anévrismal. Dans notre étude, nous avons à ce titre tenu à systématiquement inclure les données provenant des images MIP (maximum intensity projection) qui sont plus fiables puisque directement dérivées des images natives.

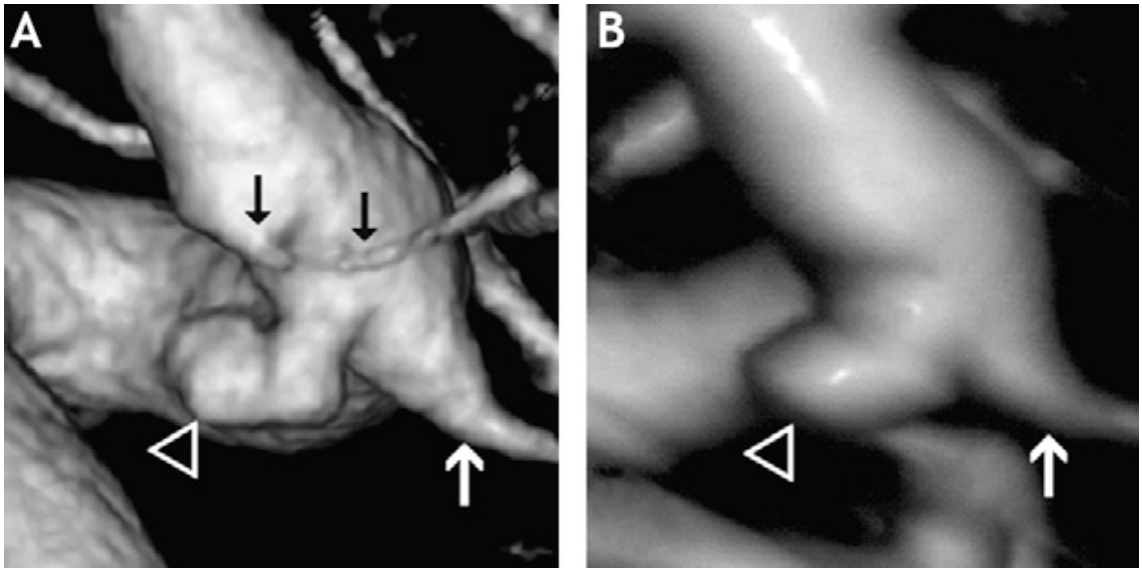

Figure 1 - *Femme âgée de 72 ans présentant une rupture d'anévrisme de l'artère communicante postérieure (patient 3). A : reconstruction tridimensionnelle (3D) en angiographie conventionnelle rotationnelle montrant un anévrisme du siphon carotidien mesurant 3 mm de diamètre (tête de flèche), situé à proximité de la naissance de l'artère communicante postérieure (flèche blanche). L'artère choroïdienne antérieure, située à distance du collet (flèches noires), est clairement visualisée ; B : l'image scanographique en rendu de volume permet de délimiter précisément l'anévrisme alors que l'artère choroïdienne antérieure n'est pas détectée. La patiente a été traitée avec succès par embolisation à l'aide de coils.*

Des études antérieures ont porté sur l'utilisation de l'angioscanner comme seul moyen diagnostic et de planning thérapeutique pour la prise en charge des anévrismes intracrâniens (3;22;38;96). Notre étude tend également à prouver que l'orientation thérapeutique des patients basée uniquement sur l'angioscanner est possible et cela en obtenant une bonne concordance avec la décision qui aurait été prise à partir de l'angiographie conventionnelle ($\kappa = 0,76$). Dans 21 cas sur 24, la décision a pu être prise

uniquement sur les données de l'angioscanner (Fig. 2 et 3). Villablanca et col. ont même rapporté avec succès dans leur étude la possibilité d'orienter de façon optimale vers le traitement chirurgical ou endovasculaire 70% des patients issus d'un groupe porteur d'anévrismes de la circulation postérieure (96), localisation où l'angioscanner est habituellement moins performant.

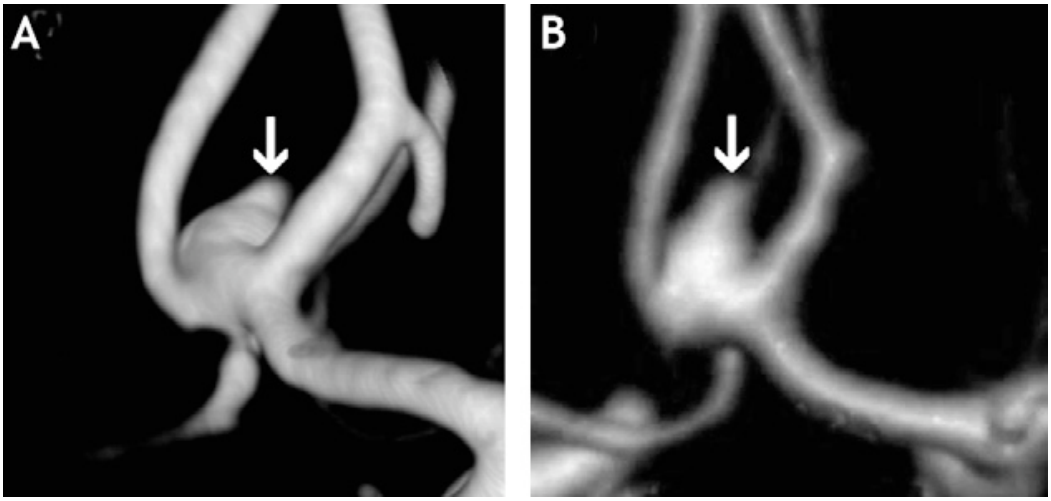

Figure 2 - *Femme âgée de 43 ans (patient 19) présentant une rupture d'un anévrisme de l'artère communicante antérieure (AcoA). a : reconstruction tridimensionnelle (3D) en angiographie conventionnelle rotationnelle montrant un anévrisme de l'AcoA mesurant 4 mm de diamètre avec une image de phlyctène à la partie distale de l'anévrisme (flèche) ; b : la morphologie de l'anévrisme (flèche) peut être évaluée sur cette image scanographique en rendu de volume. Comparé à l'angiographie conventionnelle, le collet anévrysmal apparaît discrètement plus large. L'embolisation par voie endovasculaire à l'aide de coils était proposée sur les deux modalités d'imagerie.*

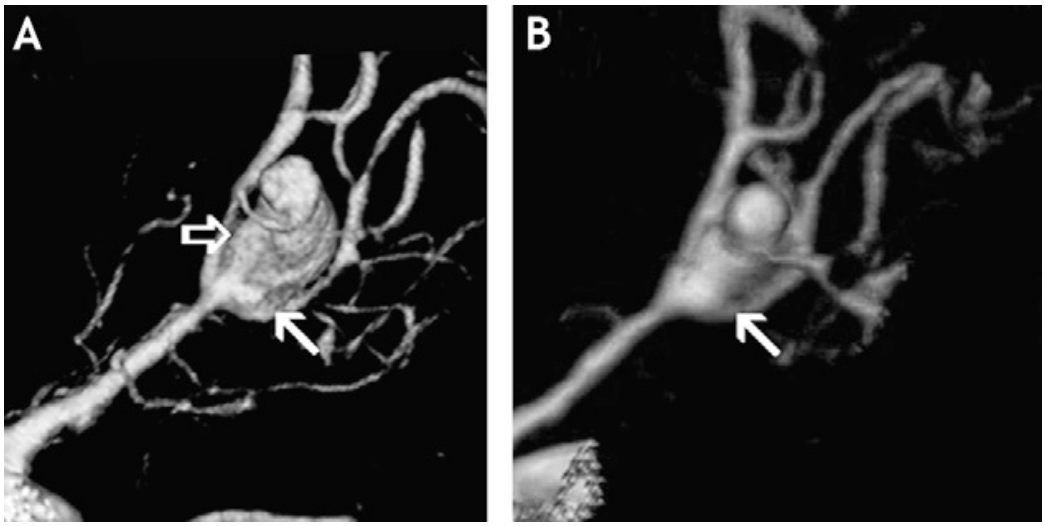

Figure 3 - *Homme âgé de 38 ans présentant une rupture d'anévrisme de la bifurcation de l'artère cérébrale moyenne (ACM) (patient 9). a : reconstruction tridimensionnelle (3D) par angiographie conventionnelle rotationnelle montrant un anévrisme irrégulier mesurant 8 mm de diamètre de l'ACM (flèche ouverte) avec présence d'une branche artérielle naissant au niveau de la base du collet de l'anévrisme (flèches blanches) ; b : les caractéristiques de l'anévrisme sur une image scanographique en rendu de volume sont en concordance avec les résultats de l'angiographie 3D avec présence d'une branche artérielle incorporée à la base de l'anévrisme (flèche blanche). Pour les deux modalités d'imagerie, un traitement chirurgical a été proposé.*

L'étude rapportée dans cette thèse présente plusieurs limitations. Nos résultats sont basés sur un échantillon de petite taille issu d'un seul centre. Les stratégies de traitement choisies auraient pu être biaisées par les habitudes de prise en charge locale. C'est pourquoi, nous avons essayé de guider la décision thérapeutique sur des critères objectifs utilisés communément pour la proposition d'un traitement endovasculaire.

La polémique persiste quant à l'utilisation exclusive de l'angioscanner pour choisir l'option thérapeutique d'un anévrisme intracrânien rompu. La limite principale de la technique semble être sa faible sensibilité à détecter les branches incorporées au sac anévrismal. En pratique clinique, si l'angioscanner multi-détecteurs devait être utilisé comme seul moyen diagnostique avant embolisation, certaines contre-indications majeures de ce traitement pourraient n'être démasquées que lors de l'angiographie rotationnelle en début de procédure endovasculaire.

Malgré ces limitations, l'angioscanner multi-détecteurs remplacera probablement progressivement l'angiographie conventionnelle à la phase diagnostique de l'HSA non traumatique. L'angiographie conventionnelle est consommatrice de temps, invasive et n'est pas toujours disponible dans chaque centre 24h/24h. L'angioscanner est une solution plus pratique, largement et facilement accessible, moins coûteuse et peu risquée. Il peut être réalisé dans le service d'accueil des urgences immédiatement après avoir fait le diagnostic d'HSA sur le scanner standard accélérant ainsi la prise en charge

thérapeutique des patients présentant une rupture anévrismale récente. Il ne faut pas minimiser, dans cet algorithme diagnostique, l'importance du post-traitement d'image et de son analyse par le neuroradiologue sur la station de travail et de la discussion collégiale qui lui fait suite en compagnie de l'équipe neurochirurgicale, préliminaire à tout choix thérapeutique.

En conclusion, l'angioscanner multi-détecteurs est un outil pratique pour la détection des anévrismes intracrâniens chez des patients se présentant avec une HSA non traumatique. De plus, cette technique fournit les informations anatomiques nécessaires à l'orientation thérapeutique de ces malades soit vers le traitement chirurgical soit vers le traitement endovasculaire. On doit cependant garder à l'esprit sa faible sensibilité (50%) pour la détection des branches artérielles partant du sac anévrismal.

Dans notre centre, cette étude a permis de valider la technique d'angioscanner pour le diagnostique des anévrismes intracrâniens rompus et pour l'orientation thérapeutique des patients victimes d'HSA. Il permet d'éviter dans la majorité des cas la réalisation d'une artériographie conventionnelle qui est maintenant réservée aux patients ayant un angioscanner non contributifs (négatif, mauvaise qualité, description insuffisante de l'anatomie anévrismale).

B. ***Localisation en IRM des anévrismes carotidiens paraclinoidiens.***

1. Etude préliminaire : développement du protocole IRM paraclinoïdien et validation anatomo-radiologique

1.1. Résumé

MRI location of the distal dural ring plane: anatomoradiological study and application to paraclinoid carotid artery aneurysms.

Thines L, Delmaire C, Le Gars D, Pruvo JP, Lejeune JP, Lehmann P, Francke JP. *Eur Radiol*. 2006 Feb;16(2):479-88.

The distal dural ring plane (DDRP) separates the intradural from the extradural paraclinoid internal carotid artery. The purpose of this study was to evaluate its position with MR imaging. The protocol used a T2 weighted sequence in two orthogonal planes: diaphragmatic (DIA-P) and carotid planes (CAR-P). The DDRP passes through 4 anatomoradiological reference points (RefP). We developed on a cadaveric model a correlation method supported by correlation lines and angles (CA) projecting the RefP toward the DDRP. RefP were correlated to the DDRP in 65-84% of cases in the DIA-P and 60-76% in the CAR-P. CA were identified and correlated to the DDRP, respectively, in 87% and 60% of cases in the DIA-P, and 60% and 51% of cases in the CAR-P (failure often related to a lack of visibility of just one RefP). A higher tissular contrast in living subjects allowed the identification of CA in 90% and 80% of cases, respectively, in the DIA-P and the CAR-P. We proposed that CA, when identified, should be considered as an approximation of the inferior radiological limit of the DDRP curve. In difficult angiographical cases, this MRI protocol could help to locate paraclinoid aneurysms on both sides of the cavernous sinus roof.

1.2. Discussion

Revue de la littérature

Depuis Punt et col. en 1979 (63), l'origine de l'artère ophtalmique sur l'angiographie cérébrale est couramment utilisée comme le repère radiologique de la

jonction entre artère carotide interne (ACI) intradurale (extra ou supracaverneuse) et extradurale (intracaverneuse). En raison de variations anatomiques fréquentes, ce marqueur radiologique, habituellement fiable, peut ne pas suffire à localiser précisément cette jonction dans environ 35% des cas. En effet, l'origine de l'artère ophtalmique est extradurale dans 10% des cas (13;46;50;63;65) ou prend naissance entre 1 mm (origine proximale) et 5mm (origine distale) au-dessus de l'anneau dural distal (ADD) dans 24% des cas (46). Depuis, la localisation radiologique de l'ADD, véritable limite anatomique entre ACI intra- et supracaverneuse, a été un problème récurrent. Certains auteurs ont créé des techniques de corrélations radiologiques utilisant certaines des structures de la base du crâne sur les vues latérale et antérieure non soustraite de l'angiographie : la base du processus clinoïde antérieur (PCA), la surface supérieure du PCA et le tuberculum sellaire, ou le planum sphénoïdal et les lignes du tuberculum sellaire (13;59;82). Des progrès récents en neuroradiologie ont permis le développement de protocoles modernes utilisant les reconstructions 3D à partir du scanner spiralé (29), l'angioscanner 3D (57) ou le cisternoscanner 3D (40). Ces procédures radiologiques étaient respectivement basées sur la visualisation du pilier optique ("optic strut"), sur l'identification d'une encoche de la paroi carotidienne à hauteur de l'ADD et sur le contraste des citernes de LCS moulant les contours de l'ACI supracaverneuse. Bien qu'intéressantes, ces méthodes ne prenaient pas en compte la complexité de l'anatomie extravasculaire de la région et particulièrement la variabilité des faisceaux duraux radiotransparents composant le toit du sinus caverneux.

Protocole paraclinoïdien et modèle de corrélation anatomique

Dans ce contexte, l'IRM est apparue comme une technique radiologique appropriée pour l'étude de l'anatomie de la région paraclinoïdienne. La résolution spatiale sur les appareils d'IRM 1.5 Tesla était suffisante pour identifier correctement sur des coupes

fines et contiguës l'ensemble des structures paraclinoïdiennes (Fig. 1) et même les faisceaux duraux du sinus caverneux. Cette visualisation directe de l'anatomie permettait au neuroradiologue de s'affranchir de la variabilité inter- et intra-individuelle si pénalisante pour les méthodes radiologiques indirectes. La précision de ce protocole était confirmée par les taux satisfaisants de visualisation des repères, des droites ou des angles de corrélations et par la qualité de la concordance interobservateur (de bonne à excellente) - Tableaux 1 et 2.

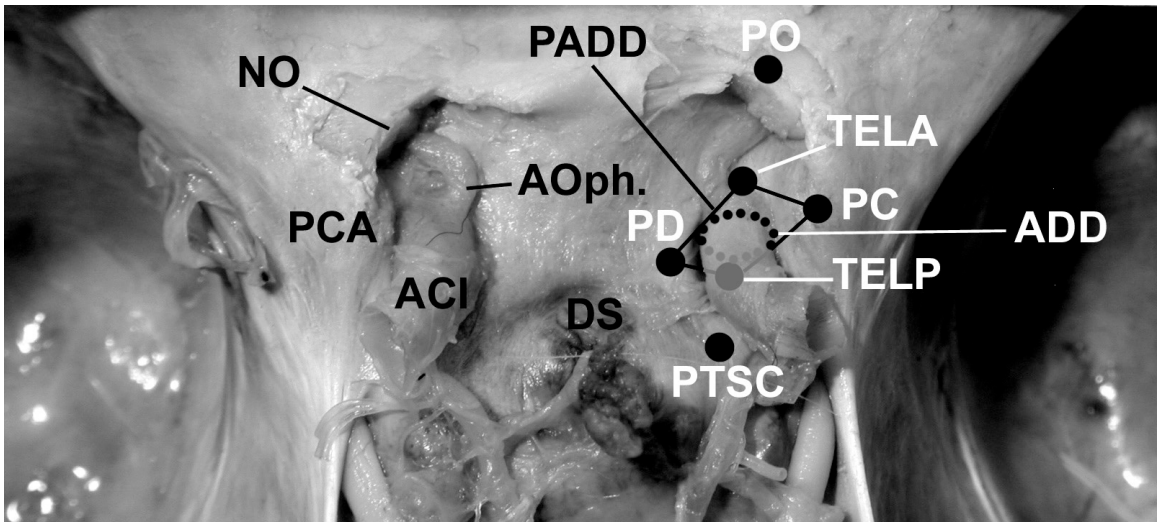

Figure 1- *Vue supérieure de la région paraclinoïdienne et repères anatomo-radiologiques (nerfs optiques et chiasma sectionnés).* ***NO****: nerf optique;* ***PCA****: processus clinoïde antérieur;* ***ACI****: artère carotide interne;* ***AOph.****: artère ophtalmique;* ***DS****: diaphragme sellaire;* ***PC****: point clinoïdien;* ***PD****: point diaphragmatique;* ***PO****: point optique;* ***TELA****: terminaison de l'encoche de LCS antérieure;* ***TELP****: terminaison de l'encoche de LCS postérieure;* ***PTSC****: point du toit du sinus caverneux;* ***ADD****: anneau dural distal;* ***PADD****: plan de l'anneau dural distal*

Une séquence T2 a été choisie pour pouvoir bénéficier du fort contraste tissulaire obtenu entre les structures osseuses, les faisceaux duraux, les artères paraclinoïdiennes, les nerfs optiques (hypo- ou isosignal) et l'hyperintensité des citernes de LCS ou du contenu du sinus caverneux. La double inclinaison du plan de l'ADD rend habituellement son indentification en imagerie difficile. Afin de résoudre ce problème,

nous avons exploré la région paraclinoïdienne à l'aide de deux plans de corrélation radiologique perpendiculaires (Fig-2) dans lesquels nous avons dessiné les droites de corrélations (Fig. 3). L'ACI était suivi de façon étroite tout au long de son trajet grâce à la création du plan carotidien (P-CAR).

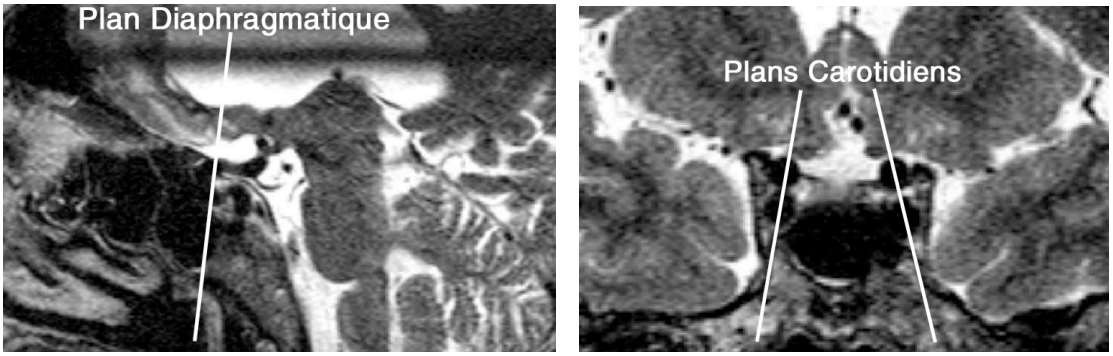

Figure 2 – *Plans radiologiques diaphragmatique et carotidien.*

Tableau 1 – *Taux (%) moyens pour la visualisation globale des repères avec les valeurs du coefficient kappa correspondantes (résultats présentés pour l'ensemble des côtés)*

Analyse globale			Modèle anatomique		Groupe contrôle	
Plans	**Type**	**Nb**	%	κ	%	κ
P-DIA	Tous les repères	**0-3**	14	0.82	7	0.70
		4	74		37	
		5	12		56	
	Points de référence	**1**	13	1	10	0.63
		2	87		90	
P-CAR	Tous les repères	**0-2**	0	0.70	0	0.60
		3-4	15		2	
		5-7	85		98	
	Points de référence	**0-2**	8	0.63	4	0.79
		3	32		16	
		4	60		80	

P-DIA: plan diaphragmatique P-CAR : plan carotidien κ: valeurs de kappa

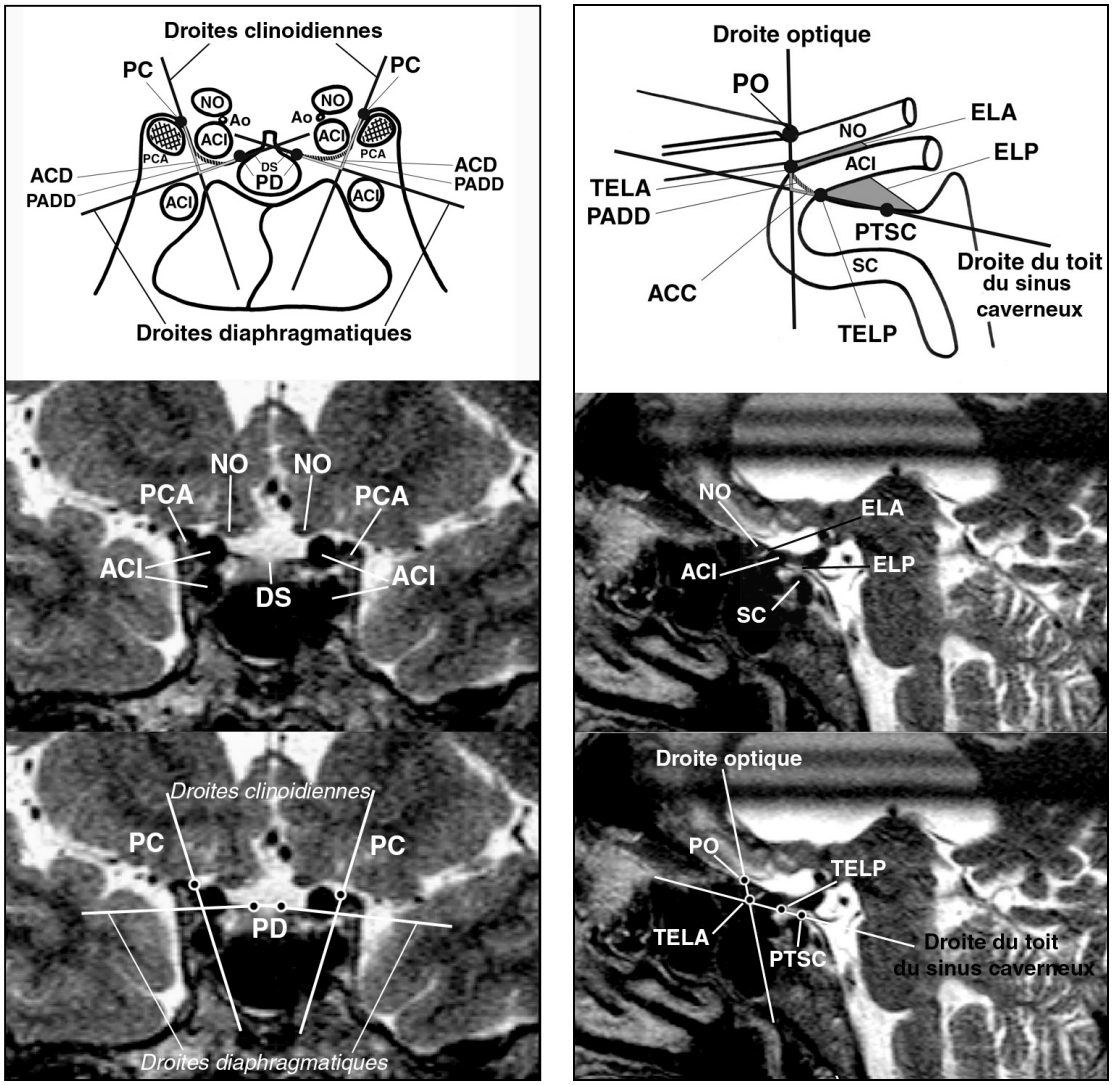

Figure. 3 – *Schéma et IRM montrant les points de référence, les droites et angles de corrélation dans le plan diaphragmatique (à gauche) et le plan carotidien (à droite).* ***NO****: nerf optique;* ***Ao****: artère ophtalmique;* ***ACI****: artère carotide interne;* ***PCA****: processus clinoïde antérieur;* ***DS****: diaphragme sellaire;* ***PC****: point clinoïdien;* ***PD****: point diaphragmatique;* ***ACD****: angle de corrélation diaphragmatique;* ***SC****: siphon carotidien;* ***PO****: point optique;* ***ELA****: encoche de LCS antérieure;* ***TELA****: terminaison de l'encoche de LCS antérieure;* ***ELP****: encoche de LCS postérieure;* ***TELP****: terminaison de l'encoche de LCS postérieure;* ***PTSC****: point du toit du sinus caverneux;* ***ACC****: angle de corrélation carotidien;* ***PADD****: plan de l'anneau dural distal*

Le contraste tissulaire obtenu in vivo (encoches de LCS) était reproduit sur le modèle anatomique en immergeant la pièce dans une solution aqueuse. Peu de modifications des rapports anatomiques étaient retrouvées sur la pièce cadavérique formolée en raison de la rigidité naturelle de l'armature de la région (PCA et faisceaux duraux) qui fixent

les artères carotides internes et les nerfs optiques en position stable, même après cathétérisation rétrograde. Des taux de visualisation comparables des encoches de LCS entre pièce anatomique et sujets vivants semblaient témoigner de peu de perturbation du signal cisternal par les artéfacts de mouvement in vivo. Ainsi la reproductibilité en IRM-T2 des repères paraclinoïdiens était établie entre les deux groupes (Tableau 2). Certains de ces repères étaient même plus facilement identifiés sur les sujets vivants en raison d'un phénomène de vide de signal intravasculaire (artère ophtalmique) ou d'hyposignal accru de la dure-mère (toit du sinus caverneux).

Tableau 2 – *Taux (%) moyens pour la visualisation et la corrélation spécifique de chaque repère et des angles de corrélation avec les valeurs du coefficient kappa correspondantes (résultats présentés pour l'ensemble des côtés)*

Analyse spécifique		**Modèle anatomique**								**Groupe contrôle**			
		P-DIA				**P-CAR**				**P-DIA**		**P-CAR**	
Classe de repères	**Type**	V+		V+/C+		V+		V+/C+		V+		V+	
		%	κ	%	κ	%	κ	%	κ	%	κ	%	κ
Points de référence	**PC**	100	nc	84	1	—	—	—	—	100	nc	—	—
	PD	87	1	65	0.88	—	—	—	—	90	0.63	—	—
	PO	—	—	—	—	100	nc	76	0.92	—	—	100	nc
	TELA	—	—	—	—	97	1			—	—	95	0.65
	TELP	—	—	—	—	91	0.84	60	0.79	—	—	85	0.87
	PT	—	—	—	—	60	0.74			—	—	95	0.65
Repères régionaux	**PCA**	100	nc	—	—	—	—	—	—	100	nc	—	—
	DS	94	0.79	—	—	—	—	—	—	100	nc	—	—
	AO	15	0.80	—	—	0	nc	—	—	60	0.72	67	0.70
	NO	—	—	—	—	100	nc	—	—	—	—	100	nc
	SC	—	—	—	—	88	0.87	—	—	—	—	100	nc
Angles de Corrélation	**ACD**	87	1	60	0,94	—	—	—	—	90	0.63	—	—
	ACC	—	—	—	—	60	0,633	51	0,84	—	—	80	0.79

V+ = visualisé, V+/C+ = visualisé + corrélé, V+ κ = concordance interobservateur en terme de visualisation, V+/C+ κ = concordance interobservateur en terme de corrélation, PC = point clinoïdien, PD = point diaphragmatique, PO = point optique, TELA = terminaison de l'encoche de LCS antérieure, TELP = terminaison de l'encoche de LCS postérieure, PT = point du toit du sinus caverneux, PCA = processus clinoïde antérieur, DS = diaphragma sellae, AO = artère ophtalmique, NO = nerf optique, SC = siphon carotidien, ACD = angle de corrélation diaphragmatique, ACC = angle de corrélation carotidien, nc = non calculable

Valeur de la méthode d'imagerie présentée

Notre étude a permis le développement d'un protocole d'IRM permettant de mettre en corrélation le plan de l'ADD avec 6 points de référence anatomiques. La limite de cette technique réside dans la nécessité de visualiser tous ces points de repères afin d'appliquer la méthode de corrélation. Cela était effectué dans un pourcentage acceptable de côtés chez le sujet vivant (90% dans le plan diaphragmatique et 80% dans le plan carotidien). Les lignes et les angles de corrélations correspondants bordaient théoriquement la limite inférieure d'inclusion du plan courbe de l'ADD. Sur les pièces anatomiques, les angles de corrélations pouvaient être tracés dans 87% et 60% des cas et corrélés au plan de l'ADD dans 60% et 51% des cas, respectivement dans les plans diaphragmatique et carotidiens. L'échec de la méthode de corrélation était dû au manque de visualisation d'un seul repère dans 33% des cas dans le plan diaphragmatique et 60% des cas dans le plan carotidien. Mais quand un angle pouvait être construit, il était corrélé au plan de l'ADD dans 68% des cas dans le plan diaphragmatique et 78% des cas dans les plans carotidiens. Un meilleur contraste tissulaire chez le sujet vivant était à l'origine d'une amélioration significative ($p< 0,05$) de la précision du protocole d'IRM paraclinoïdien avec l'identification des angles de corrélations dans 90% des cas dans le plan diaphragmatique et 80% des cas dans les plans carotidiens. Nous proposons d'admettre, quand les angles de corrélations sont identifiés clairement, que ceux-ci constituent une approximation de la limite inférieure d'inclusion du plan de l'ADD. Nous déduisons donc de ce nouveau concept que tout point (ou anévrisme) situé sous ou au-dessus de ces angles soit considéré comme étant respectivement dans l'espace extra- ou intradural.

En conclusion, avec le perfectionnement des techniques d'imagerie, les exigences des patients et des médecins en terme de précision diagnostique augmentent. La localisation de l'ADD reste un problème critique ayant des implications thérapeutiques

pour la prise en charge des anévrismes paraclinoïdiens. Dans les cas délicats où le repère habituel de l'artère ophtalmique semble pris à défaut, ce nouveau protocole d'IRM pourrait être considéré comme une méthode localisatrice non invasive complémentaire permettant de préciser la topographie exacte de l'anévrisme par rapport au toit du sinus caverneux. De plus, la précision anatomique importante de ce protocole d'IRM, en terme de visualisation des structures de la région paraclinoïdienne et de leurs rapports, pourrait être très utile à la planification de la chirurgie anévrismale dans cette région complexe.

2. Projet d'application clinique

2.1. Résumé

MRI localization of paraclinoid carotid aneurysms. Technical note

Thines L, Delmaire C, Le Gars D, Pruvo JP, Lejeune JP, Lehmann P, Francke JP. *J Neuroradiol*. 2006 Apr;33(2):115-20.

Aim : The distal dural ring plane (DDRP) separates the intracavernous from the supracavernous paraclinoid internal carotid artery. The purpose of this MRI protocol is to evaluate the position of this plane for the location of paraclinoid aneurysms.

Method : The protocol uses a T2 weighted sequence in two orthogonal planes (diaphragmatic and carotid planes) and two correlation lines in each plane. These lines pass through anatomo-radiological reference points correlated with the medio-lateral and antero-posterior margins of the DDRP. We use the intersection angle of these lines as the inferior radiological limit of the DDRP curve.

Results : An aneurysm situated above this angle is supracavernous; an aneurysm situated below this angle is intracavernous; an aneurysm crossing this angle is transitional.

Conclusion : In difficult angiographical cases, this MRI protocol could help to locate paraclinoid aneurysms on both sides of the cavernous sinus roof.

2.2. Discussion

Application aux anévrismes paraclinoïdiens

Le protocole d'IRM restitue les données perdues lors de l'angiographie concernant les rapports anatomiques de l'anévrisme *(représentation schématique: figures 1 et 2)*. La construction des angles de corrélation dans chaque plan permet d'estimer la localisation des anévrismes paraclinoïdiens par rapport au toit du sinus caverneux. Un anévrisme situé entièrement au dessus des deux angles de corrélation est considéré comme supracaverneux *(figure 3)*; un anévrisme situé entièrement en dessous des deux angles de corrélation est considéré comme intracaverneux *(figure 4)* ; un anévrisme situé à cheval sur les deux angles de corrélation est considéré comme transitionnel (intra- et supracaverneux) *(figure 5)*.

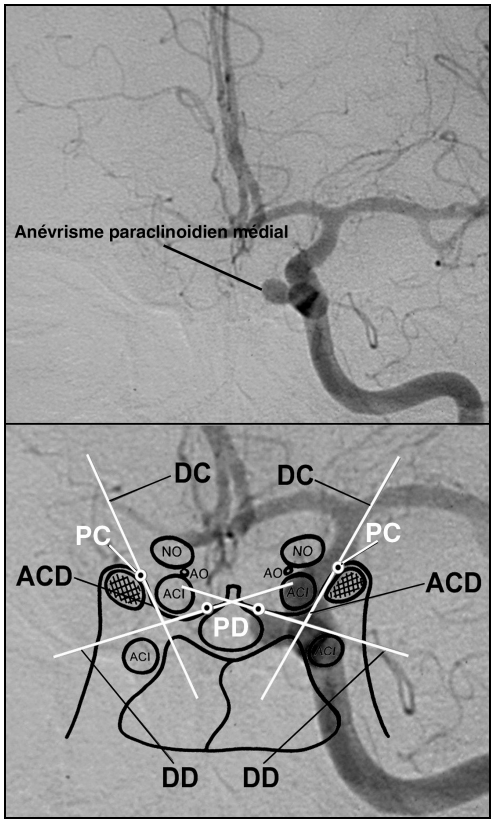

Figure 1- Superposition du schéma de corrélation diaphragmatique sur une angiographie de face d'un anévrisme paraclinoïdien gauche intracaverneux (en dessous de l'angle de corrélation diaphragmatique). **DC**: droite clinoïdienne; **DD**: droite diaphragmatique; **PC**: point clinoïdien; **PD**: point diaphragmatique; **NO**: nerf optique; **ACI**: artère carotide interne; **Ao**: artère ophtalmique; **ACD**: angle de corrélation diaphragmatique

Superimposition of the diaphragmatic correlation diagram on the angiography (anterior view) of a left intracavernous paraclinoid aneurysm (below the correlation angle).
***DC**: clinoid line; **DD**: diaphragmatic line; **PC**: clinoid point; **PD**: diaphragmatic point; **NO**: optic nerve; **ACI**: internal carotid artery; **Ao**: ophthalmic artery; **ACD**: diaphragmatic correlation angle*

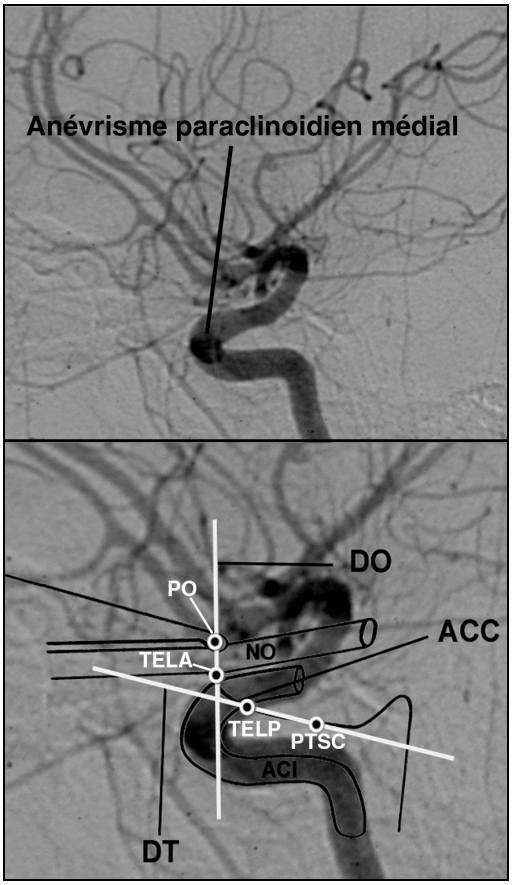

Figure 2- Superposition du schéma de corrélation carotidien sur une angiographie de profil d'un anévrisme paraclinoïdien gauche intracaverneux (en dessous de l'angle de corrélation carotidien). **DO**: droite optique; **DT**: droite du toit du sinus caverneux; **PO**: point optique; **TELA**: terminaison de l'encoche de LCS antérieure; **TELP**: terminaison de l'encoche de LCS postérieure; **PTSC**: point du toit du sinus caverneux; **NO**: nerf optique; **ACI**: artère carotide interne; **ACC**: angle de corrélation carotidien

Superimposition of the carotid correlation diagram on the angiography (lateral view) of a left intracavernous paraclinoid aneurysm (below the correlation angle). ***DO****: optic line;* ***DT****: roof line;* ***PO****: optic point;* ***TELA****: anterior CSF notch extremity;* ***TELP****: posterior CSF notch extremity;* ***PTSC****: roof of the cavernous sinus point;* ***NO****: optic nerve;* ***ACI:*** *internal carotid artery;* ***ACC****: carotid correlation angle*

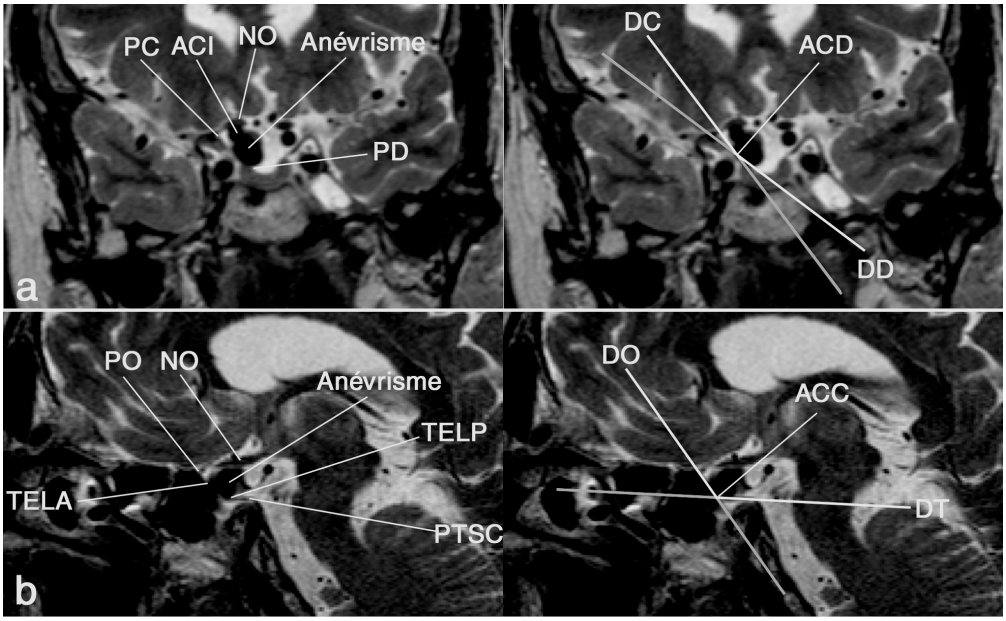

Figure 3- Anévrisme supracaverneux, situé au dessus des deux angles de corrélation. a- plan diaphragmatique ; b- plan carotidien. **ACI**: artère carotide interne; **NO**: nerf optique; **PC**: point clinoïdien; **PD**: point diaphragmatique; **PO**: point optique; **TELA**: terminaison de l'encoche de LCS antérieure; **TELP**: terminaison de l'encoche de LCS postérieure; **PTSC**: point du toit du sinus caverneux; **DC**: droite clinoïdienne; **DD**: droite diaphragmatique; **DO**: droite optique; **DT**: droite du toit; **ACD**: angle de corrélation diaphragmatique; **ACC**: angle de corrélation carotidien.

Supracavernous aneurysm, above the correlation angles. a- diaphragmatic plane ; b- carotid plane. ***ACI****: internal carotid artery;* ***NO****: optic nerve;* ***PC****: clinoid point;* ***PD****: diaphragmatic point;* ***PO****: optic point;* ***TELA****: anterior CSF notch extremity;* ***TELP****: posterior CSF notch extremity;* ***PTSC****: roof of the cavernous sinus point;* ***DC****: clinoid line;* ***DD****: diaphragmatic line;* ***DO****: optic line;* ***DT****: roof line;* ***ACD****: diaphragmatic correlation angle;* ***ACC****: carotid correlation angle*

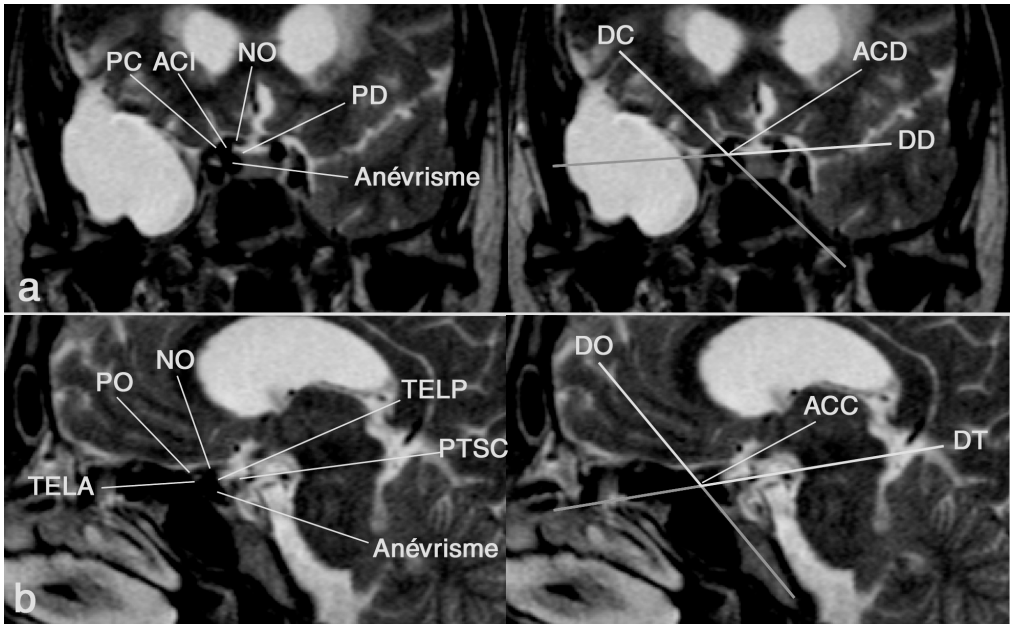

Figure 4- Anévrisme intracaverneux, situé en dessous des deux angles de corrélation. a- plan diaphragmatique ; b- plan carotidien. **ACI**: artère carotide interne; **NO**: nerf optique; **PC**: point clinoïdien; **PD**: point diaphragmatique; **PO**: point optique; **TELA**: terminaison de l'encoche de LCS antérieure; **TELP**: terminaison de l'encoche de LCS postérieure; **PTSC**: point du toit du sinus caverneux; **DC**: droite clinoïdienne; **DD**: droite diaphragmatique; **DO**: droite optique; **DT**: droite du toit; **ACD**: angle de corrélation diaphragmatique; **ACC**: angle de corrélation carotidien

Intracavernous aneurysm, below the correlation angles. a- diaphragmatic plane ; b- carotid plane. ***ACI****: internal carotid artery;* ***NO****: optic nerve;* ***PC****: clinoid point;* ***PD****: diaphragmatic point;* ***PO****: optic point;* ***TELA****: anterior CSF notch extremity;* ***TELP****: posterior CSF notch extremity;* ***PTSC****: roof of the cavernous sinus point;* ***DC****: clinoid line;* ***DD****: diaphragmatic line;* ***DO****: optic line;* ***DT****: roof line;* ***ACD****: diaphragmatic correlation angle;* ***ACC****: carotid correlation angle*

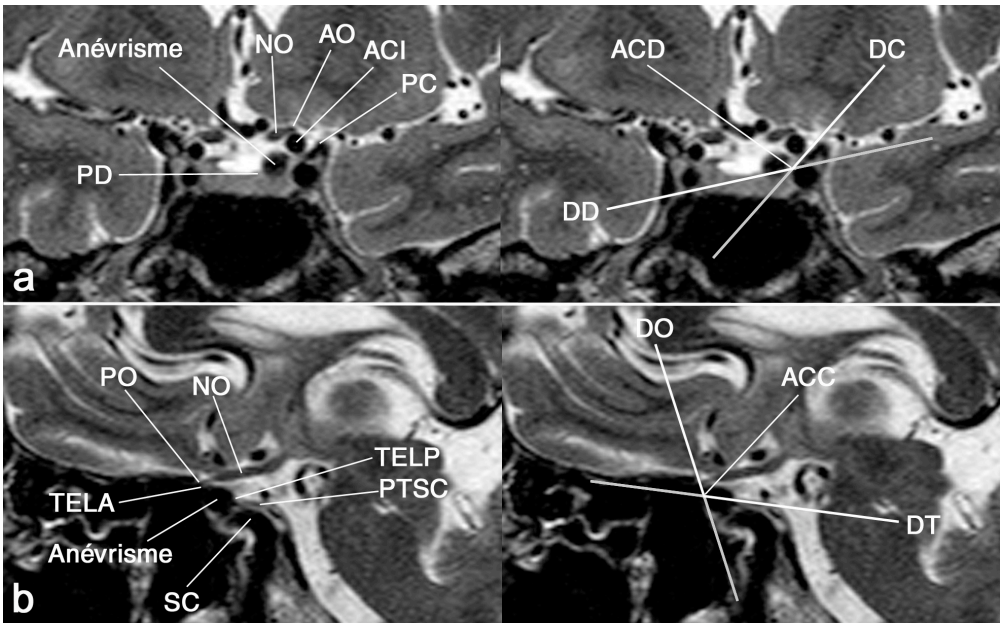

Figure 5- Anévrisme transitionnel, situé à cheval sur les deux angles de corrélation. a- plan diaphragmatique ; b- plan carotidien. **ACI**: artère carotide interne; **NO**: nerf optique; **AO**: artère ophtalmique; **SC**: siphon carotidien; **PC**: point clinoïdien; **PD**: point diaphragmatique; **PO**: point optique; **TELA**: terminaison de l'encoche de LCS antérieure; **TELP**: terminaison de l'encoche de LCS postérieure; **PTSC**: point du toit du sinus caverneux; **DC**: droite clinoïdienne; **DD**: droite diaphragmatique; **DO**: droite optique; **DT**: droite du toit; **ACD**: angle de corrélation diaphragmatique; **ACC**: angle de corrélation carotidien ;

Transitional aneurysm, crossing the correlation angles. a- diaphragmatic plane ; b- carotid plane. ***ACI****: internal carotid artery;* ***NO****: optic nerve;* ***AO****: ophthalmic artery;* **SC**: carotid siphon; ***PC****: clinoid point;* ***PD****: diaphragmatic point ;* ***PO****: optic point ;* ***TELA****: anterior CSF notch extremity ;* ***TELP****: posterior CSF notch extremity;* ***PTSC****: roof of the cavernous sinus point;* ***DC****: clinoid line;* ***DD****: diaphragmatic line;* ***DO****: optic line;* ***DT****: roof line;* ***ACD****: diaphragmatic correlation angle;* ***ACC****: carotid correlation angle*

Projet de recherche

C'est sur la base de ces données établissant l'applicabilité du protocole IRM chez les patients porteurs d'anévrismes paraclinoïdiens que nous avons mis en place une étude clinique prospective comparant IRM paraclinoïdienne et angiographie conventionnelle pour la caractérisation topographique de ces anévrismes et son influence sur leur prise en charge thérapeutique.

3. Application clinique du protocole IRM paraclinoïdien et comparaison à l'angiographie conventionnelle

3.1. Résumé

Usefulness of MR imaging for the assessment of nonophthalmic paraclinoid aneurysms.

Thines L, Gauvrit JY, Leclerc X, Le Gars D, Delmaire C, Pruvo JP, Lejeune JP. *AJNR Am J Neuroradiol*. 2008 Jan;29(1):125-9.

Background and purpose: Neuroradiological location of asymptomatic paraclinoid aneurysms is decisive for patient management. In a preliminary study, we designed a paraclinoid MR protocol (PMP) including high resolution T2-weighted images in two orthogonal planes to define the inferior limit of the distal dural ring plane that represents the borderline between the intradural and extradural internal carotid artery. In this clinical study, we compared this protocol to digital subtraction angiography for the location of paraclinoid aneurysms.

Methods: During a three year period, the PMP and conventional angiography were performed in 14 consecutive patients with 17 asymptomatic paraclinoid aneurysms. Ophthalmic aneurysms (superior aneurysms) were excluded. MRI data were reviewed by two independent observers whereas conventional angiograms were analyzed by a third experienced neuroradiologist. MRI and conventional angiography were independently analyzed and interpretations obtained with each technique were compared.

Results: PMP allowed correct visualization of the aneurysm in all patients. No significant differences ($p > 0.05$) were found between the DSA and PMP for the measurement of the aneurysmal neck *or* sac. Interobserver agreement was good. MRI was discordant with conventional angiography regarding the position around the cavernous sinus of the aneurysmal neck *and* sac in five cases. PMP images were helpful for treatment decisions in four cases.

Conclusion: PMP is an interesting tool that might be used in association with conventional angiography for the assessment of paraclinoid aneurysms.

3.2. Discussion

Valeur et limites du protocole d'IRM paraclinoïdien

La reproductibilité et la précision de ce protocole ont été documentées dans les deux travaux préliminaires de corrélation anatomo-radiologique. Dans cette étude clinique, la technique a permis pour tous les patients d'identifier et de localiser précisément ces anévrismes détectés en angiographie. Les résultats ont confirmé la reproductibilité interobservateur pour la mensuration et la localisation de l'anévrisme ainsi que la fiabilité des mesures obtenues en IRM. Dans deux cas, les données issues de ce protocole furent même confirmées lors d'une exploration chirurgicale de la région (Fig.1).

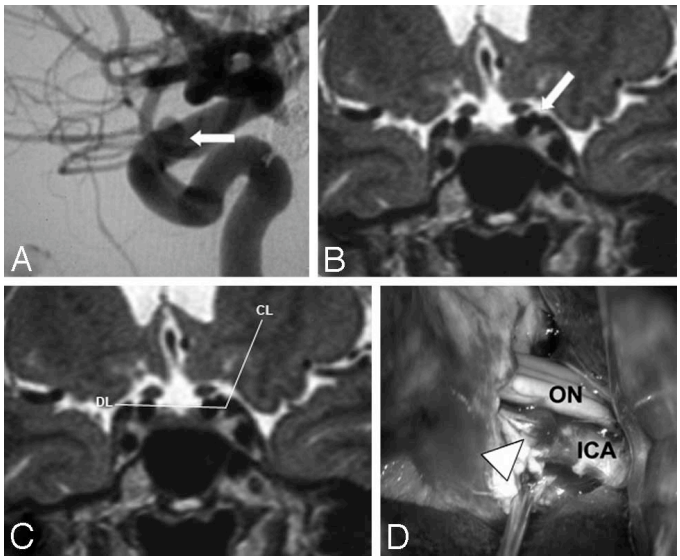

Figure 1 – Corrélation radio-chirurgicale pour un anévrisme paraclinoïdien supéro-latéral (cas 14).
A : angiographie carotidienne gauche (vue latérale) montrant un anévrisme (flèche) interprété transitionnel avec un collet intracaverneux et un sac transitionnel
B, C : protocole paraclinoïdien dans le plan diaphragmatique avec un angle de corrélation montrant une localisation intradurale pour le collet et le sac. (DL: droite diaphragmatique; CL : droite clinoïdienne).
D : Constatations opératoires confirmant la position supracaverneuse à la fois du collet et du sac et montrant, après clinoïdectomie antérieure et ouverture du ligament falciforme, les relations de l'anévrisme avec l'ACI (ICA) et le nerf optique (ON).

Comparé à l'angiographie, le protocole d'IRM paraclinoïdien fournit une vision globale de l'anatomie de cette région et une visualisation directe des faisceaux duraux dont ceux composant le toit du sinus caverneux. C'est pourquoi ce protocole permet d'améliorer l'analyse radiologique en proposant d'identifier directement l'anévrisme, de déterminer sa topographie et de mesurer dans le cas d'anévrismes transitionnels la part respective des portions supra- et intracaverneuse (Fig.2).

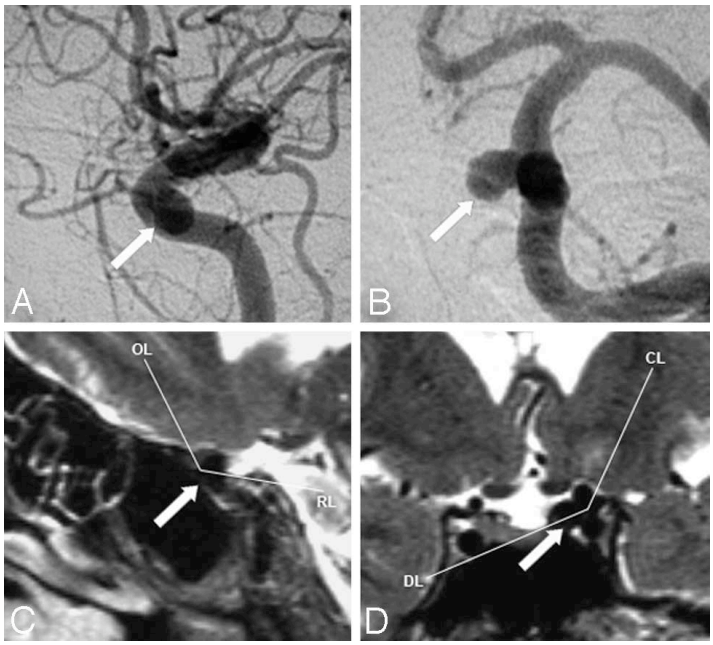

Figure – 2 Comparaison entre angiographie et IRM pour la localisation du cas 11 (flèche). Les deux examens retrouvent un anévrisme transitionnel (collet supracaverneux et sac transitionnel). Le protocole paraclinoïdien met en évidence une partie supracaverneuse plus importante que ne le laissait suspecter l'angiographie.
A, B: artériographie carotidienne gauche vue latérale et antérieure
C: protocole paraclinoïdien dans le plan carotidien (OL: droite optique; RL: droite du toit).
D: protocole paraclinoïdien dans le plan diaphragmatique (DL: droite diaphragmatique; CL: droite clinoïdienne).

Des discordances entre l'interprétation fournie par l'angiographie et celle du protocole paraclinoïdien ont été retrouvées dans 8 cas (Tableau-1). Ces différences étaient plus fréquentes pour les anévrismes à projection médiale ou postéro-médiale (5/8) et pour la localisation du sac anévrismal lui-même (7/8). L'amélioration de la localisation du sac anévrismal par rapport au toit du sinus caverneux est de toute importance si l'on considère qu'il s'agit du site habituel de rupture des anévrismes intracrâniens. Dans notre étude nous n'avons pu obtenir de confirmation chirurgicale

que dans 2 cas ainsi ces discordances entre angiographie et IRM sont à analyser prudemment. De plus, le choix arbitraire de la ligne horizontale passant par l'origine de l'artère ophtalmique comme seule limite angiographique séparant les espaces intra- et supracaverneux pourrait nous avoir conduit à mal interpréter certaines des angiographies. Certains anévrismes ont ainsi pu être mal localisés et dans ces cas, l'IRM n'aurait finalement permis que de clarifier les erreurs d'analyse artériographique.

Anévrismes	Projection de l'anévrisme		Localisation angiographique		Localisation en IRM	
	Collet	Sac	Collet	Sac	Collet	Sac
1	**MP**	**MP**	**SC**	**T**	**SC**	**SC**
2	M	M	IC	IC	IC	IC
3	**P**	**P**	**SC**	**T**	**T**	**T**
4	**M**	**M**	**IC**	**IC**	**SC**	**SC**
5	M	M	T	T	T	T
6	**P**	**P**	**SC**	**SC**	**SC**	**T**
7	MP	MP	IC	IC	IC	IC
8	MP	MP	IC	IC	IC	IC
9	MP	MP	IC	IC	IC	IC
10	**MP**	**MP**	**T**	**IC**	**SC**	**T**
11	M	MP	SC	T	SC	T
12	A	A	SC	SC	SC	SC
13	MP	MP	IC	T	IC	T
14	**LA**	**L**	**IC**	**T**	**SC**	**SC**
15	**MP**	**M**	**IC**	**IC**	**T**	**T**
16	MP	P	IC	IC	IC	IC
17	**M**	**MP**	**T**	**T**	**IC**	**IC**

Table 1 - Comparaison entre l'angiographie et le protocole d'IRM pour la localisation des anévrismes paraclinoïdiens autour du toit du sinus caverneux.

Les cas présentants des interprétations différentes sont inscrits en gras.

M: médial
L: latéral
A: antérieur
P: postérieur
IC: intracaverneux
T: transitionnel
SC: supracaverneux

Ce protocole paraclinoïdien requiert une courte période d'entraînement afin de se familiariser avec l'anatomie de la région paraclinoïdienne et de ses repères radiologiques. C'est la raison pour laquelle dans cette étude nous avons aussi fait le choix de proposer un protocole simplifié (Fig. 3) permettant de faciliter son utilisation en pratique clinique par le plus grand nombre de neuroradiologues et de neurochirurgiens.

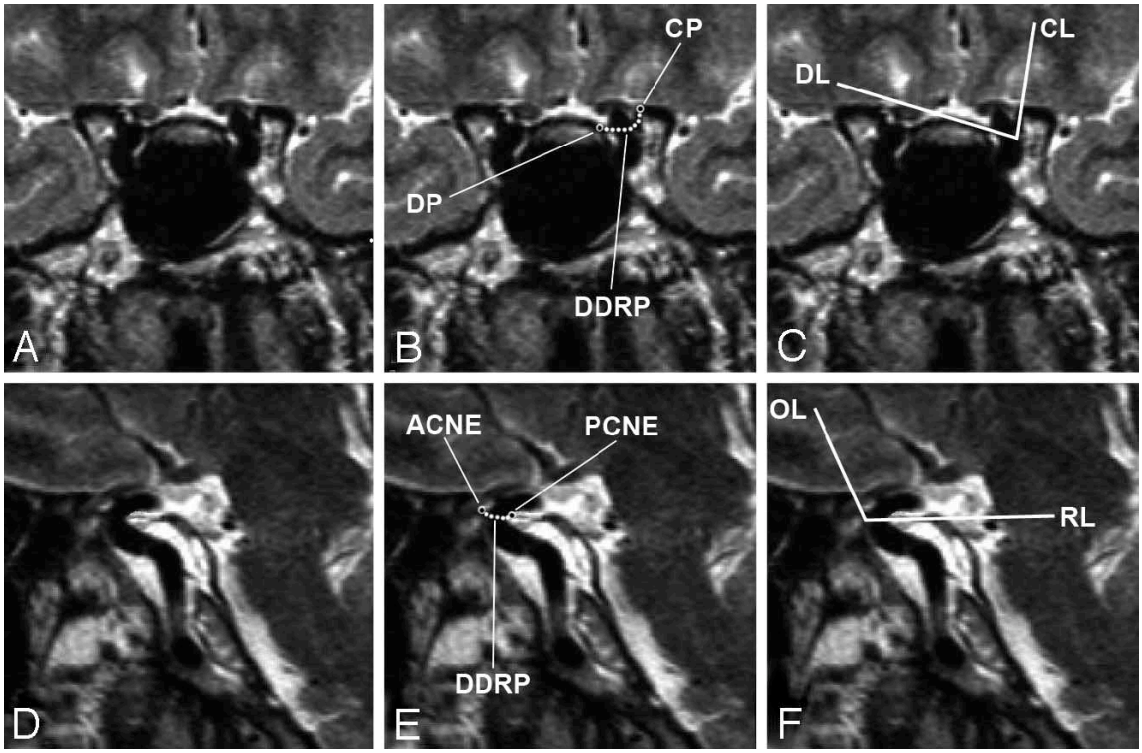

Figure 3 – Protocole d'IRM paraclinoïdien montrant chez un sujet contrôle les 4 points et les 4 lignes de référence ainsi que leurs angles d'intersection corrélés avec les limites du plan de l'anneau dural distal dans chaque plan radiologique.
A, B, C : région paraclinoïdienne dans le plan diaphragmatique
D, E, F: région paraclinoïdienne dans le plan carotidien

DP: point diaphragmatique; CP: point clinoïdien ; DL: droite diaphragmatique; CL : droite clinoïdienne, ACNE: extrémité de l'encoche de LCS antérieure; PCNE : extrémité de l'encoche de LCS postérieure; OL : droite optique; RL : droite du toit, DDRP : plan de l'anneau dural distal (*courbe pointillée*).

Implications pour la prise en charge des anévrismes paraclinoïdiens

Les progrès techniques fait en neuroradiologie ces dernières années ont conduit à l'augmentation importante du diagnostic d'anévrismes asymptomatiques. De plus, et en raison des implications thérapeutiques potentielles, la demande des patients et des praticiens en terme de précision radiologique s'est accrue. Les problèmes posés par la localisation des anévrismes paraclinoïdiens en sont une parfaite illustration. Dans la prise de décision thérapeutique, l'équipe de neurovasculaire tiens compte du rapport bénéfice-risque entre les trois options suivantes : conservative, endovasculaire ou chirurgicale. On réalise alors toute l'importance pour les anévrismes dans cette localisation d'avoir la certitude de la topographie réelle du sac. En effet celle-ci va

directement déterminer si il existe un risque potentiel ou non d'HSA, présent en cas de situation intradurale (supracaverneuse) ou transitionnelle.

Dans notre expérience clinique, le protocole paraclinoïdien nous a aidé dans de nombreux cas à mieux localiser ces anévrismes et à adapter la prise en charge thérapeutique à la situation réelle de l'anévrisme. Les anévrismes intracaverneux (Fig.4) ont été simplement surveillés, alors que les anévrismes transitionnels ou intraduraux ont été plus volontiers traités par voie endovasculaire ou chirurgicalement. Seuls les anévrismes dysplasiques ou de très petite taille ont bénéficié d'un traitement conservateur. Au total l'association de ce protocole d'IRM à l'angiographie a modifié la prise en charge de 4 anévrismes sur 17.

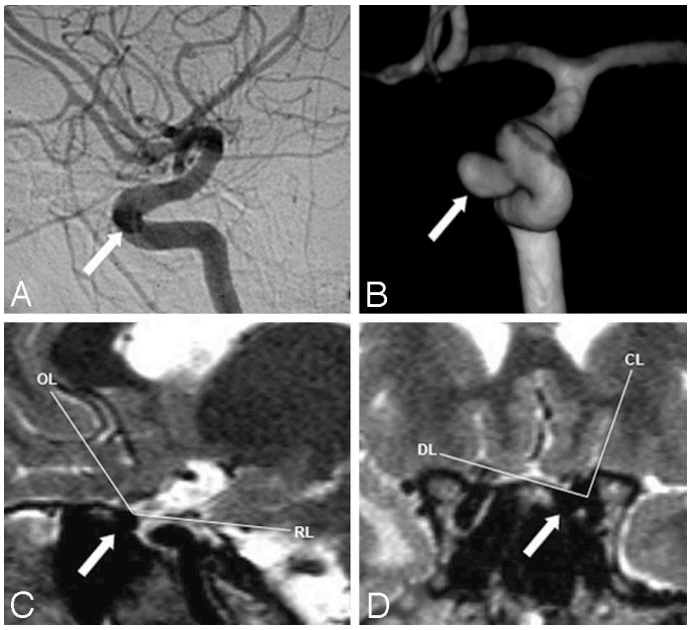

Figure – 4 Comparaison entre angiographie et IRM pour la localisation du cas 2 (flèche). Les deux examens retrouvent un anévrisme intracaverneux (collet et sac intracaverneux).
A, B: artériographie carotidienne gauche vue latérale et antérieure (3D)
C: protocole paraclinoïdien dans le plan carotidien (OL: droite optique; RL: droite du toit).
D: protocole paraclinoïdien dans le plan diaphragmatique (DL: droite diaphragmatique; CL: droite clinoïdienne).

En conclusion, ce protocole d'IRM paraclinoïdien est une technique non invasive et non irradiante complémentaire de l'artériographie pour le bilan et l'orientation de la prise en charge des anévrismes paraclinoïdiens. Ce protocole permet, de façon fiable, de mieux localiser ces anévrismes par rapport au toit du sinus caverneux. Il apporte des informations nouvelles qui permettent d'adapter le traitement au cas particulier de chaque patient et également de mieux les renseigner sur les risques évolutifs réels de

leur anévrisme. Ce protocole est maintenant bien en place au sein de notre équipe neuroradiologique et est utilisé chaque fois qu'un anévrisme de ce type pose des problèmes de localisation. Compte tenu de son excellente précision anatomique, ce protocole pourra aussi être un outil très utile au planning chirurgical des anévrismes de la région en démontrant les rapports du sac anévrismal avec le nerf optique et le chiasma d'un côté et le processus clinoïde antérieur de l'autre.

4. Perfectionnement du protocole paraclinoïdien en IRM 3.0 Tesla

4.1. Résumé

Direct imaging of the distal dural ring and paraclinoid internal carotid artery aneurysm with high resolution T2 turbo-spin echo technique at 3.0 Tesla MRI.
Thines L, Lee SK, Dedhashti A, Agid R, Willinsky RA, Wallace MC, ter Brugge KG. *Accepté dans Neurosurgery (en révision)*

The anatomic landmark separating the intra-dural and extra-dural segment of the internal carotid artery is the Distal Dural Ring (DDR). This study aimed at proving the interest of high resolution T2 turbo spin-echo magnetic resonance imaging (MRI) at 3.0 Tesla for the direct and accurate demonstration of both the DDR and aneurysms around the paraclinoid internal carotid artery. Direct visualization of the DDR and its relationship to paraclinoid internal carotid artery aneurysms with our 3.0 T MRI protocol might help to precisely locate those aneurysms. Improving the anatomical location of paraclinoid aneurysms is essential to give the appropriate information to the patient before obtaining his informed consent to a treatment. With this knowledge, patients who have an extra-dural aneurysm can negate unnecessary interventional or surgical procedures and their related risks. On the other hand, patients who have an intra-dural aneurysm, which is at risk of subarachnoid hemorrhage, can apply for an appropriate and timely management.

4.2. Discussion

Localiser précisément les anévrismes paraclinoïdiens de part et d'autre du toit du sinus caverneux est une question majeure puisque que ceux situés au-dessus de celui-ci, dans les espaces sous-arachnoïdiens, font courir aux patients un risque potentiel d'hémorragie méningée en cas de rupture.

En raison des difficultés à différencier le signal de structures anatomiques voisines et d'un manque de résolution spatiale, l'IRM a longtemps été considérée comme inadaptée à l'étude de la région paraclinoïdienne et des ses anévrismes. Récemment, Tsuboi et col. (89) ont montré l'intérêt de l'ARM 3D en temps de vol avec contraste pour améliorer le contraste entre ACI, anévrisme paraclinoïdien, parois du sinus caverneux et structures extra-vasculaires. Cette technique décrivait bien les rapports de ces anévrismes mais, comme le reconnaissaient les auteurs, manquait de résolution spatiale sur une IRM 1.5 Tesla. Rubinstein et col. (69) ont précédemment décrit l'intérêt de la séquence d'IRM TSE T2 pour la mise en évidence des rapports anatomiques des anévrismes intracrâniens. Ils estimaient qu'elle était très utile grâce à l'acquisition de coupes fines et d'un excellent rapport signal-bruit. Ainsi, des structures adjacentes telles que les vaisseaux, l'anévrisme, le parenchyme cérébral ou la dure-mère étaient parfaitement contrastées par le fort hypersignal du LCS environnant. Dans nos études précédentes, nous avions confirmé l'intérêt de cette séquence dans la localisation du plan de l'ADD et des anévrismes paraclinoïdiens (86;87).

La séquence TSE T2 utilisée dans ce nouveau travail bénéficiait à la fois de l'excellente résolution de contraste apportée dans l'analyse anatomique par l'hypersignal du LCS et d'autre part de l'accroissement important de la résolution spatiale en IRM 3.0 Tesla. Cette augmentation de la résolution globale nous a permis de visualiser, sur des coupes fines et contiguës, directement les faisceaux duraux

composant les parois du sinus caverneux ainsi que l'ADD lui-même. Sur la base de nos études préliminaires, avec la connaissance détaillée de l'anatomie de la région et l'excellente visualisation de l'ADD en IRM 3.0 Tesla, nous pensons que des corrélations chirurgicales n'étaient pas indispensables pour valider la technique. De plus, avec les progrès des techniques de neuroradiologie interventionnelle (ballonnets de protection, stents) de moins en moins d'indication opératoires sont retenues pour le traitement de ces anévrismes (hors mis pour les variétés purement supérieure ou carotido-ophtalmique) : ceux qui sont en situation intradurale ou transitionnelle sont maintenant plutôt traités par les techniques endovasculaires alors que ceux en situation intracaverneuse sont gérer de façon conservatrice.

Tableau 1- Résultats de la localisation avec les 4 modalités d'imagerie et de l'identification des repères anatomiques pour 7 anévrismes paraclinoïdiens

Patient	Age/ sexe	Angio / ARM	angioCT	Taille mm	Mode	MR anatomical analysis							Localisation en IRM	
						TRT	PCA	DS	ACI	AO	NO	ADD	Collet	Sac
1	51/F	Rt AHS	TransD	8.5	HSA	coils	+ +	+	++	++	++	++	IntraD	IntraD
2 a b	48/F	Lt CO Rt CC	IntraD ExtraD	3 2	AS	0	++	0	++	++	++	++	ExtraD ExtraD	ExtraD ExtraD
3	46/M	Rt CO	NA	7	AS	0	++	0	++	++	++	++	IntraD	IntraD
4	48/F	Rt AHS	TransD	5	AS	0	++	+	++	++	++	++	ExtraD	ExtraD
5	46/F	Rt post-ACI	IntraD	2	AS	0	++	+	++	++	++	++	IntraD	IntraD
6	34/F	Rt AHS	IntraD	5	AS	coils	++	+	++	++	++	++	IntraD	IntraD

ARM = angiographie par résonance magnétique angioCT = angioscanner TRT = traitement
HSA = hémorragie sous-arachnoïdienne AS = asymptomatique PCA = processus clinoïde antérieur DS = diaphragma sellae ACI = artère carotide interne A0 = artère ophtalmique NO = nerf optique ADD = anneau dural distal
AHS = anévrisme hypophysaire supérieur CO = anévrisme carotido-ophtalmique CC = anévrisme carotido-caverneux post-ICA = anévrisme face postérieure de carotide
IntraD = anévrisme intradural ExtraD = anévrisme extradural TransD = anévrisme transdural

Grâce à la résolution obtenue en IRM 3.0 Tesla, nous pouvons présenter dans cette étude un protocole simplifié, facilement reproductible et dont la méthode d'analyse repose uniquement sur la visualisation directe des structure anatomiques dans le plan de coupe diaphragmatique (Fig.1). En utilisant ce protocole, nous avons été capable de

localiser précisément tous les anévrismes de la série et adapter la prise en charge en fonction de ses résultats (Tableau 1). Ces données suggèrent que la précision anatomique de cette séquence TSE T2 à 3.0 Tesla pour l'imagerie de la région paraclinoïdienne est utile au clinicien afin de guider la prise en charge thérapeutique de ces anévrismes. Ce protocole offre une meilleure compréhension des rapports anatomiques de l'anévrisme et de sa localisation avant de considérer un traitement invasif qu'il soit endovasculaire ou même chirurgical.

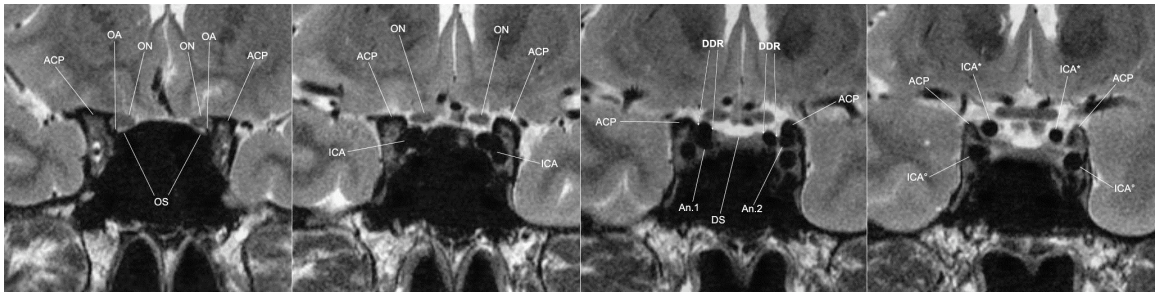

Figure 1 - (Patient 2). Quatre coupes consécutives en IRM TSE T2 à 3.0 Tesla dans le plan diaphragmatique montrant les repères radio-anatomiques de la région paraclinoïdienne.
ACP: processus clinoïde antérieur, ON: nerf optique, OA: artère ophtalmique, DS: diaphragma sellae, ICA: genou antérieur de l'artère carotide interne, ICA*: artère carotide interne supracaverneuse, ICA°: artère carotide interne intracaverneuse, DDR: anneau dural distal (noter que le pilier optique [OS] est aussi identifié e IRM), et deux anévrismes paraclinoïdiens: anévrisme 1 (An.1) est extradural (sous l'ADD) et anévrisme 2 est extradural (sous l'ADD et le processus clinoïde antérieur: anévrisme sub-clinoidien).

La limite de la technique reste paradoxalement dans sa résolution spatiale et de contraste. Quand un anévrisme vient au contact ou soulève le toit du sinus caverneux il peut ne pas être toujours facile de déterminer si le sac anévrismal est intradural ou toujours recouvert de dure-mère. Avec notre technique (18~20 cm x 18~20 cm FOV, 2 mm slice thickness, 0 space/gap, 448 x 448 Matrix) en IRM 3.0 Tesla, il n'était pas toujours simple de séparer anatomiquement l'ADD du sac quand les deux structures se rencontraient puisque toutes deux apparaissaient en hyposignal. L'utilisation d'une IRM avec contraste ou d'une ARM pourrait à ce titre améliorer la discrimination entre paroi anévrismale et paroi du toit du sinus caverneux. Une autre difficulté potentielle réside dans la localisation des petits anévrismes du cavum carotidien. Le cavum carotidien est

anatomiquement un espace virtuel sous arachnoïdien constitué, à la face médiale du siphon carotidien, par une déhiscence de la partie médiale de l'ADD. Il est situé topographiquement sous le plan de ce dernier. Dans ces cas particuliers, il est probable que, même en augmentant considérablement la puissance du champ magnétique, la résolution spatiale de l'IRM puisse ne pas être suffisante pour distinguer la solution de continuité entre ADD déhiscent et paroi supérieure du sac anévrismal.

En conclusion, cette étude finale montre l'utilité en pratique clinique d'un protocole simplifié (un seul plan de coupe, visualisation directe de l'anneau dural) en IRM 3.0 Tesla pour la prise en charge thérapeutique des anévrismes paraclinoïdiens. Cette technique apporte des informations complémentaires à l'artériographie cérébrale et à l'angioscanner.

5. Application clinique pour un cas d'anévrisme rompu dans la selle turcique

5.1. Résumé

Intrasellar rupture of a paraclinoid aneurysm with subarachnoid hemorrhage: usefulness of MR imaging in diagnosis.

Ribeiro M, Howard P, Willinsky R, ter Brugge KG, Agid R, Thines L, da Costa L. *AJNR Am J Neuroradiol*. 2008 May;29(5):980-2.

Characterization of paraclinoidal aneurysms may be difficult due to the complexity of anatomical structures involved. Differentiation between intra and extra-dural lesions is essential for management. We report a case of a unique presentation of a paraclinoid aneurysm with intrasellar hemorrhage where the presence of intrasellar blood and the relationship of the paraclinoid aneurysm neck and sack to the dural rings were elegantly demonstrated on MRI and critical in choosing the target lesion for treatment.

5.2. Discussion

La précision du protocole d'IRM paraclinoïdien à 3.0 Tesla a permis de visualiser l'ADD et de montrer que l'anévrisme était transitionnel avec un collet intradural et un sac extradural. Il révéla également la présence d'une grande quantité de sang dans la selle turcique confirmant que la rupture anévrismale s'était produite à ce niveau puis que la diffusion du sang vers les espaces sous-arachnoïdiens avait été facilitée par l'absence de septum osseux à la face médiale du cavum carotidien et un phénomène de selle vide.

C. *Vue chirurgicale à partir de l'angiographie tridimensionnelle pour le planning de la chirurgie anévrismale.*

1. Résumé

Surgical views from three-dimensional digital subtraction angiography for the planning of aneurysm surgery.

Thines L, Taschner C, Lejeune JP, Le Thuc V, Pruvo JP, Bourgeois P, Leclerc X. J Neuroradiol. 2007 Jul;34(3):205-11.

Aim. To develop a semi-automatic protocol helping to present directly and quickly three-dimensional digital subtraction angiography (3D-DSA) data in an orientation that reproduces exactly the neurosurgeon's intra-operative view.

Method. Post-processing of 3D-DSA data (volume-rendering) was performed on an Integris workstation (Philips, Best) and surgical views were obtained by reproducing the visualization of the patient's head through a fronto-pterional approach. Therefore the 3D volume was turned 135° in the sagittal plane (around X axis) and rotated by 45° and 60° in the coronal plane (around Y axis). The protocol was evaluated on a consecutive

series of nine patients harbouring ruptured or asymptomatic anterior circulation aneurysms requiring a surgical treatment. Fronto-pterional views of angiographic 3D data were compared to intra-operative views.

Results. The proposed semi-automatic algorithm is simple, fast and reproducible, and it displays directly the 3D data in an identical orientation as the intra-operative views. The surgical anatomy of the anterior communicating artery was best reproduced with a coronal rotation of 60° and with a coronal rotation of 45° for the other aneurysmal locations. In each case, the surgical reconstructions allowed a more accurate analysis of the vascular anatomy around the aneurysm and facilitate the pre- and per-operative planning.

Conclusion. The present protocol displays angiographic 3D data in a projection that reproduces precisely the vascular anatomy through a fronto-pterional approach. It may help neurosurgeons to better mentally anticipate potential difficulties in access and clip-positioning related to the specific vascular anatomy of each patient.

2. Discussion

L'angiographie soustraite digitalisée est l'examen de référence pour mettre en évidence les anévrismes intracrâniens. L'adjonction de reconstructions tridimensionnelles grâce à des techniques d'acquisition rotationnelle a considérablement amélioré l'analyse de l'architecture anévrismale, en particulier dans ses rapports avec les branches artérielles de voisinage (7;76;91). L'angiographie 3D est devenu l'outil idéal pour la planification du traitement endovasculaire (localisation, road-mapping, placement des coils) (2;7;54) ou pour son contrôle post-thérapeutique immédiat. Cette

technique est maintenant également largement utilisée pour le planning de la chirurgie anévrismale (81) et le suivi post-opératoire (42).

Dans cette étude, nous avons cherché à la rendre plus adaptée au planning du traitement chirurgical des anévrismes intracrâniens. Récemment, Siablis et col. ont publié un protocole en angioscanner permettant de reproduire la vue chirurgicale pour les anévrismes de la circulation antérieure (73). A la même période et de façon indépendante, nous étions aussi dans notre institution en phase d'évaluation d'un protocole permettant d'obtenir directement, à partir des reconstructions 3D de l'angiographie, l'orientation selon la vue opératoire.

Ce protocole fournit simplement, de façon semi-automatique et directe les planches d'angiographie 3D des anévrismes de la circulation antérieure réorientées selon l'aspect anatomique observé par une voie d'abord fronto-ptérionale. Les angles de rotations ont été approximés à partir de la position de la tête du patient ainsi que de celle de l'axe du microscope pendant la chirurgie. L'angle X correspond à la position du microscope en arrière et au-dessus de la tête du patient. L'angle Y correspond à l'inclinaison latérale du microscope nécessaire à la dissection chirurgicale et tient également compte de la rotation initiale de la tête dans la têtière de Mayfield (environ de 30°). Puis, nous avons tenté de déterminer quels angles étaient mieux adaptés à chaque localisation anévrismale (Fig.1).

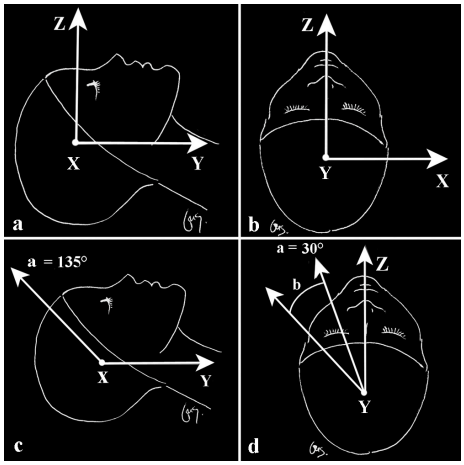

Figure 1-

(a, b): référentiel tridimensionnel inclus dans le logiciel de reconstruction

(c, d) : la rotation de l'axe Y autour de l'axe X était de 135°, positive pour un abord gauche et négative pour un abord droit. La rotation de l'axe Z autour de l'axe Y était de 45°, 60° ou 90°, positive pour un abord gauche et négative pour un abord droit. Angle a = rotation controlatérale initiale de la tête dans la têtière de Mayfield (30°), Angle b = angle de rotation additionnel de l'axe du microscope (15°, 30°, 60°).

Un angle tangentiel (60°) était requis pour représenter les conditions anatomiques de l'exploration des anévrismes de l'artère communicante antérieure (Fig.2) et dans toutes les autres localisations un angle de 45° reproduisait le plus fidèlement l'aspect opératoire (Fig.3).

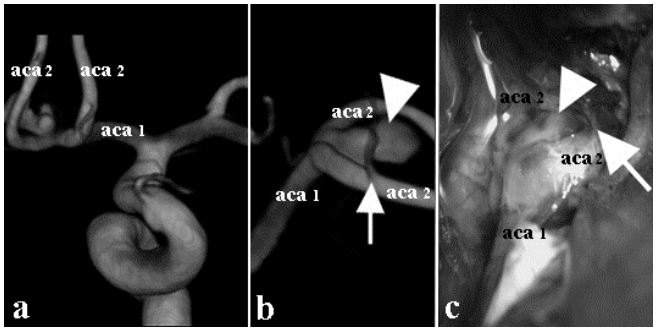

Figure 2- Anévrisme de l'artère communicante antérieure.

a : vue antérieure en angiographie tridimensionnelle ; b : vue chirurgicale en angiographie tridimensionnelle; c : vue opératoire. Tête de flèche blanche : anévrisme de l'artère communicante antérieure. Flèche blanche : artère de Heubner. aca 1 : segment A1 de l'artère cérébrale antérieure ; aca 2 : segment A2 de l'artère cérébrale antérieure

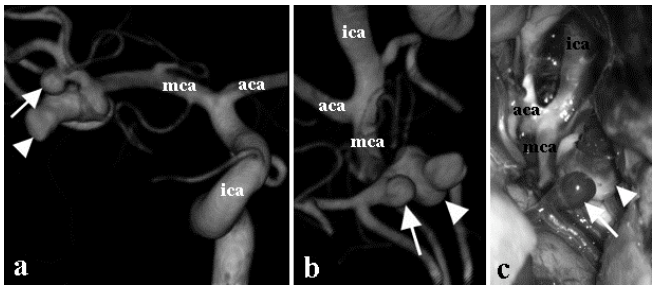

Figure 3- Anévrismes de l'artère cérébrale moyenne.

a : vue antérieure en angiographie tridimensionnelle ; b : vue chirurgicale en angiographie tridimensionnelle; c : vue opératoire. Tête de flèche blanche : large anévrisme de l'artère cérébrale moyenne. Flèche blanche : petit anévrisme de l'artère cérébrale moyenne. ica : artère carotide interne ; aca : artère cérébrale antérieure ; mca : artère cérébrale movenne

En raison des bonnes corrélations obtenues entre ces vues réorientées et les vues observées lors de la chirurgie, nous pensons que ce protocole permet de représenter de façon fiable les anévrismes de la circulation antérieure tels qu'ils seront visualisés pendant l'abord microchirurgical. Bien entendu, les vues proposées dans cette étude ne résument pas les multiples positions du microscope utilisées par le neurochirurgien pendant la procédure afin d'exposer au mieux l'anatomie vasculaire intracrânienne. Elles ne remplacent pas non plus la visualisation directe personnelle de l'anévrisme sur la station de travail et sous tous ses angles lors du planning préopératoire. Néanmoins, elles offrent une vision globale et directe de la conformation vasculaire particulière du

patient au travers d'une projection chirurgicale fronto-ptérionale. Ce protocole facilitera, en particulier pour les jeunes neurochirurgiens, la représentation mentale exacte des rapports 3D de l'anévrisme et aidera à anticiper les difficultés du clippage. Pendant l'intervention, il évitera au chirurgien de commencer sa dissection au site de rupture anévrismale, localisé sur la vue réorientée, il lui permettra de deviner la position exacte des branches collatérales à proximité de l'anévrisme, en particulier celles masquées à la face postérieure du sac anévrismal et de positionner son clip de façon sûre.

En conclusion le caractère rapide, simple et reproductible de ce protocole semi-automatique explique qu'il a été inclus facilement dans le protocole global de restitution des planches d'angiographie 3D de notre service de neuroradiologie et que ces « vues chirurgicales » sont maintenant fournies systématiquement par nos manipulateurs. Elles permettent d'améliorer à la fois le planning préopératoire mais aussi la décision chirurgicale peropératoire.

D. *Angiographie rotationnelle biplan peropératoire en chirurgie cérébrovasculaire*

1. Résumé

Intraoperative biplanar rotational angiography during neurovascular surgery: Technical Note.

Dehdashti AR, Thines L, da Costa L, Willinsky RA, ter Brugge KG, Wallace MC, Tymianski M. *Accepté dans Journal of neurosurgery (en révision)*

Object. The purpose of this study is to evaluate initial experience with integration of high-resolution rotational and biplanar angiography during neurovascular operative procedures.

Methods. Eight patients with intracerebral AVMs (6) and aneurysms (2) underwent surgical treatment of their lesions in a combined endovascular surgical suite. After initial head positioning, a preoperative biplane and rotational angiogram was performed. Surgery was then carried out for resection of the AVM or clipping of the aneurysm. A further biplane and rotational 3D angiogram were performed intraoperatively to confirm the satisfactoriness of treatment.

Results. One small AVM residual identified intra-operatively necessitated further resection. One aneurysm was clipped during endovascular inflation of an intracarotid balloon for temporary proximal control. The completeness of treatment was confirmed using intraoperative 3D rotational angiography for all cases without procedure related complications.

Conclusion. Intraoperative rotational angiography carried out in an integrated biplane angio/surgery suite is a safe and useful adjunct to surgery, and may enable combining endovascular and surgical procedures for the treatment of complex vascular lesions.

2. Discussion

Certaines équipes ont déjà réalisé lors de procédures de chirurgie vasculaire anévrismale des examens angiographiques en salle opératoire en utilisant un appareil de radiologie portable. Certaines unités neurochirurgicales utilisent de façon courante cette technique pour la chirurgie vasculaire intracrânienne. Bien que les résultats obtenus soient acceptables, la qualité des images est insuffisante pour coupler le geste à une procédure endovasculaire sophistiquée. D'un autre côté, les interventions combinées endovasculaire et chirurgicale suscitent un intérêt croissant. Il semble même que cette évolution puisse être l'avenir de la spécialité, en tout cas pour certaines lésions complexes pour lesquelles les traitements mono-modalité s'avèrent souvent inefficaces.

Lawton et col. ont rapporté leur expérience sur une série de 77 patients qui ont bénéficié d'un traitement multimodal et ont conclu que cette stratégie pourrait être incluse dans la prise en charge des cas les plus difficiles (51). Ricci et col. ont également publié leur série portant sur des anévrismes paraclinoïdiens géants ou vertébro-basilaires traités de façon combinée (66). Ils conclurent que la procédure endovasculaire avait permis l'obtention fiable d'un contrôle proximal favorisant le traitement chirurgical. Une technique combinée de réduction du flux a été décrite par Hoh et col. pour la prise en charge des anévrismes intraitables par voie chirurgicale standard ou par voie endovasculaire (37). Bien que ces travaux n'aient pas été directement réalisés dans une salle combinée angio/chirurgie, ils soulignent l'importance d'une étroite collaboration dans la prise en charge de ces lésions exceptionnelles.

Nous rapportons ici l'expérience préliminaire d'une salle vasculaire combinée (Fig.1) angiographie-chirurgie sur une série de 2 anévrismes (Tableau-1) et 6 malformations artério-veineuses cérébrales. L'angiographie peropératoire peut être appliquée à la vérification immédiate du geste afin de confirmer l'occlusion complète de l'anévrisme et la préservation de la perméabilité des branches collatérales. La réalisation de la chirurgie neurovasculaire dans une salle combinée offre d'autres avantages. Premièrement, embolisation et clippage peuvent être réalisés lors de la même anesthésie. Si la tentative de neuroradiologie interventionnelle est infructueuse, le traitement chirurgical peut immédiatement faire suite à la procédure. Deuxièmement, elle peut fournir un supplément endovasculaire

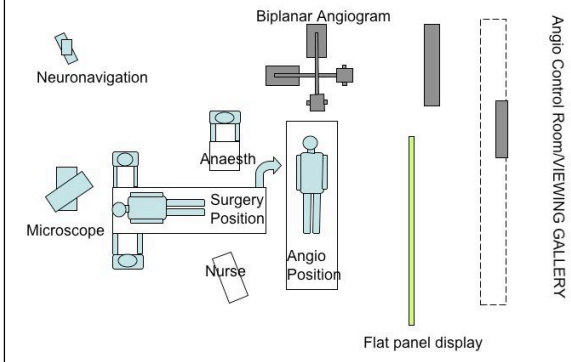

Figure 1: The illustration shows the general concept of our endovascular surgical suite

permettant d'obtenir le contrôle proximal du flux artériel au lieu de chercher à exposer proximalement les vaisseaux au niveau du cou ou à la base du crâne (ex-anévrisme paraclinoïdien). Murayama et col. ont décrit leur expérience initiale de ce type de salle combinée (56). Cependant, ils n'ont pas rapporté l'intérêt de l'utilisation d'une angiographie rotationnelle 3D peropératoire, qui offre en plus les mêmes avantages que ceux obtenus avec cette technique lors du bilan diagnostic à savoir une résolution spatiale et une précision inégalée.

Patient	Age	Sexe	Site	Taille (mm)	Abord	Commentaire	Résultats
1	60	F	Ophtalmique	22	Ptérional et clinoidectomie antérieure	Occlusion par balonner peropératoire	complet
2	57	F	Paraclinoidien	19	Ptérional et clinoidectomie antérieure	Trapping de l'ACI	complet

Tableau 1- Caractéristiques des anévrismes opérés

La limitation principale de cette salle combinée est que les mouvements de la table commune angio-chirurgie sont restreints à des mouvements orthogonaux et ne permettent pas la rotation du patient. Cela a pour conséquence de sélectionner pour ce type de procédure les patients pour lesquels des ajustements répétés de la position de la tête ne sont pas essentiels à la réalisation du geste.

En conclusion, notre expérience de l'angiographie rotationnelle 3D suggère qu'il s'agit d'une technique sûre, efficace et pratique dont les adaptations futures apporteront une sécurité accrue et une qualité de traitement supérieure en particulier pour les anévrismes complexes.

E. *Suivi postopératoires des anévrismes intracrâniens en angioscanner*

1. Résumé

Postoperative Assessment of Clipped Aneurysms with 64-Detectors Computerized Tomography Angiography.

L Thines, A Dedashti, Peter Howard, MC Wallace, M Tymianski, R.A Willinsky, KG Terbrugge, J-P Lejeune, R Agid. *Soumis à Neurosurgery*

Object: Multi-detector computerized tomography angiography (MDCTA) is now a widely accepted technique for the diagnosis and the treatment decision making of intracranial aneurysms. The goal of this study was to evaluate the accuracy of 64-MDCTA for the postoperative assessment of clipped intracranial aneurysms in place of conventional digitalized subtraction angiography (DSA).

Methods: We analysed a consecutive series of 31 patients that underwent direct clipping procedures for 38 aneurysms between November 2005 and February 2008. MDCTA used a 64-slices MDCT scanner (Aquilion 64, Toshiba). Conventional DSAs were available for comparison in all cases. Two independent neuroradiologists analysed the following data: exam quality, artifacts, aneurysm remnant and patency of collateral branches. Interobserver agreement, sensitivity, specificity with 64-MDCTA were calculated.

Results: Aneurysms locations were: anterior circulation 79% and posterior circulation 21%. Phynox (cobalt-alloy) and Titanium (titanium-alloy) Yasargil clips were used respectively in 20 and 18 cases. Important artifacts were found in both techniques with multiple clips and cobalt-alloy clips. Remnants > 2 mm were found in 21% of the cases and two patients had one collateral branch occluded. Sensitivity and specificity of 64-MDCTA for the detection of a significant remnant (> 2mm) were respectively 67% (95% CI = 0.31-0.91) and 100% (95% CI = 0.85-1). Sensitivity and

specificity of 64-MDCTA for the detection of the occlusion of a collateral branch were respectively 50% (95% CI = 0.03-0.97) and 100% (95% CI = 0.88-1). No relationship was found with the location, the type, shape, size and number of clips but missed remnants tended to be larger with cobalt-alloy clips.

Conclusions: 64-MDCTA is a non-invasive valuable exam to assess the postoperative result of clipped intracranial aneurysms and might be useful for the long term follow-up. It can't replace conventional DSA in particular conditions like cobalt-alloy or multiple clips, complex aneurysms and doubt on a collateral branch patency.

2. Discussion

L'angiographie est toujours le gold standard pour le diagnostic des anévrismes intracrâniens (7;36;54;76;91) et reste toujours l'examen de première intention pour les patients bénéficiant du bilan de lésions complexes. En raison de la résolution offerte par l'angiographie classique ou 3D, elle reste également la technique traditionnelle de contrôle du succès de l'occlusion chirurgicale des anévrismes intracrâniens (42;47;74). Les reconstructions 3D à partir de l'angiographie rotationnelle permettent de visualiser clairement à la fois le collet initial au niveau duquel se trouve(nt) le(s) clip(s) mais aussi le vaisseau porteur et ses branches collatérales. Les désavantages de l'angiographie sont les suivants : examen invasif et irradiant avec injection d'un produit de contraste iodée (risque d'allergie, d'insuffisance rénale). Ses risques sont principalement : hématome au point de ponction (4%), déficit neurologique transitoire (1%) et déficit neurologique définitif (0,1%) (35;44). L'angiographie peut aussi être de réalisation très délicate chez les sujets âgés chez qui les risques de complications thrombo-emboliques sont importants. C'est pour toutes ces raisons que nous évaluons dans cette étude les

possibilités de réaliser ce bilan post-opératoire avec l'aide d'une technique non-invasive: l'angioscanner.

La limitation principale de cette technique dans cette indication sont les artéfacts liés au(x) clip(s). Depuis le développement des clips en titane, Vieco et col. (1996) puis van Loon et col. (1997) ont pressenti que l'angioscanner pouvait être un outil utile au contrôle des anévrisme clippés (93;95). Depuis seulement 5 études ont porté sur ce sujet et évalué les possibilités de l'angioscanner multi-détecteurs dans cette indication avec des résultats parfois contradictoires et une sensibilité pour la détection des reliquats variant de 61-66% (60;70) à 100% (17;21).

L'angioscanner multi-détecteurs permet d'obtenir des images en coupe fine et se chevauchant en un temps d'acquisition très court augmentant ainsi la résolution spatiale des images natives et des reconstructions 3D. L'angioscanner multi-détecteurs est maintenant utilisé largement pour le diagnostic et la planification du traitement des anévrismes rompus (3;22;38;61;83;96). L'angioscanner 64-détecteurs a été validé par les équipes cardiovasculaires pour le contrôle post-thérapeutique des stents ou pontage coronariens avec une excellente sensibilité et spécificité (67;68). L'étude présentée ici est la première à évaluer l'application de l'angioscanner 64-détecteurs pour le contrôle des anévrismes clippés. La taille des voxels sources obtenus avec notre appareil était de 0.30 mm^3 (0.781mm×0.781mm×0.5 mm) ce qui est plus petit que ceux obtenus en IRM ou en angioscanner 16-détecteurs. Il a été prouvé que les artéfacts liés au clip sont beaucoup moins importants sur l'angioscanner 64-détecteurs en particulier avec la génération des clips titane (94). Contrairement aux études précédentes qui se sont focalisées soient sur les anévrismes de la circulation antérieure (21) soit sur les clips titane (17;21;60;70), l'intérêt de notre étude était d'inclure toutes les variétés de clip et de localisation anévrismale. La qualité technique de l'angioscanner 64-détecteurs (92%)

était comparable à celle de l'angiographie (97%) et supérieure à celle des angioscanner 16-détecteurs (8%). Comme cela avait déjà été rapporté (99), les artéfacts étaient de façon significative plus importants avec les clips cobalt en revanche aucune corrélation n'était retrouvée avec le nombre de clips. Le taux de reliquat cliniquement significatifs (>2mm) était de 21% (Fig1). Dans ce sous-groupe, la sensibilité et la spécificité de l'angioscanner 64-détecteurs étaient respectivement 67% (95% CI = 0.31-0.91) et 100% (95% CI = 0.85-1 et la corrélation inter-technique était bonne (κ = 0.75, agreement = 0.92, 95% CI = 0.49-1). Ces résultats sont compatibles avec ceux de deux séries récentes de la littérature (60;70) qui soulignaient aussi les difficultés à visualiser les reliquats de moins de 2 mm. Les caractéristiques de ces reliquats non vus (Fig.2) sont résumées dans le Tableau – 1.

Reliquats non diagnostiqués							
	Taille	**Site**	**Type clip**	**Nb clip**	**Forme de Clip**	**Taille clip (mm)**	**Artéfacts**
1	1.5 mm	AcoA	C	3	Droit	5.0, 7.0, 9.0	++
2	3 mm	AcoA	C	1	Fen. right angle	5.0 / 4.9	+
3	1 mm	D, ACS	T	1	Droit	7.0	-
4	3 mm	AcoA	C	1	Droit	5.0	+
5	1.5 mm	D, ACI term	T	1	Droit	5.0	-
6	2.5 mm	G, PICA	T	1	Droit	7.0	-

Tableau 1 – Caractéristiques des reliquats non diagnostiqués
D: doit, G: gauche, AcoA: artère communicante antérieure, ACS: artère cérébelleuse supérieure, ACI term: terminaison carotide interne, PICA: artère cérébelleuse postérieure et inférieure, C: clip cobalt, T: clip titane, ++ : important, +: présent, -: absent

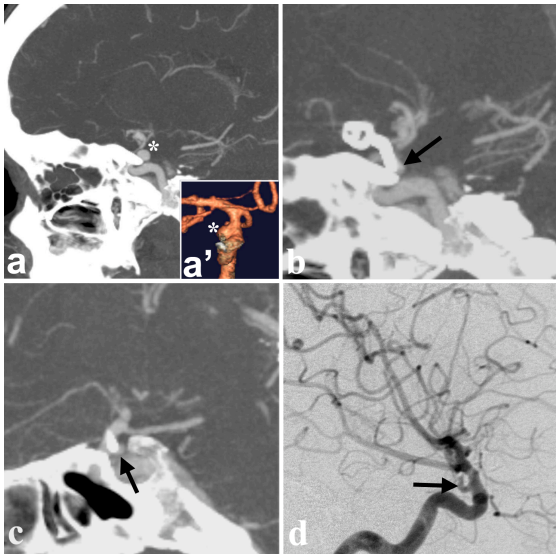

Figure 1- a, a': vue MIP sagittale à partir de l'angioscanner 64-détecteurs et reconstruction 3D à partir de l'angiographie de face montrant un anévrisme carotido-ophtalmique à projection latérale (*).

b,c: vues MIP sagittale postopératoire montrant un petit résidu anévrismal au sommet du clip (flèche)

d: angiographie rotationnelle postopératoire montrant le même résidu anévrismal (flèche).

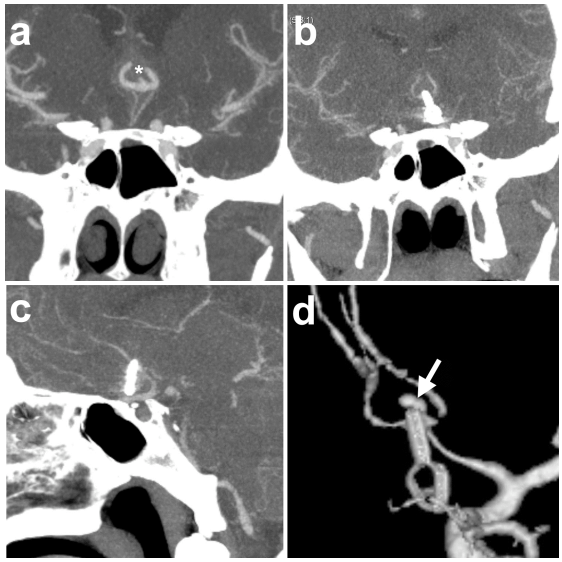

Figure 2- a: vue MIP coronale à partir de l'angioscanner 64-détecteurs montrant un anévrisme de l'artère communicante antérieure (*).

b, c: vues MIP coronale et sagittale postopératoire ne retrouvant aucun résidu

d: reconstruction 3D de l'angiographie de face mettant en évidence un reliquat (flèche) au sommet du clip.

La moitié des cas étaient liés aux artéfacts dus au(x) clip(s) et l'autre moitié à un phénomène de magnification de la taille du clip. En revanche, on ne retrouvait pas de lien avec la localisation de l'anévrisme ou son type (alliage, nombre, taille, forme). La précision de l'angioscanner 64-détecteurs pour la détection de l'occlusion d'une branche collatérale était basse mais seulement deux patients ont présentés cette complication dans la série. Au total, nous pensons que cette étude a permis de comparer l'angioscanner 64-détecteurs à l'artériographie en situation clinique réelle.

Le but de cette étude était de valider l'angioscanner 64-détecteurs pour le contrôle post-opératoire des anévrismes clippés afin de remplacer l'angiographie et ses

inconvénients. Nous avons pu à l'issue de ce travail déterminer qu'elles étaient les conditions favorables ou non à la réalisation en première intention d'un angioscanner post-opératoire (Tableau-2). De plus, nous pensons qu'une artériographie complémentaire doit être réalisée chaque fois que l'angioscanner est de mauvaise qualité : acquisition au temps veineux, artéfacts importants liés au(x) clip(s).

Conditions	64-MDCTA	DSA
Circulation antérieure	+	-
Circulation postérieure	+	-
Clips cobalt	-	+
Clips titane	+	-
Simple ou double clip(s)	+	-
Clips multiples > 2	-	+
Vasospasme	-	+
Anévrisme complexe	-	+
Occlusion d'une collatérale	-	+

Tableau 2 – Algorithme décisionnel pour le choix de l'examen de contrôle postopératoire à réaliser en première intention

Exclure par cet examen les reliquats de moins de 2mm peut être sujet à polémique car ces reliquats non diagnostiqués sont potentiellement à risque de croissance ou de rupture tardive (24;52). D'un autre côté, ces résidus ne sont habituellement pas accessibles à un traitement complémentaire et même les patients exempts de reliquats sont eux aussi à risque de présenter une nouvelle HAS différée soit par anévrisme de novo soit par récurrence anévrismale sous le clip (101-103). C'est pourquoi il est probablement plus bénéfique d'effectuer un suivi radiologique prolongé afin de dépister les lésions évolutives dont feront partie les reliquats initialement non diagnostiqués et présentant une augmentation de taille.

La première limite de ce travail est la taille de notre population. Cependant celle-ci est similaire à celle de trois des études déjà publiées. D'autre part, l'absence de réalisation prospective de cette étude peut nous avoir conduit à réduire la précision de l'angioscanner 64-détecteurs en interprétant des examens réalisés dans des conditions

potentiellement sub-optimales (thrombose temporaire du sac, mauvais remplissage vasculaire au cours d'une phase de vasospasme).

En conclusion, le contrôle de la qualité de l'occlusion anévrismale après clippage est maintenant devenue une nécessité,et cela d'autant plus que l'on souhaite comparer les résultats de la chirurgie avec le traitement endovasculaire qui possède son examen dédié, l'ARM. Cette étude a montré les capacités et les limites de l'angioscanner 64-détecteurs pour le contrôle post-opératoire des anévrismes clippés. Cette technique sera probablement plus bénéfique pour la population des anévrismes asymptomatiques à qui l'on souhaite éviter l'inconfort et les complications de l'angiographie conventionnelle. Cette dernière garde en revanche toute sa place dans les cas difficiles : clips cobalt ou multiples, anévrismes complexes, doute sur la perméabilité d'une branche collatérale.

F. *Contrôle en angioscanner de la perméabilité des pontages extra-intracrâniens associés au traitement d'un anévrisme intracrânien*

1. Résumé

Assessment of extracranial-intracranial bypass patency with 64-slice multi-detector computerized tomography angiography.

Thines L, Agid R, Dehdashti AR, da Costa L, Wallace MC, ter Brugge KG, Tymianski M. *Soumis à Journal of neurosurgery*

Object: Extracranial-intracranial (EC/IC) bypass is a useful procedure for the treatment of cerebral vascular insufficiency or complex aneurysms. We explored the role of multi-detector computed tomography angiography (MDCTA), instead of digital subtraction angiography (DSA), for the postoperative assessment of EC/IC bypass patency.

Methods: We retrospectively analysed a consecutive series of 21 MDCTAs from 17 patients that underwent 25 direct or indirect EC/IC bypass procedures between April

2003 and November 2007. Conventional DSA were available for comparison in 13 cases. MDCTA used a 64-slice MDCT scanner (Aquilion 64, Toshiba). The proximal and distal patencies were analyzed independently on MDCTA and DSA by a neuroradiologist and a neurosurgeon. The bypass was considered patent when the entire donor vessel was opacified without discontinuity from proximal to distal ends and was visibly in contact with the recipient vessel.

Results: MDCTA depicted the patency status in every patient. Bypasses were patent in 22 cases, stenosed in one and occluded in two. DSA always confirmed the results of the MDCTA (sensitivity = 100%, 95% CI = 0.655-1.0; specificity 100%, 95% CI = 0.05-1.0).

Conclusions: MDCTA is a non-invasive and accurate exam to assess the postoperative EC/IC bypass patency and could replace conventional DSA in routine follow-up.

2. Discussion

Suivi des pontages extra-intracrâniens

L'angiographie est l'examen de référence pour le diagnostic de pathologies ischémiques cérébrales telles que le Moya-moya (78). En raison de sa bonne résolution, cette technique est le moyen habituel pour le contrôle postopératoire de la réussite des pontages extra-intracrâniens (EC/IC) (71;100). Elle assure la bonne visualisation des segments extra- et intracrâniens et le cathétérisme sélectif du pontage donne une image du lit vasculaire suppléé par celui-ci. De plus, le suivi tardif en angiographie, en particulier dans le Moya-moya, permet de quantifier l'importance de la revascularisation corticale (53;79). Enfin elle permet de contrôler directement en peropératoire le résultat du pontage (10). Malgré ces avantages, l'angiographie possède les inconvénients suivants : examen invasif et irradiant avec injection d'un produit de

contraste iodée (risque d'allergie, d'insuffisance rénale). Ses risques sont principalement : hématome au point de ponction (4%), déficit neurologique transitoire (1%) et déficit neurologique définitif (0,1%) (35;44). L'angiographie peut aussi être de réalisation très délicate chez les sujets âgés chez qui les risques de complications thrombo-emboliques sont importants. C'est pour toute ces raisons que nous évaluons dans cette étude les possibilités de réaliser ce bilan post-opératoire avec l'aide d'une technique non invasive: l'angioscanner.

Certains auteurs ont déjà opté pour des techniques non invasives pour la prise en charge pré et post-opératoire des patients bénéficiant d'un pontage EC/IC. L'ARM peut dans certains cas remplacer l'angiographie en particulier chez l'enfant dans la maladie de Moya-moya (26). Pour le suivi post-opératoire, certains auteurs ont recommandé l'utilisation de l'examen clinique (palpation directe) et du doppler pour s'assurer de la perméabilité de la greffe (77). Le désavantage majeur de ce protocole est l'incertitude concernant la nature du vaisseau testé. Les progrès récents du doppler permettent maintenant la visualisation et la confirmation du bon fonctionnement du pontage mais aussi du développement de la néovascularisation après pontage direct ou indirect (62). De façon similaire, les avancées en IRM offrent la possibilité non seulement de montrer la perméabilité du pontage mais aussi d'en mesurer le flux (48;49;106)

Angioscanner 64-détecteurs

L'angioscanner multi-détecteurs permet d'obtenir des images en coupe fine et se chevauchant en un temps d'acquisition très court augmentant ainsi la résolution spatiale des images natives et des reconstructions 3D. L'angioscanner multi-détecteurs est maintenant utilisé largement pour le diagnostic et la planification du traitement des

anévrismes rompus (3;22;38;61;83;96). L'angioscanner 64-détecteurs a été valider par les équipes cardiovasculaires pour le contrôle post-thérapeutique des stents ou pontage coronariens avec une excellente sensibilité et spécificité (67;68). L'étude présentée ici est la première à évaluer l'application de l'angioscanner 64-détecteurs pour le contrôle de la perméabilité des pontages EC/IC. Quelques études ont jusqu'à présent porté sur l'apport de l'angioscanner 4-détecteurs dans cette indication (45;85;90). Le développement des scanners multi-détecteurs a augmenté de façon considérable la résolution spatiale et permis de visualiser des structures de plus en plus fines. La taille des voxels sources obtenus avec notre appareil était de 0.30 mm^3 (0.781mm×0.781mm×0.5 mm) ce qui est plus petit que ceux obtenus en IRM ou en angioscanner 4-détecteurs (0.5mm^3). En résultat, nous avons pu pour chaque cas obtenir une visualisation claire et précise des vaisseaux donneurs et receveurs ainsi que de l'ensemble du trajet du pontage. Dans tous les cas où une vérification angiographique ou chirurgicale était possible, le résultat de l'angioscanner était confirmé, donnant ainsi à la technique une spécificité et une sensibilité de 100%. Certains auteurs ont même montré que l'angioscanner pouvait aider à quantifier le degré de néovascularisation à distance du traitement (45). Le large champ de vue offert par l'angioscanner permet dans le cas des pontages haut débit (Fig.1) la démonstration simultanée de l'anastomose proximale au niveau du cou ainsi que celle en aval au niveau cortical. De plus l'angioscanner permet de visualiser les rapports du pontage avec le volet, ce qui est particulièrement utile en cas de reprise chirurgicale. La visualisation du pontage n'était par ailleurs pas altérée par la disposition de mini-clips vasculaires le long de la greffe.

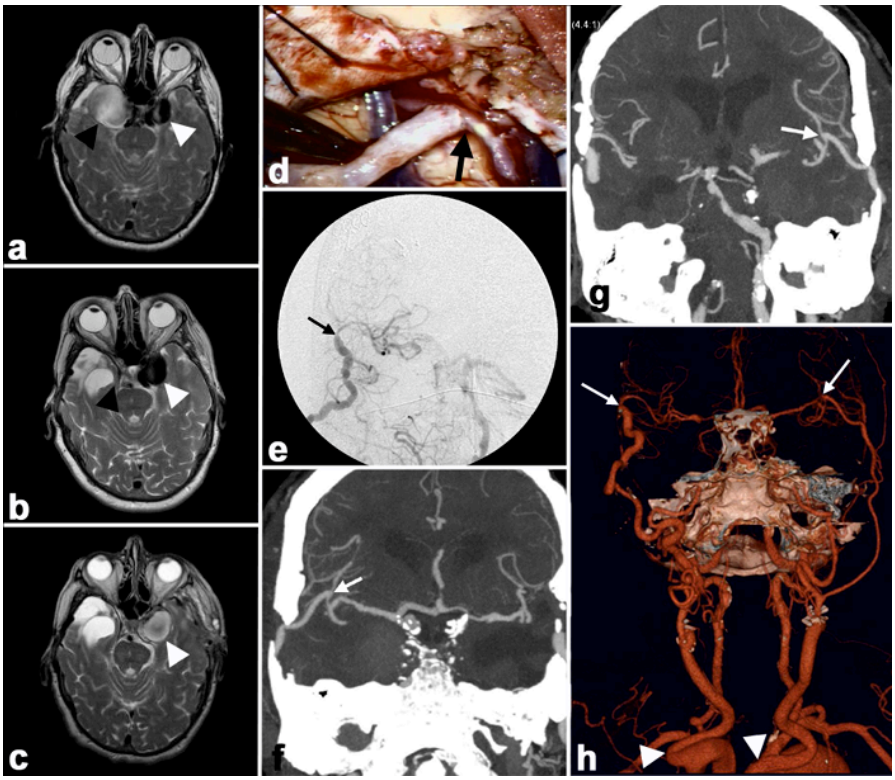

Figure -1 Cas clinique 1 –
a : IRM T2 axiale initiale montrant des anévrismes intracaverneux bilatéraux dont celui du côté droit était symptomatique par paralysie oculomotrice (tête de flèche noire). L'anévrisme du côté gauche était asymptomatique (tête de flèche blanche) ;
b : IRM T2 axiale 3 ans après un pontage EC/IC haut débit du côté droit et occlusion carotidienne montrant un anévrisme affaissé du côté droit (tête de flèche noire) et du côté gauche un anévrisme élargi et maintenant symptomatique (tête de flèche blanche) ;
c : IRM T2 axiale finale après un pontage EC/IC avec artère radiale interposée du côté gauche et occlusion carotidienne montrant l'involution de l'anévrisme de ce côté (tête de flèche blanche) ;
d : photo opératoire du pontage haut débit veineux ;
e : angiographie postopératoire sélective du pontage du côté droit (vue antérieure) montrant la perméabilité de celui-ci (flèche noire) ;
f,g : angioscanner 64-détecteurs postopératoire, vues MIP coronales montrant la perméabilité des deux pontages EC/IC (flèches blanches) ;
h : vue antérieure d'une reconstruction 3D à partir de l'angioscanner 64-détecteurs postopératoire montrant la perméabilité des deux pontages (flèches blanches). Notez la tortuosité des origines des deux artères carotides communes (têtes de flèche blanches).

Limites de l'angioscanner 64-détecteurs

L'angioscanner 64-détecteurs a plusieurs limites comparées à l'ARM par exemple. Comme l'angiographie, il expose le patient à l'injection de produit de contraste iodé et à une irradiation. L'augmentation de la résolution spatiale en angioscanner 64-détecteurs s'accompagne en parallèle d'un accroissement de la dose reçu par le patient (18;34). Cet effet peut être atténué en utilisant des logiciels ou des algorithmes « épargneurs » de dose (9;20;98;105). L'autre limite importante de l'angioscanner 64-détecteurs est qu'il ne fournit aucune information dynamique sur le sens et l'intensité du flux. Afin de palier à ce défaut, cette technique pourrait être couplée à l'ARM ou à l'écho-doppler.

Implications cliniques

Grâce aux bons résultats obtenus avec l'angioscanner 64-détecteurs, le protocole de contrôle post-opératoire peut-être modifié de la façon suivante : si le pontage est clairement visualisé sur l'ensemble de son trajet en angioscanner aucun autre examen n'est réalisé et le pontage est considéré perméable. Dans le cas contraire, une angiographie de contrôle est sollicitée pour confirmer le résultat. La facilité de réalisation et l'accessibilité de cet examen sont des qualités particulièrement utiles en cas de déficit neurologique postopératoire : en effet il permettra de faire la part entre complication intracrânienne extra ou intracérébrale et une occlusion précoce du pontage ou du vaisseau receveur.

Limitation de l'étude

La principale limitation de cette étude est la taille de la population étudiée. Elle est expliquée d'une part par le fait que ce type de procédure est rare et que d'autre part cette technique en angioscanner 64-détecteurs n'a été disponible que très récemment. Des études prospectives sur une cohorte plus large seront nécessaires avant que celle-ci ne remplace l'angiographie conventionnelle dans cette indication.

En conclusion, l'angioscanner 64-détecteurs est une technique très prometteuse pour l'évaluation postopératoire des patients bénéficiant d'un pontage EC/IC. Elle permet de s'assurer rapidement de la perméabilité du pontage et d'autre part d'effectuer le suivi à long terme.

VI. PERSPECTIVES

Au cours de ce travail de thèse nous avons eu l'occasion de montrer l'intérêt de ces nouvelles techniques d'imagerie pour l'amélioration de la prise en charge des anévrismes intracrâniens. Les résultats de nos travaux auront eu un impact réel et direct à toutes les étapes du processus de traitement et nous avons pu grâce eux et à la collaboration étroite avec les services de neuroradiologie faire changer et progresser nos habitudes professionnelles dans le souci constant de mieux soigner nos patients.

Nous avons pu mener à bien depuis plusieurs années le perfectionnement d'une séquence d'IRM entièrement dédiée à la localisation des anévrismes paraclinoïdiens. Ce protocole fait maintenant partie de notre arsenal diagnostique de base pour les anévrismes de cette région. Nous avons vu que, malgré le saut technologique permis par le passage à une IRM plus puissante (3.0 Tesla), certains anévrismes posent encore des problèmes topographiques (anévrismes du cavum). Avec l'acquisition prochaine d'une IRM 3.0 Tesla sur Lille, nous prévoyons de tester de nouvelles séquences afin d'affiner encore la description des rapports de ces anévrismes avec la paroi du toit du sinus caverneux. Nous prévoyons de coupler notre protocole paraclinoïdien à une IRM avec contraste ou une ARM haute résolution afin de mieux discriminer la paroi anévrismale elle-même de la dure-mère du toit du sinus caverneux.

Si l'artériographie conventionnelle est progressivement remplacée aux phases de diagnostic et de contrôle thérapeutique, elle garde toute sa place lors du planning du traitement. Nous avons pu mettre en place un protocole simple permettant aux manipulateurs de neuroradiologie de nous fournir directement les vues réorientées selon la vue chirurgicale. Ces planches réorientées sont particulièrement didactiques et utiles pour les neurochirurgiens en formation qui ont moins l'expérience de l'anatomie

vasculaire chirurgicale qui peut d'ailleurs être très modifiée dans certains cas après rupture anévrismale. Elles seront pour lui l'équivalent des incidences de travail si chères aux neuroradiologues et lui permettront d'anticiper les difficultés de la voie d'abord et du clippage chirurgical. Comme cela est déjà le cas sur Toronto, la modification de nos blocs opératoire, nous offrira bientôt (2012) la possibilité de traiter de façon combinée certains des anévrismes les plus complexes dans des conditions de sécurité inégalées pour les patients. Un travail d'optimisation et d'évaluation des procédures thérapeutiques sera alors à mettre en place en collaboration étroite avec nos confrères neuroradiologues.

L'angioscanner multi-détecteurs, avec ces nouvelles capacités de résolution spatiale, aura été la technique phare de cette thèse. A la phase diagnostique des anévrismes rompus, il a maintenant dans notre centre presque supplanté l'artériographie conventionnelle qui n'est plus réservée qu'aux cas les plus complexes. Cela a grandement simplifié pour les malades les modalités de cette étape de la prise en charge en supprimant surtout sa pénibilité et, d'autre part, cela aura permis de soulager nos équipes de neuroradiologie interventionnelle qui peuvent consacrer plus de temps à la mise en place de procédures de traitement de plus en plus sophistiquées. A la phase post-opératoire, l'angioscanner apporte un bénéfice certain par rapport à l'artériographie conventionnelle mais moins constant. Il convient dans cette indication de bien respecter les limites connues de la technique car elle reste encore très dépendante des artéfacts liés aux clips chirurgicaux. Probablement supplantera-t-elle définitivement l'artériographie quand seront commercialisés des clips non métalliques sur lesquels travaillent actuellement quelques laboratoires (clips en céramique).

Au cours de cette thèse, nous n'avons pas pu exploiter les capacités de l'angioscanner comme aide directe au traitement chirurgical et il a pourtant dans ce

domaine un potentiel considérable. Il sera ainsi intéressant d'évaluer ses possibilités en terme de simulation du clippage chirurgical. Deux applications pratiques découleront de ce travail. Tout d'abord tenter de simuler le clip optimal en tenant compte de l'orientation de l'anévrisme, des ses rapports vasculaires immédiats et aussi de l'orientation prévisible de la pince à clip compte tenu du côté de la voie d'abord et des interférences avec le parenchyme ou la boîte crânienne. La deuxième application visera les neurochirurgiens en formation et consistera à simuler le déroulement de l'intervention sur une console de travail, en commençant par l'orientation de la tête du patient selon la position chirurgicale, puis en réalisant le volet crânien et en terminant par la mise en place du clip. Nous avons déjà débuté en compagnie de l'ingénieur du service de neuroradiologie (V Le Thuc) les étapes préliminaires de ce travail visant à évaluer la faisabilité du projet : acquisition des données à partir de l'angioscanner préopératoire, reconstructions 3D sur le logiciel Amira®, numérisation des clips et manipulation des clips dans l'espace 3D crânien, simulation de la craniotomie. Les étapes suivantes nécessiteront de numériser la pince à clip, d'effectuer les corrélations chirurgicales entre la simulation préopératoire, le déroulement réel de l'intervention et les caractéristiques finales du clip (taille, forme, position). Cette étude aura pour but d'offrir un outil permettant d'aider les jeunes neurochirurgiens à acquérir les bases de la chirurgie cérébrovasculaire à une époque où, grâce aux progrès du traitement endovasculaire, la diminution du nombre de patients opérés rend la formation dans ce domaine de plus en plus difficile.

VII. RÉFÉRENCES

1. Unruptured intracranial aneurysms--risk of rupture and risks of surgical intervention. International Study of Unruptured Intracranial Aneurysms Investigators. **N Engl J Med** 339:1725-1733, 1998.

2. Abe T, Hirohata M, Tanaka N, Uchiyama Y, Kojima K, Fujimoto K, Norbash AM, Hayabuchi N: Clinical benefits of rotational 3D angiography in endovascular treatment of ruptured cerebral aneurysm. **AJNR Am J Neuroradiol** 23:686-688, 2002.

3. Agid R, Lee SK, Willinsky RA, Farb RI, terBrugge KG: Acute subarachnoid hemorrhage: using 64-slice multidetector CT angiography to "triage" patients' treatment. **Neuroradiology** 48:787-794, 2006.

4. Agid R, Willinsky RA, Lee SK, Terbrugge KG, Farb RI: Characterization of aneurysm remnants after endovascular treatment: contrast-enhanced MR angiography versus catheter digital subtraction angiography. **AJNR Am J Neuroradiol** 29:1570-1574, 2008.

5. Anderson GB, Findlay JM, Steinke DE, Ashforth R: Experience with computed tomographic angiography for the detection of intracranial aneurysms in the setting of acute subarachnoid hemorrhage. **Neurosurgery** 41:522-527, 1997.

6. Anderson GB, Steinke DE, Petruk KC, Ashforth R, Findlay JM: Computed tomographic angiography versus digital subtraction angiography for the diagnosis and early treatment of ruptured intracranial aneurysms. **Neurosurgery** 45:1315-1320, 1999.

7. Anxionnat R, Bracard S, Ducrocq X, Trousset Y, Launay L, Kerrien E, Braun M, Vaillant R, Scomazzoni F, Lebedinsky A, Picard L: Intracranial aneurysms: clinical value of 3D digital subtraction angiography in the therapeutic decision and endovascular treatment. **Radiology** 218:799-808, 2001.

8. Audibert G, Pottie JC, Hummer M, Torrens J: [Anesthesia and intensive care of subarachnoid hemorrhage. A survey on practice in 32 centres]. **Ann Fr Anesth Reanim** 15:338-341, 1996.

9. Bahner ML, Bengel A, Brix G, Zuna I, Kauczor HU, Delorme S: Improved vascular opacification in cerebral computed tomography angiography with 80 kVp. **Invest Radiol** 40:229-234, 2005.

10. Barrow DL, Boyer KL, Joseph GJ: Intraoperative angiography in the management of neurovascular disorders. **Neurosurgery** 30:153-159, 1992.

11. Beck J, Rohde S, Berkefeld J, Seifert V, Raabe A: Size and location of ruptured and unruptured intracranial aneurysms measured by 3-dimensional rotational angiography. **Surg Neurol** 65:18-25, 2006.

12. Beck J, Rohde S, el BM, Zimmermann M, Berkefeld J, Seifert V, Raabe A: Difference in configuration of ruptured and unruptured intracranial aneurysms determined by biplanar digital subtraction angiography. **Acta Neurochir (Wien)** 145:861-865, 2003.

13. Beretta F: The paraclinoid aneurysms and the distal dural ring: a new classification. **J Neurosurg Sci** 48:161-175, 2004.

14. Castel JP, Frerebeau P, Lagarrigue J, Moreau JJ: **[Neurosurgical treatment of intracranial aneurysms]**. **Neurochirurgie 40**:31-66, 1994 (abstr).

15. Chappell ET, Moure FC, Good MC: Comparison of computed tomographic angiography with digital subtraction angiography in the diagnosis of cerebral aneurysms: a meta-analysis. **Neurosurgery** 52:624-631, 2003.

16. Chawla S: Advances in multidetector computed tomography: applications in neuroradiology. **J Comput Assist Tomogr** 28 Suppl 1:S12-S16, 2004.

17. Chen W, Yang Y, Qiu J, Peng Y, Xing W: Sixteen-row multislice computerized tomography angiography in the postoperative evaluation of patients with intracranial aneurysms. **Br J Neurosurg** 22:63-70, 2008.

18. Coles DR, Smail MA, Negus IS, Wilde P, Oberhoff M, Karsch KR, Baumbach A: Comparison of radiation doses from multislice computed tomography coronary angiography and conventional diagnostic angiography. **J Am Coll Cardiol** 47:1840-1845, 2006.

19. Dammert S, Krings T, Moller-Hartmann W, Ueffing E, Hans FJ, Willmes K, Mull M, Thron A: Detection of intracranial aneurysms with multislice CT: comparison with conventional angiography. **Neuroradiology** 46:427-434, 2004.

20. Deetjen A, Mollmann S, Conradi G, Rolf A, Schmermund A, Hamm CW, Dill T: Use of automatic exposure control in multislice computed tomography of the coronaries: comparison of 16-slice and 64-slice scanner data with conventional coronary angiography. **Heart** 93:1040-1043, 2007.

21. Dehdashti AR, Binaghi S, Uske A, Regli L: Comparison of multislice computerized tomography angiography and digital subtraction angiography in the postoperative evaluation of patients with clipped aneurysms. **J Neurosurg** 104:395-403, 2006.

22. Dehdashti AR, Rufenacht DA, Delavelle J, Reverdin A, de TN: Therapeutic decision and management of aneurysmal subarachnoid haemorrhage based on computed tomographic angiography. **Br J Neurosurg** 17:46-53, 2003.

23. Ferre JC, Carsin-Nicol B, Morandi X, Carsin M, de Kersaint-Gilly A, Gauvrit JY, Desal HA: Time-of-flight MR angiography at 3T versus digital subtraction angiography in the imaging follow-up of 51 intracranial aneurysms treated with coils. **Eur J Radiol** 2008.

24. Feuerberg I, Lindquist C, Lindqvist M, Steiner L: Natural history of postoperative aneurysm rests. **J Neurosurg** 66:30-34, 1987.

25. Forbes G, Fox AJ, Huston J, III, Wiebers DO, Torner J: Interobserver variability in angiographic measurement and morphologic characterization of intracranial aneurysms: a report from the International Study of Unruptured Intracranial Aneurysms. **AJNR Am J Neuroradiol** 17:1407-1415, 1996.

26. Fukui M: Guidelines for the diagnosis and treatment of spontaneous occlusion of the circle of Willis ('moyamoya' disease). Research Committee on Spontaneous Occlusion of the Circle of Willis (Moyamoya Disease) of the Ministry of Health and Welfare, Japan. **Clin Neurol Neurosurg** 99 Suppl 2:S238-S240, 1997.

27. Gauvrit JY, Leclerc X, Caron S, Taschner CA, Lejeune JP, Pruvo JP: Intracranial aneurysms treated with Guglielmi detachable coils: imaging follow-up with contrast-enhanced MR angiography. **Stroke** 37:1033-1037, 2006.

28. Germanson TP, Lanzino G, Kongable GL, Torner JC, Kassell NF: Risk classification after aneurysmal subarachnoid hemorrhage. **Surg Neurol** 49:155-163, 1998.

29. Gonzalez LF, Walker MT, Zabramski JM, Partovi S, Wallace RC, Spetzler RF: Distinction between paraclinoid and cavernous sinus aneurysms with computed tomographic angiography. **Neurosurgery** 52:1131-1137, 2003.

30. Gouliamos A, Gotsis E, Vlahos L, Samara C, Kapsalaki E, Rologis D, Kapsalakis Z, Papavasiliou C: Magnetic resonance angiography compared to intra-arterial digital subtraction angiography in patients with subarachnoid haemorrhage. **Neuroradiology** 35:46-49, 1992.

31. Guglielmi G, Vinuela F, Duckwiler G, Dion J, Lylyk P, Berenstein A, Strother C, Graves V, Halbach V, Nichols D, .: Endovascular treatment of posterior circulation aneurysms by electrothrombosis using electrically detachable coils. **J Neurosurg** 77:515-524, 1992.

32. Hamada J, Morioka M, Miura M, Fujioka S, Marubayashi T, Ushio Y: Management outcome for ruptured anterior circulation aneurysms with a Hunt and Hess clinical grade of III in patients in the 9th decade of life. **Surg Neurol** 56:294-300, 2001.

33. Harrison MJ, Johnson BA, Gardner GM, Welling BG: Preliminary results on the management of unruptured intracranial aneurysms with magnetic resonance angiography and computed tomographic angiography. **Neurosurgery** 40:947-955, 1997.

34. Hausleiter J, Meyer T, Hadamitzky M, Huber E, Zankl M, Martinoff S, Kastrati A, Schomig A: Radiation dose estimates from cardiac multislice computed tomography in daily practice: impact of different scanning protocols on effective dose estimates. **Circulation** 113:1305-1310, 2006.

35. Heiserman JE, Dean BL, Hodak JA, Flom RA, Bird CR, Drayer BP, Fram EK: Neurologic complications of cerebral angiography. **AJNR Am J Neuroradiol** 15:1401-1407, 1994.

36. Hochmuth A, Spetzger U, Schumacher M: Comparison of three-dimensional rotational angiography with digital subtraction angiography in the assessment of ruptured cerebral aneurysms. **AJNR Am J Neuroradiol** 23:1199-1205, 2002.

37. Hoh BL, Putman CM, Budzik RF, Carter BS, Ogilvy CS. Combined surgical and endovascular techniques of flow alteration to treat fusiform and complex wide-necked intracranial aneurysms that are unsuitable for clipping or coil embolization. **J Neurosurg** 95, 24-35. 2008.

38. Hoh BL, Cheung AC, Rabinov JD, Pryor JC, Carter BS, Ogilvy CS: Results of a prospective protocol of computed tomographic angiography in place of catheter angiography as the only diagnostic and pretreatment planning study for cerebral aneurysms by a combined neurovascular team. **Neurosurgery** 54:1329-1340, 2004.

39. Hutchinson PJ, Power DM, Tripathi P, Kirkpatrick PJ: Outcome from poor grade aneurysmal subarachnoid haemorrhage--which poor grade subarachnoid haemorrhage patients benefit from aneurysm clipping? **Br J Neurosurg** 14:105-109, 2000.

40. Ito K, Hongo K, Kakizawa Y, Kobayashi S: Three-dimensional contrast medium-enhanced computed tomographic cisternography for preoperative evaluation of surgical anatomy of intradural paraclinoid aneurysms of the internal carotid artery: technical note. **Neurosurgery** 51:1089-1092, 2002.

41. Jayaraman MV, Mayo-Smith WW: Multi-detector CT angiography of the intra-cranial circulation: normal anatomy and pathology with angiographic correlation. **Clin Radiol** 59:690-698, 2004.

42. Kang HS, Han MH, Kwon BJ, Jung SI, Oh CW, Han DH, Chang KH: Postoperative 3D angiography in intracranial aneurysms. **AJNR Am J Neuroradiol** 25:1463-1469, 2004.

43. Kassell NF, Torner JC, Haley EC, Jr., Jane JA, Adams HP, Kongable GL: The International Cooperative Study on the Timing of Aneurysm Surgery. Part 1: Overall management results. **J Neurosurg** 73:18-36, 1990.

44. Kaufmann TJ, Huston J, III, Mandrekar JN, Schleck CD, Thielen KR, Kallmes DF: Complications of diagnostic cerebral angiography: evaluation of 19,826 consecutive patients. **Radiology** 243:812-819, 2007.

45. Kikuchi M, Asato M, Sugahara S, Nakajima K, Sato M, Nagao K, Kumagai N, Muraosa Y, Ito K, Hoshino H: Evaluation of surgically formed collateral circulation in moyamoya disease with 3D-CT angiography: comparison with MR angiography and X-ray angiography. **Neuropediatrics** 27:45-49, 1996.

46. Kim JM, Romano A, Sanan A, van Loveren HR, Keller JT: Microsurgical anatomic features and nomenclature of the paraclinoid region. **Neurosurgery** 46:670-680, 2000.

47. Kivisaari RP, Porras M, Ohman J, Siironen J, Ishii K, Hernesniemi J: Routine cerebral angiography after surgery for saccular aneurysms: is it worth it? **Neurosurgery** 55:1015-1024, 2004.

48. Kodama T, Ueda T, Suzuki Y, Yano T, Watanabe K: MRA in the evaluation of EC-IC bypass patency. **J Comput Assist Tomogr** 17:922-926, 1993.

49. Kodoma T, Suzuki Y, Yano T, Watanabe K, Ueda T, Asada K: Phase-contrast MRA in the evaluation of EC-IC bypass patency. **Clin Radiol** 50:459-465, 1995.

50. Kyoshima K, Oikawa S, Kobayashi S: Interdural origin of the ophthalmic artery at the dural ring of the internal carotid artery. Report of two cases. **J Neurosurg** 92:488-489, 2000.

51. Lawton MT, Quinones-Hinojosa A, Sanai N, Malek JY, Dowd CF. Combined microsurgical and endovascular management of complex intracranial aneurysms. **Neurosurgery** 52, 263-274. 2003.

52. Lin T, Fox AJ, Drake CG: Regrowth of aneurysm sacs from residual neck following aneurysm clipping. **J Neurosurg** 70:556-560, 1989.

53. Matsushima T, Inoue T, Suzuki SO, Fujii K, Fukui M, Hasuo K: Surgical treatment of moyamoya disease in pediatric patients--comparison between the results of indirect and direct revascularization procedures. **Neurosurgery** 31:401-405, 1992.

54. Missler U, Hundt C, Wiesmann M, Mayer T, Bruckmann H: Three-dimensional reconstructed rotational digital subtraction angiography in planning treatment of intracranial aneurysms. **Eur Radiol** 10:564-568, 2000.

55. Molyneux A, Kerr R, Stratton I, Sandercock P, Clarke M, Shrimpton J, Holman R: International Subarachnoid Aneurysm Trial (ISAT) of neurosurgical clipping versus endovascular coiling in 2143 patients with ruptured intracranial aneurysms: a randomised trial. **Lancet** 360:1267-1274, 2002.

56. Murayama Y, Saguchi T, Ishibashi T, Ebara M, Takao H, Irie K, Ikeuchi S, Onoue H, Ogawa T, Abe T. Endovascular operating suite: future directions for treating neurovascular disease. **J Neurosurg** . 104, 925-930. 2006. Ref Type: Generic

57. Murayama Y, Sakurama K, Satoh K, Nagahiro S: Identification of the carotid artery dural ring by using three-dimensional computerized tomography angiography. Technical note. **J Neurosurg** 95:533-536, 2001.

58. Murphy KJ, Houdart E, Szopinski KT, Levrier O, Guimaraens L, Kuhne D, Solymosi L, Bartholdy NJ, Rufenacht DA: Mechanical detachable platinum coil: report of the European phase II clinical trial in 60 patients. **Radiology** 219:541-544, 2001.

59. Oikawa S, Kyoshima K, Kobayashi S: Surgical anatomy of the juxta-dural ring area. **J Neurosurg** 89:250-254, 1998.

60. Pechlivanis I, Koenen D, Engelhardt M, Scholz M, Koenig M, Heuser L, Harders A, Schmieder K: Computed tomographic angiography in the evaluation of clip placement for intracranial aneurysm. **Acta Neurochir (Wien)** 2008.

61. Pechlivanis I, Schmieder K, Scholz M, Konig M, Heuser L, Harders A: 3-Dimensional computed tomographic angiography for use of surgery planning in patients with intracranial aneurysms. **Acta Neurochir (Wien)** 147:1045-1053, 2005.

62. Perren F, Horn P, Vajkoczy P, Schmiedek P, Meairs S: Power Doppler imaging in detection of surgically induced indirect neoangiogenesis in adult moyamoya disease. **J Neurosurg** 103:869-872, 2005.

63. Punt J: Some observations on aneurysms of the proximal internal carotid artery. **J Neurosurg** 51:151-154, 1979.

64. Raabe A, Beck J, Rohde S, Berkefeld J, Seifert V: Three-dimensional rotational angiography guidance for aneurysm surgery. **J Neurosurg** 105:406-411, 2006.

65. Renn WH, Rhoton AL, Jr.: Microsurgical anatomy of the sellar region. **J Neurosurg** 43:288-298, 1975.

66. Ricci G, Ricci A, Gallucci M, Zotta D, Scogna A, Costagliola C, Galzio RJ. Combined endovascular and microsurgical approach in the treatment of giant paraclinoid and vertebrobasilar aneurysms. J Neurosurg Sci 49, 6-1. 2008. Ref Type: Generic

67. Rixe J, Achenbach S, Ropers D, Baum U, Kuettner A, Ropers U, Bautz W, Daniel WG, Anders K: Assessment of coronary artery stent restenosis by 64-slice multi-detector computed tomography. **Eur Heart J** 27:2567-2572, 2006.

68. Ropers D, Pohle FK, Kuettner A, Pflederer T, Anders K, Daniel WG, Bautz W, Baum U, Achenbach S: Diagnostic accuracy of noninvasive coronary angiography in patients after bypass surgery using 64-slice spiral computed tomography with 330-ms gantry rotation. **Circulation** 114:2334-2341, 2006.

69. Rubinstein D, Sandberg EJ, Breeze RE, Sheppard SK, Perkins TG, Cajade-Law AG, Simon JH: T2-weighted three-dimensional turbo spin-echo MR of intracranial aneurysms. **AJNR Am J Neuroradiol** 18:1939-1943, 1997.

70. Sakuma I, Tomura N, Kinouchi H, Takahashi S, Otani T, Watarai J, Mizoi K: Postoperative three-dimensional CT angiography after cerebral aneurysm clipping with titanium clips: detection with single detector CT. Comparison with intra-arterial digital subtraction angiography. **Clin Radiol** 61:505-512, 2006.

71. Schmiedek P, Piepgras A, Leinsinger G, Kirsch CM, Einhupl K: Improvement of cerebrovascular reserve capacity by EC-IC arterial bypass surgery in patients with ICA occlusion and hemodynamic cerebral ischemia. **J Neurosurg** 81:236-244, 1994.

72. Schmieder K, Falk A, Hardenack M, Heuser L, Harders A: Clinical utility of magnetic resonance angiography in the evaluation of aneurysms from a neurosurgical point of view. **Zentralbl Neurochir** 60:61-67, 1999.

73. Siablis D, Kagadis GC, Karamessini MT, Konstantinou D, Karnabatidis D, Petsas T, Nikiforidis GC: Intracranial aneurysms: reproduction of the surgical view using 3D-CT angiography. **Eur J Radiol** 55:92-95, 2005.

74. Sindou M, Acevedo JC, Turjman F: Aneurysmal remnants after microsurgical clipping: classification and results from a prospective angiographic study (in a consecutive series of 305 operated intracranial aneurysms). **Acta Neurochir (Wien)** 140:1153-1159, 1998.

75. Sprengers ME, van Rooij WJ, Sluzewski M, Rinkel GJ, Velthuis BK, de Kort GA, Majoie CB: MR Angiography Follow-Up 5 Years after Coiling: Frequency of New Aneurysms and Enlargement of Untreated Aneurysms. **AJNR Am J Neuroradiol** 2008.

76. Sugahara T, Korogi Y, Nakashima K, Hamatake S, Honda S, Takahashi M: Comparison of 2D and 3D digital subtraction angiography in evaluation of intracranial aneurysms. **AJNR Am J Neuroradiol** 23:1545-1552, 2002.

77. Sundt TM, Jr., Whisnant JP, Fode NC, Piepgras DG, Houser OW: Results, complications, and follow-up of 415 bypass operations for occlusive disease of the carotid system. **Mayo Clin Proc** 60:230-240, 1985.

78. Suzuki J, Takaku A: Cerebrovascular "moyamoya" disease. Disease showing abnormal net-like vessels in base of brain. **Arch Neurol** 20:288-299, 1969.

79. Suzuki Y, Negoro M, Shibuya M, Yoshida J, Negoro T, Watanabe K: Surgical treatment for pediatric moyamoya disease: use of the superficial temporal artery for both areas supplied by the anterior and middle cerebral arteries. **Neurosurgery** 40:324-329, 1997.

80. Tampieri D, Leblanc R, Oleszek J, Pokrupa R, Melancon D: Three-dimensional computed tomographic angiography of cerebral aneurysms. **Neurosurgery** 36:749-754, 1995.

81. Tanoue S, Kiyosue H, Kenai H, Nakamura T, Yamashita M, Mori H: Three-dimensional reconstructed images after rotational angiography in the evaluation of intracranial aneurysms: surgical correlation. **Neurosurgery** 47:866-871, 2000.

82. Taptas JN: Intradural and extradural ICA. **J Neurosurg** 51:877-878, 1979.

83. Taschner CA, Thines L, Lernout M, Lejeune JP, Leclerc X: Treatment decision in ruptured intracranial aneurysms: comparison between multi-detector row CT angiography and digital subtraction angiography. **J Neuroradiol** 34:243-249, 2007.

84. Teksam M, McKinney A, Casey S, Asis M, Kieffer S, Truwit CL: Multi-section CT angiography for detection of cerebral aneurysms. **AJNR Am J Neuroradiol** 25:1485-1492, 2004.

85. Teksam M, McKinney A, Truwit CL: Multi-slice CT angiography in evaluation of extracranial-intracranial bypass. **Eur J Radiol** 52:217-220, 2004.

86. Thines L, Delmaire C, Le GD, Pruvo JP, Lejeune JP, Lehmann P, Francke JP: MRI location of the distal dural ring plane: anatomoradiological study and application to paraclinoid carotid artery aneurysms. **Eur Radiol** 16:479-488, 2006.

87. Thines L, Gauvrit JY, Leclerc X, Le GD, Delmaire C, Pruvo JP, Lejeune JP: Usefulness of MR Imaging for the Assessment of Nonophthalmic Paraclinoid Aneurysms. **AJNR Am J Neuroradiol** 29:125-129, 2008.

88. Tipper G, King-Im JM, Price SJ, Trivedi RA, Cross JJ, Higgins NJ, Farmer R, Wat J, Kirollos R, Kirkpatrick PJ, Antoun NM, Gillard JH: Detection and evaluation of intracranial aneurysms with 16-row multislice CT angiography. **Clin Radiol** 60:565-572, 2005.

89. Tsuboi T, Tokunaga K, Shingo T, Itoh T, Mandai S, Kinugasa K, Date I: Differentiation between intradural and extradural locations of juxta-dural ring aneurysms by using contrast-enhanced 3-dimensional time-of-flight magnetic resonance angiography. **Surg Neurol** 67:381-387, 2007.

90. Tsuchiya K, Aoki C, Katase S, Hachiya J, Shiokawa Y: Visualization of extracranial-intracranial bypass using multidetector-row helical computed tomography angiography. **J Comput Assist Tomogr** 27:231-234, 2003.

91. Tu RK, Cohen WA, Maravilla KR, Bush WH, Patel NH, Eskridge J, Winn HR: Digital subtraction rotational angiography for aneurysms of the intracranial anterior circulation: injection method and optimization. **AJNR Am J Neuroradiol** 17:1127-1136, 1996.

92. van Gijn J, Rinkel GJ: Subarachnoid haemorrhage: diagnosis, causes and management. **Brain** 124:249-278, 2001.

93. van Loon JJ, Yousry TA, Fink U, Seelos KC, Reulen HJ, Steiger HJ: Postoperative spiral computed tomography and magnetic resonance angiography after aneurysm clipping with titanium clips. **Neurosurgery** 41:851-856, 1997.

94. van dS, I, van LM, Vlassenbroek A, Velthuis B: Minimizing clip artifacts in multi CT angiography of clipped patients. **AJNR Am J Neuroradiol** 27:60-66, 2006.

95. Vieco PT, Morin EE, III, Gross CE: CT angiography in the examination of patients with aneurysm clips. **AJNR Am J Neuroradiol** 17:455-457, 1996.

96. Villablanca JP, Hooshi P, Martin N, Jahan R, Duckwiler G, Lim S, Frazee J, Gobin YP, Sayre J, Bentson J, Vinuela F: Three-dimensional helical computerized tomography angiography in the diagnosis, characterization, and

management of middle cerebral artery aneurysms: comparison with conventional angiography and intraoperative findings. **J Neurosurg** 97:1322-1332, 2002.

97. Vinuela F, Duckwiler G, Mawad M: Guglielmi detachable coil embolization of acute intracranial aneurysm: perioperative anatomical and clinical outcome in 403 patients. **J Neurosurg** 86:475-482, 1997.

98. Waaijer A, Prokop M, Velthuis BK, Bakker CJ, de Kort GA, van Leeuwen MS: Circle of Willis at CT angiography: dose reduction and image quality--reducing tube voltage and increasing tube current settings. **Radiology** 242:832-839, 2007.

99. Watanabe Y, Kashiwagi N, Yamada N, Higashi M, Fukuda T, Morikawa S, Onishi Y, Iihara K, Miyamoto S, Naito H: Subtraction 3D CT angiography with the orbital synchronized helical scan technique for the evaluation of postoperative cerebral aneurysms treated with cobalt-alloy clips. **AJNR Am J Neuroradiol** 29:1071-1075, 2008.

100. Weinstein PR, Baena R, Chater NL: Results of extracranial-intracranial arterial bypass for intracranial internal carotid artery stenosis: review of 105 cases. **Neurosurgery** 15:787-794, 1984.

101. Wermer MJ, Greebe P, Algra A, Rinkel GJ: Incidence of recurrent subarachnoid hemorrhage after clipping for ruptured intracranial aneurysms. **Stroke** 36:2394-2399, 2005.

102. Wermer MJ, Rinkel GJ, Greebe P, Albrecht KW, Dirven CM, Tulleken CA: Late recurrence of subarachnoid hemorrhage after treatment for ruptured aneurysms: patient characteristics and outcomes. **Neurosurgery** 56:197-204, 2005.

103. Wermer MJ, van dS, I, Velthuis BK, Algra A, Buskens E, Rinkel GJ: Follow-up screening after subarachnoid haemorrhage: frequency and determinants of new aneurysms and enlargement of existing aneurysms. **Brain** 128:2421-2429, 2005.

104. Wintermark M, Ko NU, Smith WS, Liu S, Higashida RT, Dillon WP: Vasospasm after subarachnoid hemorrhage: utility of perfusion CT and CT angiography on diagnosis and management. **AJNR Am J Neuroradiol** 27:26-34, 2006.

105. Yang CY, Chen YF, Lee CW, Huang A, Shen Y, Wei C, Liu HM: Multiphase CT Angiography versus Single-Phase CT Angiography: Comparison of Image Quality and Radiation Dose. **AJNR Am J Neuroradiol** 2008.

106. Zhao M, Charbel FT, Alperin N, Loth F, Clark ME: Improved phase-contrast flow quantification by three-dimensional vessel localization. **Magn Reson Imaging** 18:697-706, 2000.

VIII. ARTICLES

Journal of Neuroradiology ▫▫ (2007) ▫▫▫

ORIGINAL ARTICLE

Treatment decision by embolization versus surgery in patients with ruptured intracranial aneurysm: accuracy of multi-detector row CT angiography compared with digital subtraction angiography

Décision du traitement par embolisation versus chirurgie chez les patients présentant un anévrisme rompu intracrânien : précision de l'angioscanner multibarrette comparée à l'angiographie conventionnelle

C.-A. Taschner[a,*], L. Thines[b], M. Lernout[a], J.-P. Lejeune[b], X. Leclerc[a]

[a] *Department of neuroradiology, hôpital Roger-Salengro, CHRU Lille, rue Émile-Laine, 59037 Lille cedex, France*
[b] *Department of neurosurgery, hôpital Roger-Salengro, University Hospital Lille, Lille, France*

KEYWORDS
CT angiography;
Digital substraction angiography;
Endovascular treatment;
Intracranial aneurysms;
Multidetector-row technology;
Surgical clipping

Abstract

Objective. — The aim of this study was to determine the accuracy of multi-detector row computed tomography angiography (CTA) for the triage of patients with acutely ruptured aneurysms, and to assess how therapeutic decisions based on this method compared with digital subtraction angiography (DSA).

Methods. — Twenty-seven consecutive patients with acute subarachnoid hemorrhage were included, and underwent both CTA and DSA. CTA was performed on a 16-detector row CT scanner with a 0.75-mm collimation and a 0.558-beam pitch. Two readers reviewed the CTA data, and two different readers reviewed the DSA data. Aneurysm characteristics were recorded and treatment by surgical clipping or endovascular coil embolization was proposed.

Results. — A total of 24 aneurysms were identified on DSA in 21 patients. Sensitivity and specificity for CTA were 100% and 83%, respectively, on a per-aneurysm-basis. The correlation between DSA and CTA for the determination of sac and neck sizes was very good ($r = 0.92$, and $r = 0.95$, respectively, $P < 0.0001$). Sensitivity and specificity for the detection of arterial branches incorporated into the aneurysmal sac or neck were 50% and 100%, respectively. In

* Corresponding author.
E-mail address: c.taschner@web.de (C.-A. Taschner).

0150-9861/$ - see front matter © 2007 Published by Elsevier Masson SAS.
doi:10.1016/j.neurad.2007.07.006

Please cite this article as: C.-A. Taschner et al., Treatment decision by embolization versus surgery in patients with ruptured intracranial aneurysm: accuracy of..., Journal of Neuroradiology (2007), doi: 10.1016/j.neurad.2007.07.006.

three aneurysms, readers judged CTA inappropriate for triage, because peri-aneurysmal branches were not properly visualized. Overall agreement between CTA and DSA regarding the therapeutic decision between surgical clipping and endovascular coil embolization in 24 aneurysms was good (κ = 0.76).

Conclusion. — Multi-detector row CTA provides accurate anatomic information for aneurysm location as well as sac and neck sizes; however, the technique appears to have a low sensitivity in detecting branches incorporated into the aneurysmal sac.

MOTS CLÉS
Anévrismes intracrâniens ;
Angiographie conventionnelle ;
Technologie multibarrette ;
Angioscanner ;
Traitement endovascular ;
Clippage chirurgical

Résumé

Objectif. — Le but de ce travail était de déterminer la précision de l'angioscanner multibarrette pour le triage des patients présentant un anévrisme rompu intracrânien et d'étudier la précision de cette méthode pour la décision thérapeutique comparée à l'angiographie conventionnelle.

Matériel et méthode. — Vingt-sept patients consécutifs admis pour une hémorragie sous-arachnoïdienne ont été inclus et ont bénéficié d'un angioscanner et d'une angiographie conventionnelle. Les examens scanographiques étaient réalisés sur un scanner 16 barrettes avec des coupes de 0,75 mm et un pitch de 0,558. Deux lecteurs ont analysé les données du scanner et deux autres lecteurs ont analysé les angiographies conventionnelles. Les caractéristiques de l'anévrisme étaient notées, et un traitement par chirurgie ou par embolisation était proposé.

Résultats. — Un total de 24 anévrismes chez 21 patients était identifié en angiographie conventionnelle. La sensibilité et la spécificité de l'angioscanner pour la détection d'un anévrisme étaient de 100 et 83 % respectivement. La corrélation entre l'angioscanner et l'angiographie conventionnelle pour la détermination de la taille du sac et du collet était très bonne ($r = 0,92$, and $r = 0,95$ respectively, $p < 0,0001$). La sensibilité et la spécificité de l'angioscanner pour la détection d'une branche artérielle incorporée au sac ou au collet de l'anévrisme étaient 50 et 100 % respectivement. Pour trois anévrismes, les lecteurs ont jugé l'angioscanner inapproprié pour le triage avant traitement, car les branches artérielles périanévrysmales n'étaient pas visualisées correctement. La concordance globale entre angioscanner et angiographie conventionnelle pour la décision thérapeutique entre chirurgie et embolisation était jugée bonne pour 24 anévrismes.

Conclusion. — Le scanner multibarrette fournit des informations anatomiques précises tant pour la localisation de l'anévrisme que pour la mesure de sac et du collet. Cependant, cette technique semble avoir une sensibilité faible pour la détection des branches artérielles incorporées au sac anévrysmal.

Introduction

Intracranial aneurysms have a reported prevalence of 0.65–9% in the general population [11,14,22]. The incidence of aneurysm rupture lies in the range of 1:10 000 per year [12]. Case-fatality rates reported in the literature for acutely ruptured aneurysms range from 32–67%, with up to 20% of all patients remaining severely disabled with long-term loss of independence [7]. The principle of treatment is to prevent rebleeding by excluding the aneurysm from the intracranial circulation. This can be achieved by positioning a clip at the base of the ruptured aneurysm via a neurosurgical approach. With the publication of the ISAT study, endovascular coil embolization, first described in 1991, has become an accepted treatment of intracranial aneurysms worldwide [6,13].

Precise information on the aneurysms morphology is mandatory for patient triage between endovascular coil embolization and surgical clipping. So far, digital subtraction angiography (DSA) has been regarded as the standard-of-reference for the detection and characterization of intracranial aneurysms in patients with acute subarachnoid hemorrhage (SAH). Three-dimensional (3D) DSA data acquired with rotational angiography techniques is an important adjunct for the pre-therapeutic evaluation of ruptured aneurysms. The ample availability of novel CT techniques with multi-detector row acquisition, considerably improving the spatial resolution of CTA data, has started to change the diagnostic algorithm in patients with acute SAH. A number of comparative studies have shown that multi-detector row CTA has high sensitivity and specificity for the detection of intracranial aneurysms in patients with acute SAH [4,8,9,15,17,21,23]. CTA has also been used as unique pre-therapeutic tool in the preparatory phase of aneurysm clipping [1,5,16,20,21].

The purpose of this study was to determine the accuracy of multi-detector row computed tomography angiography (CTA) for triage in patients with acutely ruptured intracra-

Q2 Please cite this article as: C.-A. Taschner et al., Treatment decision by embolization versus surgery in patients with ruptured intracranial aneurysm: accuracy of..., Journal of Neuroradiology (2007), doi: 10.1016/j.neurad.2007.07.006.

nial aneurysms, and to assess, how therapeutic decisions based on this method compared with DSA.

Subjects and methods

Patients

From November 2005 through February 2006, 27 consecutive patients (15 women and 12 men; mean age: 49 years, range: 19–72 years) admitted for a non-traumatic SAH were enrolled in this prospective study and had both, multi-detector row CTA and DSA as part of the diagnostic and pre-therapeutic work-up. The diagnosis of SAH was made by CT ($N = 25$), or lumbar puncture ($N = 2$). Exclusion criteria were poor clinical grade, patient agitation, renal insufficiency, and known allergy to iodinated contrast agents. Two patients presenting with SAH could not be enrolled into the study due to a poor clinical grade. The study was approved by the local ethics committee.

Multi-detector row CTA

CT examinations were carried out on a 16-detector row scanner (Volume Zoom, Siemens, Erlangen, Germany). Parameters for the CTA acquisition were 0.75 mm section thickness, 0.5 mm section interval, 100 kVp, 200 mAs, and 160 mm field of view with a scanning time of approximately 8 s. The table feed was 13.4 mm/s at a scan revolution time of 0.5 s resulting in a beam pitch of 0.558. The scanned volume provided full anatomic coverage of all potential intracranial aneurysmal sites from the axis to the vertex. A total of 80 mL Iomeprol (Iomeron 400, Bracco S.p.a, Milan, Italy) were administered intravenously with a power injector at a rate of 3.5 ml/s via a venous line. The correct timing of contrast media injection was achieved by applying a bolus tracking technique. Acquisition of the CTA was started when the density of a predefined region of interest set within the aortic arch passed a value of 120 HU.

Intra-arterial DSA

Intra-arterial DSA was performed on a monoplane digital angiographic unit (Allura, Philips Medical Systems, Best, the Netherlands), via a transfemoral approach with bilateral selective injections of the internal carotid and vertebral arteries with frontal and lateral views. In addition, a rotational acquisition with 3D reconstructions was performed for any aneurysm diagnosed. Images were acquired with a 22 cm field-of-view, and a 102 4 × 1024 matrix.

Image interpretation

Two sets of readers composed of one interventional neuroradiologist and one cerebrovascular neurosurgeon each, retrospectively and independently reviewed the CTA data (X.L., J.P.L.) and the DSA data (C.A.T., L.T.). This protocol recreates the pre-therapeutic situation when the cerebrovascular neurosurgeon and the interventional neuroradiologists make a joint decision regarding the treatment strategy for the revealed intracranial aneurysms.

CTA data was evaluated on a computer workstation (Syngo, Siemens, Erlangen, Germany) by using preset volume-rendered and maximum intensity projection display algorithms on InSpace (Siemens, Erlangen, Germany). In addition source images and multiplanar reformations were reviewed at a window width of 500 HU and a window level of 200 HU. Conventional DSA data was reviewed on hardcopies; 3D reformats of rotational DSA were assessed on a dedicated workstation (Integris 3D-RA, Philips, Best, the Netherlands). Angiographic images were displayed using volume rendered and maximum intensity projection display algorithms. Aneurysm sizes and neck sizes were determined with the caliper tool on 3D reconstructions for both modalities. The presence and location of aneurysms, their largest diameter, neck size, and the presence of side branches originating from the aneurysmal sac were recorded on a scoring sheet.

Patient triage

Triage of patients with ruptured aneurysms between endovascular coil embolization and surgical clipping is based on the evaluation and critical consideration of the clinical grade, the patient age, the extent of the intracranial hemorrhage, the location of the intracranial aneurysm, as well as morphologic features of the underlying malformation. As the aim of the present survey was to evaluate the impact of CTA on medical decision making, patient triage in this study was exclusively based on morphologic criteria of the underlying aneurysm. Readers were asked to identify any contraindications to endovascular coil embolization related to the aneurysms morphologic features. Contraindications to endovascular coil embolization were branches arising from the aneurysmal neck or sac, unfavorable dome – neck ratio, small aneurysmal size (< 2 mm), and inaccessibility of the aneurysmal sac due to vascular pathologies. In the absence of these contraindications, aneurysms were assigned to endovascular coil embolization, when present, aneurysms were allocated to surgical clipping. The treatment option finally recommended, was based on a consensual decision made by the interventional neuroradiologist and the vascular neurosurgeon.

Statistical analysis

Two-by-two tables were constructed from true-positive, false-positive, false-negative, and true-negative results for multi-detector row CTA compared with intra-arterial DSA serving as standard-of-reference. We calculated sensitivity, specificity, positive and negative predictive values regarding the detection of intracranial aneurysms with multi-detector row CTA on a per-aneurysm basis. The calculation of the positive and negative predictive values was based on a supposed prevalence of ruptured intracranial aneurysms in 85% of patients presenting with SAH [19]. Sensitivity and specificity were calculated for the detection of branches originating from the aneurysmal sac on a per-aneurysm basis. Linear regression analysis with calculation of a Pearson correlation coefficient was used to assess the intermodality correlation for the largest aneurysmal diameter and the neck size. Statistical significance was set at

Q2 Please cite this article as: C.-A. Taschner et al., Treatment decision by embolization versus surgery in patients with ruptured intracranial aneurysm: accuracy of..., Journal of Neuroradiology (2007), doi: 10.1016/j.neurad.2007.07.006.

$P < 0.001$. Kappa statistics were calculated to determine the agreement in the proposed treatment of the diagnosed aneurysms based on anatomical information deriving from either multi-detector row CTA or DSA on a per-aneurysm basis. MedCalc (Medisoftware, Mariakerke, Belgium) was used for statistical analysis.

Results

Technical efficacy

In 27 CT angiograms and 27 DSA, no procedural complications, or allergic reactions to the contrast agent were observed. All exams were of diagnostic quality.

Diagnostic efficacy

In 21 of 27 patients, a total of 24 aneurysms were identified by DSA (Table 1). All aneurysms were identified on CTA. One aneurysm of the anterior communicating artery diagnosed by CTA was not confirmed by DSA. In the remaining five patients no further aneurysm was diagnosed with either modality. Three patients carried two aneurysms. CTA had a sensitivity of 100% and a specificity of 83.3% for the detection of intracranial aneurysms with a positive predictive value of 97.14%, a negative predictive value of 100%, and a likelihood ratio of 6.000.

The average aneurysm diameter measured 5.6 mm (SD CTA: ± 2.06, DSA: ± 2.16; range 3–10 mm) with an aneurysm neck of 3.3 mm (SD CTA: ± 1.30, DSA: ± 1.46, range 2–8 mm) for both techniques. The calculation of Pearsons' linear correlation coefficient for aneurysm size and neck size on a per-aneurysm basis ($N = 24$) demonstrated a very good agreement between techniques with $r = 0.92$ ($P < 0.0001$, 95% confidence interval for $r = 0.8248$ to 0.9646) and $r = 0.95$ ($P < 0.0001$, 95% confidence interval for $r = 0.8876$ to 0.9779), respectively (Figs. 1 and 2).

The sensitivity and specificity of CTA for the detection of arterial branches originating from the aneurysm were 50% and 100%, respectively. In three aneurysms of the communicating segment of the internal carotid artery (ICA) neither the posterior communicating artery nor the anterior choroi-

Table 1 Aneurysm characteristics in 27 patients admitted for subarachnoid hemorrhage
Tableau 1 Charactéristiques des anévrismes chez 27 patients admis pour une hémorragie sous-arachnoïdienne

Patient number	Aneurysm number	Age/Sex	Aneurysm detected		Aneurysm location	Aneurysm size diameter/neck (in mm)		Incorporated branches		Proposed treatment		Treatment
			CTA	*DSA*		*CTA*	*DSA*	*CTA*	*DSA*	*CTA*	*DSA*	
1	1	49/female	+	+	Pcom	5/3	6/3	-	+	Coil	Coil	Coil
2	2	35/female	+	+	Acom	7/4	7/4	-	+	Coil	Coil	Coil
	3		+	+	Pcom	3/2	3/2	n.a.	+	n.a.	Clip	Clip
3	4	72/female	+	+	Pcom	4/2	3/2	-	-	Coil	Coil	Coil
4	5	69/female	+	+	Pcom	6/5	7/4	n.a.	-	n.a.	Coil	Coil
5	6	57/female	+	+	MCA	4/3	4/3	+	+	Clip	Clip	Clip
6	7	44/female	+	+	CB	9/3	10/2	-	-	Coil	Coil	Coil
7	8	56/male	+	+	MCA	7/3	7/3	-	-	Clip	Clip	Clip
8	9	39/male	+	+	MCA	8/8	7/8	-	+	Clip	Clip	Clip
9	10	38/male	+	+	MCA	10/6	9/5	+	+	Clip	Clip	Clip
10	11	53/female	+	+	Acom	6/4	5/3	-	+	Coil	Coil	Coil
	12		+	+	Pcom	6/3	5/3	n.a.	+	n.a.	Coil	Coil
11	13	44/female	+	+	AC	3/2	4/2	-	-	Coil	Coil	Coil
12	14	47/female	+	+	MCA	9/5	10/6	+	+	Clip	Clip	Clip
13	15	63/male	+	+	CB	5/3	4/3	-	-	Coil	Coil	Coil
14	16	51/male	+	+	MCA	6/3	6/3	+	+	Clip	Clip	Clip
	17		+	+	M1-MCA	3/3	3/3	-	-	Clip	Clip	Clip
15	18	50/male	+	+	Acom	7/3	7/4	-	-	Coil	Coil	Coil
16	19	57/female	+	+	Acom	3/2	3/2	-	-	Coil	Coil	Coil
17	20	51/male	+	+	MCA	5/3	5/3	-	-	Coil	Coil	Coil
18	21	46/male	+	+	Acom	5/2	6/3	-	-	Coil	Coil	Coil
19	22	43/female	+	+	Acom	6/4	4/3	-	-	Coil	Coil	Coil
20	23	46/female	+	+	Acom	4/2	4/3	-	-	Coil	Coil	Coil
21	24	50/female	+	+	BA	3/3	3/3	-	-	Coil	Coil	Coil
22		66/male	-	-						0	0	
23		19/male	+	-	*Acom*	2/2				0	0	
24		51/male	-	-						0	0	
25		54/female	-	-						0	0	
26		24/female	-	-						0	0	
27		53/male	-	-						0	0	

Pcom: posterior communicating segment of the internal carotid artery (ICA); Acom: anterior communicating artery; MCA: Bifurcation of the middle cerebral artery; CB: bifurcation of the intracranial ICA; AC: anterior cerebral artery; M1-MCA: M1 segment of the middle cerebral artery; BA: basilar artery; +: aneurysm present; -; no aneurysm found, n.a.; not assessable; Coil: Absence of contraindication to endovascular coil embolization; Clip: Presence of contraindication to endovascular coil embolization.

Q2 Please cite this article as: C.-A. Taschner et al., Treatment decision by embolization versus surgery in patients with ruptured intracranial aneurysm: accuracy of..., Journal of Neuroradiology (2007), doi: 10.1016/j.neurad.2007.07.006.

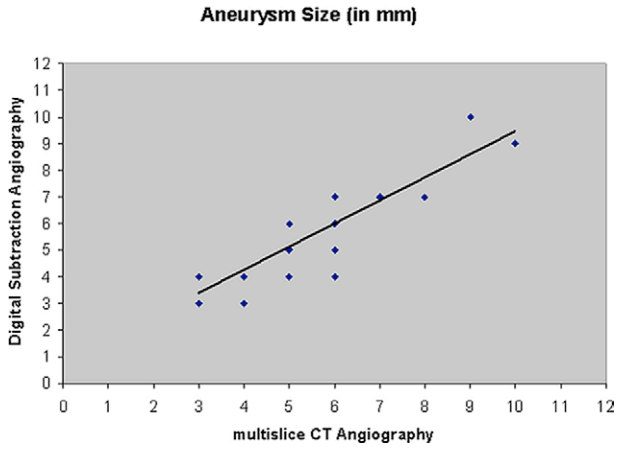

Figure 1 Scatterplot displays the correlation of aneurysmal sizes determined by digital subtraction angiography and multislice CT angiography measures ($r = 0.92$; slope = 0.880, $P < 0.0001$).

Figure 1 Représentation de la dispersion des mesures de l'anévrisme par angiographies cérébrale conventionnelle et angioscanner multibarrette ($r = 0,92$; slope = 0,880, $p < 0,0001$).

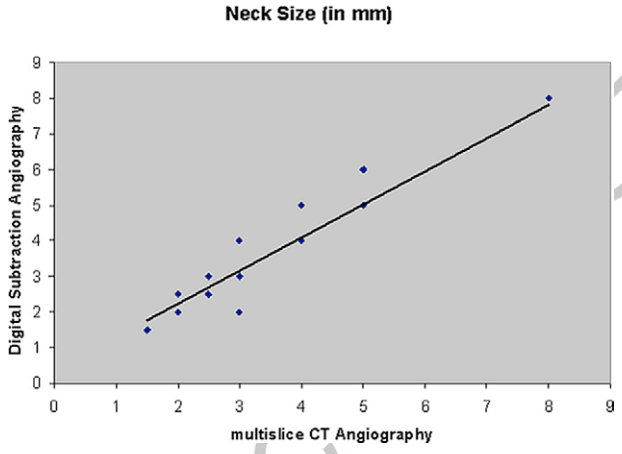

Figure 2 Scatterplot shows the correlation of neck sizes measured on digital subtraction angiographies compared to multislice CT angiography measures ($r = 0.95$; slope = 0.845, $P < 0.0001$).

Figure 2 Représentation de la dispersion des mesures du collet de l'anévrisme par angiographie cérébrale conventionnelle et angioscanner multibarrette ($r = 0,95$; slope = 0,845, $p < 0,0001$).

dal artery could be identified (aneurysms 3,5,12) on CTA images.

Therapeutic efficacy

The assignment to endovascular coil embolization or surgical clipping was based on morphologic features only. Endovascular coil embolization was considered the preferential therapeutic option, and patients were assigned to coil embolization in the absence of any contraindication to endovascular treatment (Fig. 3).

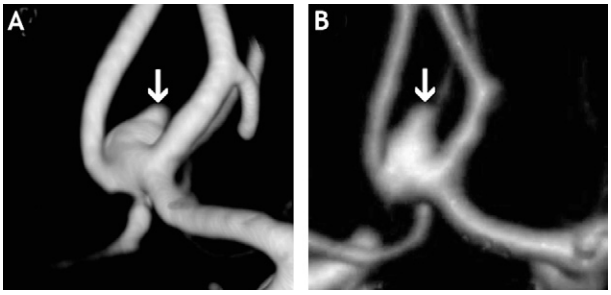

Figure 3 Forty-three year old woman (patient 19) with a ruptured aneurysm of the anterior communicating artery (ACom). (a) Three-dimensional (3D) reconstruction from rotational digital subtraction angiography (DSA) showing a 4-mm diameter aneurysm of ACom with a blister at the distal part of the aneurysm (arrow); (b) the morphology of the aneurysm (arrow) can be evaluated on this volume rendered CT image. When compared to DSA the aneurysmal neck appears slightly larger. Endovascular coil embolization was the proposed treatment for both imaging modalities.

Figure 3 Femme âgée de 43 ans (patient 19) présentant une rupture d'un anévrisme de l'artère communicante antérieure (ACom). a : reconstruction tridimensionnelle (3D) en angiographie conventionnelle rotationnelle montrant un anévrisme de l'ACom mesurant 4 mm de diamètre avec une image de phlyctène à la partie distale de l'anévrisme (fleche) ; b : la morphologie de l'anévrisme (flèche) peut être évaluée sur cette image scanographique en rendu de volume. Comparé à l'angiographie conventionnelle, le collet anévrysmal apparaît discrètement plus large. L'embolisation par voie endovasculaire à l'aide de coils était proposée sur les deux modalités d'imagerie.

Readers were unable to decide on the therapeutic choice based on CTA data in 3 of 24 aneurysms because important perianeurysmal vessels – an important element for the risk allocation – could not be identified. Of the remaining 21 aneurysms, 14 were allocated to endovascular coil embolization and seven were assigned to surgical clipping. When compared to the therapeutic decision based on DSA data, identical therapeutic choices were made for these 21 aneurysms. We included the three CTAs that were non-diagnostic for the presence of perianeurysmal branches for the calculation of the intermodality agreement. The kappa score for the overall agreement between CTA and DSA regarding the therapeutic decision between surgical clipping and endovascular coil embolization in 24 aneurysms was 0.76.

Principal contraindication to endovascular coil embolization was an unfavorable dome-neck-ratio in five of seven aneurysms, present on both imaging modalities (Fig. 4). An additional incorporated artery was demonstrated on DSA in four cases, three of these were visualized on CTA (aneurysms 6,10+14). Endovascular coil embolization was not considered in another aneurysm due to an unfavorable dome-to-neck ratio without incorporated artery visible on neither imaging modality (aneurysm 17), and in one case, surgical clipping was proposed due to a major branch originating at the base of a MCA bifurcation aneurysm – visualized on both CTA and DSA (aneurysm 16).

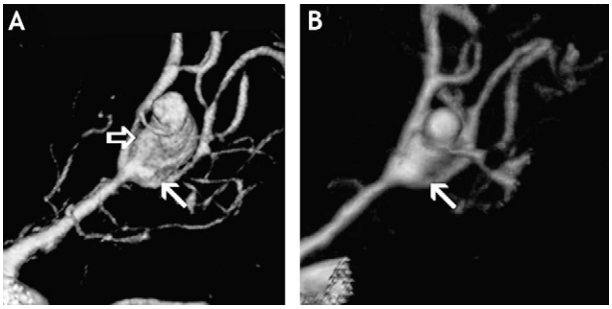

Figure 4 Thirty-eight year old man with a ruptured aneurysm of the middle cerebral artery (MCA) bifurcation (patient 9). (a) Three-dimensional (3D) reconstruction from rotational digital subtraction angiography (DSA) showing an irregular 8-mm diameter aneurysm of the MCA (open arrow) with an arterial branch arising from the base of the aneurysmal neck (white arrows); (b) Aneurysm characteristics on volume rendered CT image are in agreement with 3D DSA findings with incorporation of an arterial branch originating from the base of the aneurysm (white arrow). For both imaging modalities, a treatment by surgical clipping was suggested.

Figure 4 Homme âgé de 38 ans présentant une rupture d'anévrisme de la bifurcation de l'artère cérébrale moyenne (ACM) (patient 9). a : reconstruction tridimentionnelle (3D) par angiographie conventionnelle rotationnelle montrant un anévrisme irrégulier mesurant 8 mm de diamètre de l'ACM (flèche ouverte) avec présence d'une branche artérielle naissant au niveau de la base du collet de l'anévrisme (flèches blanches) ; b : les caractéristiques de l'anévrisme sur une image scanographique en rendu de volume sont en concordance avec les résultats de l'angiographie 3D avec présence d'une branche artérielle incorporée à la base de l'anévrisme (flèche blanche). Pour les deux modalités d'imagerie, un traitement par chirurgie a été proposé.

Discussion

The present study corroborates findings of previous studies that multi-detector row CTA is an appropriate means for the diagnostic work-up of SAH [1,4,8,9,15,17,20,21,23]. In our study, the sensitivity and specificity for the detection of intracranial aneurysms were 100% and 83.3%, respectively, applying 16-row detector CTA techniques.

A meta-analysis by Chappell et al. based on 21 studies published between 1995 and 2002 including 1252 patients resulted in a sensitivity of 93.3% and a specificity of 87.8% for the detection of intracranial aneurysms [2]. However, most of the studies included were based on single beam, spiral CTA techniques. Major advances have been made by the introduction of multi-detector row scanners. This new technology allows investigation of a large volume with a high x-axis resolution in a very short time with multiple detector rows receiving the attenuated radiation. Multi-detector row CT allows for faster scan coverage and larger z-axis coverage/rotation. With its high spatial resolution and thin slices, the method provides data sets with isotropic voxel size improving the quality of multiplanar reformats and 3D-rendered images [3]. Recent studies applying multi-detector row CTA have reported improved detection rates of intracranial aneurysms in patients presenting with SAH. Kadri et al. reported a sensitivity of 86% and a specificity of 100% for the detection of acutely ruptured aneurysms with CTA [9]. Jayaraman et al. obtained a sensitivity of 90% and a specificity of 93% when applying CTA with four detector rows [8]. Tipper et al. used a 16-row detector CTA and reported a sensitivity of 96.2%, and a specificity of 100% for the detection of intracranial aneurysms in patients presenting with intracranial hemorrhage [17]. Teksam et al. report on a series applying multi-detector row CT with 4-detector row technique [15]. They stratified the aneurysms detected and calculated sensitivities according to aneurysmal size. They found an overall sensitivity of 84% for small (< 4 mm), 97% for medium-size (4-10 mm), and 100% for large (> 10 mm) aneurysms. These results seem to justify the exclusive application of multi-detector row CTA for the detection of intracranial aneurysms in patients presenting with SAH, reserving DSA for cases of uncertainty.

The exact characterization of the largest aneurysmal diameter, the neck size, variations of the circle of Willis, and of branches arising from the aneurysmal sac are important issues for the pre-therapeutic risk assessment. In our survey, CTA provided precise information on aneurysms morphology including the largest diameter and the neck size. The efficacy of CTA in detecting small branches originating in the vicinity of, or directly from the aneurysmal sac was restricted in aneurysms located close to the skull base (Fig. 5). This limitation of CTA has been described earlier and is technically related to beam-hardening artifacts from the dense bone of the skull base [21]. For the non-invasive characterization of paraclinoid aneurysms MR Angiography might be more appropriate [16]. Another factor limiting the clinical performance of CTA might have been the application of volume rendering techniques, which often include an automatically generated threshold, which may suppress valuable image information such as small vessels. In our study we systematically included complementary information deriving from maximum intensity projections which are more consistent, as they directly rely on source images [18].

Previous reports on CTA serving as the only diagnostic and pre-treatment planning study for cerebral aneurysms have been reported in the literature [5,21]. This study agrees that patient triage based on multi-detector row CTA data is possible, and that a good correlation with therapeutic decisions based on DSA data can be obtained. Villablanca et al. have published a study that determined whether multi-detector row CTA could be used to identify and characterize aneurysms of the posterior circulation and to guide optimal treatment selection [21]. They successfully used CTA to triage patients between endovascular and neurosurgical treatment in a significant proportion of cases and based treatment planning in more than 70% of treated cases on CTA data.

The present study includes various limitations. Our observations are based on a small sample size obtained from a single centre. Management strategies for the treatment of intracranial aneurysms obviously differ according to local preferences, which might have biased the therapeutic decision. Therefore, we have tried to base patient

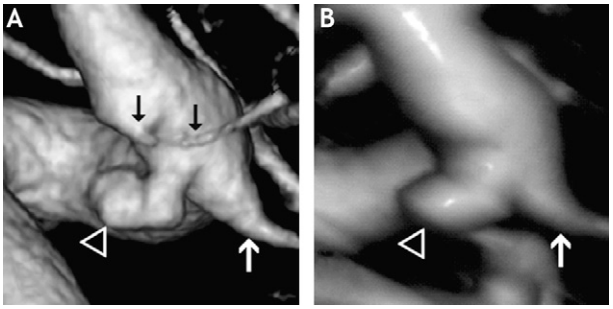

Figure 5 Seventy-two year old woman with a ruptured aneurysm of the posterior communicating artery (patient 3). (a) Three-dimensional (3D) reconstruction from rotational digital subtraction angiography (DSA) showing a 3-mm diameter aneurysm (arrow head) of the carotid siphon close to the origin of the posterior communicating artery (white arrow). The anterior choroidal artery located distal to the neck (black arrows) is clearly visualize; (b) volume rendered 3D CT image clearly delineating the aneurysm, whereas the anterior choroidal artery is not depicted. The patient was successfully treated by endovascular coil embolization.

Figure 5 Femme âgée de 72 ans présentant une rupture d'anévrisme de l'artère communicante postérieure (patient 3). a : reconstruction tridimensionnelle (3D) en angiographie conventionnelle rotationnelle montrant un anévrisme du siphon carotidien mesurant 3 mm de diamètre (tête de flèche), situé à proximité de la naissance de l'artère communicante postérieure (flèche blanche). L'artère choroïdienne antérieure, située à distance du collet (flèches noires), est clairement visualisée ; b : l'image scanographique en rendu de volume permet de délimiter précisément l'anévrisme alors que l'artère choroïdienne antérieure n'est pas détectée. Le patient a été traité avec succès par embolisation à l'aide de coils.

triage on objective criteria, used for the general risk allocation of endovascular coil embolization as described in the methods section.

It remains debatable, whether CTA can be applied exclusively for the pre-therapeutic risk allocation and therapeutic assignment of ruptured intracranial aneurysms. The major restriction of the technique seems to lie in the low sensitivity in detecting branches incorporated into the aneurysmal sac. In clinical practice, if multi-detector row CTA was used as the sole diagnostic procedure before coil embolization, a major contraindication to endovascular treatment might in some cases not be revealed until the three-dimensional DSA at the beginning of the endovascular procedure.

Despite these limitations, multi-detector row CTA will probably replace DSA in the work-up of patients with non-traumatic SAH. Intra-arterial DSA is time consuming, invasive, and might not be available on a 24 h basis in all institutions. CTA is a more practicable option, as it is widely available, less expensive and offers a great procedural safety. It can be performed in the emergency setting right after diagnosing a SAH, thereby accelerating the diagnostic work-up and the process of medical decision making in patients with acutely ruptured intracranial aneurysms.

Conclusion

Multislice CTA is a practical tool for the detection of intracranial aneurysms in patients presenting with acute non-traumatic SAH. In addition, the technique provides anatomical information necessary for the assignment of ruptured aneurysms to either endovascular coil embolization or surgical clipping; however, the technique appears to have a low sensitivity in detecting branches incorporated into the aneurysmal sac.

Uncited reference

[10]. Q1

References

[1] Agid R, Lee SK, Willinsky RA, Farb RI, Terbrugge KG. Acute subarachnoid hemorrhage: using 64-slice multidetector CT angiography to "triage" patients' treatment. Neuroradiology 2006;48:787–94.

[2] Chappell ET, Moure FC, Good MC. Comparison of computed tomographic angiography with digital subtraction angiography in the diagnosis of cerebral aneurysms: a meta-analysis. Neurosurgery 2003;52:624–31.

[3] Chawla S. Advances in multidetector computed tomography: applications in neuroradiology. J Comput Assist Tomogr 2004; 28(Suppl 1):S12–6.

[4] Dammert S, Krings T, Moller-Hartmann W, Ueffing E, Hans FJ, Willmes K, et al. Detection of intracranial aneurysms with multislice CT: comparison with conventional angiography. Neuroradiology 2004;46:427–34.

[5] Dehdashti AR, Rufenacht DA, Delavelle J, Reverdin A, de Tribolet N. Therapeutic decision and management of aneurysmal subarachnoid haemorrhage based on computed tomographic angiography. Br J Neurosurg 2003;17:46–53.

[6] Guglielmi G, Vinuela F, Dion J, Duckwiler G. Electrothrombosis of saccular aneurysms via endovascular approach- Part 2: Preliminary clinical experience. J Neurosurg 1991;75:8–14.

[7] Hop JW, Rinkel GJ, Algra A, van Gijn J. Case-fatality rates and functional outcome after subarachnoid hemorrhage: a systematic review. Stroke 1997;28:660–4.

[8] Jayaraman MV, Mayo-Smith WW, Tung GA, Haas RA, Rogg JM, Mehta NR, et al. Detection of intracranial aneurysms: multidetector row CTA compared with DSA. Radiology 2004;230: 510–8.

[9] Kadri S, Brunel H, Bourbotte G, Delort P, Lust S, Bonafe A. Can multislice helical computed tomography replace conventional angiography in the diagnosis of non traumatic subarachnoid hemorrhage? J Neuroradiol 2006;33:45–50.

[10] Matsumoto M, Sato M, Nakano M, Endo Y, Watanabe Y, Sasaki T, et al. Three-dimensional computerized tomography angiography-guided surgery of acutely ruptured cerebral aneurysms. J Neurosurg 2001;94:718–27.

[11] McCormick WF, Nafzinger JD. Saccular intracranial aneurysms: an autopsy study. J Neurosurg 1965;22:155–9.

[12] Menghini VV, Brown Jr. RD, Sicks JD, O'Fallon WM, Wiebers DO. Incidence and prevalence of intracranial aneurysms and hemorrhage in Olmsted County, Minnesota, 1965 to 1995. Neurology 1998;51:405–11.

[13] Molyneux A, Kerr R, Stratton I, Sandercock P, Clarke M, Shrimpton J, et al. International Subarachnoid Aneurysm Trial (ISAT) of neurosurgical clipping versus endovascular coiling in 2143 patients with ruptured intracranial aneurysms: a randomised trial. Lancet 2002;360:1267–74.

[14] Rinkel GJ, Djibuti M, Algra A, van Gijn J. Prevalence and risk of rupture of intracranial aneurysms: a systematic review. Stroke 1998;29:251–6.

[15] Teksam M, McKinney A, Casey S, Asis M, Kieffer S, Truwit CL. Multi-section CTA for detection of cerebral aneurysms. AJNR Am J Neuroradiol 2004;25:1485–92.

[16] Thines L, Delmaire C, Le Gars D, Pruvo JP, Lejeune JP, Lehmann P, et al. MRI localization of paraclinoid carotid aneurysms. J Neuroradiol 2006;33:115–20.

[17] Tipper G, U-King-Im JM, Price SJ, Trivedi RA, Cross JJ, Higgins NJ, et al. Detection and evaluation of intracranial aneurysms with 16-row multislice CTA. Clin Radiol 2005;60:565–72.

[18] Tomandl BF, Kostner NC, Schempershofe M, Huk WJ, Strauss C, Anker L, et al. CT angiography of intracranial aneurysms: a focus on postprocessing. Radiographics 2004;24:637–55.

[19] van Gijn J, Rinkel GJ. Subarachnoid haemorrhage: diagnosis, causes and management. Brain 2001;124:249–78.

[20] Velthuis BK, Van Leeuwen MS, Witkamp TD, Ramos LM, Berkelbach van Der Sprenkel JW, Rinkel GJ. Computerized tomography angiography in patients with subarachnoid hemorrhage: from aneurysm detection to treatment without conventional angiography. J Neurosurg 1999;91:761–7.

[21] Villablanca JP, Achiriolaie A, Hooshi P, Martin N, Duckwiler G, Jahan R, et al. Aneurysms of the posterior circulation: detection and treatment planning using volume-rendered three-dimensional helical computerized tomography angiography. J Neurosurg 2005;103:1018–29.

[22] Winn HR, Jane Sr. JA, Taylor J, Kaiser D, Britz GW. Prevalence of asymptomatic incidental aneurysms: review of 4568 arteriograms. J Neurosurg 2004;96:43–9.

[23] Wintermark M, Uske A, Chalaron M, Regli L, Maeder P, Meuli R, et al. Multislice computerized tomography angiography in the evaluation of intracranial aneurysms: a comparison with intraarterial digital subtraction angiography. J Neurosurg 2003;98:828–36.

Q2 Please cite this article as: C.-A. Taschner et al., Treatment decision by embolization versus surgery in patients with ruptured intracranial aneurysm: accuracy of..., Journal of Neuroradiology (2007), doi: 10.1016/j.neurad.2007.07.006.

Eur Radiol (2006) 16: 479–488
DOI 10.1007/s00330-005-2879-6

NEURO

Laurent Thines
Christine Delmaire
Daniel Le Gars
Jean-Pierre Pruvo
Jean-Paul Lejeune
Pierre Lehmann
Jean-Paul Francke

MRI location of the distal dural ring plane: anatomoradiological study and application to paraclinoid carotid artery aneurysms

Received: 12 April 2005
Revised: 13 June 2005
Accepted: 28 July 2005
Published online: 23 August 2005

L. Thines · J.-P. Lejeune
Department of Neurosurgery,
University Hospital,
Lille, France

C. Delmaire · J.-P. Pruvo
Department of Neuroradiology,
University Hospital,
Lille, France

D. Le Gars
Department of Neurosurgery,
University Hospital,
Amiens, France

D. Le Gars
Department of Anatomy,
University Hospital,
Amiens, France

P. Lehmann
Department of Neuroradiology,
University Hospital,
Amiens, France

J.-P. Francke
Department of Anatomy,
University Hospital,
Lille, France

L. Thines (✉)
Clinique Neurochirurgicale,
Hôpital Roger-Salengro,
CHRU,
59037 Lille Cedex, France
e-mail: Laurent.Thines@wanadoo.fr
Tel.: +33-32-0446615
Fax: +33-32-0446623

Abstract The distal dural ring plane (DDRP) separates the intradural from the extradural paraclinoid internal carotid artery. The purpose of this study was to evaluate its position with MR imaging. The protocol used a T2-weighted sequence in two orthogonal planes: diaphragmatic (DIA-P) and carotid (CAR-P). The DDRP passes through four anatomoradiological reference points (RefP). We developed on a cadaveric model a correlation method supported by correlation lines and angles (CA) projecting the RefP toward the DDRP. RefP were correlated to the DDRP in 65–84% of cases in the DIA-P and 60–76% of cases in the CAR-P. CA were identified and correlated to the DDRP, respectively, in 87% and 60% of cases in the DIA-P, and 60% and 51% of cases in the CAR-P (failure often related to a lack of visibility of just one RefP). A higher tissular contrast in living subjects allowed the identification of CA in 90% and 80% of cases, respectively, in the DIA-P and the CAR-P. We propose that CA, when identified, should be considered as an approximation of the inferior radiological limit of the DDRP curve. In difficult angiographical cases, this MRI protocol could help to locate paraclinoid aneurysms on both sides of the cavernous sinus roof.

Keywords Dural ring · Internal carotid artery · Anatomical study · Paraclinoid aneurysms · Magnetic resonance imaging

Introduction

Progress in neuroimaging leads to the diagnosis of an increasing number of incidental lesions. In paraclinoid vascular pathology, determination of the relationship between asymptomatic aneurysms and the cavernous sinus roof may be a neuroradiological challenge [1–13]. Indeed, aneurysms entirely located below this plane cannot cause subarachnoid hemorrhage and do not have the same morbidity after rupture as intradural subarachnoid aneurysms. The distal dural ring (DDR) represents the anatomical borderline between the extradural (intracavernous or clinoid segment) and the intradural (extracavernous or ophthalmic segment) internal carotid artery (ICA) [14–18]. This magnetic resonance

imaging (MRI) study was designed to evaluate the position of the distal dural ring plane (DDRP), defined as the curved plane passing through the DDR.

Materials and methods

Anatomical material and cadaveric correlation model

Forty paraclinoid regions and ICA were dissected from 20 adult, formalin-fixed, human cadaveric heads. No vascular injection was performed. Then, we developed a cadaveric correlation model (Fig. 1) comprised of a skull base in which ICA were ligatured on a venous central catheter filled with echographic gel. The catheter tip was positioned to correspond to the inferior level of the DDRP. For MRI acquisition, the model was fixed upside down in a tank filled with an isotonic saline solution.

Control group

In order to evaluate the reproducibility of the results obtained from cadaveric specimens, we included in our study 15 adult patients referred to our institution for a cerebral MRI. Patients were selected on the following criteria: informed consent, absence of pregnancy in women, absence of previous history of meningitis or subarachnoid hemorrhage, and absence of disease involving the paraclinoid region (no aneurysms).

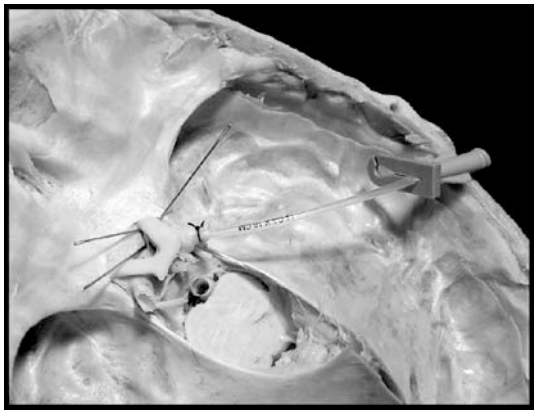

Fig. 1 Left posterolateral view of the cadaveric correlation model. The catheter tip was very strictly positioned. First, we pierced the internal carotid artery (ICA) with three fine needles parallel to the distal dural ring plane (DDRP) surface in such a manner that they crossed at the centre of the ICA. Then, the catheter insertion was stopped at the level of the needles' intersection. The third time, the ICA was ligatured on the catheter to avoid its migration, and the needles were removed. So, in this cadaveric model, the catheter tip corresponded to the level of the DDRP

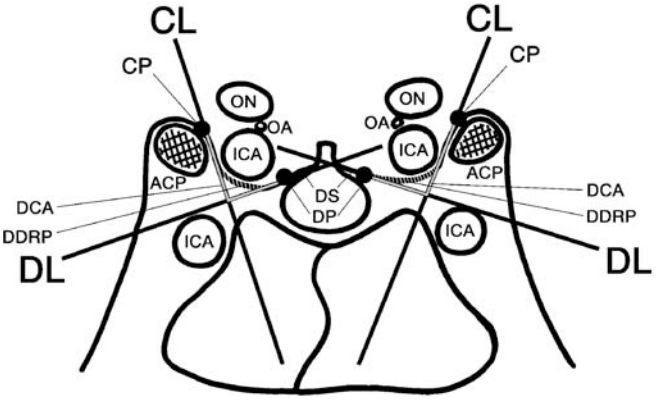

Fig. 2 Diagram depicting regional markers, reference points, and correlation lines and angles in the diaphragmatic plane (DIA-P). *ICA* Internal carotid artery, *ACP* anterior clinoid process, *ON* optic nerve, *OA* ophthalmic artery, *DS* diaphragma sellae, *CP* clinoid point, *DP* diaphragmatic point, *CL* clinoid line, *DL* diaphragmatic line, *DCA* diaphragmatic correlation angle, *DDRP* distal dural ring plane

Paraclinoid markers, correlation lines, correlation angles, and correlation planes

Definitions of the DDRP and the paraclinoid markers were based on previous anatomical, surgical or radiological reports [3, 7, 9, 14–37] and on our own anatomical or neuroradiological observations.

Regional markers (Figs. 2, 3, 4) were essential to the overall radiological analysis of the paraclinoid region. They included the anterior clinoid process (ACP), the

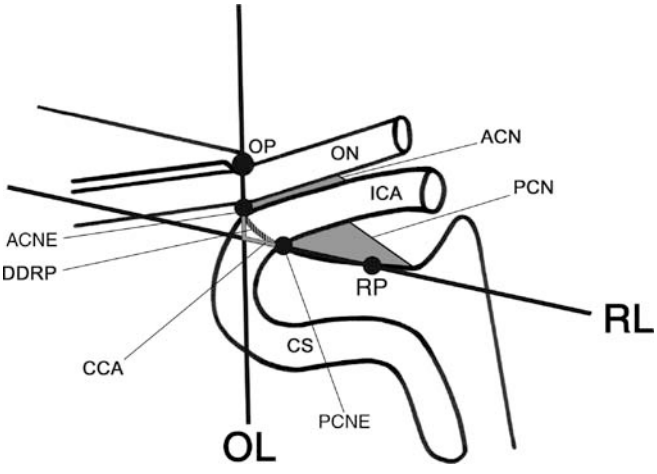

Fig. 3 Diagram depicting regional markers, reference points and correlation lines and angles in the carotid plane (CAR-P). *ICA* Internal carotid artery, *ON* optic nerve, *CS* carotid siphon, *OP* optic point, *ACN* anterior CSF notch, *ACNE* anterior CSF notch extremity, *PCN* posterior CSF notch, *PCNE* posterior CSF notch extremity, *RP* roof of the cavernous sinus point, *OL* optic line, *RL* roof line, *CCA* carotid correlation angle, *DDRP* distal dural ring plane

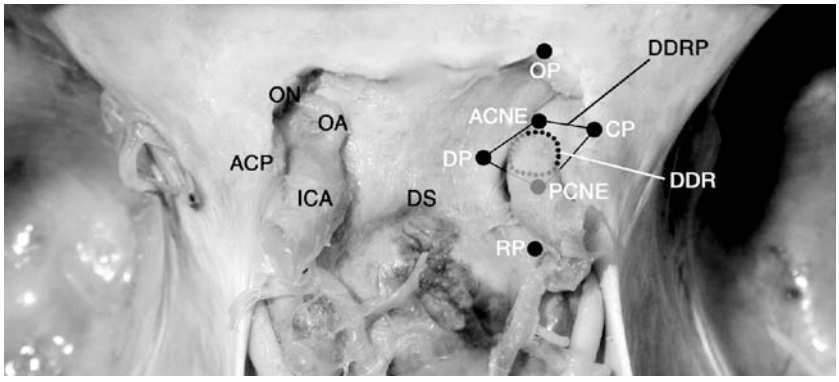

Fig. 4 Superior view of the paraclinoid and parasellar regions showing the location of the regional markers, the reference points, the distal dural ring (DDR) and the distal dural ring plane (DDRP) (the optic nerves and chiasm are removed). *ICA* Internal carotid artery, *ACP* anterior clinoid process, *ON* optic nerve, *OA* ophthalmic artery, *DS* diaphragma sellae, *CP* clinoid point, *DP* diaphragmatic point, *OP* optic point, *ACNE* anterior CSF notch extremity, *PCNE* posterior CSF notch extremity, *RP* roof of the cavernous sinus point

diaphragma sellae (DS), the ophthalmic artery (OA), the optic nerve (ON), and the carotid siphon (CS).

Reference points (Figs. 2, 3, 4) were anatomically correlated with the mediolateral and anteroposterior margins of the DDRP. The diaphragmatic point (DP) was at the borderline between the diaphragma sellae and the roof of the cavernous sinus. The clinoid point (CP) was at the medial ridge of the superior surface of the ACP. These two points corresponded, respectively, to the medial and lateral attachment of the dura extending between the diaphragma sellae and the ACP, and they represented the medial and lateral edges of the DDRP. The anterior and posterior CSF notches (ACN and PCN) were indirect markers formed by CSF, respectively between the optic nerve or the cavernous sinus roof and the anterior or posterior aspects of the ICA. They fitted closely to the anterior and posterior walls of the ICA in the paraclinoid region and stopped at the dural surface. So, the extremities of these notches represented the anterior and posterior edges of the DDRP: anterior and posterior CSF notch extremities (ACNE, PCNE). The optic point (OP) corresponded to the depression formed on the upper surface of the optic nerve at the level of the falciform ligament. It projected vertically at the anterior border of the DDRP. The cavernous sinus roof point or roof point (RP) was chosen on the retrocarotid surface of the cavernous sinus roof that separates the intradural space from the extradural intracavernous space. In this anatomical model, the DDRP was a curved plane passing through four radiological reference points: CP, DP, ACNE, and PCNE (Fig. 4).

Correlation lines (Figs. 2, 3) were used to radiologically project these reference points toward the catheter tip that represented the inferior level of the DDRP in the cadaveric model. The clinoid line (CL) passed through the CP and was drawn parallel or tangential to the first 0.5 mm segment of dura mater, extending inferomedially from the upper surface of the ACP toward the ICA. The diaphragmatic line (DL) passed through the DP and was drawn parallel or tangential to the extension of the dura mater lateral to the DP. The optic line (OL) passed through the OP and the ACNE. The roof line (RL) passed through the RP and the PCNE.

Correlation planes were selected for their accuracy in locating these anatomoradiological markers. The diaphragmatic plane (DIA-P) was a coronal plane perpendicular to the diaphragma sellae (Fig. 5). It is used in routine investigations for sellar, parasellar, and paraclinoid anomalies. The carotid plane (CAR-P), especially designed for the study, was a sagittal oblique plane, strictly anteroposterior and passing through the carotid siphon axis (Fig. 6). This axis was defined by both section centers of the carotid on the first slice posterior to the anterior carotid siphon knee. The anatomoradiological markers or lines were identified on each plane as follows: DIA-P (ACP, DS, OA, DP, CP, CL, DL) and CAR-P (ON, CS, OA, ACNE, PCNE, OP, RP,

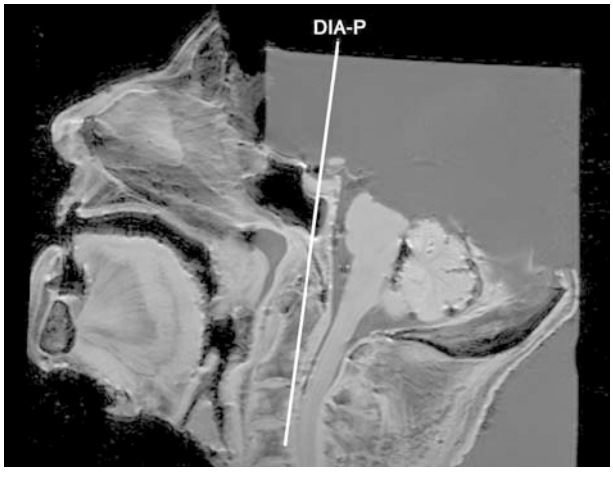

Fig. 5 The diaphragmatic plane

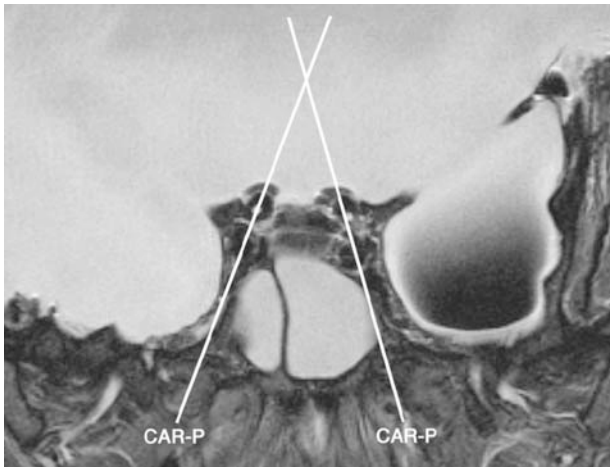

Fig. 6 The carotid planes

OL, RL). The angles corresponding to the CL–DL and OL–RL intersections were named, respectively, diaphragmatic and carotid correlation angles (DCA, CCA) according to the plane in which they were drawn (Figs. 2, 3).

Magnetic resonance imaging paraclinoid protocol

MRI were performed with a 1.5-T MR systems (1.5-T Vision, Siemens AG, Medical Solutions, Erlangen, Germany, and 1.5-T Signa Horizon LX 9.0, General Electric, GE Medical Systems, Milwaukee, WI, USA). A TSE-T2-weighted sequence (TR/TE: 5000/120 ms; nex: 2; contiguous slice thickness: 2.0-mm; field of view: 32 cm; matrix: 512×512) was chosen. Sections were obtained in three correlation planes: DIA-P, and right and left CAR-P.

Descriptive analysis

On cadaveric correlation models, we studied the visibility of the catheter tip, which was considered as identified when the tip quotation was "normal" (N) or "positive artifact" (A+, allowing identification of the catheter) and unidentified when quotation was "negative artifact" (A−, masking the catheter tip) or "invisible" (O). We analyzed the visibility (V+) or absence of visibility (V−) of regional markers, reference points, and correlation angles. Then, we determined whether the reference points or correlation angles identified were correlated (C+) to the DDRP or not (C−). The correlation lines were drawn on the slice where the catheter tip lay. They allowed the radiological projection of the reference points at the DDRP level materialized by the catheter tip. If the lines passed through or were tangent to the catheter tip, the corresponding reference points or correlation angle were considered as correlated. When a point was not identified, it was considered as not correlated as well as the corresponding correlation angle. On control subjects, we analyzed the V+ or V− of regional markers, reference points, and correlation angles. Data were reviewed independently by two observers (the author and an experienced neuroradiologist).

Statistical analysis

We studied the interobserver agreement using the kappa coefficient [38] for each item (number of catheter tips identified, number of markers identified, number of reference points identified and correlated, number of correlation angles drawn and correlated). The agreement was considered moderate, good, or excellent according to the respective kappa coefficient values: 0.41–0.60, 0.61–0.80, ≥0.81.

We compared the results obtained on the cadaveric correlation model with the results obtained on control subjects for each observer and for each correlation plane. The *t* test was applied to the number of markers identified. Fischer's exact test was applied to the visualization of each regional marker, of each reference point, and of each correlation angle.

Results

Cadaveric study

The cadaveric correlation model was built on both sides in 19 heads. In one specimen, we were unable to insert the catheter into the right ICA because of severe atherosclerosis. Considering the identification of the catheter tip (N, A+), the mean percentage was 95% in the DIA-P and 97% in the CAR-P, and the kappa coefficient was 1 (excellent agreement) in both correlation planes.

Mean percentages for global visualization frequencies of markers (all markers taken together and only reference points), for specific visualization or correlation frequencies of each marker or correlation angles, and kappa coefficient values for each item are summarized in Tables 1 and 2. In the DIA-P (Fig. 7), the global mean values of markers identified per side were 3.9 and 4 out of 5. The mean value of reference points identified per side was 1.9 out of 2 for both observers. In the CAR-P (Fig. 8), the global mean values of markers identified per side were 5.3 and 5.4 out of 7. The mean values of reference points identified per side were 3.4 and 3.5 out of 4. We identified all the reference points and thus drew the correlation angles in 87% of cases in the DIA-P and 60% in the CAR-P.

We found a radiological correlation between the DDRP and reference points in 65– 84% of cases in the DIA-P and 60–76% in the CAR-P. The correlation angles were drawn and correlated to the DDRP in 60% of cases in the DIA-P and 51% in the CAR-P. The lack of visibility of only one reference point was responsible for the correlation method failure in 33% of cases in the DIA-P and 60% in the CAR-P.

Table 1 Mean percentages for global visualization of the markers with corresponding kappa (K) coefficients (results are presented all sides taken together)

Global analysis			Cadaveric model		Control group	
Plane	Type	Nb	%	K	%	K
DIA-P	All markers	0–3	14	0.82	7	0.70
		4	74		37	
		5	12		56	
	Reference points	1	13	1	10	0.63
		2	87		90	
CAR-P	All markers	0–2	0	0.70	0	0.60
		3–4	15		2	
		5–7	85		98	
	Reference points	0–2	8	0.63	4	0.79
		3	32		16	
		4	60		80	

DIA-P diaphragmatic plane, *CAR-P* carotid plane

Control subjects study

Mean percentages for global visualization frequencies of markers (all markers taken together and only reference points), for specific visualization frequencies of each marker, and for visualization of correlation angles are summarized in Tables 1 and 2. In the DIA-P (Fig. 9), the global mean value of markers identified per side was 4.5 out of 5 for both observers. Mean value of reference points identified per side was 1.9 out of 2 for both observers. In the CAR-P (Fig. 10), the global mean values of markers identified per side were 6.3 and 6.4 out of 7. Mean values of reference points identified per side were 3.7 and 3.8 out of 4. Kappa coefficient values for each item are summarized in Tables 1 and 2. We identified all the reference points and thus drew the correlation angles in 90% of cases in the DIA-P and 80% in the CAR-P.

Control subjects study versus cadaveric study

In the DIA-P, the global visualization of regional markers was statistically better in patients than in cadaveric specimens ($p<0.05$). There was no significant difference in terms of global visualization of reference points or correlation angles and in terms of specific visualization of each

Table 2 Mean percentages for specific visualization and correlation of each marker and correlation angle with corresponding kappa (K) coefficients (results are presented all sides taken together)

Specific analysis		Cadaveric model								Control group			
		DIA-P				CAR-P				DIA-P		CAR-P	
Markers class	Type	V+		V+/C+		V+		V+/C+		V+		V+	
		%	K	%	K	%	K	%	K	%	K	%	K
Reference points	CP	100	nc	84	1	–	–	–	–	100	nc	–	–
	DP	87	1	65	0.88	–	–	–	–	90	0.63	–	–
	OP	–	–	–	–	100	nc	76	0.92	–	–	100	nc
	ACNE	–	–	–	–	97	1			–	–	95	0.65
	PCNE	–	–	–	–	91	0.84	60	0.79	–	–	85	0.87
	RP	–	–	–	–	60	0.74			–	–	95	0.65
Regional markers	ACP	100	nc	–	–	–	–	–	–	100	nc	–	–
	DS	94	0.79	–	–	–	–	–	–	100	nc	–	–
	OA	15	0.80	–	–	0	nc	–	–	60	0.72	67	0.70
	ON	–	–	–	–	100	nc	–	–	–	–	100	nc
	CS	–	–	–	–	88	0.87	–	–	–	–	100	nc
Correlation angles	DCA	87	1	60	0,94	–	–	–	–	90	0.63	–	–
	CCA	–	–	–	–	60	0.63	51	0,84	–	–	80	0.79

V+ visualized, *V+/C+* visualized + correlated, *V+K* interobserver agreement in terms of visualization, *V+/C+K* interobserver agreement in terms of correlation, *CP* clinoid point, *DP* diaphragmatic point, *OP* optic point, *ACNE* anterior CSF notch extremity, *PCNE* posterior CSF notch extremity, *RP* roof of the cavernous sinus point, *ACP* anterior clinoid process, *DS* diaphragma sellae, *OA* ophthalmic artery, *ON* optic nerve, *CS* carotid siphon, *DCA* diaphragmatic correlation angle, *CCA* carotid correlation angle, *nc* noncalculable (when a marker was always identified or nonidentified on every side by both observers, the kappa coefficient could not be calculated)

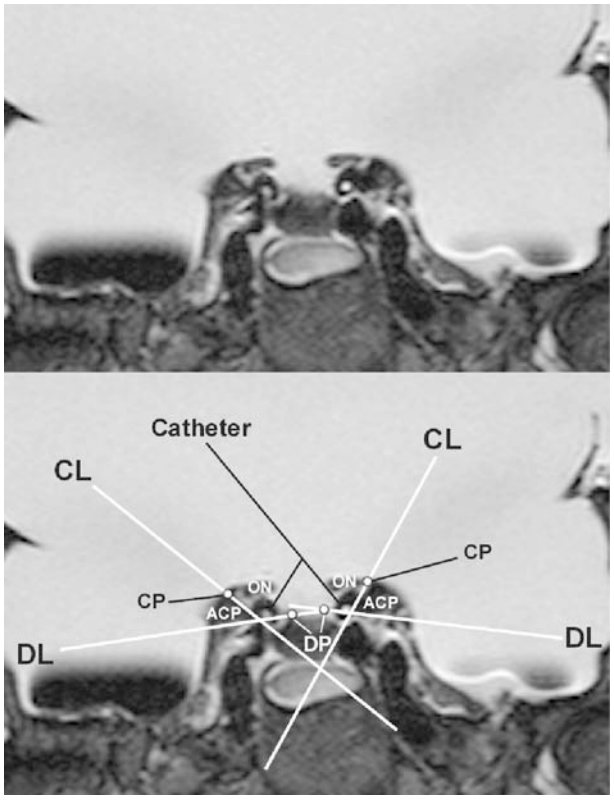

Fig. 7 MRI paraclinoid protocol of a cadaveric correlation model showing regional markers, reference points, and correlation lines in the diaphragmatic plane (DIA-P). *ACP* Anterior clinoid process, *ON* optic nerve, *CP* clinoid point, *DP* diaphragmatic point, *CL* clinoid line, *DL* diaphragmatic line. The catheter tip is correlated with the reference points

marker ($p>0.05$) excepted for the OA, which was more often identified in patients ($p<0.05$). In the CAR-P, the global visualization of regional markers and correlation angles was statistically better in patients than in cadaveric specimens ($p<0.05$). Concerning the global visualization of reference points, the difference was found to be significant by one observer ($p<0.05$) and nonsignificant by the other ($p>0.05$). There was no significant difference in terms of specific visualization of each marker ($p>0.05$) excepted for the RP and the OA, which were more often identified in patients ($p<0.05$).

Discussion

Review of the literature

Since Punt in 1979 [39], the origin of the ophthalmic artery on cerebral angiography is commonly used as the radiological marker of the junction between the intradural (extracavernous) and the extradural (intracavernous) ICA. Because of anatomic variations, this reliable marker may fail to locate precisely this junction in about 35% of cases. Indeed, the origin of the ophthalmic artery is extradural in 10% of cases [14, 15, 20, 37, 39] or arises within 1 mm (proximal origin) to 5 mm (distal origin) of the DDR in 24% of cases [14]. Since then, the neuroradiological location of the DDR has been a recurring concern. Some authors designed radiographic correlation techniques using some of the skull-base bone structures on lateral and anterior nonsubtracted angiography: the base of the ACP (Taptas [40]), the superior surface of the ACP, and the tuberculum sellae (Oikawa et al. [16]) or the planum sphenoidale and tuberculum sellae lines (Beretta [20]). Recent advances in neuroradiology allowed the development of modern protocols using three-dimensional computerized tomography (Gonzales et al. [41], three-dimensional computerized tomography angiography (Murayama et al. [42]), or three-dimensional contrast-medium-enhanced tomographic cisternography (Ito et al. [43]). These radiological procedures were respectively based on the visualization of the optic strut, on the identification of a surface concavity at the level of the DDR, and on the CSF cisterns contrast around the ICA. Although effective, these protocols did not take into account the complexity of the extravascular anat-

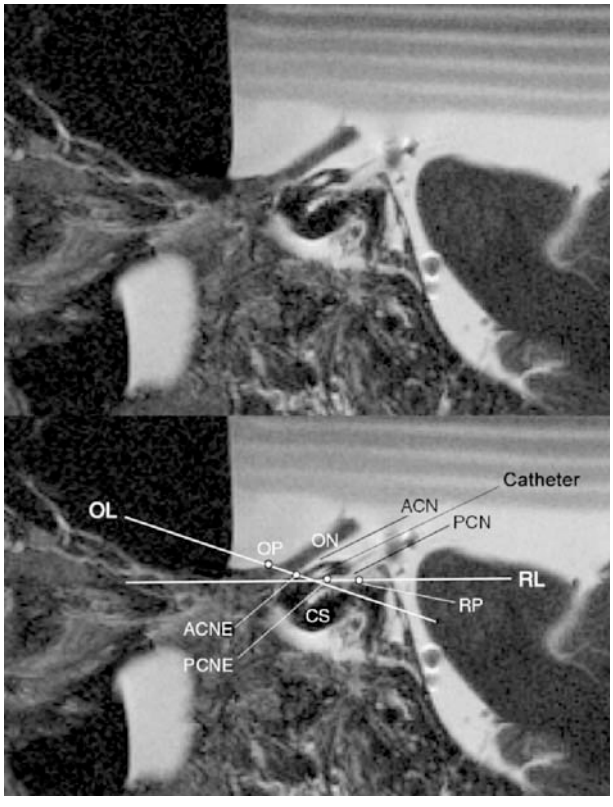

Fig. 8 MRI paraclinoid protocol of a cadaveric correlation model showing regional markers, reference points, and correlation lines in the carotid plane (CAR-P). *ON* Optic nerve; *CS* carotid siphon; *OP* optic point, *ACN* anterior CSF notch, *ACNE* anterior CSF notch extremity, *PCN* posterior CSF notch, *PCNE* posterior CSF notch extremity, *RP* roof of the cavernous sinus point, *OL* optic line; *RL* roof line. The catheter tip is correlated with the reference points

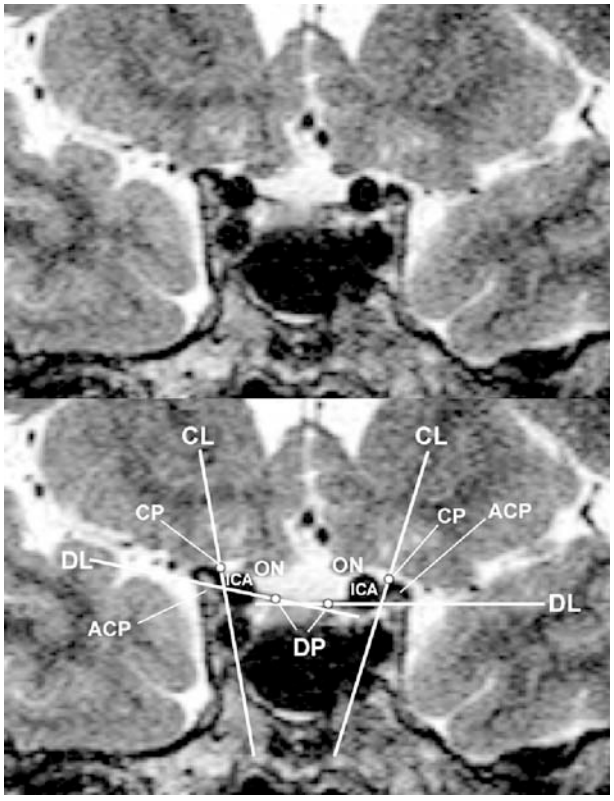

Fig. 9 MRI paraclinoid protocol of a control subject showing regional markers, reference points, and correlation lines in the diaphragmatic plane (DIA-P). *ICA* Internal carotid artery, *ACP* anterior clinoid process, *ON* optic nerve, *CP* clinoid point, *DP* diaphragmatic point, *CL* clinoid line, *DL* diaphragmatic line

omy of the paraclinoid region, particularly of the radiotransparent dural folds of the cavernous sinus walls. An indirect approach and interindividual radiological variability were the major limitations of those techniques.

MRI paraclinoid protocol and cadaveric correlation model

In this context, MRI appeared as an appropriate radiological technique for the study of the paraclinoid region anatomy. The spatial resolution on the 1.5-T MR system was sufficient to correctly identify on thin and contiguous slices the paraclinoid structures, even the dural folds of the cavernous sinus. This direct visualization releases the neuroradiologist from the interindividual variability encountered with other methods. The accuracy of the protocol was confirmed by satisfactory rates of visualization of the markers, correlation lines, or correlation angles and by the quality of the interobserver agreement (good to excellent) although only two observers reviewed the data (Tables 1 and 2). A T2-weighted MRI sequence was chosen to benefit from the high tissular contrast obtained between bone structures, dural folds, paraclinoid arteries, optic nerves, and the hyperintensity of the CSF cisterns and cavernous sinus content. The double inclination of the DDRP usually makes its radiological identification very difficult. In order to solve this problem, we explored the paraclinoid region using two orthogonal correlation planes in which we drew the correlation lines. The ICA was strictly followed along all its paraclinoid course owing to the creation of a new radiological study plane: the carotid plane (CAR-P).

The tissular contrast obtained in vivo (CSF notches) was reproduced in the cadaveric model after immersion in a water solution. Few modifications of anatomical relationship should be expected on formalin-fixed cadaver because of the natural rigidity of the paraclinoid structures (ACP and dural folds) that fixes the ICA and ON in position, even after catheterization. Comparable visualization rates of CSF notches between cadaver and living subjects seem to imply few modifications of the paraclinoid cisterns signal by CSF motion artifacts in vivo. So the reproducibility on MRI T2-weighted images of the paraclinoid markers was proven between the two groups (Table 2). Some of the

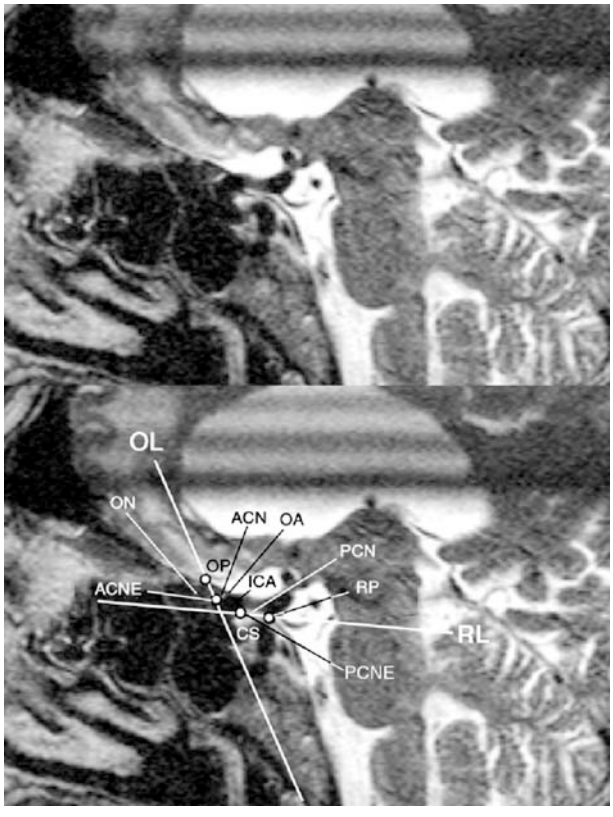

Fig. 10 MRI paraclinoid protocol of a control subject showing regional markers, reference points, and correlation lines in the carotid plane (CAR-P). *ON* Optic nerve, *ICA* internal carotid artery, *OA* ophthalmic artery, *CS* carotid siphon, *OP* optic point, *ACN* anterior CSF notch, *ACNE* anterior CSF notch extremity, *PCN* posterior CSF notch, *PCNE* posterior CSF notch extremity, *RP* roof of the cavernous sinus point, *OL* optic line, *RL* roof line

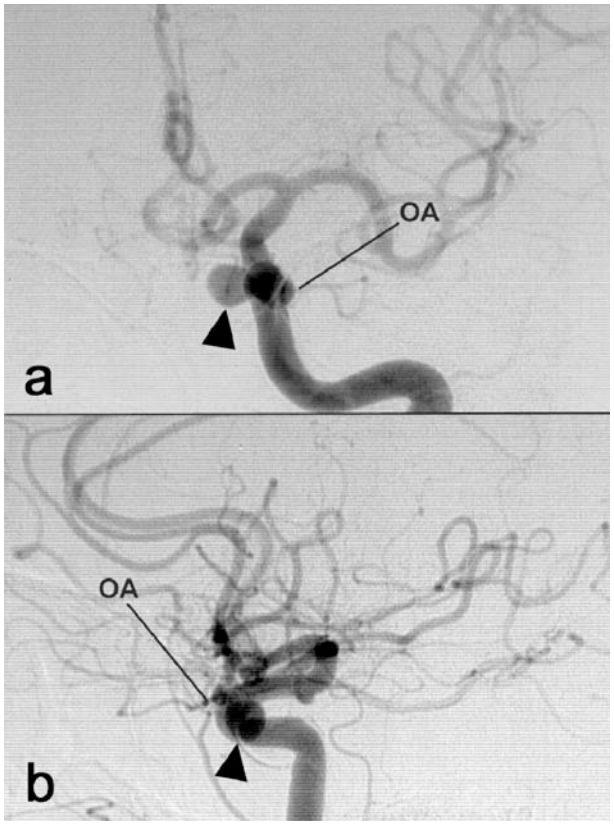

Fig. 11 Left anterior (**a**) and lateral (**b**) angiogram showing an aneurysm arising from the medial wall of the paraclinoid carotid artery and projecting below the origin of the ophthalmic artery (OA). *Arrowheads* indicate the aneurysm

markers were even easily identified in control subjects because of intravascular flow void (ophthalmic artery) or increased hypointensity of the dura mater (cavernous sinus roof).

Value of the proposed imaging method

Our MRI study allowed the development of a radiological correlation method between the DDRP and six anatomical reference points. The limit of our method lies in the necessity of identifying all those reference points. This was done in an acceptable proportion of sides in living subjects (90% in the DIA-P and 80% in the CAR-P). The corresponding correlation lines and angles bounded theoretically the inferior limits of the curve and slope of the DDRP. On cadaveric specimen, the correlation angles were drawn in 87% and 60% of cases and drawn/correlated to the DDRP in 60% and 51% of cases, respectively, in the DIA-P and in the CAR-P. Failure of the correlation method was related to a lack of visibility of just one reference point in 33% of cases in the DIA-P and 60% of cases in the CAR-P. But when an angle was identified, it was correlated to the DDRP in 68% of cases in the DIA-P and 78% of cases in the CAR-P. A higher tissular contrast in living subjects led to a statistically ($p<0.05$) better accuracy of the MRI paraclinoid protocol with the identification of the correlation angles in 90% of cases in the DIA-P and 80% in the CAR-P. Although we could not prove it directly in living subjects, we expected from these results a higher efficiency of the protocol for the DDRP level identification in vivo. That is why we propose to consider, when the correlation angles are identified, that they should approximate to the inferior inclusion limits of the DDRP in each correlation plane. We infer from this new concept that a point (or an aneurysm) situated below or above these correlation angles should be suspected to be located respectively in the extra- or intradural space.

With the perfecting of neuroradiological techniques, clinicians' and patients' demands in terms of diagnosis accuracy grows. The location of the DDR remains a critical problem for the therapeutic and technical management of paraclinoid aneurysms. The origin of the ophthalmic artery

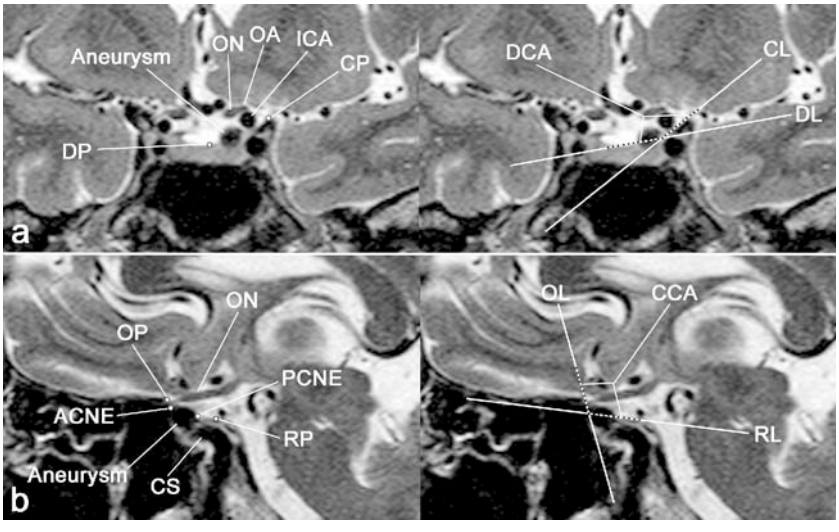

Fig. 12 MRI paraclinoid protocol in the diaphragmatic plane (DIA-P) (**a**) and in the carotid plane (CAR-P) (**b**). Half of the aneurysm is located above the diaphragmatic (DCA) and carotid correlation (CCA) angles: transitional aneurysm. *DP* Diaphragmatic point, *ON* optic nerve, *OA* ophthalmic artery, *ICA* internal carotid artery, *CP* clinoid point, *CL* clinoid line, *DL* diaphragmatic line, *ACNE* anterior CSF notch extremity, *OP* optic point, *ON* optic nerve, *PCNE* posterior CSF notch extremity, *RP* roof point, *CS* carotid siphon, *OL* optic line, *RL* roof line

on conventional or three-dimensional computerized cerebral angiography is usually a reliable marker of the DDR position. But in difficult cases, it might fail to position a small aneurysm on both sides of its plane. In those cases, the MRI paraclinoid protocol designed in this study should be considered as a noninvasive and complementary examination allowing a more accurate approximation of its location. Furthermore, this protocol provides a direct and precise overview of the anatomical relationship in the paraclinoid region, particularly important for planning of paraclinoid aneurysmal surgery.

Illustrative case

A 52-year-old woman complained of sudden headache. A CT scan of the brain found a right sylvian subarachnoid hemorrhage associated with a small posterior sylvian hemorrhagic infarct. Cerebral angiography disclosed aspects of unilateral Moya–Moya disease of the right middle cerebral artery and a left asymptomatic paraclinoid aneurysm (Fig. 11a, b). The aneurysm projected on the inferomedial part of the paraclinoid ICA below the origin of the ophthalmic artery and seemed to be completely extradural (intracavernous). The MRI paraclinoid protocol (Fig. 12a, b) proved that this aneurysm was transitional, with half of the sac being in the intradural (extracavernous) space. Because of the risk of subarachnoid rupture and the angioarchitectural aspects of the aneurysm, a decision of an endovascular treatment was made. Complete occlusion was obtained with endosaccular coil embolization.

Conclusions

This "MRI paraclinoid protocol" provides a direct overview of the paraclinoid region anatomy and a reliable identification of the DDR paraclinoid markers, allowing an approximation of the DDRP position. This complementary protocol will be very helpful each time we need to assess whether a paraclinoid aneurysm is located in the intradural space or not, which is of great importance in the management decision. Clinical benefits of this protocol will certainly be greater for small and asymptomatic paraclinoid aneurysms than for ruptured or giant aneurysms. After a short learning curve, the analysis of the MRI data may become a routine practice in an experienced neuroradiological team. A multicentric study should be conducted on a large group of patients to confirm the value of this technique. We propose to collect and analyze clinical, radiological (MRI paraclinoid protocol, cerebral angiography), and surgical (operative location) data. Contributors will be acknowledged and cited as coauthors in case of publication.

Acknowledgements We would like to thank Chadi Khalil for his contribution in the translation of this article.

References

1. al Rodhan NR, Piepgras DG, Sundt TM Jr (1993) Transitional cavernous aneurysms of the internal carotid artery. Neurosurgery 33:993–996
2. Andaluz N, Tew JM Jr (2003) Intradural aneurysm arising from the posterior genu of the cavernous carotid artery mimicking a posterior communicating aneurysm: case report. Neurosurgery 53:432–435
3. Day AL (1990) Aneurysms of the ophthalmic segment. A clinical and anatomical analysis. J Neurosurg 72:677–691
4. Heros RC (2002) Paraclinoid aneurysms. J Neurosurg 96:647–648
5. Kupersmith MJ, Hurst R, Berenstein A, Choi IS, Jafar J, Ransohoff J (1992) The benign course of cavernous carotid artery aneurysms. J Neurosurg 77:690–693
6. Linskey ME, Sekhar LN, Horton JA, Hirsch WL Jr, Yonas H (1991) Aneurysms of the intracavernous carotid artery: a multidisciplinary approach to treatment. J Neurosurg 75:525–534
7. Nagasawa S, Deguchi J, Arai M, Tanaka H, Kawanishi M, Ohta T (1997) Topographic anatomy of paraclinoid carotid artery aneurysms: usefulness of MR angiographic source images. Neuroradiology 39:341–343
8. Nutik S (1978) Carotid paraclinoid aneurysms with intradural origin and intracavernous location. J Neurosurg 48:526–533
9. Tanaka Y, Hongo K, Tada T, Nagashima H, Horiuchi T, Goto T, Koyama J, Kobayashi S (2002) Radiometric analysis of paraclinoid carotid artery aneurysms. J Neurosurg 96:649–653
10. Thornton J, Aletich VA, Debrun GM, Alazzaz A, Misra M, Charbel F, Ausman JI (2000) Endovascular treatment of paraclinoid aneurysms. Surg Neurol 54:288–299
11. White JA, Horowitz MB, Samson D (1999) Dural waisting as a sign of subarachnoid extension of cavernous carotid aneurysms: a follow-up case report. Surg Neurol 52:607–609
12. Wilms G, van Calenbergh F, Stockx L, Demaerel P, van Loon J, Goffin J (2000) Endovascular treatment of a ruptured paraclinoid aneurysm of the carotid syphon achieved using endovascular stent and endosaccular coil placement. AJNR Am J Neuroradiol 21:753–756
13. Zhang QJ, Kobayashi S, Toriyama T, Kyoshima K, Hongo K, Kuroyanagi T (1993) Angiographic differentiation of carotid cave aneurysms from ventral paraclinoid carotid aneurysms of Nutik type. Neurosurg Rev 16:283–289
14. Kim JM, Romano A, Sanan A, van Loveren HR, Keller JT (2000) Microsurgical anatomic features and nomenclature of the paraclinoid region. Neurosurgery 46:670–680

15. Kyoshima K, Oikawa S, Kobayashi S (2000) Interdural origin of the ophthalmic artery at the dural ring of the internal carotid artery. Report of two cases. J Neurosurg 92:488–489
16. Oikawa S, Kyoshima K, Kobayashi S (1998) Surgical anatomy of the juxtadural ring area. J Neurosurg 89:250–254
17. Seoane E, Rhoton AL Jr, de Oliveira E (1998) Microsurgical anatomy of the dural collar (carotid collar) and rings around the clinoid segment of the internal carotid artery. Neurosurgery 42:869–884
18. Umansky F, Valarezo A, Elidan J (1994) The superior wall of the cavernous sinus: a microanatomical study. J Neurosurg 81:914–920
19. Batjer HH, Kopitnik TA, Giller CA, Samson DS (1994) Surgery for paraclinoidal carotid artery aneurysms. J Neurosurg 80:650–658
20. Beretta F (2004) The paraclinoid aneurysms and the distal dural ring: a new classification. J Neurosurg Sci 48:161–175
21. Bouthillier A, van Loveren HR, Keller JT (1996) Segments of the internal carotid artery: a new classification. Neurosurgery 38:425–432
22. De Jesus O, Sekhar LN, Riedel CJ (1999) Clinoid and paraclinoid aneurysms: surgical anatomy, operative techniques, and outcome. Surg Neurol 51:477–487
23. Erturk M, Kayalioglu G, Govsa F (2004) Anatomy of the clinoidal region with special emphasis on the caroticoclinoid foramen and interclinoid osseous bridge in a recent Turkish population. Neurosurg Rev 27:22–26
24. Evans JJ, Hwang YS, Lee JH (2000) Pre- versus post-anterior clinoidectomy measurements of the optic nerve, internal carotid artery, and opticocarotid triangle: a cadaveric morphometric study. Neurosurgery 46:1018–1021
25. Gibo H, Kobayashi S, Kyoshima K, Hokama M (1988) Microsurgical anatomy of the arteries of the pituitary stalk and gland as viewed from above. Acta Neurochir (Wien) 90:60–66
26. Gibo H, Lenkey C, Rhoton AL Jr (1981) Microsurgical anatomy of the supraclinoid portion of the internal carotid artery. J Neurosurg 55:560–574
27. Hokama M, Hongo K, Gibo H, Kyoshima K, Kobayashi S (2001) Microsurgical anatomy of the ophthalmic artery and the distal dural ring for the juxta-dural ring aneurysms via the pterional approach. Neurol Res 23:331–335
28. Kakizawa Y, Tanaka Y, Orz Y, Iwashita T, Hongo K, Kobayashi S (2000) Parameters for contralateral approach to ophthalmic segment aneurysms of the internal carotid artery. Neurosurgery 47:1130–1136
29. Knosp E, Muller G, Perneczky A (1988) The paraclinoid carotid artery: anatomical aspects of a microneurosurgical approach. Neurosurgery 22:896–901
30. Kobayashi S, Kyoshima K, Gibo H, Hegde SA, Takemae T, Sugita K (1989) Carotid cave aneurysms of the internal carotid artery. J Neurosurg 70:216–221
31. Koyama T, Gibo H, Okudera H, Kobayashi S (2000) Computer generated microsurgical anatomy of the supraclinoid portion of the internal carotid artery. J Clin Neurosci 7:52–56
32. Krisht AF, Barrow DL, Barnett DW, Bonner GD, Shengalaia G (1994) The microsurgical anatomy of the superior hypophyseal artery. Neurosurgery 35:899–903
33. Nagasawa S, Ohta T, Tsuda E (1996) Surgical results and the related topographic anatomy in paraclinoid internal carotid artery aneurysms. Neurol Res 18:401–408
34. Nishihara M, Tamaki N (2001) Usefulness of volume-rendered three-dimensional computed tomographic angiography for surgical planning in treating unruptured paraclinoid internal carotid artery aneurysms. Kobe J Med Sci 47:221–230
35. Nishio S, Matsushima T, Fukui M, Sawada K, Kitamura K (1985) Microsurgical anatomy around the origin of the ophthalmic artery with reference to contralateral pterional surgical approach to the carotid-ophthalmic aneurysm. Acta Neurochir (Wien) 76:82–89
36. Reisch R, Vutskits L, Filippi R, Patonay L, Fries G, Perneczky A (2002) Topographic microsurgical anatomy of the paraclinoid carotid artery. Neurosurg Rev 25:177–183
37. Renn WH, Rhoton AL Jr (1975) Microsurgical anatomy of the sellar region. J Neurosurg 43:288–298
38. Cohen J (1960) A coefficient of agreement for nominal scales. Educ Psychol Meas 20:27–46
39. Punt J (1979) Some observations on aneurysms of the proximal internal carotid artery. J Neurosurg 51:151–154
40. Taptas JN (1979) Intradural and extradural ICA. J Neurosurg 51:877–878
41. Gonzalez LF, Walker MT, Zabramski JM, Partovi S, Wallace RC, Spetzler RF (2003) Distinction between paraclinoid and cavernous sinus aneurysms with computed tomographic angiography. Neurosurgery 52:1131–1137
42. Murayama Y, Sakurama K, Satoh K, Nagahiro S (2001) Identification of the carotid artery dural ring by using three-dimensional computerized tomography angiography. Technical note. J Neurosurg 95:533–536
43. Ito K, Hongo K, Kakizawa Y, Kobayashi S (2002) Three-dimensional contrast medium-enhanced computed tomographic cisternography for preoperative evaluation of surgical anatomy of intradural paraclinoid aneurysms of the internal carotid artery: technical note. Neurosurgery 51:1089–1092

Journal of Neuroradiology, 2006 Apr;33(2):115-20

LE PROTOCOLE D'IRM PARACLINOIDIEN: DISTINCTION ENTRE ARTERE CAROTIDE INTERNE INTRA- ET SUPRACAVERNEUSE. APPLICATION AUX ANEVRISMES PARACLINOIDIENS. NOTE TECHNIQUE.

L. THINES, C. DELMAIRE, D. LE GARS, J.P. PRUVO, J.P. LEJEUNE, P. LEHMANN,

J.P. FRANCKE

Clinique Neurochirurgicale (L.T., J.P.L.), Service de Neuroradiologie (C.D., J.P.P.) et Laboratoire d'Anatomie (J.P.F.), CHRU de Lille, France.

Service de Neurochirurgie (D.L.), Service de Neuroradiologie (P.L.) et Laboratoire d'Anatomie (D.L.), CHRU d'Amiens, France.

Correspondance à: Dr **Laurent Thines**, Clinique Neurochirurgicale, Hôpital Roger-Salengro, CHRU, 59037 Lille Cedex, France.

Tel : (33) 03 20 44 66 15 Fax : (33) 03 20 44 66 23 Email : Laurent.Thines@wanadoo.fr

RÉSUMÉ

But : le plan de l'anneau dural distal (PADD) sépare les portions intra- et supracaverneuse de l'artère carotide interne paraclinoïdienne. Le but de ce protocole d'IRM est d'évaluer la position de ce plan pour la localisation des anévrismes paraclinoïdiens.
Méthode : le protocole est basé sur une séquence T2 dans deux plans orthogonaux (plans diaphragmatique et carotidien) et sur deux droites de corrélation dans chaque plan. Ces droites passent par des points anatomo-radiologiques de référence corrélés aux limites médio-latérales et antéro-postérieures du PADD. Nous utilisons l'angle d'intersection de ces droites comme la limite radiologique inférieure du PADD.
Résultats : un anévrisme situé au dessus de cet angle est supracaverneux; un anévrisme situé en dessous de cet angle est intracaverneux; un anévrisme situé à cheval sur cet angle est transitionnel.
Conclusion : ce protocole d'IRM permettra de mieux situer de part et d'autre du toit du sinus caverneux les anévrismes paraclinoïdiens difficiles à localiser en angiographie.

Mots-clés : IRM, anévrisme, paraclinoïdien, anneau dural distal, artère carotide interne

SUMMARY

MRI paraclinoid protocol: distinction between intra and supracavernous internal carotid artery and application to paraclinoid aneurysms. Technical note.

Aim : the distal dural ring plane (DDRP) separates the intracavernous from the supracavernous paraclinoid internal carotid artery. The purpose of this MRI protocol is to evaluate the position of this plane for the location of paraclinoid aneurysms.
Method : the protocol uses a T2 weighted sequence in two orthogonal planes (diaphragmatic and carotid planes) and two correlation lines in each plane. These lines pass through anatomo-radiological reference points correlated with the medio-lateral and antero-posterior margins of the DDRP. We use the intersection angle of these lines as the inferior radiological limit of the DDRP curve.
Results : an aneurysm situated above this angle is supracavernous; an aneurysm situated below this angle is intracavernous; an aneurysm crossing this angle is transitional.
Conclusion : in difficult angiographical cases, this MRI protocol could help to locate paraclinoid aneurysms on both sides of the cavernous sinus roof.

Key words: MRI, aneurysm, paraclinoid, distal dural ring, internal carotid artery

INTRODUCTION

La prise en charge thérapeutique des anévrismes asymptomatiques de l'artère carotide interne paraclinoïdienne (ACIP) repose sur la connaissance de leur topographie par rapport au toit du sinus caverneux. Cette localisation détermine directement leur risque hémorragique et fixe donc les modalités de leur prise en charge.
Malgré les progrès récents des techniques de neuroradiologie [1, 3, 4, 7, 8, 12], l'analyse précise de la localisation de ce type d'anévrisme demeure difficile pour les équipes neurovasculaires. Dans la plupart des cas, c'est l'origine de l'artère ophtalmique en angiographie qui sert de repère [9]. Mais dans environ un tiers des cas, elle ne permet pas une localisation fiable (origine distale ou intra-caverneuse) [1, 5, 6, 9, 10]. La limite anatomique entre ACIP intra- et supra-caverneuse est représentée au niveau du toit du sinus caverneux par l'anneau dural distal [1, 2, 5, 8, 11, 14], qui n'est pas facilement repérable par les techniques d'imagerie habituelles.
C'est pourquoi nous avons développé un protocole d'IRM spécifique, appelé « protocole paraclinoïdien » permettant d'estimer la position du plan de cet anneau dural distal (PADD) [13].

METHODE

Paramètres de la séquence
L'étude a été réalisée sur une IRM de 1.5-T (1.5-T Vision, Siemens AG, Medical Solutions, Erlangen, Germany et 1.5-T Signa Horizon LX 9.0, General Electric, GE Medical Systems, Milwaukee, WI, USA).
Une séquence TSE-T2 a été choisie: TR/TE: 5000/120 ms; nex: 2; contiguous slice; thickness: 2.0-mm; field of view: 32 cm; matrix: 512 x 512.

Plans de coupe
Deux plans de coupe ont été sélectionnés. Un plan coronal perpendiculaire au diaphragme sellaire, le plan diaphragmatique *(figure 1)*, utilisé couramment pour l'exploration de la pathologie hypophysaire. Un plan sagittal oblique, le plan carotidien *(figure 2)*, spécialement développé pour cette étude et passant par l'axe du siphon carotidien. Cet axe est déterminé par les centres des deux sections du siphon carotidien sur la coupe située juste en arrière de son genou antérieur. Dans chacun des plans, nous avons défini les repères anatomo-radiologiques du PADD, appelés points de référence.

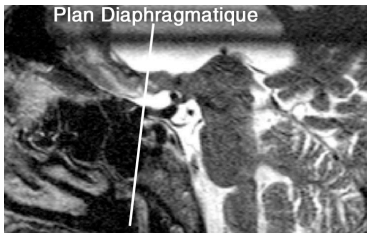

Figure 1- Le plan diaphragmatique
Diaphragmatic plane

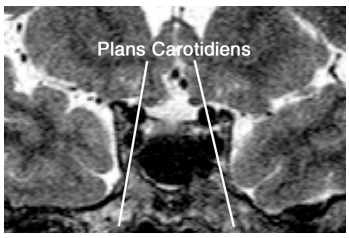

Figure 2- Les plans carotidiens
Carotid planes

Points de référence
Six points de référence, corrélés anatomiquement aux limites médio-latérales et antéro-postérieures du PADD ont été définis *(figure 3)*:

- Le point diaphragmatique (PD) est à la jonction entre toit du sinus caverneux et diaphragme sellaire. Il représente la limite médiale du PADD.
- Le point clinoïdien (PC) est situé sur le rebord médial de la face supérieure du processus clinoïde antérieur. Il représente la limite latérale du PADD.
- Le point optique (PO) représente la dépression faite à la face supérieure du nerf optique par le ligament falciforme et se projette verticalement au niveau de la limite antérieure de l'anneau dural distal.
- Les terminaisons des encoches de LCS antérieure (TELA) et postérieure (TELP). Ces encoches de LCS, visualisables sur la séquence T2, sont situées respectivement entre la face antérieure de l'ACIP et le nerf optique, et la face postérieure de l'ACIP et la partie postérieure du toit du sinus caverneux. Elles se terminent toutes les deux à la surface du toit du sinus caverneux et au contact des limites antérieure et postérieure de l'anneau dural distal.
- Le point du toit du sinus caverneux (PTSC) est choisi sur la surface rétro-carotidienne du toit du sinus caverneux.

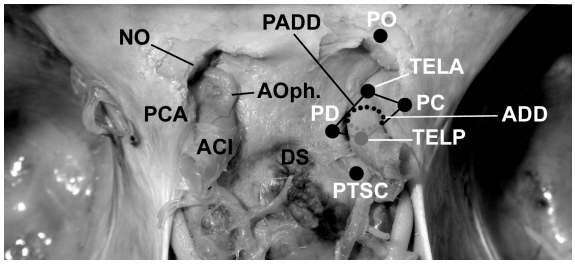

Figure 3- Vue supérieure de la région paraclinoïdienne et repères anatomo-radiologiques (nerfs optiques et chiasma sectionnés). **NO**: nerf optique; **PCA**: processus clinoïde antérieur; **ACI**: artère carotide interne; **AOph**.: artère ophtalmique; **DS**: diaphragme sellaire; **PC**: point clinoïdien; **PD**: point diaphragmatique; **PO**: point optique; **TELA**: terminaison de l'encoche de LCS antérieure; **TELP**: terminaison de l'encoche de LCS postérieure; **PTSC**: point du toit du sinus caverneux; **ADD**: anneau dural distal; **PADD**: plan de l'anneau dural distal

*Superior view of the paraclinoid region showing the location of the reference points (the optic nerves and chiasm are removed). **NO**: optic nerve; **PCA**: anterior clinoid process; **ACI**: internal carotid artery; **AOph**: ophthalmic artery; **DS**: diaphragma sellae; **PC**: clinoid point; **PD**: diaphragmatic point; **PO:** optic point; **TELA**: anterior CSF notch extremity; **TELP**: posterior CSF notch extremity; **PTSC**: roof of the cavernous sinus point; **ADD**: distal dural ring; **PADD**: distal dural ring plane*

Méthode de corrélation

Elle est basée sur la construction de deux droites de corrélation dans chaque plan. Les droites diaphragmatique et clinoïdienne passent dans le plan diaphragmatique respectivement par le PD et le PC, et sont tracées de façon tangentielle ou parallèle à la dure-mère du diaphragme sellaire et de la face médiale du processus clinoïde antérieur *(figure 4)*. Les droites optique et du toit du sinus caverneux passent dans le plan carotidien respectivement par les couples de points PO/TELA et TELP / PTSC *(figure 5)*.

L'angle d'intersection de chacun des couples de droites, dans chaque plan (angles de corrélation diaphragmatique et carotidien), représente alors l'estimation de la limite d'inclusion inférieure du PADD.

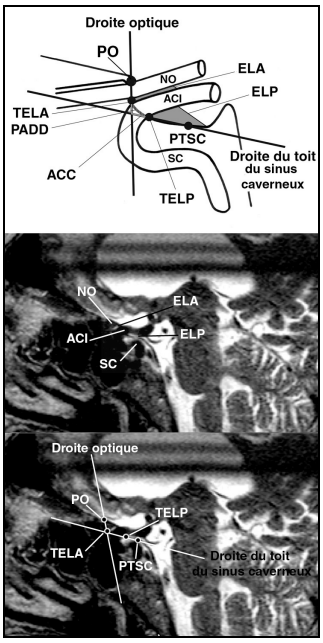

Figure 4- Schéma et IRM montrant les points de référence, les droites et angles de corrélation dans le plan diaphragmatique. **NO**: nerf optique; **Ao**: artère ophtalmique; **ACI**: artère carotide interne; **PCA**: processus clinoïde antérieur; **DS**: diaphragme sellaire; **PC**: point clinoïdien; **PD**: point diaphragmatique; **ACD**: angle de corrélation diaphragmatique; **PADD**: plan de l'anneau dural distal

*Diagram and MRI depicting the reference points, the correlation lines and angles in the diaphragmatic plane. **NO**: optic nerve; **Ao**: ophthalmic artery; **ACI**: internal carotid artery; **PCA**: anterior clinoid process; **DS**: diaphragma sellae; **PC**: clinoid point; **PD**: diaphragmatic point; **ACD**: diaphragmatic correlation angle; **PADD**: distal dural ring plane*

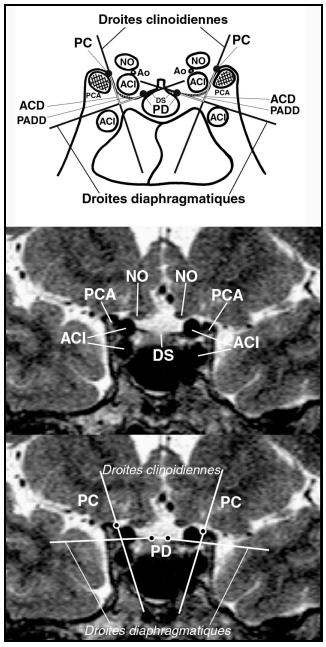

Figure 5- Schéma et IRM montrant les points de référence, les droites et angles de corrélation dans le plan carotidien. **NO**: nerf optique; **ACI**: artère carotide interne; **SC**: siphon carotidien; **PO**: point optique; **ELA**: encoche de LCS antérieure; **TELA**: terminaison de l'encoche de LCS antérieure; **ELP**: encoche de LCS postérieure; **TELP**: terminaison de l'encoche de LCS postérieure; **PTSC**: point du toit du sinus caverneux; **ACC**: angle de corrélation carotidien; **PADD**: plan de l'anneau dural distal

*Diagram and MRI depicting the reference points, the correlation lines and angles in the carotid plane. **NO**: optic nerve; **ACI**: internal carotid artery; **SC**: carotid siphon; **PO**: optic point; **ELA**: anterior CSF notch; **TELA**: anterior CSF notch extremity; **ELP**: posterior CSF notch; **TELP**: posterior CSF notch extremity; **PTSC**: roof of the cavernous sinus point; **ACC**: carotid correlation angle; **PADD**: distal dural ring plane*

APPLICATION AUX ANEVRISMES PARACLINOIDIENS

Le protocole d'IRM restitue les données perdues lors de l'angiographie concernant les rapports anatomiques de l'anévrisme *(représentation schématique: figures 6 et 7)*. La construction des angles de corrélation dans chaque plan permet d'estimer la localisation des anévrismes paraclinoïdiens par rapport au toit du sinus caverneux. Un anévrisme situé entièrement au dessus des deux angles de corrélation est considéré comme supracaverneux *(figure 8)*; un anévrisme situé entièrement en dessous des deux angles de corrélation est considéré comme intracaverneux *(figure 9)* ; un anévrisme situé à cheval sur les deux angles de corrélation est considéré comme transitionnel (intra- et supracaverneux) *(figure 10)*.

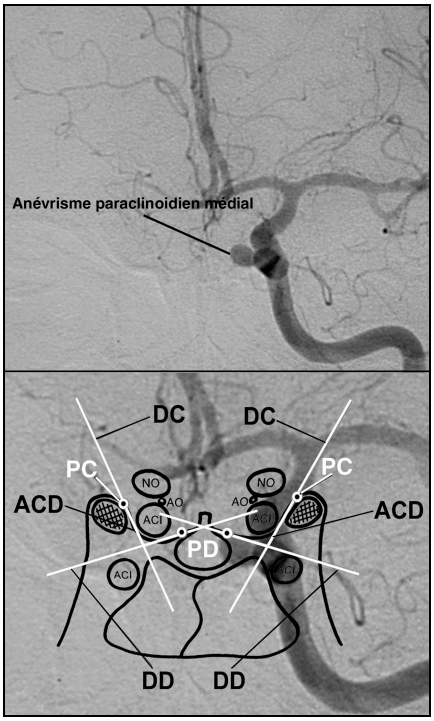

Figure 6- Superposition du schéma de corrélation diaphragmatique sur une angiographie de face d'un anévrisme paraclinoïdien gauche intracaverneux (en dessous de l'angle de corrélation diaphragmatique). **DC**: droite clinoïdienne; **DD**: droite diaphragmatique; **PC**: point clinoïdien; **PD**: point diaphragmatique; **NO**: nerf optique; **ACI**: artère carotide interne; **Ao**: artère ophtalmique; **ACD**: angle de corrélation diaphragmatique

Superimposition of the diaphragmatic correlation diagram on the angiography (anterior view) of a left intracavernous paraclinoid aneurysm (below the correlation angle).
***DC**: clinoid line; **DD**: diaphragmatic line; **PC**: clinoid point; **PD**: diaphragmatic point; **NO**: optic nerve; **ACI**: internal carotid artery; **Ao**: ophthalmic artery; **ACD**: diaphragmatic correlation angle*

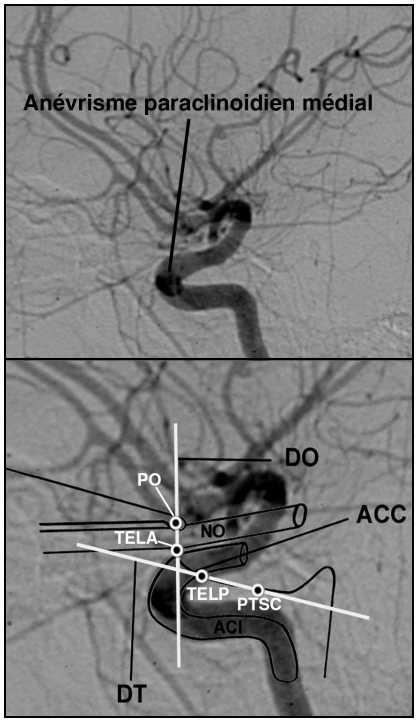

Figure 7- Superposition du schéma de corrélation carotidien sur une angiographie de profil d'un anévrisme paraclinoïdien gauche intracaverneux (en dessous de l'angle de corrélation carotidien). **DO**: droite optique; **DT**: droite du toit du sinus caverneux; **PO**: point optique; **TELA**: terminaison de l'encoche de LCS antérieure; **TELP**: terminaison de l'encoche de LCS postérieure; **PTSC**: point du toit du sinus caverneux; **NO**: nerf optique; **ACI**: artère carotide interne; **ACC**: angle de corrélation carotidien

Superimposition of the carotid correlation diagram on the angiography (lateral view) of a left intracavernous paraclinoid aneurysm (below the correlation angle). ***DO**: optic line; **DT**: roof line; **PO**: optic point; **TELA**: anterior CSF notch extremity; **TELP**: posterior CSF notch extremity; **PTSC**: roof of the cavernous sinus point; **NO**: optic nerve; **ACI:** internal carotid artery; **ACC**: carotid correlation angle*

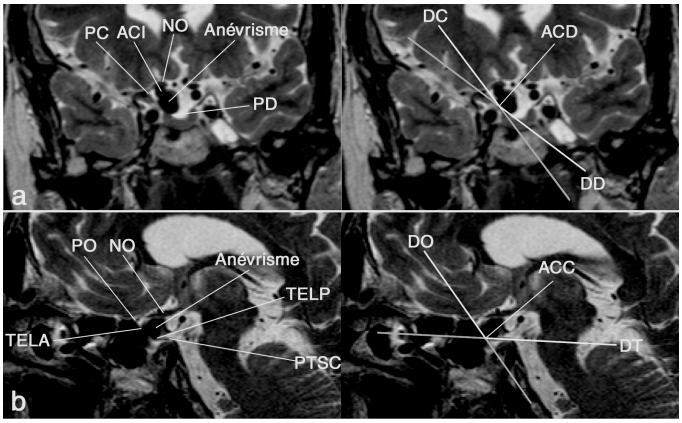

Figure 8- Anévrisme supracaverneux, situé au dessus des deux angles de corrélation. a- plan diaphragmatique ; b- plan carotidien. **ACI**: artère carotide interne; **NO**: nerf optique; **PC**: point clinoïdien; **PD**: point diaphragmatique; **PO**: point optique; **TELA**: terminaison de l'encoche de LCS antérieure; **TELP**: terminaison de l'encoche de LCS postérieure; **PTSC**: point du toit du sinus caverneux; **DC**: droite clinoïdienne; **DD**: droite diaphragmatique; **DO**: droite optique; **DT**: droite du toit; **ACD**: angle de corrélation diaphragmatique; **ACC**: angle de corrélation carotidien

*Supracavernous aneurysm, above the correlation angles. a- diaphragmatic plane ; b- carotid plane. **ACI**: internal carotid artery; **NO**: optic nerve; **PC**: clinoid point; **PD**: diaphragmatic point; **PO**: optic point; **TELA**: anterior CSF notch extremity; **TELP**: posterior CSF notch extremity; **PTSC**: roof of the cavernous sinus point; **DC**: clinoid line; **DD**: diaphragmatic line; **DO**: optic line; **DT**: roof line; **ACD**: diaphragmatic correlation angle; **ACC**: carotid correlation angle*

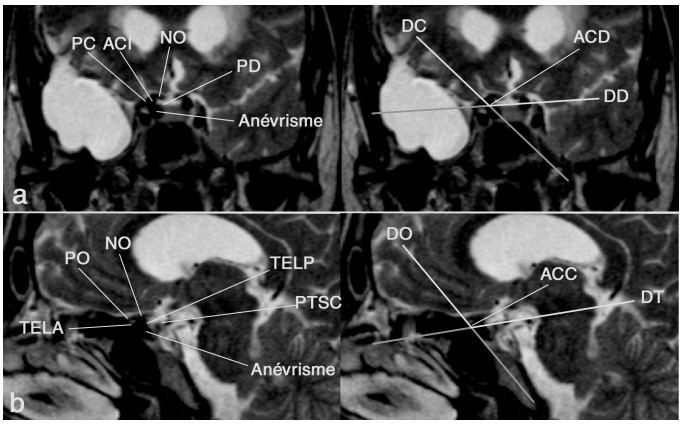

Figure 9- Anévrisme intracaverneux, situé en dessous des deux angles de corrélation. a- plan diaphragmatique ; b- plan carotidien. **ACI**: artère carotide interne; **NO**: nerf optique; **PC**: point clinoïdien; **PD**: point diaphragmatique; **PO**: point optique; **TELA**: terminaison de l'encoche de LCS antérieure; **TELP**: terminaison de l'encoche de LCS postérieure; **PTSC**: point du toit du sinus caverneux; **DC**: droite clinoïdienne; **DD**: droite diaphragmatique; **DO**: droite optique; **DT**: droite du toit; **ACD**: angle de corrélation diaphragmatique; **ACC**: angle de corrélation carotidien

*Intracavernous aneurysm, below the correlation angles. a- diaphragmatic plane ; b- carotid plane. **ACI**: internal carotid artery; **NO**: optic nerve; **PC**: clinoid point; **PD**: diaphragmatic point; **PO**: optic point; **TELA**: anterior CSF notch extremity; **TELP**: posterior CSF notch extremity; **PTSC**: roof of the cavernous sinus point; **DC**: clinoid line; **DD**: diaphragmatic line; **DO**: optic line; **DT**: roof line; **ACD**: diaphragmatic correlation angle; **ACC**: carotid correlation angle*

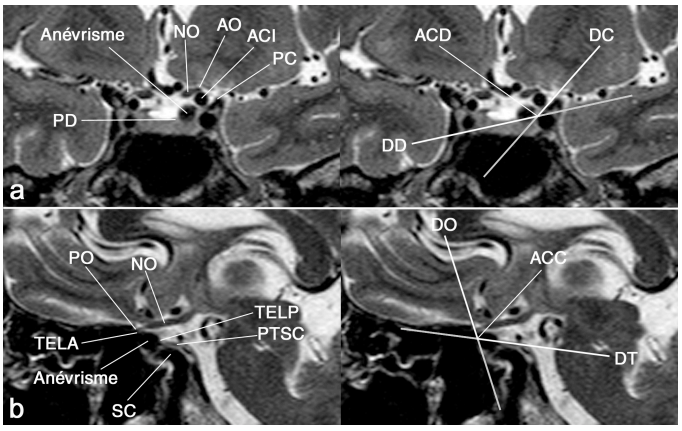

Figure 10- Anévrisme transitionnel, situé à cheval sur les deux angles de corrélation. a- plan diaphragmatique ; b- plan carotidien. **ACI**: artère carotide interne; **NO**: nerf optique; **AO**: artère ophtalmique; **SC**: siphon carotidien; **PC**: point clinoïdien; **PD**: point diaphragmatique; **PO**: point optique; **TELA**: terminaison de l'encoche de LCS antérieure; **TELP**: terminaison de l'encoche de LCS postérieure; **PTSC**: point du toit du sinus caverneux; **DC**: droite clinoïdienne; **DD**: droite diaphragmatique; **DO**: droite optique; **DT**: droite du toit; **ACD**: angle de corrélation diaphragmatique; **ACC**: angle de corrélation carotidien ;

*Transitional aneurysm, crossing the correlation angles. a- diaphragmatic plane ; b- carotid plane. **ACI**: internal carotid artery; **NO**: optic nerve; **AO**: ophthalmic artery;* **SC**: carotid siphon; ***PC**: clinoid point; **PD**: diaphragmatic point ; **PO**: optic point ; **TELA**: anterior CSF notch extremity ; **TELP**: posterior CSF notch extremity; **PTSC**: roof of the cavernous sinus point; **DC**: clinoid line; **DD**: diaphragmatic line; **DO**: optic line; **DT**: roof line; **ACD**: diaphragmatic correlation angle; **ACC**: carotid correlation angle*

CONCLUSION

Ce protocole d'IRM paraclinoïdien permet une analyse anatomique précise de la région paraclinoïdienne et une estimation fiable de la position de l'anneau dural distal et donc de la limite entre artère carotide interne intra- et supracaverneuse. Cet examen complémentaire est très utile pour localiser les anévrismes paraclinoïdiens de part et d'autre du toit du sinus caverneux, ce qui est d'une grande importance pour le choix thérapeutique de cette pathologie. C'est sur la base de ce protocole que nous proposons de mener une étude prospective comparant IRM et angiographie pour la prise en charge des patients porteurs d'anévrismes paraclinoïdiens.

REFERENCES

1. Beretta F. The paraclinoid aneurysms and the distal dural ring: a new classification. J Neurosurg Sci 2004;48:161-175
2. Bouthillier A, van Loveren HR, Keller JT. Segments of the internal carotid artery: a new classification. Neurosurgery 1996;38:425-432
3. Gonzalez LF, Walker MT, Zabramski JM, Partovi S, Wallace RC, Spetzler RF. Distinction between paraclinoid and cavernous sinus aneurysms with computed tomographic angiography. Neurosurgery 2003;52:1131-1137
4. Ito K, Hongo K, Kakizawa Y, Kobayashi S. Three-dimensional contrast medium-enhanced computed tomographic cisternography for preoperative evaluation of surgical anatomy of intradural paraclinoid aneurysms of the internal carotid artery: technical note. Neurosurgery 2002;51:1089-1092
5. Kim JM, Romano A, Sanan A, van Loveren HR, Keller JT. Microsurgical anatomic features and nomenclature of the paraclinoid region. Neurosurgery 2000;46:670-680
6. Kyoshima K, Oikawa S, Kobayashi S. Interdural origin of the ophthalmic artery at the dural ring of the internal carotid artery. Report of two cases. J Neurosurg 2000;92:488-489
7. Murayama Y, Sakurama K, Satoh K, Nagahiro S. Identification of the carotid artery dural ring by using three-dimensional computerized tomography angiography. Technical note. J Neurosurg 2001;95:533-536
8. Oikawa S, Kyoshima K, Kobayashi S. Surgical anatomy of the juxta-dural ring area. J Neurosurg 1998;89:250-254
9. Punt J. Some observations on aneurysms of the proximal internal carotid artery. J Neurosurg 1979;51:151-154
10. Renn WH, Rhoton AL, Jr. Microsurgical anatomy of the sellar region. J Neurosurg 1975;43:288-298
11. Seoane E, Rhoton AL, Jr., de Oliveira E. Microsurgical anatomy of the dural collar (carotid collar) and rings around the clinoid segment of the internal carotid artery. Neurosurgery 1998;42:869-884
12. Taptas JN. Intradural and extradural ICA. J Neurosurg 1979;51:877-878
13. Thines L, Delmaire C, Le Gars D, Pruvo JP, Lejeune JP, Lehmann P, Francke JP. MRI location of the distal dural ring plane : anatomo-radiological study and application to paraclinoid carotid artery aneurysms. Eur Radiol 2005 (In press)
14. Umansky F, Valarezo A, Elidan J. The superior wall of the cavernous sinus: a microanatomical study. J Neurosurg 1994;81:914-920

ORIGINAL RESEARCH

Usefulness of MRI for the Assessment of Nonophthalmic Paraclinoid Aneurysms

AQ: A

L. Thines
J.-Y. Gauvrit
X. Leclerc
D. Le Gars
C. Delmaire
J.-P. Pruvo
J.-P. Lejeune

BACKGROUND AND PURPOSE: The neuroradiologic location of asymptomatic paraclinoid aneurysms is decisive for patient management. In a preliminary study, we designed a paraclinoid MR protocol (PMP) including high-resolution T2-weighted images in 2 orthogonal planes to define the inferior limit of the distal dural ring plane that represents the borderline between the intradural and extradural internal carotid artery (ICA). In this clinical study, we compared this protocol with digital subtraction angiography (DSA) for the location of paraclinoid aneurysms.

MATERIALS AND METHODS: During a 3-year period, we performed PMP and conventional angiograms in 14 consecutive patients with 17 asymptomatic paraclinoid aneurysms. Ophthalmic (superior) aneurysms were excluded. Two independent observers reviewed MR imaging data, and a third experienced neuroradiologist analyzed the conventional angiograms. MR imaging and conventional angiograms were independently analyzed, and interpretations obtained with each technique were compared.

RESULTS: PMP allowed correct visualization of the aneurysms in all patients. No significant differences ($P > .05$) were found between the DSA and PMP for the measurement of the aneurysmal neck or sac. Interobserver agreement was good. MR imaging was discordant with conventional angiography regarding the position around the cavernous sinus of the aneurysmal neck and sac in 5 cases. PMP images were helpful for treatment decisions in 4 cases.

CONCLUSION: PMP is an interesting tool that might be used in association with conventional angiography for the assessment of paraclinoid aneurysms.

Paraclinoid aneurysms (PA) represent only 5% to 11% of asymptomatic intracranial aneurysms.[1-5] The main goal of the treatment is to prevent subarachnoid hemorrhage (SAH) from aneurysmal rupture, which is associated to high rates of morbidity and mortality.[6] Asymptomatic extradural (intracavernous) aneurysms are at lower risk of subarachnoid hemorrhage than transitional or intradural aneurysms (1.4% of SAH and exceptional cataclysmic epistaxis)[7]. However, they can result in mass effect (cranial neuropathies), carotid-cavernous fistulas, or distal embolization when partly fusiform. Conversely, the rupture of an intradural (supracavernous) aneurysm is life threatening. The precise location of PA on both sides of the roof of the cavernous sinus is of great importance for patient management. The distal dural ring is the anatomic limit between the intracavernous and supracavernous internal carotid artery (ICA). Unfortunately, the distal dural ring is not easily identifiable because of its small size. We developed a paraclinoid MR protocol (PMP), which allows us to estimate the position of the distal dural ring plane. This protocol was validated previously with use of correlations between a cadaveric model and MR imaging.[8,9] Our study compares the PMP with digital subtraction angiography (DSA) in clinical conditions.

Materials and Methods

Patients and Selection of Aneurysms

We evaluated PMP in 14 consecutive female patients (median age, 45± 14 years) harboring 17 asymptomatic PA between June 2002 and June 2005. PA were defined as aneurysms arising from the C4, C5, or C6 segments according to the Bouthillier classification of the ICA segments.[10] We studied carotid-cave projecting aneurysms (arising from the medial wall of the ICA, most often at the level of the origin of the superior hypophyseal artery), high-located, cavernous, subclinoid, and low-located posterior carotid aneurysms. Giant aneurysms and purely anterior (superior or "carotid-ophthalmic") aneurysms were excluded.

Angiographic Technique and Classification

We performed conventional angiograms on an Integris Allura V5000 (Philips Medical Systems, Best, the Netherlands) using the propeller rotation technique.[11] We then performed postprocessing of dynamic angiographic data, including volume rendering, using the Integris workstation (Philips Medical Systems).

The orientation of the aneurysmal neck and sac was determined according to the angiographic classification described by De Jesus et al.[2] as follows: we distinguished medial or lateral projections on the anterior view and anterior or posterior projections on the lateral view. To locate on DSA the aneurysmal neck and sac in comparison with the roof of the cavernous sinus and to ensure the reproducibility of the method, we chose the limit represented by the horizontal line passing through the origin of the ophthalmic artery on the lateral and anterior views. We classified the aneurysmal neck and sac as supracavernous, above the ophthalmic line; transitional, crossing the ophthalmic line; and intracavernous, beneath the ophthalmic line. Cases with an obvious intracavernous origin of the ophthalmic artery were excluded.

Paraclinoid MR Protocol

Brain MR imaging was performed on a 1.5T MR system (Vision; Siemens, Erlangen, Germany). A turbo spin-echo T2-weighted sequence (TR, 5000 ms; TE, 120 ms; NEX, 2; contiguous section thickness, 2.0 mm; field of view, 32 cm; matrix, 512 × 512) was performed. For each aneurysm, we obtained sections in 2 planes: a coronal plane perpendicular to the diaphragma sellae (so-called diaphragmatic

Received December 7, 2006; accepted after revision May 13, 2007.

Departments of Neurosurgery (L.T., J.-P.L.) and Neuroradiology (J.-Y.G., X.L., C.D., J.-P.P.), Centre Hospitalier Régional et Universitaire, Lille, France; Departments of Neurosurgery and Anatomy (D.L.), Centre Hospitalier Régional et Universitaire, Amiens, France.

Please address correspondence to Dr. Thines Laurent, Clinique Neurochirurgicale, Hôpital Roger-Salengro, CHRU, 59037 Lille Cedex, France; e-mail: laurent.thines@ wanadoo.fr

DOI 10.3174/ajnr.A0734

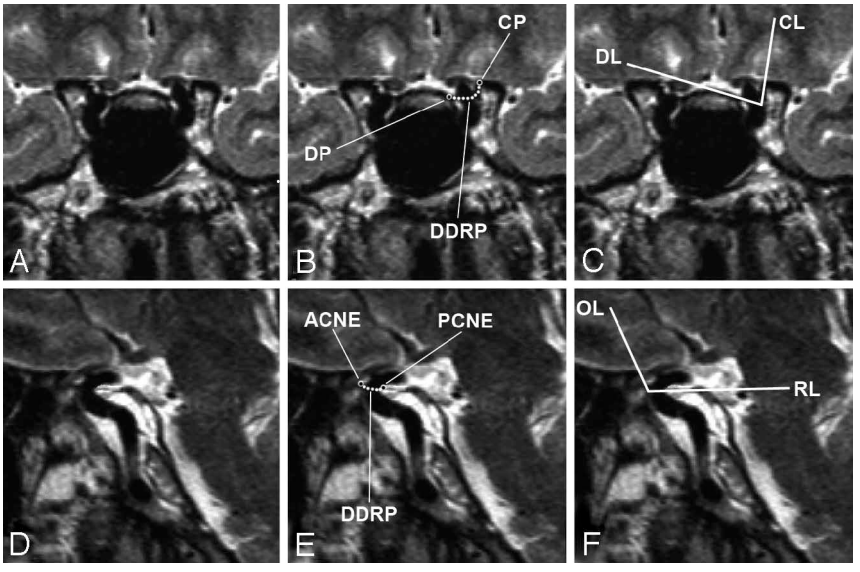

Fig 1. Paraclinoid MR protocol in a control subject showing the 4 reference points. The 4 lines and their angles of intersection correlated with the limits of the distal dural ring plane in each cutting plane. *A, B, C,* Paraclinoid region in the diaphragmatic plane. *D, E, F,* Paraclinoid region in the carotid plane. DP indicates diaphragmatic point; CP, clinoid point; DL, diaphragmatic line; CL, clinoid line, ACNE, anterior CSF notch extremity; PCNE, posterior CSF notch extremity; OL, optic line; RL, roof line, DDRP, distal dural ring plane (*dotted curve*).

plane) and a sagittal oblique plane, strictly anteroposterior passing through the axis of the carotid siphon (so-called carotid plane).

In preliminary studies, we defined the reference points, correlation lines, and angles that correlated with the limits of the distal dural ring plane in both cutting planes.[8,9] We used 40 paraclinoid regions (dissected from 20 formalin-fixed human cadaveric heads) to correlate the MR data with a cadaveric model. In our study, the PMP angles allowed us to accurately locate the distal dural ring plane in the diaphragmatic and carotid planes in 70% and 80% of the cases, respectively.

In our study, we propose a simple and practical method allowing the use of the PMP protocol in clinical practice (Fig 1). The distal dural ring plane is a curved plane passing through 4 radiologic reference points: the diaphragmatic point (in the diaphragmatic plane) at the borderline between the diaphragma sellae and the roof of the cavernous sinus; the clinoid point (in the diaphragmatic plane) at the medial ridge of the superior surface of the anterior clinoid process; the anterior and posterior CSF (CSF) notches extremity (in the carotid plane); and indirect markers formed by CSF cisterns around the ICA, respectively, between the optic nerve or the roof of the cavernous sinus and the anterior or posterior aspects of the ICA. The inferior limit of the distal dural ring plane is estimated in each cutting plane by the intersection angle formed by the lines passing through these 4 points. Rapid and simple drawing of those 4 lines can be achieved as follows: diaphragmatic line (through the diaphragmatic point); clinoid line (through the clinoid point); and roof line (through the posterior CSF notch extremity), respectively, tangential to the diaphragma sellae, the inner dural surface of the anterior clinoid process and the cavernous sinus roof, and optic line (through the anterior CSF notch extremity) perpendicular to the optic nerve at the level of its penetrating point in the optic canal.

We determined the orientation of the aneurysmal neck and sac compared with the ICA by distinguishing medial or lateral projections in the diaphragmatic plane, and anterior or posterior projections in the carotid plane.

The MR positioning of the aneurysmal neck and sac compared with the roof of the cavernous sinus was based on their relationship with each intersection angle in both planes as follows: supracavernous (above both intersection angles), transitional (crossing 1 or both intersection angles), and intracavernous (beneath both intersection angles).

Treatment of the Aneurysms

All cases of asymptomatic aneurysms at our institution are managed by a multidisciplinary neurovascular team. For PA, we took into account principally the location of the aneurysmal sac, the history of a previous SAH, and the ages of the patients. When the sac was intracavernous, we chose conservative management. For a transitional or supracavernous sac, embolization or surgery was usually required because of the risk of hemorrhage. An exception was made for some of the transitional or supracavernous aneurysms that were too small ($<$1–2 mm) for endovascular or surgical treatment, or for those aneurysms associated with carotid dysplasia.

Descriptive Analysis

Epidemiologic data for each patient was documented. Angiograms were reviewed on films from anterior, lateral, and 3D views by an experienced neuroradiologist specialized in endovascular treatment of the cerebral aneurysms (X.L.). MR imaging data were reviewed independently by 2 investigators (L.T., J.-Y.G.). We measured the ratio of the neck and sac of each aneurysm and assessed the projection of the aneurysmal neck and sac around the ICA (anterior, posterior, medial, lateral) and their locations regarding the roof of the cavernous sinus. Therapeutic modalities of the management for each patient were recorded. For patients in whom an operation was performed, we took operative field shots to make radiologic-surgical correlations.

Statistical Analysis

The angiographic and MR imaging results in terms of measurement of the sac and neck, and the sac-to-neck ratio were compared with the *t* test. The intrinsic validity of the PMP was evaluated with aneurysmal measurement (sac, neck, and sac-to-neck ratio) with the *t* test and interobserver agreement for the aneurysmal projection around the ICA and location around the roof of the cavernous sinus with the κ coefficient. The agreement was considered as low, moderate, good, or excellent according to the respective κ coefficient values: $\leq$0.40, 0.41–0.60, 0.61–0.80, $\geq$0.81. A P value $<$.05 was regarded as significant.

Results

General Data

Fourteen patients (17 PA) were enrolled in the study. After angiography, most patients were found to have at least 1 additional vascular disease: 10 patients with at least 1 associated aneurysm (1 dysplasia) and 1 patient each with contralateral Moyamoya disease and contralateral arteriovenous malformation. Seventeen associated aneurysms were found: carotid-ophthalmic (5), posterior carotid (5), PA (3), basilar (2), middle cerebral artery (1), and proximal ICA (1). Ten PA were incidentally discovered, and 7 were diagnosed after SAH as a result of an associated vascular disease.

Angiographic Results

We performed DSA with 3D-reconstructions on most of the PA (14/17). The mean sizes of the necks and sacs were 3.1 ± 1 mm and 5.9 ± 4 mm, respectively. The mean sac-to-neck ratio was 1.9 ± 0.9. Seven PA were located in the intracavernous position, 8 were transitional, and 2 were supracavernous.

MR Imaging Results

The mean sizes of the necks and sacs were 3.5 ± 1.3 to 1.4 mm and 6.2 to 6.3 ± 3.8 mm, respectively. The mean sac-to-neck ratio was 1.8 ± 0.7. Six PA were located in an intracavernous position, 7 were transitional, and 4 were supracavernous. No significant differences ($P > .05$) were found between the investigators for the measurement of the aneurysmal neck or sac. The interobserver agreement for the projections of the aneurysmal neck or sac ($\kappa = 0.87{:}1$) and for the location of PA around roof of the cavernous sinus ($\kappa = 1$) were "excellent."

Treatment of the Aneurysms

Ten PA including 6 intracavernous and 4 transitional or supracavernous—but very small (<2 mm) or associated with severe intracranial arterial dysplasia—were managed conservatively. Six patients with PA underwent endovascular treatment because of the supracavernous (2 cases) and transitional (4 cases) locations of the sac in young patients or in patients with previous SAH. One patient underwent direct surgical treatment of PA.

Surgical Results

A young patient was operated on after failure of coil embolization for a supracavernous aneurysm, which was revealed by the rupture of an associated aneurysm (case 14). Another patient was operated on for a carotid-ophthalmic aneurysm (superior location) associated with an intracavernous PA (case 16). In both cases, the aneurysmal locations provided by the PMP were similar to the surgical findings. The first aneurysm
F2 was supracavernous and was clipped (Fig 2). The second was not seen after full dissection of the paraclinoid region down to the distal dural ring and was supposed to be intracavernous.

Comparison between the PMP and DSA

No significant difference ($P > .05$) was found between DSA and the PMP for the measurement of the aneurysmal necks or
T1 sacs (table). In 9 cases (2, 5, 7–9, 11–13, and 16), DSA and the
F5 PMP gave the same aneurysmal location (Figs 3, 4 and 5). Interpretations on DSA in cases 1, 3, and 6 were different from the PMP for the locations of the neck or sac. Interpretations on DSA in cases 4, 10, 14, 15, and 17 were different from the PMP for the locations of the neck and sac (Fig 2).

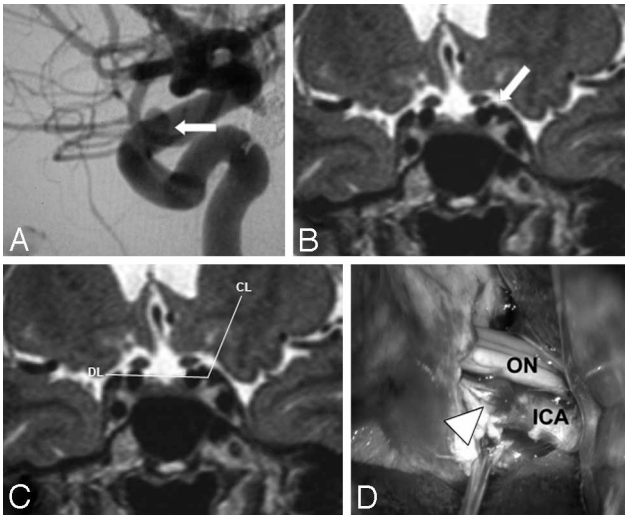

Fig 2. Radiologic-surgical correlation for a left superolateral paraclinoid aneurysm (case 14). *A,* DSA of the left ICA (lateral view) showing an aneurysm (*arrows*) interpreted as transitional with an intracavernous neck and a transitional sac. *B, C,* PMP in the diaphragmatic plane with an intersection angle showing a supracavernous location of the neck and the sac (DL indicates diaphragmatic line; CL, clinoid line). *D,* Operative findings confirming the supracavernous location of both neck and sac and showing, after anterior clinoidectomy and opening of the falciform ligament, the aneurysmal (*arrowhead*) relationship between the ICA and the optic nerve (ON).

Discussion

Review of the Literature

The origin of the ophthalmic artery is commonly used as the angiographic limit between the intracavernous and supracavernous ICA.[4] Because of its interindividual variability,[4,12-16] this reliable marker may sometimes fail to locate this junction precisely, anatomically represented by the distal dural ring.

Comparison between DSA and the PMP for the location of paraclinoid aneurysms around the roof of the cavernous sinus

	Aneurysmal Projection		Angiographic Location		PMP Location	
Aneurysms	Neck	Sac	Neck	Sac	Neck	Sac
1*	MP*	MP*	SC*	T*	SC*	SC*
2	M	M	IC	IC	IC	IC
3*	P*	P*	SC*	T*	T*	T*
4*	M*	M*	IC*	IC*	SC*	SC*
5	M	M	T	T	T	T
6*	P*	P*	SC*	SC*	SC*	T*
7	MP	MP	IC	IC	IC	IC
8	MP	MP	IC	IC	IC	IC
9	MP	MP	IC	IC	IC	IC
10*	MP*	MP*	T*	IC*	SC*	T*
11	M	MP	SC	T	SC	T
12	A	A	SC	SC	SC	SC
13	MP	MP	IC	T	IC	T
14*	LA*	L*	IC*	T*	SC*	SC*
15*	MP*	M*	IC*	IC*	T*	T*
16	MP	P	IC	IC	IC	IC
17*	M*	MP*	T*	T*	IC*	IC*

Note:—M indicates medial; L, lateral; A, anterior; P, posterior; IC, intracavernous; T, transitional; SC, supracavernous.
* Cases with different interpretations.

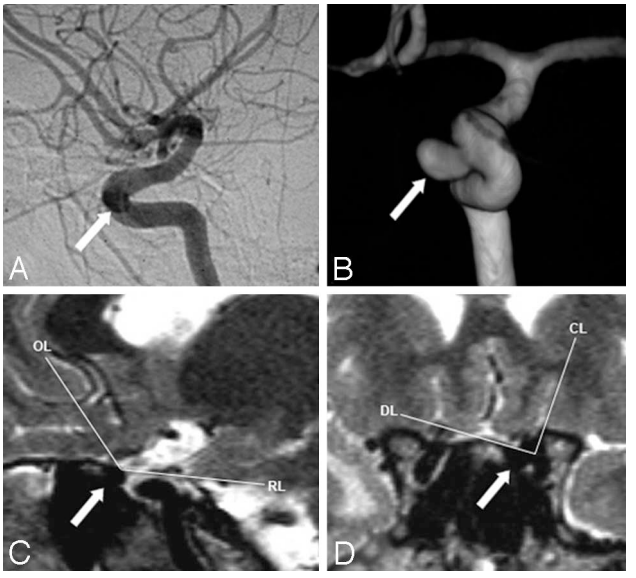

Fig 3. Comparison between angiogram and PMP for the location of case 2 (*arrows*). Both examinations show an intracavernous aneurysm (neck and sac intracavernous). *A,* DSA of the left ICA in the lateral view. *B,* 3D-DSA of the left ICA in the anterior view. *C,* PMP in the carotid plane (OL indicates optic line; RL, roof line). *D,* PMP in the diaphragmatic plane (DL indicates diaphragmatic line; CL, clinoid line).

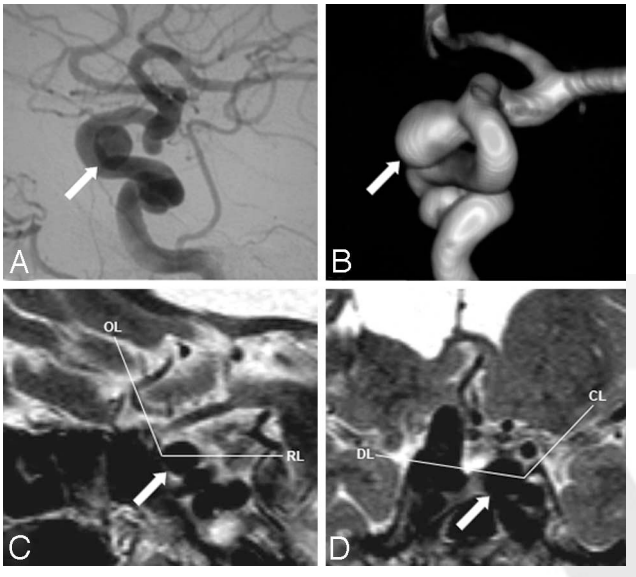

Fig 4. Comparison between angiogram and the PMP for the location of case 13 (*arrows*). Both examinations show a transitional aneurysm (neck intracavernous and sac transitional). The PMP depicts a widest supracavernous portion than it is suspected on initial DSA. *A,* DSA of the left ICA in the lateral view. *B,* 3D-DSA of the left ICA in the anterior view. *C,* PMP in the carotid plane (OL indicates optic line; RL, roof line). *D,* PMP in the diaphragmatic plane (DL indicates diaphragmatic line; CL, clinoid line).

The ophthalmic artery may arise from the ICA in the extradural space, most often far below the distal dural ring (artery of the foramen rotundum, inferolateral trunk) and is easily recognized as anomalous and unreliable but rarely near the distal dural ring (clinoid space, interdural location). Most ophthalmic arteries originate in the intradural space, but the distance between the origin and the distal dural ring may vary in 24% to 50% of cases. This variability led some to design techniques of radiographic correlation using some of the bony structures of the skull base on lateral and anterior nonsubtracted angiograms: the base of the anterior clinoid process,[17]

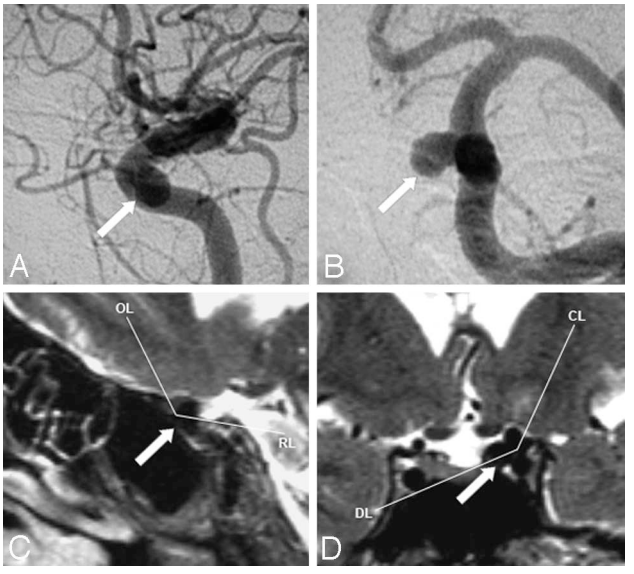

Fig 5. Comparison between angiogram and PMP for the location of case 11 (*arrows*). Both examinations show a transitional aneurysm (neck supracavernous and sac transitional). The PMP depicts a widest supracavernous portion than it is suspected on initial DSA. *A,* DSA of the left ICA in the lateral view. *B,* DSA of the left ICA in the anterior view. *C,* PMP in the carotid plane (OL indicates optic line; RL, roof line). *D,* PMP in the diaphragmatic plane (DL indicates diaphragmatic line; CL, clinoid line).

the superior surface of the anterior clinoid process and the tuberculum sellae[18] or the planum sphenoidale, and lines of the tuberculum sellae.[16] Recently, 3D reconstructions from CT scans,[19] CT angiograms,[20] or contrast medium-enhanced tomographic cisternograms[21] have been used. These radiologic procedures were respectively based on the visualization of the strut of the optic canal, identification of a surface concavity at the level of the distal dural ring, and CSF cisterns contrast around the ICA. Although effective, these protocols did not take into account the complexity of the extravascular anatomy of the paraclinoid region, particularly of the radiotransparent dural folds of the walls of the cavernous sinus. An indirect approach and interindividual radiologic variability were the major limitations of the above techniques.

Value and Limitations of the PMP

Reproducibility and accuracy of the PMP was proved in preliminary anatomoradiologic studies.[8,9] In this clinical study, the MR technique allowed the identification and the precise positioning of the PA detected with DSA for all patients. The results confirmed the interobserver reproducibility for the aneurysmal measurement and location, and the reliability of the aneurysmal dimensions obtained with the PMP. In 2 cases, the results of the PMP were confirmed by surgical exploration of the paraclinoid region. Compared with DSA, the PMP provides a global view of the paraclinoid anatomy and direct visualization of the radiotransparent dural folds comprising the roof of the cavernous sinus. Therefore, the PMP could increase the quality of the overall radiologic analysis by providing direct visualization of the aneurysm and a reliable evaluation of the size of the intracavernous and supracavernous portions of transitional aneurysms.

Discordance between interpretations of DSA and PMP were found in 8 cases. Differences were more frequent for medial or medial-posterior projecting PA (5/8) and for the location of the

aneurysmal sacs (7/8). Improvement of the location of the aneurysmal sac around the roof of the cavernous sinus is of importance, considering that it is the most usual site of rupture. In our study, we had surgical correlations in 2 cases only, so the discordances between DSA and the PMP should be carefully analyzed. Furthermore, the arbitrary choice of the horizontal line passing through the origin of the ophthalmic artery as the only angiographic limit between the intracavernous and extracavernous spaces could have led us to misinterpret some of the DSA. Some aneurysms could have been quoted in the wrong location. In those cases, the PMP technique has perhaps helped us only to clarify misinterpretations on DSA.

This PMP technique requires a short training period to become familiar with the MR imaging anatomy of the paraclinoid region. Therefore, a simplified protocol that could be applied in clinical practice by all neuroradiologists is proposed.

Potential Implications for the Management of PA

Advances in neuroradiologic techniques are responsible for the increased diagnosis of asymptomatic aneurysms. Furthermore, because of therapeutic implications, clinicians' and patients' demands for radiologic accuracy have grown. The location of PA compared with the roof of the cavernous sinus illustrates this situation perfectly. In the treatment decision making, the neurovascular team takes into account the benefit-to-risk ratio among 3 therapeutic options: conservative, endovascular, or surgical. The rates of morbidity and mortality related to endovascular and surgical treatment of asymptomatic aneurysms are, respectively, 1% and 4%[6,22] and 2.6% and 10.9%,[22,23] the surgical morbidity being slightly higher for PA.[24] The spontaneous risk of rupture of these aneurysms (sizes are approximately 6 mm and are located on the anterior circulation) varies between 0.05% and 0.5% per year, whether there is a previous history of SAH from an associated aneurysm (7/17 cases in this study).[25] In women with a mean age of 45 years and a life expectancy of approximately 84 years, the cumulative risk of rupture (conservative treatment) can reach 1.95% to 19.5% and is not so different from the risk of endovascular or surgical treatment, especially if there are individual risks of aneurysmal growth such as arterial hypertension, smoking, or a familial history of SAH or connective tissue disease.[6,26-28] The decision of curative treatment for a PA relies on the certainty that they are supracavernous or transitional aneurysms (at risk of SAH).

In our own clinical experience, the PMP allowed us to differentiate among intracavernous, supracavernous, and transitional aneurysms more precisely and to adapt the therapeutic management to the aneurysmal location. Intracavernous aneurysmal sacs were conservatively managed, whereas supracavernous or transitional aneurysmal sacs were treated with endovascular or surgical intervention. Only very small or dysplastic supracavernous or transitional sacs were not treated. Overall, the association of DSA and PMP benefited the treatment decisions in 4 patients (cases 10, 14, 15, and 17).

Conclusions

The paraclinoid MR protocol is a noninvasive and nonradiating alternative technique, complementary to DSA. It is efficient for the location around the roof of the cavernous sinus of small and asymptomatic PA. This protocol might help to provide patients with more appropriate information about their disease and therapeutic solutions adjusted in relationship to the potential risk of their aneurysm(s).

References

1. Day AL. **Aneurysms of the ophthalmic segment. A clinical and anatomical analysis.** *J Neurosurg* 1990;72:677–91
2. De Jesūs O, Sekhar LN, Riedel CJ. **Clinoid and paraclinoid aneurysms: surgical anatomy, operative techniques, and outcome**. *Surg Neurol* 1999;51:477–87; discussion 487–88
3. Gurian JH, Viñuela F, Guglielmi G, et al. **Endovascular embolization of superior hypophyseal artery aneurysms.** *Neurosurgery* 1996;39:1150–54; discussion 1154–56
4. Punt J. **Some observations on aneurysms of the proximal internal carotid artery.** *J Neurosurg* 1979;51:151–54
5. Knosp E, Muller G, Perneczky A. **The paraclinoid carotid artery: anatomical aspects of a microneurosurgical approach.** *Neurosurgery* 1988;22:896–901
6. Wardlaw JM, White PM. **The detection and management of unruptured intracranial aneurysms.** *Brain* 2000;123:205–21
7. Kupersmith MJ, Hurst R, Berenstein A, et al. **The benign course of cavernous carotid artery aneurysms.** *J Neurosurg* 1992;77:690–93
8. Thines L, Delmaire C, Le Gars D, et al. **MRI location of the distal dural ring plane: anatomoradiological study and application to paraclinoid carotid artery aneurysms.** *Eur Radiol* 2006;16:479–88
9. Thines L, Delmaire C, Le Gars D, et al. [**MRI localization of paraclinoid carotid aneurysms**]. *J Neuroradiol* 2006;33:115–20
10. Bouthillier A, van Loveren HR, Keller JT. **Segments of the internal carotid artery: a new classification.** *Neurosurgery* 1996;38:425–32; discussion 432–33
11. Gauvrit JY, Leclerc X, Vermandel M, et al. **3D rotational angiography: use of propeller rotation for the evaluation of intracranial aneurysms.** *AJNR Am J Neuroradiol* 2005;26:163–65
12. Huynh-Le P, Natori Y, Sasaki T. **Surgical anatomy of the ophthalmic artery: its origin and proximal course.** *Neurosurgery* 2005;57(4 suppl):236–41; discussion 236–41
13. Kim JM, Romano A, Sanan A, et al. **Microsurgical anatomic features and nomenclature of the paraclinoid region.** *Neurosurgery* 2000;46:670–80; discussion 680–82
14. Kyoshima K, Oikawa S, Kobayashi S. **Interdural origin of the ophthalmic artery at the dural ring of the internal carotid artery. Report of two cases.** *J Neurosurg* 2000;92:488–89
15. Renn WH, Rhoton AL. **Microsurgical anatomy of the sellar region.** *J Neurosurg* 1975;43:288–98
16. Beretta F. **The paraclinoid aneurysms and the distal dural ring: a new classification.** *J Neurosurg Sci* 2004;48:161–75
17. Taptas JN. **Intradural and extradural ICA.** *J Neurosurg* 1979;51:877–78
18. Oikawa S, Kyoshima K, Kobayashi S. **Surgical anatomy of the juxta-dural ring area.** *J Neurosurg* 1998;89:250–54
19. Gonzalez LF, Walker MT, Zabramski JM, et al. **Distinction between paraclinoid and cavernous sinus aneurysms with computed tomographic angiography.** *Neurosurgery* 2003;52:1131–37; discussion 1138–39
20. Murayama Y, Sakurama K, Satoh K, et al. **Identification of the carotid artery dural ring by using three-dimensional computerized tomography angiography. Technical note.** *J Neurosurg* 2001;95:533–36
21. Ito K, Hongo K, Kakizawa Y, et al. **Three-dimensional contrast medium-enhanced computed tomographic cisternography for preoperative evaluation of surgical anatomy of intradural paraclinoid aneurysms of the internal carotid artery: technical note.** *Neurosurgery* 2002;51:1089–92; discussion 1092–93
22. Molyneux A, Kerr R, Stratton I, et al. **International Subarachnoid Aneurysm Trial (ISAT) of neurosurgical clipping versus endovascular coiling in 2143 patients with ruptured intracranial aneurysms: a randomised trial.** *Lancet* 2002;360:1267–74
23. Raaymakers TW, Rinkel GJ, Limburg M, et al. **Mortality and morbidity of surgery for unruptured intracranial aneurysms: a meta-analysis.** *Stroke* 1998;29:1531–38
24. Kumon Y, Sakaki S, Kohno K, et al. **Asymptomatic, unruptured carotid-ophthalmic artery aneurysms: angiographical differentiation of each type, operative results, and indications.** *Surg Neurol* 1997;48:465–72
25. Anonymous. **Unruptured intracranial aneurysms–risk of rupture and risks of surgical intervention. International Study of Unruptured Intracranial Aneurysms Investigators.** *N Engl J Med* 1998;339:1725–33
26. Broderick JP, Viscoli CM, Brott T, et al. **Major risk factors for aneurysmal subarachnoid hemorrhage in the young are modifiable.** *Stroke* 2003;34:1375–81
27. Qureshi AI, Sung GY, Suri MF, et al. **Factors associated with aneurysm size in patients with subarachnoid hemorrhage: effect of smoking and aneurysm location.** *Neurosurgery* 2000;46:44–50
28. Raaymakers TW, Rinkel GJ, Ramos LM. **Initial and follow-up screening for aneurysms in families with familial subarachnoid hemorrhage.** *Neurology* 1998;51:1125–30

Neurosurgery

(Accepted minor corrections)

Direct Imaging of the Distal Dural Ring and Paraclinoid Internal Carotid Artery Aneurysms with High Resolution T2 Turbo-Spin Echo Technique at 3.0 Tesla MRI

Laurent Thines [1,2,3,5], MD., Amir R. Dehdashti [2,3,5], MD., Ronit Agid [4,5], MD., Karel G. Terbrugge [4,5], MD., M. Christopher Wallace [2,3,5], MD, MSc., SeonKyu Lee [4,5], M.D, PhD

[1] Department of Neurosurgery, Lille University Hospital, Lille, France
[2] Division of Neurosurgery, Toronto Western Hospital, Ontario, Canada
[3] Department of Surgery, University of Toronto, Ontario, Canada.
[4] Department of Medical Imaging, Toronto Western Hospital, Ontario, Canada
[5] the University of Toronto Brain Vascular Malformation Study Group, Toronto Western Hospital, Ontario, Canada

Corresponding author: Seon Kyu Lee, M.D.,PhD.
Staff Interventional Neuroradiologist, Department of Radiology
Lahey Clinic Medical Center, #41 Mall Road, Burlington, MA, 01805
Tel: 781-744-3330 Fax:781-744-5630 Email: seonkyu.lee@lahey.org

Abstract

Objective: To evaluate the feasibility of the direct visualization of the distal dural ring (DDR) and adjacent anatomical structures in patients with paraclinoid internal carotid artery aneurysms at 3.0 Tesla Magnetic Resonance Imaging (MRI).

Methods: Six consecutive patients [male:female=1:5, mean age=45.5 (range: 34~51)] who underwent a 3.0 T MRI examination for the evaluation of 7 paraclinoid carotid artery aneurysms were reviewed retrospectively. MR images were acquired using a T2 turbo spin-echo sequence, 2-mm thickness without gap on the coronal plane perpendicular to the diaphragma sellae. Identifications of the DDR, adjacent regional anatomical landmarks and paraclinoid aneurysms were analyzed. The locations of the paraclinoid aneurysms were categorized into intradural (aneurysm neck and sac located above the DDR), transdural (aneurysm neck or sac were straddling the DDR) and extra-dural (aneurysm neck and sac located below the DDR). Inter-study agreement between CTA and 3T MRI for the anatomical location of the paraclinoid aneurysms was accessed in 6 patients which underwent both exams.

Results: In all cases, the DDR was clearly identified and the relationship between the DDR and the paraclinoid aneurysm was successfully determined on 3 T MRI. The aneurysm locations with 3T MRI were: 4 intradural, 1 transdural and 2 extradural. Comparison between CTA and 3T MRI found discordant anatomical locations in 3 aneurysms (3/6, 50%).

Conclusion: Direct visualization of the DDR as well as precise evaluation of paraclinoid aneurysm location with high resolution 3 T MRI is possible. This study suggests that high resolution 3 T MRI could be an important imaging method to determine the appropriate management for patients with paraclinoid aneurysms.

Running title: Direct Imaging of the Distal Dural Ring at 3.0 T MRI

Keywords: distal dural ring, paraclinoid aneurysm, internal carotid artery, magnetic resonance imaging, management

The distal dural ring (DDR) is a dural fold embedded in the cavernous sinus roof which delineates the border between the supracavernous and intracavernous spaces and is recognized as the anatomical boundary between the intradural and extradural segments of the internal carotid artery (ICA) in the paraclinoid region [7, 9, 13, 17].

Since an intradural arterial aneurysm carries potential risk of subarachnoid hemorrhage (SAH), it is a challenging issue to determine whether a paraclinoid aneurysm is located intradurally or not. Two potential anatomical landmarks have been suggested for this purpose including the origin of the ophthalmic artery [10] on ICA digital subtraction angiography (DSA) and the location of the aneurysm compared to the optic strut [3, 4] on computerized tomography angiography (CTA). However, these are indirect anatomical landmarks, and as such are not always reliable.

In this study, we analyzed the interest of 3.0 Tesla (3T) Magnetic Resonance Imaging (MRI) for the direct visualization of the DDR itself and the localization of associated paraclinoid aneurysms.

Material and Methods

This study was approved by the Research Ethics Board of our institution

Patients

MRI studies of 6 consecutive patients with seven paraclinoid aneurysms were retrospectively reviewed. Our patient group included five female and one male patient. The age range was 34 to 51 (mean=45.5). Indications for MRI studies included pre-therapeutic assessment (n=5) of paraclinoid aneurysm and follow-up of a known paraclinoid aneurysm (n=2). Among those 7 paraclinoid aneurysms, 6 aneurysms were unruptured. Two aneurysms were treated with endovascular techniques and 5 aneurysms remained untreated.

MRI and analysis

All MRI studies were performed using a 3.0 Tesla MR scanner (GE, Milwakee, WI, USA) with a standard head and neck coil. Coronal T2 weighted images using Fast Recovery Fast Spine Echo (FRFSE) sequence was obtained using the following parameters: 18~20 cm x 18~20 cm FOV, 2 mm slice thickness, 0 space/gap, 448 x 448 Matrix, 4 NEX, Echo train length of 17. TR was 4700~6550 ms and TE was 104.6~110.6 ms.

MRI studies were independently reviewed by a neuroradiologist (S.K.L.) and a neurosurgeon (L.T.). Identification of the DDR, the relationship between the DDR and the neck/sac of each aneurysm were evaluated. Identification of the regional anatomical markers, such as the ICA, the anterior clinoid process, the diaphragma sellae, the ophthalmic artery and the optic nerve, was also evaluated.

The DDR is identified as the dural reflection that surrounds the ICA when it exits the cavernous sinus roof (Fig 1). It is contained in a curved dural plane that projects infero-medialy between the medial ridge of the upper surface of the anterior clinoid process and the diaphragma sellae. The DDR also extends infero-posteriorly between the floor of the optic canal and the posterior part of the cavernous sinus roof.

According to their relationship with the DDR, the paraclinoid aneurysms were categorized as follows: intradural if the aneurysm neck and sac were located above the

DDR, transdural if the aneurysm neck or sac was straddling the DDR and extra-dural if the aneurysm neck and sac were located below the DDR. Interobserver agreement for the aneurysm location on MRI was analyzed with the kappa correlation coefficient.

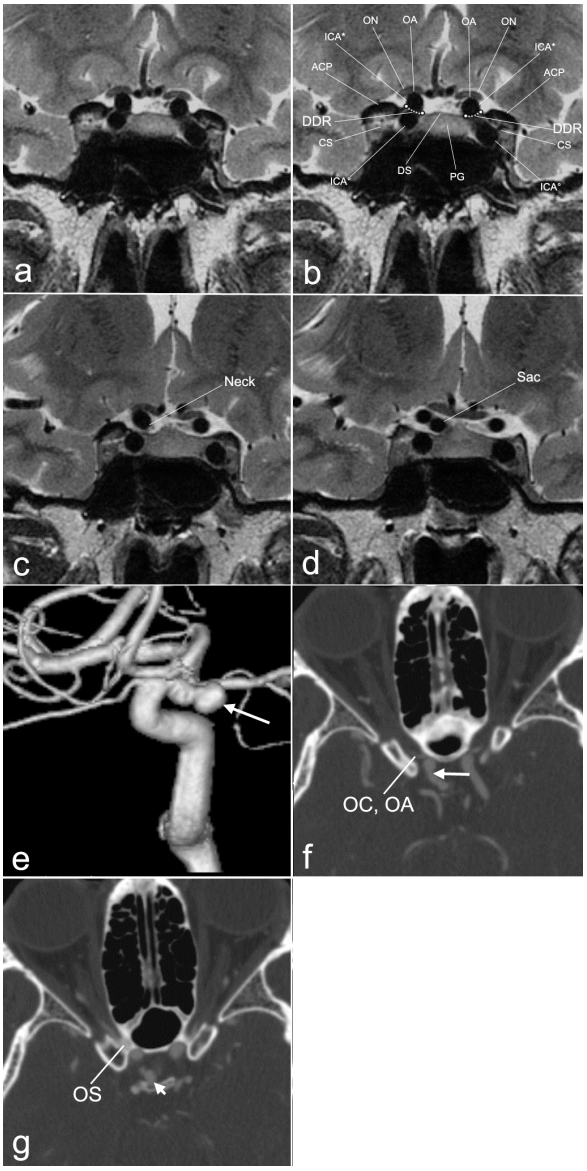

Figure 1 - (Patient 5). T2 turbo spin-echo MR images at 3.0 Tesla in the coronal plane demonstrate: (a,b) the anatomo-radiological markers of the paraclinoid region. ACP: anterior clinoid process, ON: optic nerve, OA: ophthalmic artery, CS: cavernous sinus, DS: diaphragma sellae, PG: pituitary gland, ICA*: supracavernous internal carotid artery, ICA°: intracavernous internal carotid artery, DDR: distal dural ring; (c,d) on following posterior slices, an intradural paraclinoid aneurysm is evidenced, the neck and the sac are located above the DDR ; (e) : three-dimensional reconstruction from the DSA (medial view) showing the same aneurysm (arrow); (f,g): axial CTA of the same patient showing on adjacent slices an intradural aneurysm located above the optic strut (OS), arrow-f: aneurysm neck, arrow-g: aneurysm sac, OC: optic canal, OA: ophthalmic artery.

Anatomic localization of paraclinoid aneurysms using indirect anatomical landmarks

1. ***Digital Subtraction Angiography / Magnetic Resonance Angiography (MRA)***
   DSA and rotational angiography with 3 D reconstruction using volume rendering technique and/or Gadolinium enhanced MRA were reviewed. The technical details of MRA were described previously [2]. The origin of the ophthalmic artery was used as the landmark to determine whether the aneurysm was intradural or not. The anatomical location of each aneurysm was further detailed by using

conventional angiographic classification as follows: cavernous, paraophthalmic, superior hypophyseal and posterior ICA.

2. ***Computerized Tomography Angiography***

CTA was performed from the aortic arch to the vertex using a 64-slice multidetector CT scanner (Aquilion 64, Toshiba Medical Systems, Tokyo, Japan). CTA images were acquired following the intravenous timed injection of a contrast agent using an auto-triggered mechanical injector. The study was performed with automated z axis modulation technique with: maximum allowed current of 300 mAs, 120 kVp, matrix size 512×512, FOV 28–32 cm, slice thickness 0.5 mm, pitch 1.0, and isotropic voxel size of 0.5 mm^3.

CTA studies were independently reviewed by a neuroradiologist (S.K.L.) and a neurosurgeon (L.T.). The ipsilateral optic struts on the axial source images of the CTAs were used as the landmarks to determine whether the aneurysms were intradural or not [3, 4]. If the aneurysm neck and sac were above the level of the optic strut, it was considered as intradural. If the aneurysm neck and sac were below the level of the optic strut, it was considered as extradural. However, if the aneurysm neck or sac was straddling the optic strut, it was considered as transdural. Interobserver agreement for the aneurysm localization on CTA was analyzed with the kappa correlation coefficient.

The determined anatomical location of each aneurysm with CTA was compared to that of MRI to evaluate inter-study agreement.

Results

All paraclinoid regional anatomical markers (Fig 2) were always identified on the MRI (table 1). The DDR was always seen on both sides and its visualization allowed the precise localization of the neck and the sac of the aneurysm in all cases. The DSA/MRA showed 6 intradural and 1 extradural aneurysms including superior-hypophyseal aneurysms (n=3), paraophthalmic aneurysms (n=2), cavernous aneurysm (n=1) and posterior ICA aneurysm (n=1). The CTA using the optic strut as the anatomical landmark showed: 3 intradural, 2 transdural and 1 extradural aneurysms. The 3 T MRI localization of paraclinoid aneurysm showed 4 intradural and 3 extradural aneurysms. The interobserver agreements for the anatomical localization of each aneurysm by both CTA and MRI techniques were perfect (κ=1). Among 6 aneurysms which have both CTA and 3 T MRI, the anatomical localizations obtained with 3 T MRI were discordant with those from CTA in 3 aneurysms (Fig 3).

Table 1-Results for the location of paraclinoid aneurysms with the four imaging modalities and for the MR anatomical analysis of the paraclinoid markers in seven paraclinoid aneurysms.

Patient	Age/ sex	Angio MRA	CTA	Size mm	Mode	MR anatomical analysis							MR location	
						TRT	ACP	DS	ICA	OA	ON	DDR	Neck	Sac
1	51/F	Rt SHA	TransD	8.5	SAH	coils	+ +	+	++	++	++	++	IntraD	IntraD
2 a b	48/F	Lt CO Rt CC	IntraD ExtraD	3 2	AS	none	++	0	++	++	++	++	ExtraD ExtraD	ExtraD ExtraD
3	46/M	Rt CO	NA	7	AS	none	++	0	++	++	++	++	IntraD	IntraD
4	48/F	Rt SHA	TransD	5	AS	none	++	+	++	++	++	++	ExtraD	ExtraD
5	46/F	Rt post-ICA	IntraD	2	AS	none	++	+	++	++	++	++	IntraD	IntraD
6	34/F	Rt SHA	IntraD	5	AS	coils	++	+	++	++	++	++	IntraD	IntraD

MRA = magnetic resonance angiography CTA = computerized tomography angiography TRT = treatment SAH = subarachnoid hemorrhage AS = asymptomatic ACP = anterior clinoid process DS = diaphragma sellae ICA = internal carotid artery OA = ophthalmic artery ON = optic nerve DDR = distal dural ring SHA = superior hypophyseal aneurysm CO = carotido-ophthalmic aneurysm CC = carotido-cavernous aneurysm post-ICA = posterior ICA aneurysm IntraD = intradural aneurysm ExtraD = extradural aneurysm TransD = transdural aneurysm

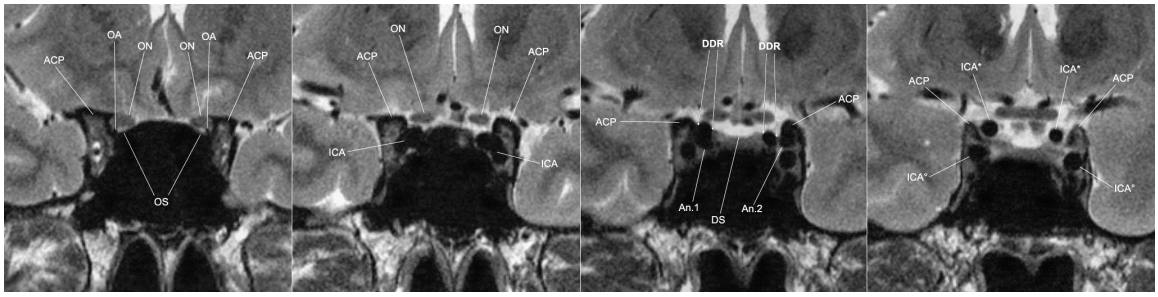

Figure 2 - (Patient 2). Four consecutive T2 turbo spin-echo MR images at 3.0 Tesla in the coronal plane show, the anatomo-radiological markers of the paraclinoid region: ACP: anterior clinoid process, ON: optic nerve, OA: ophthalmic artery, DS: diaphragma sellae, ICA: anterior loop of the internal carotid artery, ICA*: supracavernous internal carotid artery, ICA°: intracavernous internal carotid artery, DDR: distal dural ring (note that the optic strut [OS] is also identified on MR images), and two paraclinoid aneurysms: Aneurysm 1 (An.1) is extradural (under the DDR) and Aneurysm 2 is extradural (under the DDR and the clinoid process: sub-clinoid aneurysm).

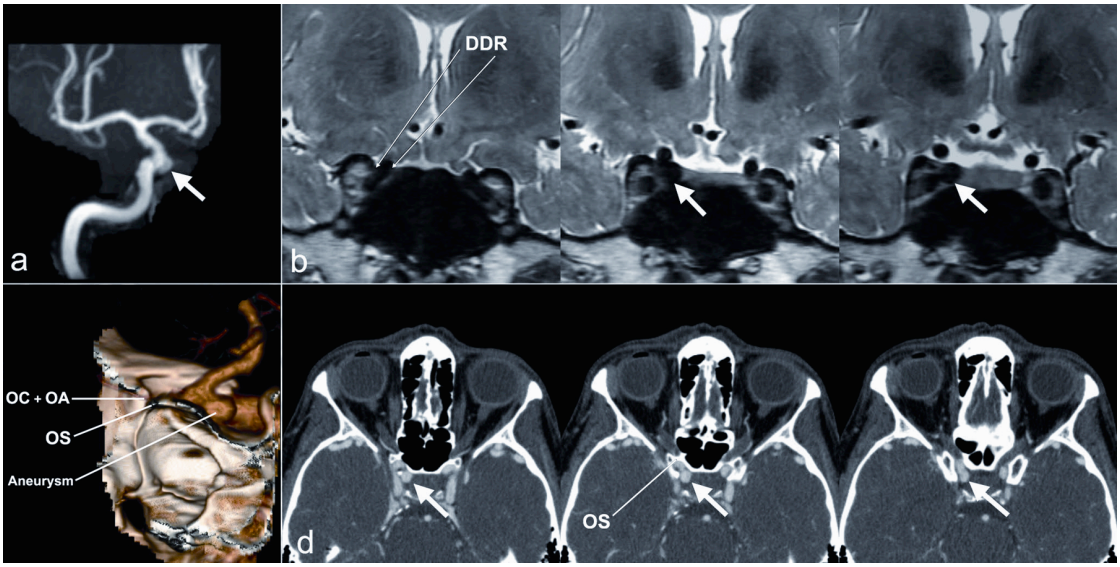

Figure 3 - (Patient 4). a) magnetic resonance (MR) angiography showing a right superior hypophyseal aneurysm (arrow); b) successive T2 turbo spin-echo MR images at 3.0 Tesla in the coronal plane clearly showing an extradural aneurysm (arrow), under the DDR (distal dural ring); c) medial view of a three-dimensional reconstruction from computerized tomography angiography (CTA) showing a right superior hypophyseal aneurysm (arrow) which sac is projecting on both sides of the optic strut (OS) level, OC: optic canal; d) CTA images in the axial plane quoting the aneurysm (arrow) as "transdural" (intra-extradural) because its sac is identified on both sides of the optic strut (OS) plane.

Discussion

The precise localization of paraclinoid aneurysms around the roof of the cavernous sinus is a major clinical issue since an aneurysm located beyond the DDR, in the subarachnoid space, carries future risk of SAH [18].

Several imaging landmarks including the origin of the ophthalmic artery on DSA and the level of the optic strut on CTA have been proposed for this purpose. The ophthalmic artery is often used as the angiographic landmark between the intracavernous and supracavernous ICA [10]. However, it is not always reliable to determine the precise anatomical location of a paraclinoid aneurysm since its origin is very variable and extradural or distal intradural origins are not infrequent [1, 6-8, 11]. Bony landmarks on unsubtracted angiography were also used including the base of the anterior clinoid process [14], the superior surface of the anterior clinoid process and the tuberculum sellae [9] or the planum sphenoidale and the tuberculum sellae lines [1]. More recently, the optic strut was proposed as a reliable bony landmark on the CTA to determine the anatomical location of paraclinoid aneurysms [3, 4]. However, the anatomy of the radiotransparent dural folds of the paraclinoid region is highly variable compared to bony structures. So, the above described indirect landmarks don't take into account the complexity of the extravascular anatomy of this region and the interindividual variability in the shape of the superior wall of the cavernous sinus which contains the DDR. Therefore, these bony landmarks, including the optic strut, might not be reliable to determine the accurate localization of paraclinoid region aneurysm either.

Because of difficulties to differentiate the signal of neighbouring anatomical structures and lack of spatial resolution, MRI has long been considered to be inadequate for the analysis of the paraclinoid region and paraclinoid aneurysms. However, Tsuboi et al. [16] used contrast-enhanced three-dimensional time-of-flight MRA to improve the contrast between the ICA, paraclinoid aneurysm, cavernous sinus walls and extravascular structures. This technique well depicts the relationship of paraclinoid aneurysms but the authors acknowledged that the spatial resolution might be insufficient particularly on 1.5T MRI scanners. Rubinstein et al. have described T2-weighted TSE MRI for the imaging of intracranial aneurysm [12]. It was thought to be helpful because it allowed thin slice acquisition with high signal-to-noise ratio. Thus, adjacent anatomical structures such as brain parenchyma, vascular structures and dura mater were well contrasted by the high signal intensity of surrounding cerebrospinal fluid. Recent exploration of this sequence in the evaluation of the paraclinoid region for the location of the DDR also confirmed the good tissue contrast obtained among the above described anatomical structures [15].

The T2-weighted TSE sequence used in this study benefited from both higher contrast resolution of the paraclinoid anatomical structures due to the hyperintense signal of surrounding cisternal CSF and considerable increase in the spatial resolution at 3T MRI. This increased resolution allowed us to demonstrate, on thin and contiguous slices, the dural folds of the cavernous sinus roof and to identify the DDR. With detailed and precise knowledge of the anatomy of this region and the excellent visualization of the DDR at 3T MRI, we believe that surgical correlations to validate the accuracy of this technique were not required. Furthermore, with the advances in the interventional techniques (stents), those who are supposed to be intradural are more frequently occluded endovascularly, and those who are supposed to be in an extradural location are managed conservatively.

Our protocol is easy to apply and to interpret since it only uses a coronal plane which is perpendicular to the diaphragm sellae. Using this technique, we were able to precisely locate all the paraclinoid aneurysms in our patients and adapt the therapeutic management accordingly. These findings suggest that the anatomical accuracy of the T2-weighted TSE MRI at 3T for the imaging of the paraclinoid region can help the clinician to recommend the appropriate therapeutic management for patients with paraclinoid aneurysms. It gives a more accurate localization of the aneurysm and a better understanding of its anatomical relationship before considering any invasive treatment, including interventional treatment or even surgical obliteration.

The limitation of this technique, however, still remains in the capacity of spatial and contrast resolution of MRI. When an extradural paraclinoid ICA aneurysm abuts or makes upward displacement of the DDR, it may not be easy to appreciate if the aneurysm dome is above the DDR or is still covered with the dura. With our technique of 18~20 cm x 18~20 cm FOV, 2 mm slice thickness, 0 space/gap, 448 x 448 Matrix at 3T MRI, it was still not easy to anatomically separate the DDR from the aneurysm dome when both structures meet (Fig. 3). Since both the DDR and the aneurysm dome show low signal intensities on MRI, contrast enhanced MRI or MR angiography could be used to differentiate paraclinoid aneurysms wall from the DDR itself. Another potential difficulty could be the precise localization of small carotid cave aneurysm. The carotid cave is a small subarachnoid recess along the medial or posteromedial aspect of the DDR [5] which is an intradural space but below the DDR level. In such cases, even in very high magnetic

fields, the resolution of the MRI might not be enough to differentiate the aneurismal dome from the DDR.

In conclusion, this study demonstrated a simple and reliable protocol at 3T MRI which helped to directly visualize the DDR as well as it demonstrated its anatomical relationship with paraclinoid aneurysms. With a more accurate anatomical localization of paraclinoid aneurysms and a better understanding of the paraclinoid imaging anatomy, we believe that more appropriate management recommendations can be provided to the patients.

References

1. Beretta F: The paraclinoid aneurysms and the distal dural ring: a new classification. **J Neurosurg Sci 48**:161-175, 2004
2. Farb RI, Nag S, Scott JN, et al: Surveillance of intracranial aneurysms treated with detachable coils: a comparison of MRA techniques. **Neuroradiology 47**:507-515, 2005
3. Gonzalez LF, Walker MT, Zabramski JM, et al: Distinction between paraclinoid and cavernous sinus aneurysms with computed tomographic angiography. **Neurosurgery 52**:1131-1137, 2003
4. Hashimoto K, Nozaki K, Hashimoto N: Optic strut as a radiographic landmark in evaluating neck location of a paraclinoid aneurysm. **Neurosurgery 59**:880-895, 2006
5. Hitotsumatsu T, Natori Y, Matsushima T, et al: Micro-anatomical study of the carotid cave. **Acta Neurochir (Wien) 139**:869-874, 1997
6. Huynh-Le P, Natori Y, Sasaki T: Surgical anatomy of the ophthalmic artery: its origin and proximal course. **Neurosurgery 57**:236-241, 2005
7. Kim JM, Romano A, Sanan A, et al: Microsurgical anatomic features and nomenclature of the paraclinoid region. **Neurosurgery 46**:670-680, 2000
8. Kyoshima K, Oikawa S, Kobayashi S: Interdural origin of the ophthalmic artery at the dural ring of the internal carotid artery. Report of two cases. **J Neurosurg 92**:488-489, 2000
9. Oikawa S, Kyoshima K, Kobayashi S: Surgical anatomy of the juxta-dural ring area. **J Neurosurg 89**:250-254, 1998
10. Punt J: Some observations on aneurysms of the proximal internal carotid artery. **J Neurosurg 51**:151-154, 1979
11. Renn WH, Rhoton AL, Jr.: Microsurgical anatomy of the sellar region. **J Neurosurg 43**:288-298, 1975
12. Rubinstein D, Sandberg EJ, Breeze RE, et al: T2-weighted three-dimensional turbo spin-echo MR of intracranial aneurysms. **AJNR Am J Neuroradiol 18**:1939-1943, 1997
13. Seoane E, Rhoton AL, Jr., de Oliveira E: Microsurgical anatomy of the dural collar (carotid collar) and rings around the clinoid segment of the internal carotid artery. **Neurosurgery 42**:869-884, 1998
14. Taptas JN: Intradural and extradural ICA. **J Neurosurg 51**:877-878, 1979
15. Thines L, Delmaire C, Le GD, et al: MRI location of the distal dural ring plane: anatomoradiological study and application to paraclinoid carotid artery aneurysms. **Eur Radiol 16**:479-488, 2006
16. Tsuboi T, Tokunaga K, Shingo T, et al: Differentiation between intradural and extradural locations of juxta-dural ring aneurysms by using contrast-enhanced 3-dimensional time-of-flight magnetic resonance angiography. **Surg Neurol 67**:381-387, 2007
17. Umansky F, Valarezo A, Elidan J: The superior wall of the cavernous sinus: a microanatomical study. **J Neurosurg 81**:914-920, 1994
18. Wiebers DO, Whisnant JP, Huston J, III, et al: Unruptured intracranial aneurysms: natural history, clinical outcome, and risks of surgical and endovascular treatment. **Lancet 362**:103-110, 2003

CASE REPORT

Intrasellar Rupture of a Paraclinoid Aneurysm with Subarachnoid Hemorrhage: Usefulness of MR Imaging in Diagnosis

M. Ribeiro
P. Howard
R. Willinsky
K. ter Brugge
R. Agid
L. Thines
L. da Costa

SUMMARY: Characterization of paraclinoid aneurysms may be difficult because of the complexity of anatomic structures involved, and differentiation between intradural and extradural lesions is crucial. We report a case of a patient with a unique presentation of a paraclinoid aneurysm with intrasellar hemorrhage in which the presence of intrasellar blood and the relationship of the paraclinoid aneurysmal neck and sac to the dural rings were elegantly demonstrated on MR imaging and were critical in choosing the target lesion for treatment.

The anatomy of the paraclinoid region is complex, and sometimes it is hard to properly characterize aneurysms arising in that region. Differentiation between an intradural and extradural location is of the utmost importance because it may determine patient prognosis and management strategy. Intracavernous internal carotid artery (ICA) aneurysms usually have a benign natural history, and treatment is reserved for patients with unbearable pain or progressive neurologic deficits. An intradural aneurysm carries a risk for subarachnoid hemorrhage and may require treatment. We report an unusual case of multiple intracranial aneurysms including a ruptured paraclinoid carotid aneurysm presenting with intrasellar bleeding followed by subarachnoid extension.

Case Report

A 45-year-old man presented with good clinical grade subarachnoid hemorrhage. CT revealed blood in the basal cisterns and Sylvian fissures with symmetric distribution (Fig 1*A*,*B*). A digital subtraction angiography (Fig 1*C*, *D*) and a CT angiogram (CTA) demonstrated 2 aneurysms, a larger one arising from the right paraclinoid carotid and a smaller one at the right middle cerebral artery (MCA) bifurcation. The neck of the paraclinoid aneurysm could be seen at the level of the optic strut, with the sac pointing posteriorly and inferomedially, in close relationship with the sella turcica. (Fig 2). MR imaging was performed with the hope of being able to clarify if the paraclinoid aneurysm was intradural or extradural; results showed the aneurysmal neck to be intradural and its dome below the dural ring, extradural. In addition, an enlarged sella turcica was noted, with inferior displacement of the pituitary gland and a large amount of blood filling the sella and extending into the subarachnoid space (Fig 3). We concluded that the paraclinoid aneurysm had ruptured into the sella with subarachnoid extension. The paraclinoid aneurysm was successfully coiled.

Received November 20, 2007; accepted December 20.

From the Department of Neuroradiology (M.R.), Hospital São Marcos, Braga, Portugal; and Department of Medical Imaging (P.H., R.W., K.t.B., R.A., L.d.C.) and Division of Neurosurgery (L.T.), Department of Surgery, Toronto Western Hospital, University of Toronto, Toronto, Ontario, Canada.

Please address correspondence to Manuel Ribeiro, MD, Hospital São Marcos, Largo Engenheiro Carlos Amarante, Apartado 2242, Braga, Portugal, 4701–965; e-mail: manuelqr@portugalmail.pt

DOI 10.3174/ajnr.A1022

Discussion

The establishment of either an intradural or extradural location of paraclinoid aneurysms has critical implications for treatment and prognosis. Extradural aneurysms have a good prognosis and very low risks for a subarachnoid hemorrhage and major neurologic complications.[1] Treatment is reserved for symptomatic lesions or for those lesions with extension into the subarachnoid space.[2] Intradural aneurysms carry a risk for subarachnoid hemorrhage and may require treatment. Most paraclinoid aneurysms can be localized by their direction of projection on angiograms.[3] However, the complex anatomy of the juxtadural ring area and individual variability in this region can sometimes make it difficult to define the relationship of the aneurysm to the dural ring, which differentiates extradural (below the dural ring) and intradural (above the dural ring) lesions.

Different techniques with several anatomic references have been used to differentiate intradural from extradural aneurysms. The simplest method uses the ophthalmic artery as the landmark for the transition of the extradural and intradural location. The major drawback of this method is that the origin of the ophthalmic artery is extradural in 10% of cases,[4] leading to the erroneous assumption that an aneurysm is intradural when it is intracavernous. In our patient, the aneurysm arises distal to the ophthalmic artery, but its inferior direction places it below the plane of this artery (Fig 1*D*).

A reliable landmark for identification of the proximal dural ring, which defines the roof of cavernous sinus, is the optic strut.[4-6] Lesions above this level are considered intradural, and below, intracavernous, extradural. In our case, the neck of the aneurysm is located at the exact level of the optic strut, and its fundus projects downward and medially, into the sella turcica. The aneurysm could be classified as a carotid cave aneurysm, arising between the 2 dural rings and growing into the cavernous sinus. The carotid cave is a pouch located in the posteromedial side of the distal dural ring,[7] above the proximal ring, which may or may not have a communication with the subarachnoid space.

The diffuse subarachnoid hemorrhage demonstrated on CT could have been caused by either lesion, so it was important to determine if the proximal aneurysm was intradural or extradural. If the paraclinoid aneurysm was extradural, our treatment choice for the MCA aneurysm (Fig 1*C*) would have

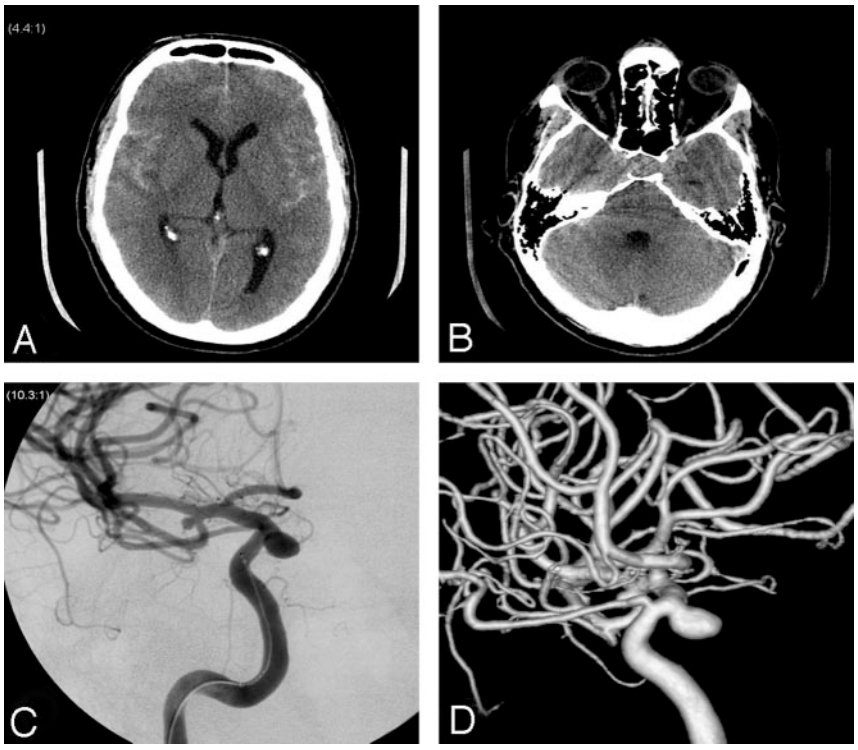

Fig 1. *A,* Axial unenhanced CT shows diffuse symmetric subarachnoid hemorrhage. *B,* Questionable hyperattenuation at the level of the sella turcica is difficult to interpret given adjacent streak artifact. *C,* Frontal view of right internal carotid angiogram shows MCA bifurcation and paraclinoid aneurysms. *D,* 3D right ICA angiogram in lateral view reveals the paraclinoid aneurysm arising distal to the ophthalmic artery but pointing inferiorly below the plane of the ophthalmic artery.

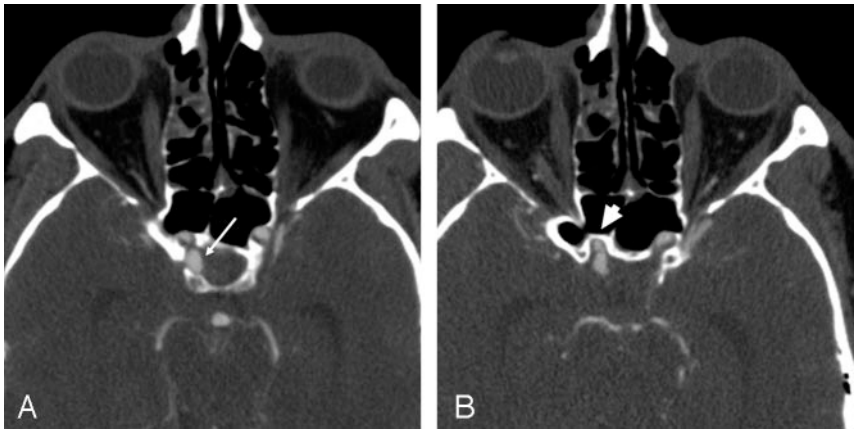

Fig 2. *A,* Axial CT angiography shows the sac of the paraclinoid aneurysm (*arrow*) adjacent to the sella, without intervening septum. *B,* At the level of the superior margin of the optic strut (*arrowhead*), the aneurysmal neck and body extend posteriorly from the ICA.

been clipping (small size, relatively wide neck), but if it was intradural, our first choice of treatment would be coiling. CT and CTA alone were insufficient to define the location of the paraclinoid aneurysm and did not reveal the large intrasellar hemorrhage. In retrospect, after MR imaging revealed the intrasellar hemorrhage, intrasellar blood could be suspected on the plain CT head (Fig 1*B*).

MR imaging at 3T was used to visualize the dural ring[8] and showed that the neck of the aneurysm was intradural and its dome, clearly extradural. More importantly, it revealed a large amount of blood inside an enlarged sella turcica, confirming that the paraclinoid aneurysm had bled. The large amount of intrasellar blood, the relatively small volume of blood in the subarachnoid space, and the empty sella syndrome lead to the hypothesis that the aneurysm had bled primarily into the sella and secondarily through an incompetent diaphragma sellae into the subarachnoid space. Absence of a bony septum in the posteromedial segment of the carotid cave[9] allows direct contact of the pulsatile aneurysmal dome with the dura, which eventually could cause its progressive erosion and the intrasellar hemorrhage. Advanced MR imaging techniques have improved our ability to identify the ruptured lesion in cases of multiple intracranial aneurysms, where MR imaging may identify a parenchymal clot adjacent to an aneurysm and recently has been used to determine an intradural or extradural location in unruptured paraclinoid aneurysms.

Conclusion

We report the case of a patient with a unique presentation of a paraclinoid aneurysm with intrasellar hemorrhage. Lesions located in the paraclinoid carotid can be difficult to clearly define as intradural or extradural. In this case, localization of the paraclinoid lesion (intradural vs extradural) and identification of the aneurysm responsible for the subarachnoid hemorrhage were critical in choosing a treatment strategy. The presence of intrasellar blood and the relationship of the paraclinoid aneurysm to the dura elegantly demonstrated on MR

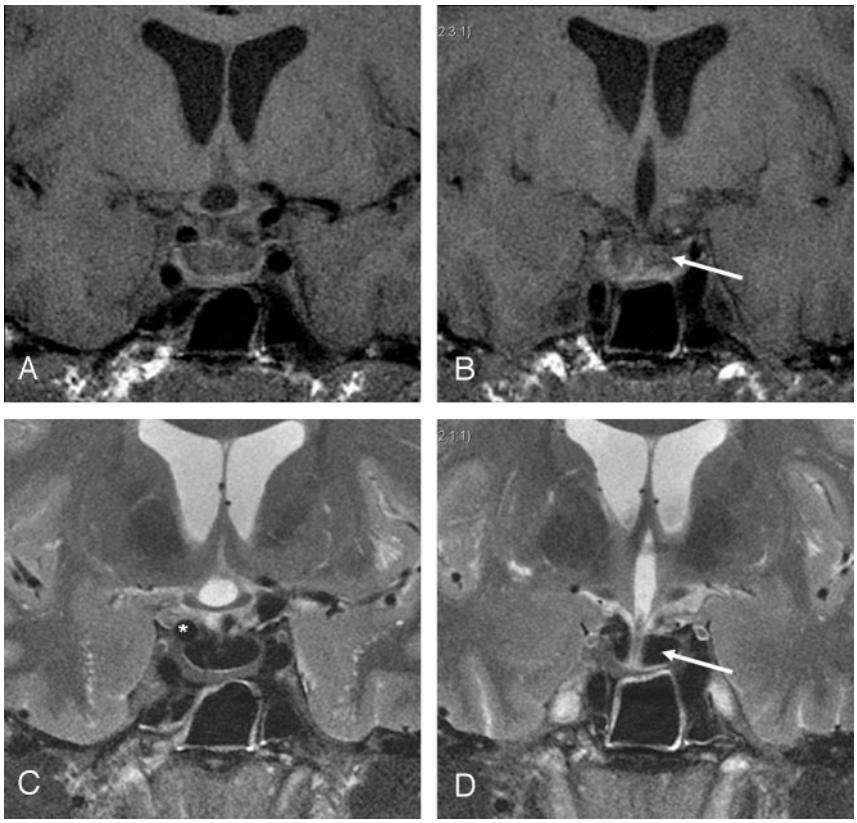

Fig 3. Coronal T1- and T2-weighted 3T MR imaging through anterior (*A,C*) and posterior (*B,D*) sella. *C,* Junction of aneurysmal neck and body (*), which projects partly superior to dural ring (*interface with CSF*) and partly inferior to the dural ring (*interface with blood within sella*). Note the large sella turcica filled with blood (*arrows*) showing homogeneous hypointensity on T2-weighted images and isointensity on T1-weighted images, consistent with intracellular deoxyhemoglobin. Note that the blood in the suprasellar cisterns has different signal intensity. *D,* The infundibulum can be traced to the compressed pituitary.

imaging were critical in choosing the target lesion for treatment.

References

1. Kupersmith MJ, Stiebel-Kalish H, Huna-Baron R, et al. **Cavernous carotid aneurysms rarely cause subarachnoid hemorrhage or major neurologic morbidity.** *J Stroke Cerebrovasc Dis* 2002;11:9–14
2. Linskey ME, Sekhar LN, Hirsch WL Jr, et al. **Aneurysms of the intracavernous carotid artery: natural history and indications for treatment.** *Neurosurgery* 1990;26:933–37
3. Nutik SL. **Subclinoid aneurysms.** *J Neurosurg* 2003;98:731–36
4. Beretta F, Sepahi AN, Zuccarello M, et al. **Radiographic imaging of the distal dural ring for determining the intradural or extradural location of aneurysms.** *Skull Base* 2005;15:253–61
5. Gonzalez LF, Walker MT, Zabramski JM, et al. **Distinction between paraclinoid and cavernous sinus aneurysms with computed tomographic angiography.** *Neurosurgery* 2003;52:1131–39
6. Hashimoto K, Nozaki K, Hashimoto N. **Optic strut as a radiographic landmark in evaluating neck location of a paraclinoid aneurysm.** *Neurosurgery* 2006;59:880–95
7. Oikawa S, Kyoshima K, Kobayashi S. **Surgical anatomy of the juxta-dural ring area.** *J Neurosurg* 1998;89:250–54
8. Thines L, Gauvrit JY, Leclerc X, et al. **Usefulness of MR imaging for the assessment of nonophthalmic paraclinoid aneurysms.** *AJNR Am J Neuroradiol* 2008;29:125–29
9. Hitotsumatsu T, Natori Y, Matsushima T, et al. **Micro-anatomical study of the carotid cave.** *Acta Neurochir (Wien)* 1997;139:869–74

Journal of Neuroradiology 34 (2007) 205–211

TECHNICAL NOTE

Surgical views from three-dimensional digital subtraction angiography for the planning of aneurysm surgery

Vues chirurgicales à partir de l'angiographie tridimensionnelle pour le planning de la chirurgie anévrismale

L. Thines[a,*], C. Taschner[b], J.-P. Lejeune[a], V. Le Thuc[c], J.-P. Pruvo[b], P. Bourgeois[a], X. Leclerc[b]

[a] *Department of Neurosurgery, University Hospital of Lille, Lille, France*
[b] *Department of Neuroradiology, University Hospital of Lille, Lille, France*
[c] *Department of Radiology, University Hospital of Lille, Lille, France*

KEYWORDS
Cerebral aneurysm;
Three-dimensional angiography;
Volume-rendering;
Image processing;
Surgical simulation

Abstract

Aim. — To develop a semi-automatic protocol helping to present directly and quickly three-dimensional digital subtraction angiography (3D-DSA) data in an orientation that reproduces exactly the neurosurgeon's intraoperative view.

Method. — Post-processing of 3D-DSA data (volume-rendering) was performed on an Integris workstation (Philips, Best); surgical views were obtained by visualization of the patient's head through a frontopterional approach: the 3D volume was turned 135° in the sagittal plane (around the *X* axis) and rotated by 45° and 60° in the coronal plane (around the *Y* axis). The protocol was evaluated on a consecutive series of nine patients who had ruptured or asymptomatic anterior circulation aneurysms requiring surgical treatment. Frontopterional views of angiographic 3D data were compared with intraoperative views.

Results. — The proposed semi-automatic algorithm is simple, fast and reproducible, and displays the 3D data in an orientation identical to the intraoperative views. The surgical anatomy of the anterior communicating artery was best reproduced with a coronal rotation of 60°, with a coronal rotation of 45° for the other aneurysm locations. In each case, the surgical reconstructions allowed a more accurate analysis of the vascular anatomy around the aneurysm, and facilitated pre- and perioperative planning.

Conclusion. — The present protocol displays angiographic 3D data in a projection that exactly reproduces the vascular anatomy through a frontopterional approach. It may help neurosur-

* Corresponding author. Clinique neurochirurgicale, hôpital Roger-Salengro, CHRU, 59037 Lille cedex, France.
E-mail address: Laurent.Thines@wanadoo.fr (L. Thines).

0150-9861/$ - see front matter
doi:10.1016/j.neurad.2007.02.001

geons to better anticipate any potential difficulties during access and clip-positioning arising due to the specific vascular anatomy of a given patient.

MOTS CLÉS
Anévrysme intracrânien ;
Angiographie 3D ;
Rendu volumique ;
Post-traitement d'images ;
Simulation chirurgicale

Résumé
But. — Développer un protocole semi-automatique permettant de présenter directement et rapidement les vues d'angiographie tridimensionnelle (ATD) selon une orientation qui reproduise exactement la vue opératoire du neurochirurgien.
Méthode. — Le post-traitement des données d'ATD a été réalisé sur une station de travail Integris (Philips, Best) et les vues chirurgicales ont été obtenues en reproduisant la visualisation de la tête du patient selon un abord frontoptérional. Pour cela, le volume 3D était tourné de 135° dans le plan sagittal (autour de l'axe des X) et tourné de 45 et 60° dans le plan coronal (autour de l'axe des Y). Le protocole a été évalué sur une série consécutive de neuf patients présentant un anévrisme rompu ou non de la circulation antérieure nécessitant un traitement chirurgical. Les vues frontoptérionales d'ATD ont été comparées aux vues opératoires.
Résultats. — L'algorithme semi-automatique proposé est simple, rapide et reproductible, et il fournit directement les vues 3D dans une orientation identique à celle de la vue opératoire. L'anatomie chirurgicale de l'artère communicante antérieure était mieux reproduite avec une rotation coronale de 60° et avec une rotation coronale de 45° pour toutes les autres localisations anévrismales. Dans chaque cas, les reconstructions chirurgicales ont permis une analyse plus précise de l'anatomie vasculaire autour de l'anévrisme et ont facilité le planning pré- et peropératoire.
Conclusion. — Le protocole présenté fournit des vues d'ATD selon une orientation qui reproduit précisément l'anatomie vasculaire selon un abord frontoptérional. Il aidera les neurochirurgiens à mieux anticiper les difficultés potentielles de l'abord et du clippage liées à l'anatomie vasculaire spécifique de chaque patient.

Introduction

Various factors determine the success of cerebral aneurysm surgery. One of them is the ability of the neurosurgeon to anticipate potential difficulties in dissecting and clipping the aneurysm. Three-dimensional radiological techniques, 3D-computerized tomography angiography (3D-CTA) and three-dimensional digital subtraction angiography (3D-DSA) are useful tools for analysis of the arterial relationships and projection of intracranial aneurysms and, therefore, may help to predict the pitfalls and risks of surgery.

This study aimed to develop a semi-automatic 3D-DSA protocol to display views of the arterial tree in the same orientation as through a frontopterional approach, and to validate this algorithm using intraoperative views. The objective was to increase the quality of the pre- and perioperative planning of anterior circulation aneurysm surgery.

Method

Patients

The 3D-DSA surgical view protocol was evaluated on a consecutive series of nine patients who had ruptured or asymptomatic anterior circulation aneurysms requiring surgical treatment (Table 1). Thirteen aneurysms were studied: seven middle cerebral artery aneurysms, three posterior carotid artery aneurysms, two anterior communicating artery (ACoA) aneurysms and one carotid artery termination aneurysm.

Angiographic technique

The patient's head was positioned on a standard headrest. Rotational DSA covering 240° at 55° per s was performed on an Allura V 5000 (Philips, Best, the Netherlands) during selective injection of a non-ionic contrast material into the internal carotid artery (ICA) at a flow-rate of 4 ml/s using the propeller rotation technique. Post-processing of dynamic angiographic data, including volume-rendering, was performed on an Integris workstation (Philips). The initial reconstructed volume could be viewed interactively. This allowed the vessel morphology to be displayed in any spatial orientation. The surgical reconstructions were printed on film.

Surgical reconstruction technique

At the 3D-DSA workstation, the head of the patient was centered according to a three-dimensional coordinate system included in the reconstruction software (Fig. 1a, b). The *X* axis was defined as the horizontal axis, the *Y* axis as the vertical axis and the *Z* axis as the anteroposterior axis. The surgical reconstructions were obtained by successive rotations of the 3D-DSA volume from the lateral view (automatically displayed by the software) as follows (Fig. 1c, d):

Table 1 Characteristics of the patient series
Tableau 1 Caractéristiques de la série des patients

	Side	Aneurysm 1: site/measurements	Aneurysm 2: site/measurements
Patient 1	Left	**Posterior ICA**/*S: 4.2 N: 1.6*	**ICA Termination**/*S: 3 N: 1.5*
Patient 2	Left	**Posterior ICA**/*S: 20 N: 3*	—
Patient 3	Left	**Posterior ICA**/*S: 10 N: 5*	**MCA**/*S: 2 N: 4*
Patient 4	Left	**MCA**/*S: 5 N: 3*	**MCA**/*S: 20 N: 5*
Patient 5	Left	**ACoA**/*S: 6 N: 2*	—
Patient 6	Right	**MCA**/*S: 10 N: 4*	**MCA**/*S: 2.7 N: 2.4*
Patient 7	Left	**MCA**/*S: 6.5 N: 8.3*	—
Patient 8	Right	**MCA**/*S: 6 N: 4*	—
Patient 9	Left	**ACoA**/*S: 8 N: 5*	—

S: size of the sac in mm; N: size of the neck in mm.

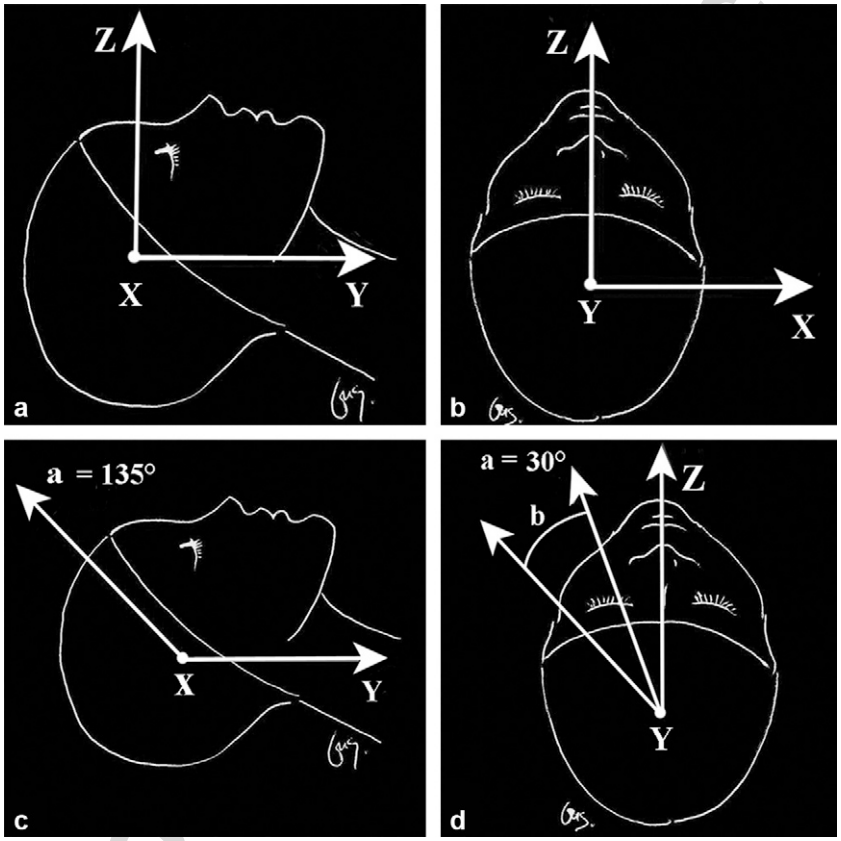

Figure 1 a, b: Three-dimensional coordinate system included in the reconstruction software; c, d: Rotation of the *Y* axis around the *X* axis was 135°, positive for a left approach and negative for a right approach. The rotation of the *Z* axis around the *Y* axis was 45°, 60° or 90°, positive for a left approach and negative for a right approach. Angle *a* = initial contralateral rotation of the head in the Mayfield device (30°). Angle *b* = additional rotational angle of the microscope axis (15°, 30°, 60°).
Figure 1 a, b : Référentiel tridimensionnel inclus dans le logiciel de reconstruction ; c, d : La rotation de l'axe Y autour de l'axe X était de 135°, positive pour un abord gauche et négative pour un abord droit. La rotation de l'axe Z autour de l'axe Y était de 45°, 60° ou 90°, positive pour un abord gauche et négative pour un abord droit. Angle a = rotation controlatérale initiale de la tête dans la têtière de Mayfield (30°), Angle b = angle de rotation additionnel de l'axe du microscope (15°, 30°, 60°).

- the rotation around the *Z* axis was 0;
- the rotation of the *Y* axis around the *X* axis was 135°, positive for a left approach and negative for a right approach;
- the rotation of the *Z* axis around the *Y* axis was 45°, 60° or 90°, positive for a left approach and negative for a right approach.

Surgical technique

The patient was positioned in the dorsal position; the head was fixed in a Mayfield device with a slight extension and a 30° rotation to the opposite side of the frontopterional approach. A semicircular incision was extended from the tragus to the frontal midline. A classic frontopterional

bone flap and an arciform dural opening were made. Large dissection of the sylvian fissure and the anterior part of the cerebral arterial circle were achieved. After aneurysm delineation, a titanium Yasargil clip was applied.

Validation

Direct comparisons were made between the 3D-DSA surgical views and the operative field shots. We determined the most suitable rotational *Y* angle for the best representation of the surgical view for each aneurysm location. We studied the quality of the visualizations of the arterial tree and the aneurysms (sac and neck). These reconstructions were also compared with standard 3D-DSA views (lateral, anterior, posterior and superior).

Results

The application of this protocol was feasible in all patients. The reconstruction technique was very fast (about 5 min). The suitable rotational angle around the *Y* axis for visualization of ACoA aneurysms was 60° (Fig. 2), and 45° for the other aneurysm locations (Figs. 3 and 4). Radiosurgical correlations were excellent for each specific rotational angle (Table 2). There was no discordant case with the technique itself although, in case 4, the arterial tree was only partially visualized during surgery because of a narrow dissec-

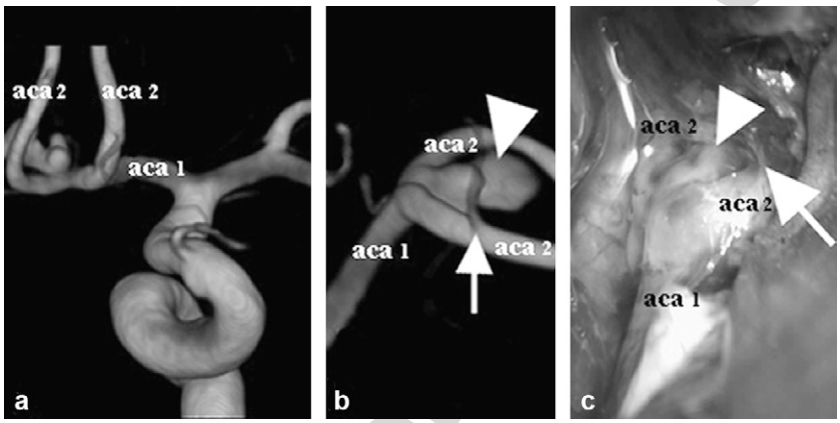

Figure 2 ACoA aneurysm: a: 3D-DSA anterior view; b: 3D-DSA surgical view; c: operative view. White arrowhead: AcoA aneurysm. White arrow: Heubner recurrent artery. ACA 1: A1 segment of the anterior cerebral artery; ACA 2: A2 segment of the anterior cerebral arteries.

Figure 2 Anévrisme de l'artère communicante antérieure. a : vue antérieure en angiographie tridimensionnelle ; b : vue chirurgicale en angiographie tridimensionnelle ; c : vue opératoire. Tête de flèche blanche : anévrisme de l'artère communicante antérieure. Flèche blanche : artère de Heubner. aca 1 : segment A1 de l'artère cérébrale antérieure ; aca 2 : segment A2 de l'artère cérébrale antérieure.

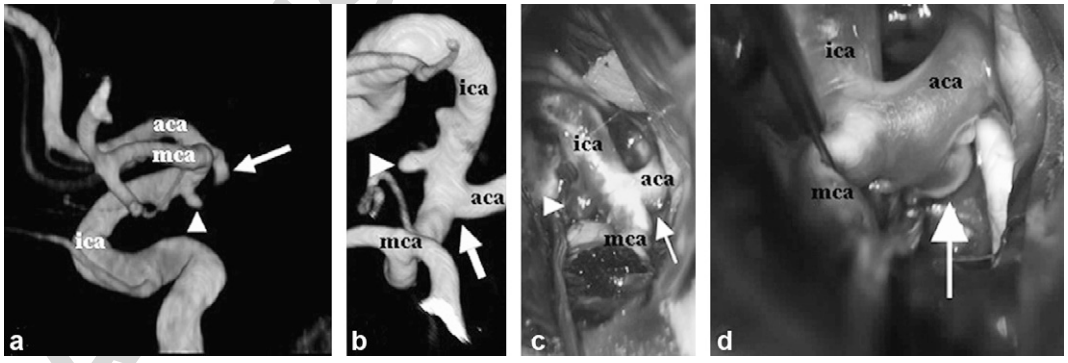

Figure 3 Posterior carotid artery and carotid artery bifurcation aneurysms. a: 3D-DSA lateral view; b: 3D-DSA surgical view; c: global operative view; d: operative view after carotid bifurcation mobilization. White arrowhead: posterior carotid artery aneurysm. White arrow: carotid artery bifurcation aneurysm (hidden by the bifurcation). ICA: internal carotid artery; ACA: anterior cerebral artery; MCA: middle cerebral artery.

Figure 3 Anévrismes de la face postérieure et de la terminaison carotidienne. a : vue latérale en angiographie tridimensionnelle ; b : vue chirurgicale en angiographie tridimensionnelle ; c : vue opératoire globale ; d : vue opératoire après mobilisation la terminaison carotidienne. Tête de flèche blanche : anévrisme de la face postérieure de l'artère carotide interne. Flèche blanche : anévrisme de la terminaison de l'artère carotide interne (caché par la bifurcation). ica : artère carotide interne ; aca : artère cérébrale antérieure ; mca : artère cérébrale moyenne.

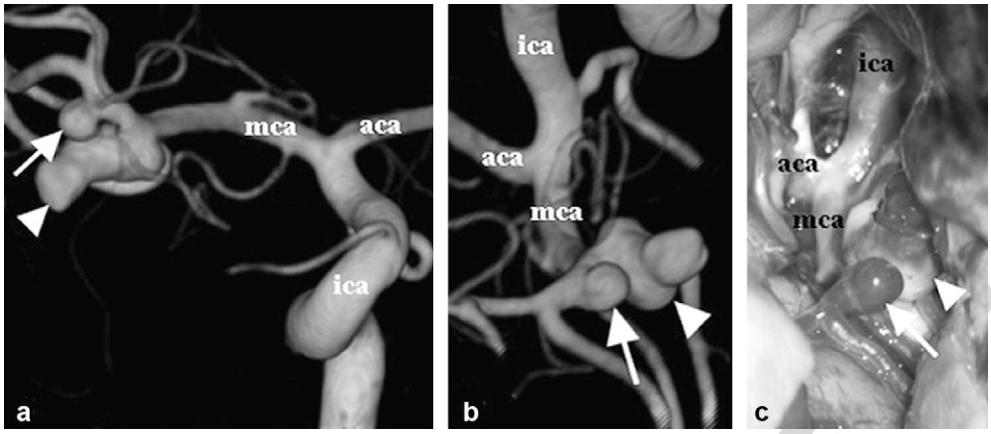

Figure 4 Middle cerebral artery aneurysms. a: 3D-DSA anterior view; b: 3D-DSA surgical view; c: operative view. White arrowhead: large MCA aneurysm. White arrow: small MCA aneurysm. ICA: internal carotid artery; ACA: anterior cerebral artery; MCA: middle cerebral artery.

Figure 4 Anévrismes de l'artère cérébrale moyenne. a : vue antérieure en angiographie tridimensionnelle ; b : vue chirurgicale en angiographie tridimensionnelle; c : vue opératoire. Tête de flèche blanche : large anévrisme de l'artère cérébrale moyenne. Flèche blanche : petit anévrisme de l'artère cérébrale moyenne. ica : artère carotide interne ; aca : artère cérébrale antérieure ; mca : artère cérébrale moyenne.

Table 2 Radiosurgical correlations
Tableau 2 Corrélations radiochirurgicales

	Aneurysm	Neck visualization	Sac visualization	Arterial tree visualization	Preferential coronal angle (°)
Patient 1	Number 1	+	+	+	45
	Number 2	+	+		45
Patient 2	—	+	+	+	45
Patient 3	Number 1	+	+	+	45
	Number 2	+	+		45
Patient 4	Number 1	+	+	nc	45
	Number 2	+	+		45
Patient 5	—	+	+	+	60
Patient 6	Number 1	+	+	+	45
	Number 2	+	+		45
Patient 7	—	+	+	+	45
Patient 8	—	+	+	+	45
Patient 9	—	+	+	+	60

nc = non-comparable data.

tion of the sylvian fissure (non-comparable data). Comparisons between the standard 3D-DSA and frontopterional views are summarized in Table 3.

Discussion

DSA is used in many centers for intracranial aneurysm detection [3,9,11]. Adjunctive three-dimensional reconstructions improve the accuracy of the radiological analysis: neck and sac measurement, and neck and sac relationship to parent artery and neighboring branches. 3D-DSA is perfectly adapted to planning (neck location, road-mapping, coil placement) [1,2,7] and to postoperative management [5,6] of endovascular treatment. This technique is also widely used for preoperative evaluation [10] and postoperative follow-up of clipped aneurysms [4].

It can also optimalize planning of aneurysm surgery. Recently, colleagues of the University of Patras (Rion, Greece) published a 3D-CTA protocol allowing reproduction of the surgical view of anterior circulation aneurysms [8]. Simultaneously and independently at our institution, we were evaluating the value of an equivalent 3D-DSA protocol (presented in this paper). Overall, the methodology of our study was similar, except that the coordinate system axes were automatically included in the reconstruction software we used. Also, although the Greeks used a different terminology for their axes, we found approximately the same rotational angles for each location with one exception: we used exactly opposite angles for the analysis of a right or a left frontopterional approach.

This protocol displayed semi-automatic and direct 3D-DSA reconstructed surgical views of the anterior circulation arteries oriented for a frontopterional approach. The rotational angles were approximated by observation of the patient's head position and the microscope's axis orientation during surgery (Fig. 5). The *X* angle corresponds to the microscope positioned beside and above the patient's head. The *Y* angle corresponds to a lateral course of the

Table 3 Comparisons between standard 3D-DSA views and surgical views
Tableau 3 Comparaisons entre vues standards d'angiographie tridimensionnelle et vues chirurgicales

	Aneurysm	Objective
Patient 1	Number 1	Identification of relationship to the anterior choroidal artery
	Number 2	Location of the aneurysm (hidden by the carotid termination)
Patient 2	—	Identification of relationship to the anterior choroidal artery hidden by the aneurysm sac
Patient 3	Number 1	Identification of relationship to the posterior communicating artery at the neck (hidden by the sac and the ICA)
	Number 2	Identification of relationship to MCA branches
Patient 4	Number 1	Identification of relationship to the temporal branch of the MCA
	Number 2	Identification of relationship to MCA branches
Patient 5	—	Evaluation of sac projection/Identification of relationship to the ACA1 and ACA2 plus Heubner recurrent artery
Patient 6	Number 1	Identification of relationship to MCA branches
	Number 2	Identification of relationship to MCA branches and between the two aneurysm necks
Patient 7	—	Identification of relationship to MCA branches
Patient 8	—	Identification of relationship to MCA branches
Patient 9	—	Evaluation of sac projection/Identification of relationship to the ACA1 and ACA2

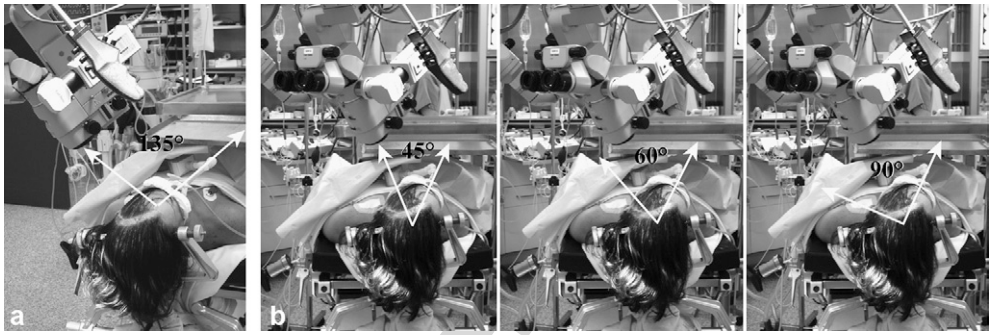

Figure 5 a: Sagittal rotation of the microscope axis (*X* angle); b: coronal rotation of the microscope axis (*Y* angle).
Figure 5 a : rotation sagittale de l'axe du microscope (angle X) ; b : rotation coronale de l'axe du microscope (angle Y).

microscope for the surgical dissection, and takes into account the initial contralateral rotation of the head in the Mayfield device (about 30°). We then determined which angle corresponded to each specific aneurysm location. A more tangential angle (60°) was suitable for the exploration of ACoA aneurysms whereas, in other locations, a 45° rotational angle gave the best results.

According to the good radiosurgical correlations obtained with this small series of patients, this 3D-DSA protocol appears to be a reliable technique for the surgical representation of anterior circulation aneurysms. However, these angles do not summarize the multiple positions of the microscope used for this surgery, and such reconstructions cannot replace viewing the 3D data from multiple angles on the workstation. Nevertheless, they provide a global and direct view of the vascular conformation through a frontopterional approach as seen by the neurosurgeon after exposure of the anterior circulation and the aneurysm. Preoperatively, this protocol facilitates mental representation of the exact three-dimensional arterial relationships of the aneurysm, and allows anticipation of any potential difficulties in the clipping procedure. Perioperatively, it avoids beginning the dissection at the site the aneurysm bleb, and it shows the exact three-dimensional orientation of the aneurysm sac and the precise positions of neighboring branches (particularly those next to the aneurysm sac), thus allowing adjustment of clip position.

This semi-automatic protocol is fast, simple and reproducible. It gives additional information on the vascular anatomy that the neurosurgeon will encounter during the frontopterional approach. It allows for better pre- and perioperative planning for surgical clipping by predicting the surgical position of the aneurysm and its surrounding blood vessels. It should be of particular interest in difficult operations such as giant or calcified aneurysm surgery.

References

[1] Abe T, Hirohata M, Tanaka N, Uchiyama Y, Kojima K, Fujimoto K, et al. Clinical benefits of rotational 3D angiography in endovascular treatment of ruptured cerebral aneurysm. AJNR Am J Neuroradiol 2002;23:686–8.

[2] Anxionnat R, Bracard S, Ducrocq X, Trousset Y, Launay L, Kerrien E, et al. Intracranial aneurysms: clinical value of 3D digital subtraction angiography in the therapeutic decision and endovascular treatment. Radiology 2001;218:799–808.

[3] Hochmuth A, Spetzger U, Schumacher M. Comparison of three-dimensional rotational angiography with digital subtraction angiography in the assessment of ruptured cerebral aneurysms. AJNR Am J Neuroradiol 2002;23:1199–205.

[4] Kang HS, Han MH, Kwon BJ, Jung SI, Oh CW, Han DH, et al. Postoperative 3D angiography in intracranial aneurysms. AJNR Am J Neuroradiol 2004;25:1463–9.
[5] Kiyosue H, Okahara M, Tanoue S, Nakamura T, Nagatomi H, Mori H. Detection of the residual lumen of intracranial aneurysms immediately after coil embolization by three-dimensional digital subtraction angiographic virtual endoscopic imaging. Neurosurgery 2002;50:476–84.
[6] Kiyosue H, Tanoue S, Okahara M, Hori Y, Nakamura T, Nagatomi H, et al. Anatomic features predictive of complete aneurysm occlusion can be determined with three-dimensional digital subtraction angiography. AJNR Am J Neuroradiol 2002;23:1206–13.
[7] Missler U, Hundt C, Wiesmann M, Mayer T, Bruckmann H. Three-dimensional reconstructed rotational digital subtraction angiography in planning treatment of intracranial aneurysms. Eur Radiol 2000;10:564–8.
[8] Siablis D, Kagadis GC, Karamessini MT, Konstandinou, D, Karnabatidis D, Petsas T, et al. Intracranial aneurysms: reproduction of the surgical view using 3D-CT angiography. Eur J Radiol 2005;55:92–5.
[9] Sugahara T, Korogi Y, Nakashima K, Hamatake S, Honda S, Takahashi M. Comparison of 2D and 3D digital subtraction angiography in evaluation of intracranial aneurysms. AJNR Am J Neuroradiol 2002;23:1545–52.
[10] Tanoue S, Kiyosue H, Kenai H, Nakamura T, Yamashita M, Mori H. Three-dimensional reconstructed images after rotational angiography in the evaluation of intracranial aneurysms: surgical correlation. Neurosurgery 2000;47:866–71.
[11] Tu RK, Cohen WA, Maravilla KR, Bush WH, Patel, NH, Eskridge J, et al. Digital subtraction rotational angiography for aneurysms of the intracranial anterior circulation: injection method and optimization. AJNR Am J Neuroradiol 1996;17:1127–36.

Journal of Neurosurgery
(Accepted)

Intraoperative biplanar rotational angiography during neurovascular surgery: Technical Note

Amir R. Dehdashti MD, Laurent Thines MD, Leodante B. Da Costa MD, Karel G. terBrugge MD, Robert A. Willinsky MD, M. Christopher Wallace MD, Michael Tymianski MD PHD

Division of Neurosurgery and Division of Neuroradiology, Department of Medical Imaging, Toronto Western Hospital, University of Toronto, Toronto, Ontario, Canada

Corresponding author: Michael Tymianski MD

Division of Neurosurgery, Toronto Western Hospital, 399 Bathurst Street,4th Floor, University of Toronto , Toronto, M5T 2S8, Ontario, Canada

Email: mike.tymianski@rogers.com Tel: 1 416 6035800 ext 2896 Fax: 1 416 6035298

Running title: Intraoperative rotational angiography

Key words: intraoperative angiography, rotational angiography, three dimensional angiography, endovascular surgical suite, aneurysm, arteriovenous malformation

Abstract

Object. The purpose of this study is to evaluate initial experience with integration of high-resolution rotational and biplanar angiography during neurovascular operative procedures.

Methods. Eight patients with intracerebral AVMs (6) and aneurysms (2) underwent surgical treatment of their lesions in a combined endovascular surgical suite. After initial head positioning, a preoperative biplane and rotational angiogram was performed. Surgery was then carried out for resection of the AVM or clipping of the aneurysm. A further biplane and rotational 3D angiogram were performed intraoperatively to confirm the satisfactoriness of treatment.

Results. One small AVM residual identified intra-operatively necessitated further resection. One aneurysm was clipped during endovascular inflation of an intracarotid balloon for temporary proximal control. The completeness of treatment was confirmed using intraoperative 3D rotational angiography for all cases without procedure related complications.

Conclusion. Intraoperative rotational angiography carried out in an integrated biplane angio/surgery suite is a safe and useful adjunct to surgery, and may enable combining endovascular and surgical procedures for the treatment of complex vascular lesions.

In the past decades, angiography has evolved with the introduction of rotational angiography, 3D morphometry and 3D rotational angiography (6, 7, 12, 16). This technique permits the assessment and improves identification of anatomical details of neurovascular pathologies including aneurysm shape, size, relationship to neighboring vessels and AVM characteristics along with their 3D angioanatomy(6, 7). To date, this novel angiographic procedure has been used in neuroradiology to visualize complex vascular pathologies, and to provide optimal treatment using high resolution, high quality imaging. To date, such high quality imaging has been restricted to angiography suites, whereas conventional intraoperative angiography is most commonly performed using portable fluoroscopic equipment. The latter provides lower resolution, single plane images.

There are advocates for routine intraoperative angiography performed immediately after treatment with portable equipment, or post-operatively in angiography suites (1, 4, 9, 14, 15). A recent meta-analysis has shown that routine intraoperative angiography remains the most cost-effective form of confirming satisfactoriness of surgical aneurysm clipping (14). However, conventional equipment has limitations associated with suboptimal image quality, uniplanar image guidance and lack of 3D acquisition. The integration of high resolution 3D biplane angiography in the setting of an endovascular/surgical suite is a promising step towards improved intra-operative diagnostics and endovascular support during neurovascular surgery (3, 11). We describe herewith our initial experience with intraoperative rotational angiography in aneurysm and AVM surgery done in our combined endovascular/surgical suite. The feasibility of intraoperative rotational angiography in the management of aneurysms and AVMs is evaluated.

Clinical material and methods

Since combining surgery with intraoperative 3D rotational angiography had not been previously carried out, we applied this technique to cases of progressively increasing complexity to confirm its feasibility, practicality and utility. During 4 consecutive months, 8 patients with intracranial vascular lesions (6 AVMs and two large aneurysms) were surgically treated in our combined endovascular/surgical suite. This suite consists of a fully-equipped operating theater combined with full biplane and rotational digital subtraction (DS) equipment (GE Advantx LCN Plus biplanar DSA Unit, GE medical system, Milwaukee, WI) a DS angiography control room and a computer room(GE workstation Advantage 4.2, GE medical system). Ample operative space (12 x 10 m) is required for performance of endovascular procedures and microsurgery (Figure 1).

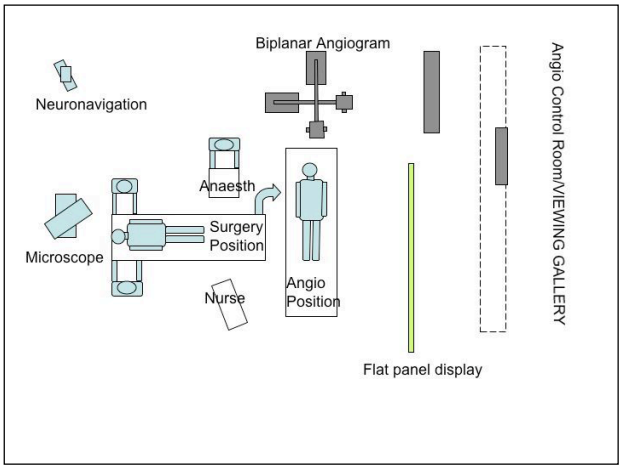

Figure 1: The illustration shows the general concept of our endovascular surgical suite as described in the method section.

The DS angiographic system consists of a standard biplane C-arm unit comprising a floor-mounted frontal plane and a ceiling mounted lateral plane, allowing for both biplanar fluoroscopy with digital acquisition and rotational 3D angiography capability. The angiography table is equipped with a radiolucent head fixation system. The table is mounted on a pivot, capable of laterally rotating the long axis of the table 180 degrees in order to switch the patients' orientation from a position that enables angiography (Figure 2), to a position (usually a 90 degree turn) that brings the patient into a surgical field (Figure 3). Seven flat – panel display monitors are installed in the suite to enable the surgical and endovascular operators to view biplane angiographic images and 3D images. A neuronavigation system (Medtronic,Stealth®) and microscope (Zeiss NC4, OPMI neuro) are also installed.

Figure 2 - Patient's position during intraoperative angiography and rotational

Figure 3- Patient's position during the surgery. The table is rotated 90 degrees from

Endovascular and surgical procedures setup

Patients are transferred to the endovascular/surgical suite and undergo general anesthesia. The patient's head is fixed in the head fixation apparatus and positioned according to the location of the vascular abnormality. The radiolucent frame enables the positioning of the head about 20 degrees above the heart axis. The angiographic catheter is introduced at the beginning of the procedure. Thereafter, a diagnostic biplane angiogram and a rotational 3D angiogram is performed with the head fixed in the desired position (Figure 2) for the purpose of obtaining baseline imaging, to optimize quality and to ascertain that the head position does not preclude complete movement of the 3D rotational gantry around the surgical field. Rotational images are obtained by 200 degrees rotation of the Carm in 5 seconds. Following this, the table is laterally rotated to the surgical area (Figure 3) and the surgery is carried out using routine methods. Whenever an angiogram is required, the bone flap is returned to the head and fixated with a single miniplate thus decreasing air artifact. The patient is then covered with a sterile plastic covering (Figure 4) and rotated back to the angiographic position. These maneuvers take approximately 5 minutes. Then intraopertive biplane and rotational imaging are performed **(See movie file),** providing image quality identical to that of a routine diagnostic 3D angiogram. The patient is then rotated back to the surgical field for continuation of surgery.

Initially (first three cases) the angiogram was repeated at the end of the procedure to reconfirm satisfactoriness of treatment (AVM resection or aneurysm clipping). However, due

to the high quality of the imaging obtained intraoperatively, we are re-evaluating the need to repeat the angiogram at the end of the procedure.

Figure 4 - The sterile plastic covering protects the patient's head during the rotation to the angiographic position. These maneuvers take approximately 5 minutes.

Special considerations in aneurysm surgery

Intraoperative angiography may be applied to assess adequacy of aneurysm obliteration, but also as an endovascular adjunct for obtaining proximal flow control instead exposing proximal vessels in the neck, or in the paraclinoidal region. After initial surgical exposure of the aneurysm, the patient is rotated to the angiographic position and a balloon catheter is introduced via the femoral route and the tip positioned in the parent artery, ready to perform the balloon occlusion. The patient is the rotated back to the surgical field and the procedure continues. When proximal vascular control is desired, the patient is rotated back to the angiographic position and the balloon inflated under direct fluoroscopic vision, and the patient rotated back for continuation of surgery. Anticoagulation by heparin is introduced as a single bolus of 100 IU/kg during the balloon occlusion which last a few minutes. Clipping of the aneurysm neck is then carried out with the aneurysm softened, and the balloon is then deflated. No further anticoagulation is needed. With the patient back in the angiographic position, a biplane and 3D angiograms are performed to assess the clipping.

Results

The technique was applied successfully in all 8 cases. There were 6 AVM patients. In one of the AVM cases consisting of a small post-operative residual lesion, the preoperative angiogram after head positioning showed spontaneous obliteration of the AVM. Due to this, further surgical exploration was deemed unnecessary and the patient was scheduled for follow-up angiography in 6 months.

All other 5 AVM cases underwent surgical removal and in one case a small residual was identified at the time of intraoperative angiography, necessitating continuation of the surgery to achieve total resection. There were no new neurological complications after the combined endovascular and surgical treatment in the AVM series.

Both aneurysms in this series were large and unruptured. Surgical exclusion of the aneurysm was confirmed after the intraoperative standard and rotational angiogram. In one case, a balloon catheter was inflated for 3 min. in the high cervical internal carotid artery to provide proximal vascular control and softening of the aneurysm. There were no procedure-related complications. A preoperative visual deficit present in one patient improved moderately after decompression of the aneurysm.

Rotational angiography provided excellent quality images in all cases with reliable interpretation allowing a definite diagnosis of the exclusion of AVMs or total obliteration of the two aneurysms with patency of parent vessels.

Case illustration (AVM patient no.6):

A19 year-old male had presented with right posterior frontal hemorrhage causing a moderate left hemiparesis and cerebral angiogram showed a small diffuse parasagittal precentral gyrus AVM (Fig. 5a). He subsequently underwent surgery at another institution. Postoperatively, a residual AVM was identified and radiosurgery was suggested. Follow-up angiogram at 3 years showed no change in the size of the residual AVM and the patient was transferred to our institution for further management. After discussion in our multidisciplinary AVM clinic, surgical resection of the residual AVM was considered as the most effective treatment. Figure 5b shows the immediate preoperative angiogram performed with the patient's head positioned in the radiolucent head frame. After craniotomy and resection of the AVM, an intraoperative angiogram and rotational angiogram were performed and showed a persistent shunt with a residual micronidus (Figure 5c and 5d). Further exploration and resection of the suspicious area was performed and the final angiogram confirmed total excision of the AVM (Figure 5e).

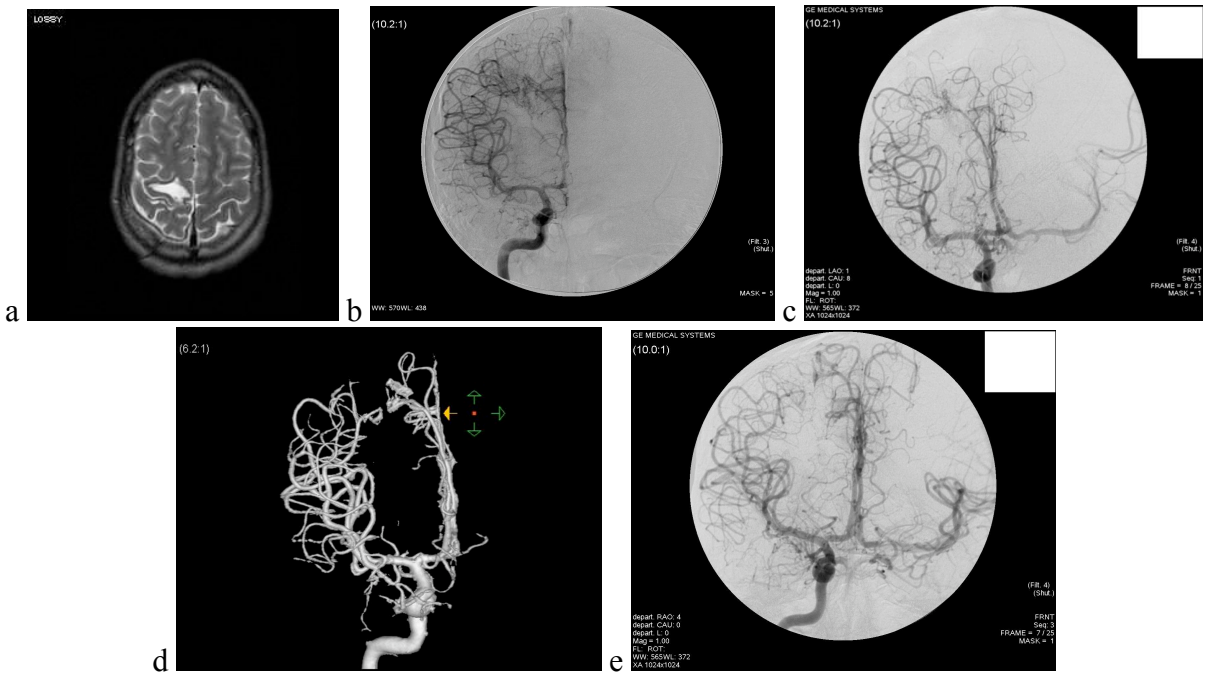

Figure 5 - 5a: Axial T2 MR shows location of the previous hemorrhage in the precentral gyrus due to a diffuse parasagittal posterior frontal AVM ; 5b: Immediate preoperative angiogram (AP view) performed with the patient's head positioned in the radiolucent head frame showing the residual AVM ; 5c: Intraoperative rotational angiogram showing a persistent shunt with a residual micronidus necessitating further exploration ; 5d: Intraoperative 3D image confirms the presence of a residual micronidus ; 5e: Final intraoperative angiogram confirming the total resection of the AVM.

Identification of this micro residual AVM would have been more difficult without high quality intraoperative imaging and 3D reconstruction. The patient's post operative course was uneventful without new neurological deficit.

Discussion

Endovascular intervention has been performed in the operative room by using a portable C-arm system especially in the setting of general vascular surgery and triple-A aneurysm repair (5). Many neurosurgical units still use this technique in routine intracranial vascular surgery. Although the results are acceptable, the quality of images is insufficient for neurovascular interventions. Furthermore, the limitations of this technique preclude sophisticated imaging like rotational angiography and 3D acquisition. On the other hand, combined endovascular and microsurgical approaches for intracranial vascular pathologies have gained further attention and it has been suggested that evolving endovascular technologies need to be integrated into the microsurgical management of these lesions. Conventional therapy with a single treatment modality has shown its failure in some complex vascular cases. Lawton et al. have reported their series of 77 patients who underwent multimodality treatment and concluded that this strategy should be adopted in the management armamentarium of complex and complicated vascular cases (10). Ricci et al. have reported on a small series of giant paraclinoidal and vertebrobasilar aneurysms treated by combined endo/microsurgery approach. They concluded that endovascular procedure allowed for a safe and reliable proximal control during microsurgical treatment of the aneurysm (13). A combined technique of flow alteration has been described by Hoh et al. for treatment of aneurysms unsuitable for clipping or coiling (8). Although these reports of different application of combined treatment in neurovascular pathologies were not performed in the angio/surgery suite, but they emphasize the importance of close collaboration in the management of these formidable lesions.

Neurovascular surgery performed in the endovascular/surgical unit has several advantages (11). First, coil embolization and aneurysm clipping can be performed in the same setting and under one single general anesthesia. If the attempt for coiling is unsuccessful, the surgical repair can immediately follow the procedure. Second, post operative angiography can immediately confirm the position of the clip after clipping of the aneurysm or exclusion of the AVM. Third, combined surgical exposure can be performed through an endovascular procedure when this approach is considered optimal or when a transarterial-venous approach proves unsuccessful, such as in dural arteriovenous fistulas with isolated sinus. Fourth, excellent quality images along with rotational angiography and 3D acquisition can be performed and finally superficial landmarks on the surface of the brain or in the resection site can help in exact localization of a possible residual AVM(2). Murayama et al. have described their initial experience with an endovascular operating suite and have also confirmed its effectiveness and practicality in intracranial vascular procedures (11). However, they had not reported the use of intraoperative rotational 3D angiography. In our view, the addition of rotational 3D angiography in the intraoperative setting offers the surgeon the same additional advantages with respect to improved assessment of the angioarchitecture, as those afforded by 3D angiography in the routine diagnostic setting (7). Our preliminary experience with this concept and intraoperative rotational angiogram has encouraged us to perform more neurovascular procedures in the endovascular/surgical suite.

Current limitations of the endovascular/surgical suite

Currently, movements of the operating/angio table are restricted to orthogonal (X,Y,Z plane) movements. Most conventional angiography tables do not provide for tilt and yaw like conventional surgical tables. This limits patient selection to those in whom significant adjustments of table position are not required. This limitation exists also for the current

endovascular operating suite which will be hopefully addressed with new table designs in the future.

Our initial experience with intraoperative 3D rotational angiography suggests that this technique is safe, efficacious, and practical. We believe that this technique will improve the accuracy and quality of intraoperative imaging and provides increased safety and completeness in the management of neurovascular patients.

Conclusion

The addition of high quality intraoperative 3D rotational angiography to intracranial vascular neurosurgery provides a safe and useful adjunct to the diagnostic and therapeutic approach to neurovascular pathologies.

References

1. Alexander TD, Macdonald RL, Weir B, Kowalczuk A: Intraoperative angiography in cerebral aneurysm surgery: a prospective study of 100 craniotomies. **Neurosurgery** 39:10-17; discussion 17-18, 1996.

2. Ayad M, Ulm AJ, Yao T, Eskioglu E, Mericle RA: Real-time image guidance for open vascular neurosurgery using digital angiographic roadmapping. **Neurosurgery** 61:55-61; discussion 61-52, 2007.

3. Calligaro KD, Dougherty MJ, Patterson DE, Raviola CA, DeLaurentis DA: Value of an endovascular suite in the operating room. **Ann Vasc Surg** 12:296-298, 1998.

4. Chiang VL, Gailloud P, Murphy KJ, Rigamonti D, Tamargo RJ: Routine intraoperative angiography during aneurysm surgery. **J Neurosurg** 96:988-992, 2002.

5. Fillinger MF, Weaver JB: Imaging equipment and techniques for optimal intraoperative imaging during endovascular interventions. **Semin Vasc Surg** 12:315-326, 1999.

6. Gauvrit JY, Leclerc X, Vermandel M, Lubicz B, Despretz D, Lejeune JP, Rousseau J, Pruvo JP: 3D rotational angiography: use of propeller rotation for the evaluation of intracranial aneurysms. **AJNR Am J Neuroradiol** 26:163-165, 2005.

7. Hoff DJ, Wallace MC, terBrugge KG, Gentili F: Rotational angiography assessment of cerebral aneurysms. **AJNR Am J Neuroradiol** 15:1945-1948, 1994.

8. Hoh BL, Putman CM, Budzik RF, Carter BS, Ogilvy CS: Combined surgical and endovascular techniques of flow alteration to treat fusiform and complex wide-necked intracranial aneurysms that are unsuitable for clipping or coil embolization. **J Neurosurg** 95:24-35, 2001.

9. Klopfenstein JD, Spetzler RF, Kim LJ, Feiz-Erfan I, Han PP, Zabramski JM, Porter RW, Albuquerque FC, McDougall CG, Fiorella DJ: Comparison of routine and selective use of intraoperative angiography during aneurysm surgery: a prospective assessment. **J Neurosurg** 100:230-235, 2004.

10. Lawton MT, Quinones-Hinojosa A, Sanai N, Malek JY, Dowd CF: Combined microsurgical and endovascular management of complex intracranial aneurysms. **Neurosurgery** 52:263-274; discussion 274-265, 2003.

11. Murayama Y, Saguchi T, Ishibashi T, Ebara M, Takao H, Irie K, Ikeuchi S, Onoue H, Ogawa T, Abe T: Endovascular operating suite: future directions for treating neurovascular disease. **J Neurosurg** 104:925-930, 2006.

12. Raabe A, Beck J, Rohde S, Berkefeld J, Seifert V: Three-dimensional rotational angiography guidance for aneurysm surgery. **J Neurosurg** 105:406-411, 2006.

13. Ricci G, Ricci A, Gallucci M, Zotta D, Scogna A, Costagliola C, Galzio RJ: Combined endovascular and microsurgical approach in the treatment of giant paraclinoid and vertebrobasilar aneurysms. **J Neurosurg Sci** 49:1-6, 2005.

14. Stein SC, Burnett MG, Zager EL, Riina HA, Sonnad SS: Completion angiography for surgically treated cerebral aneurysms: an economic analysis. **Neurosurgery** 61:1162- 1167; discussion 1167-1169, 2007.

15. Tang G, Cawley CM, Dion JE, Barrow DL: Intraoperative angiography during aneurysm surgery: a prospective evaluation of efficacy. **J Neurosurg** 96:993-999, 2002.

16. Willems PW, van Walsum T, Woerdeman PA, van de Kraats EB, de Kort GA, Niessen WJ, van der Sprenkel JW: Image-guided vascular neurosurgery based on threedimensional rotational angiography. Technical note. **J Neurosurg** 106:501-506, 2007.

Neurosurgery ***(submitted)***

64-detectors computerized tomography angiography for the postoperative assessment of clipped aneurysms.

LAURENT THINES [1,2,4], AMIR R. DEHDASHTI [2,4], MD., PETER HOWARD [3,4], MD., LEODANTE DA COSTA [3,4], MD., M. CHRISTOPHER WALLACE [2,4], MD, MSc., ROBERT A WILLINSKY, MD., MICHAEL TYMIANSKI [2,4], MD., PhD., JEAN-PAUL LEJEUNE [1] MD., RONIT AGID [3,4], MD

[1] Department of Neurosurgery, Lille University Hospital, Lille, France
[2] Division of Neurosurgery, Department of Surgery, Toronto Western Hospital, Toronto, Ontario, Canada
[3] Division of Neuroradiology, Department of Medical Imaging, Toronto Western Hospital, Ontario, Canada
[4] University of Toronto Brain Vascular Malformation Study Group, Toronto Western Hospital, Toronto, Ontario, Canada

Running title: 64-MDCTA post-clipping

Keywords: aneurysm remnant, cerebrovascular surgery, clipping, cerebral aneurysm, multi-detector computerized tomography angiography

Corresponding author: Dr. Michael Tymianski
Toronto Western Hospital, Division of Neurosurgery, 4W-435, 399 Bathurst Street, Toronto, ON, M5T-2S8, Canada
Tel: 416-603-5896 Fax: 416-603-5298 Email: mike.tymianski@uhn.on.ca

Object: Multi-detector computerized tomography angiography (MDCTA) is now a widely accepted technique for the diagnosis and the treatment decision making of intracranial aneurysms. The goal of this study was to evaluate the accuracy of 64-MDCTA for the postoperative assessment of clipped intracranial aneurysms in place of conventional digitalized subtraction angiography (DSA).

Methods: We analysed a consecutive series of 31 patients that underwent direct clipping procedures for 38 aneurysms between November 2005 and February 2008. MDCTA used a 64-slices MDCT scanner (Aquilion 64, Toshiba). Conventional DSAs were available for comparison in all cases. Two independent neuroradiologists analysed the following data: exam quality, artifacts, aneurysm remnant and patency of collateral branches. Interobserver agreement, sensitivity, specificity with 64-MDCTA were calculated.

Results: Aneurysms locations were: anterior circulation 79% and posterior circulation 21%. Phynox (cobalt-alloy) and Titanium (titanium-alloy) Yasargil clips were used respectively in 20 and 18 cases. Important artifacts were found in both techniques with multiple clips and cobalt-alloy clips. Remnants > 2 mm were found in 21% of the cases and two patients had one collateral branch occluded. Sensitivity and specificity of 64-MDCTA for the detection of a significant remnant (> 2mm) were respectively 67% (95% CI = 0.31-0.91) and 100% (95% CI = 0.85-1). Sensitivity and specificity of 64-MDCTA for the detection of the occlusion of a collateral branch were respectively 50% (95% CI = 0.03-0.97) and 100% (95% CI = 0.88-1). No relationship was found with the location, the type, shape, size and number of clips but missed remnants tended to be larger with cobalt-alloy clips.

Conclusions: 64-MDCTA is a non-invasive valuable exam to assess the postoperative result of clipped intracranial aneurysms and might be useful for the long term follow-up. It can't replace conventional DSA in particular conditions like cobalt-alloy or multiple clips, complex aneurysms and doubt on a collateral branch patency.

Keywords: aneurysm remnant, cerebrovascular surgery, clipping, cerebral aneurysm, multi-detector computerized tomography angiography

Introduction

The goal of intracranial aneurysm treatment is to obtain the complete obliteration of the aneurysm while preserving the patency of the parent and collateral vessels. Incomplete treatment expose the patient to regrowth and (re)bleeding (5;6;13;24;35;36) thus emphasizing the need for an accurate radiological technique documenting the quality of the treatment. Postoperatively, clipped aneurysms have traditionally been assessed using digitalized subtraction angiography (DSA), and this has remained the gold standard for this purpose. Recent advances in non-invasive imaging technologies have raised the possibility of replacing DSA in order to reduce constraints and risks associated with this technique (18;22). Computerized tomography angiography (CTA) is now a recognized valuable technique for the diagnosis and treatment decision of ruptured intracranial aneurysms (1;11;15;16;20;29;39;45). Because of artifacts related to the coils, CTA is not a suitable exam for the follow-up of embolized aneurysms and magnetic resonance angiography (MRA) is the technique of choice for this purpose (2;12;14;25;30;37;41). The advent of multi-detector computerized tomography (MDCT) scanners has reduced clips related artifacts and made it possible to reliably depict aneurysm remnants after surgical obliteration on CTA. Results about MDCTA capacities are sometimes contradictory in the literature (10;28;33;47). The goal of this study was to evaluate in real clinical practice the accuracy of recent 64-multidetector computerized tomography angiography (64-MDCTA) for the postoperative assessment of clipped intracranial aneurysms and to determine to which extent it could replace conventional DSA for this purpose.

Clinical Material and Methods

Study population

This study was approved by the Research Ethics Board of our institution. We analysed retrospectively a consecutive series of patients who underwent 64-MDCTA and DSA for the postoperative assessment of a clipped intracranial aneurysm between November 2005 and February 2008. Aneurysms were all obliterated with Yasargil clips (Braun-Aesculap®) either Phynox clips (cobalt-alloy) or Titanium clips (titanium-alloy). Type, size and shape of all clips were recorded. Patient's demographics and aneurysms locations were also documented.

64-MDCTA

All patients underwent a MDCTA from the aortic arch to the vertex using a 64-slices MDCT scanner (Aquilion 64, Toshiba Co., Tochigi-ken, Japan). MDCTA images were acquired following an intravenous timed injection of contrast (Visipaque 270, Amersham Health) using an auto-triggered injector. The injection parameters were: injection rate of 4ml/sec to a total volume of 40cc of contrast followed by the immediate injection of 20cc of normal saline. The scanning parameters were: 300 mAs, 120 kV, Matrix 512x512, FOV 28-32 cm, slice thickness 0.5 mm, Pitch 1.0, isotropic voxel size = 0.5 mm, acquisition time 11-16 seconds. The image processing consisted of standarized axial, coronal and sagittal multi-planar volume reformatted (MPVR) images, maximum intensity projections (MIP) images as well as three-dimensional (3D) Volume-Rendered (VR) reconstructions. Post-processing of the source images was done using a dedicated workstation (Advantage Windows version 4.2 workstation, GE medical systems).

Digitalized subtraction angiography

Conventional intra-arterial cerebral angiography was performed with a biplane angiography unit (LUA or LCN; GE Medical Systems, France). Anteroposterior and lateral

views of the vessels of interest were acquired. Three-dimensional reconstructions and subspin angiogram were obtained from the rotational acquisition as well. The diagnostic catheter used was a 4 or 5-F Berenstein catheter (Angiodynamics, Queensbury, NY) with the help of an angled 0.35-inch radiofocus guide wire (Terumo, Meditech, Watertown, MA). Intermittent flushing techniques with heparinized saline were used to prevent clots from developing in the catheter. The contrast media used for injections was nonionic (Omnipaque 300, Nycomed, Oslo, Norway). Injections were performed with a power injector (Mark V, Medrad, Indianola, Pa). Standard injection rates and volumes were as follows: 4–6 mL/sec for 8–12 mL for common carotid artery, 4–5 mL/sec for 8–10 mL for internal carotid artery.

Radiological analysis

Both 64-MDCTA and conventional DSA were analysed independently on a workstation by two experienced neuroradiologists (A.R, P.H). Both observers analysed the following parameters: exam quality, presence of clip related artifacts, presence of an aneurysmal remnant and patency of collateral vessels around the aneurysm neck. Interobserver agreement was assessed with the kappa coefficient. Sensitivity and specificity of 64-MDCTA with respect to remnant and collateral branch patency detections were calculated. Differences between cobalt-alloy and titanium-alloy clips or multiple/single-clips in terms of artifacts and remnant detection were assessed with the Fisher's test. Difference between cobalt-alloy and titanium-alloy clips in terms of missed remnant size was assessed with the t-test.

Results

General data

Thirty-one patients were involved in this study. Sex ratio was 0.5 and mean age was 55 years (range 35-76). Both CTA and DSA were used for the postoperative assessment of 38 ruptured and unruptured aneurysms (Table 1). Aneurysms were preferentially located on the anterior circulation (79%). Single clipping was applied in 26 aneurysms, a total of 53 clips were used (cobalt-alloy clips 30, titanium-alloy clips 23) with a mean of 1.4 clips per aneurysm and global clipping types were: cobalt-alloy 57%, titanium-alloy 43%.

Conventional DSA

The injection quality was good in 97% of the cases. Three-dimensional reconstructions were available in 74% of the cases. Important artifacts were found in 21% of the cases and were associated in 50% and 67% of the cases respectively with multiple clipping and cobalt-alloy clips. An aneurysm remnant was diagnosed in 31% of the cases (12/38) but this residue was larger than 2mm in 21% of the cases. Those remnants were only seen on 3D-reconstructions or subspin angiogram in two third of the cases. An occlusion of a collateral branch was found in 2 cases. In the first case, the anterior communicating artery (AcoA) had to be sacrificed because of a tearing extending from the sac to the neck of an AcoA aneurysm. In the second case, a collateral branch of the distal posterior inferior cerebellar artery (PICA) was occluded after the obliteration of a dissecting aneurysm.

64-MDCTA

The injection quality was good in 92% of the cases. Important artifacts were found in 13% of the cases and were associated in 60% and 100% of the cases respectively with multiple clips and cobalt-alloy clips. An aneurysm remnant was diagnosed in 6 cases (Fig.1 and 2). So, the global detection rate was 6/12 but for residue larger than 2mm, this rate reached 6/9 (Fig.3 and 4). The smallest missed remnant (1mm) was only seen on DSA after angioplasty of the parent artery. Characteristics of missed aneurysm remnants on CTA are summarized in Table 2. One of the collateral branch occlusion (AcoA aneurysm) was detected on 64-MDCTA (Fig.5) but the other one (close to the distal PICA aneurysm and already hardly visualized on the preoperative CTA) was missed.

Data analysis

Interobserver correlation for remnant detection was for all aneurysms moderate ($\kappa = 0.58$, agreement = 0.84, 95% CI = 0.30-0.86) and for remnants greater than 2mm good ($\kappa = 0.75$, agreement = 0.92, 95% CI = 0.49-1).

Sensitivity and specificity of 64-MDCTA compared with conventional DSA for the global detection of remnants and the detection of remnants greater than 2mm were respectively: 50% (95% CI = 0.22-0.78), 100% (95% CI = 0.84-1), and 67% (95% CI = 0.31-0.91), 100% (95% CI = 0.85-1). Sensitivity and specificity of 64-MDCTA compared with conventional DSA for the detection of collateral branch occlusions were respectively 50% (95% CI = 0.03-0.97) and 100% (95% CI = 0.88-1).

Missed remnants (Table-2) were not statistically associated with type of clip (p=0.43) or number of clips (p=0.5). Artifacts on 64-MDCTA were statistically more frequent with cobalt-alloy clips ($p<0.001$) but not on DSA (p=0.18). No significant association was found between the number of clips (Fig.5) and observed artifacts on 64-MDCTA or DSA (p= 0.15 and p=0.11). Although not significant, missed remnant sizes tended to be larger with cobalt-alloy clips (mean=2.5mm) than titanium-alloy clips (mean=1.7mm).

Discussion

Intracranial aneurysms postoperative follow-up

DSA has been the gold standard for the preoperative diagnosis of intracranial aneurysms (3;19;26;38;40) and is still the primary exam for patients undergoing evaluation of complex aneurysms. Due to the resolution afforded by DSA and 3D-rotational DSA, it has been also the traditional mean to assess the technical success of the surgical obliteration of intracranial aneurysms (21;23;34). DSA and its 3D-reconstructions allow the clear depiction of both the site of the previous aneurysm neck along which the clips can clearly be visualized and the patency of the parent vessel and its collateral branches close to the clip(s). Despite all those advantages, cerebral angiography can produce patient discomfort and is also associated with the following risks (18;22): groin haematoma (4%), transitory neurological symptoms (1-2%) and possible permanent neurological deficits (0.14-0.5%). Also, DSA can be technically very challenging in elderly patients because of atherosclerotic arterial changes that may limit vascular access, and impose a higher risk of embolic events.

For those reasons, some have opted for less invasive techniques for the postoperative and the routine follow-up of patients undergoing intracranial aneurysm clipping. The main limitation of those non invasive techniques are the clip related artifacts radiologically obscuring the area around the aneurysm neck. If developments in MR imaging made MRA a widely accepted technique for the post-therapeutic assessment and follow-up of coiled aneurysms (2;12;14;25;30;37;41), the artifacts caused by the clips preclude evaluating the dome and the neck of the aneurysm with MRA (42). Since the advent of titanium-alloy clips in 1995, Vieco et al. (1996) then van Loon et al. (1997) already felt that CTA could become a useful tool to evaluate clipped aneurysms (42;44). Since then, five studies evaluated MDCTA on single or 16-detectors MDCT scanners and proved its feasibility and its accuracy compared with conventional DSA (7;10;28;33;47). Results obtained in those studies were sometimes contradictory and for example the sensitivity of MDCTA for remnant detection was varying between 61-66% (28;33) and 100% (7;10). Those discrepancies led us to evaluate the interest in the clinical setting of a recent 64-MDCT scanner for the postoperative assessment of clipped aneurysms.

64-MDCTA

MDCT scanners enable the acquisition of thin overlapping images in a short scanning time thus increasing the spatial resolution of 2D source images and 3D reconstructions and allowing the recognition of smaller and smaller structures. Because of its low probability of complication and its accuracy, MDCTA is now worldwide used by cerebrovascular teams as a primary imaging method for the diagnosis and treatment planning of ruptured intracranial aneurysms (1;11;20;29;39;45). 64-MDCTA has already been validated by cardiovascular teams for the postoperative follow-up of coronary stents and bypasses (31;32) with high sensitivity (100%) and specificity (94%). The present study is the first using 64-MDCTA for the post-operative assessment of clipped aneurysms. The source voxel dimension obtained with our 64-MDCTA is 0.30 mm^3 (0.781mm×0.781mm×0.5 mm) which is smaller than that obtained with MRA or 16-MDCTA. Clip related artifacts (particularly with titanium-alloy clips) are proven to be considerably reduced at 64-MDCTA (43). The interest of our study is that it included various kinds of aneurysms in terms of locations and types of clip compared with previous studies that mainly focused on anterior circulation aneurysms (10) or aneurysms obliterated only with titanium-alloy clips (7;10;28;33). The imaging quality of 64-MDCTA (92%) was comparable to that of DSA (97%) and interestingly artifacts were reduced on 64-MDCTA. Poor imaging quality (8%) was less frequent than with older MDCT scanners (14%) (10). It was mainly the result of a delayed acquisition time with partial imaging of the venous phase and was rarely due to clip or motion artifacts. As it was previously reported (47), artifacts were significantly more important with cobalt-alloy clips (Fig.6) than titanium-alloy clips. No significant relationship was found between artifacts and number of clips. The high rate of remnants observed in this series might be explained by the fact that most of them were only seen on 3D-reconstructions from the conventional DSA. This technique allows a very precise analysis around the aneurysms neck and might not have been always available in older series of the literature (23;27;34). This high remnant rate was at some point beneficial for the study itself because it increased the statistical significance of the results. The rate of significant remnants (that could benefit from re-treatment), that is remnant greater than 2mm, was 21%. In this clinically relevant subgroup, the sensitivity and specificity of 64-MDCTA for the detection of remnants were respectively 67% (95% CI = 0.31-0.91) and 100% (95% CI = 0.85-1 and the inter-technique agreement was good (κ = 0.75, agreement = 0.92, 95% CI = 0.49-1). Those data are similar to the results of two recent studies (28;33) which emphasized the difficulty to depict on MDCTA remnants smaller than 2mm. Characteristics of the missed remnant cases are summarized in Table-2. Half of those cases was associated with clip related artifacts and the other half was most likely due to a magnification phenomenon of the clip size precluding the detection of the smallest remnants (Fig. 7). Surprisingly we didn't find any significant relationship between the aneurysmal location or the clip types (alloy, number, size or shape) and the inability to detect the remnant. The accuracy of 64-MDCTA for the diagnosis of a collateral branch occlusion was low but only two patients experienced this complication in the series. Overall, we think that this study compared the capacities of MDCTA versus conventional DSA for the postoperative assessment of clipped aneurysms in every clinical situations in terms of aneurysms locations (anterior and posterior circulations) and diversity of clips applied (cobalt-alloy and titanium-alloy). Because of the very high spatial resolution expected with 64-MDCTA and the high remnant rate in this series, this study might better delineate the real limits of the technique with respect to aneurysm remnant and collateral branch occlusion detection. Compared with other non invasive techniques, MDCTA carries, as DSA does, the risks of contrast material administration. The potential increased radiation dose delivered to the patient accompanying the increase in spatial and temporal resolution with 64-MDCTAs (8;17) can be reduced as needed and optimized by dose-saving algorithms or software (4;9;46;51).

Clinical implications

The purpose of this study was similar to those who led to the validation of MDCTA for the therapeutic management of intracranial aneurysms: to reduce the inconvenience and morbidity related to conventional DSA and to simplify the imaging protocol. The good results obtained with 64-MDCTA encouraged us to progressively modify our postoperative radiological algorithm for the assessment of clipped aneurysms. Favourable and unfavourable conditions for the use in first instance of 64-MDCTA to assess the post-clipping results are summarized in Table 3. Furthermore, a complimentary DSA should be performed each time the MDCTA is technically of bad quality – poor injection or important artifacts around the clip(s).

Excluding with 64-MDCTA the subgroup of remnants smaller than 2mm might be controversial because those misdiagnosed residues might still be at risk of growth or late rupture (13;24). On the other hand, those residual aneurysms are usually not considered suitable for a complimentary treatment. Furthermore, even without having a postoperative remnant, some patients are still at risk of developing de novo aneurysms or aneurysm regrowth at the clip site and may still present late subarachnoid hemorrhage (SAH) recurrence (48-50). Hence, a systematic follow-up with 64-MDCTA at 5, 10 and 15 years (according to the mean dates of diagnosis of known aneurysms growth, de novo aneurysms formation or recurrent aneurysms appearance), might be more beneficial by detecting delayed clinically significant aneurysms (> 2mm), including those growing remnants initially underestimated, and prevent repeated SAH.

The necessity for assessing the anatomical result of intracranial aneurysm treatment is now widely accepted. MRA became the dedicated method for post-coiling assessment. MDCTA could have the same role for the post-clipping long term follow-up and could allow comparisons between the two therapeutic options, which would be particularly helpful for randomized multicentric studies. MDCTA could also be very useful in the subgroup of asymptomatic aneurysms for which a less invasive imaging technique would be more beneficial.

Although the ultimate objective of the surgical treatment is to obtain the most perfect balance between complete obliteration of the aneurysm and preservation of collateral branches patency, the result of this study might to some extent influence the surgical technique itself. At the time of the clipping, the surgeon will also have to consider that the way he will proceed with the clipping, will automatically condemn the patient to an invasive or a non-invasive follow-up.

Study Limitations

The first limitation of our study is the relatively small number of patients enrolled. The population sample was however similar to that of three of the five previous studies (7;28;47). This default was to some extent compensated by the high rate of aneurysm remnants in the series improving the statistical accuracy of the results. Second, the lack of a prospective evaluation and of a timely planned radiological follow-up might have reduced the accuracy of 64-MDCTA. Initial aneurysm remnant thrombosis or reduced vessels filling (related to vasospasm) might have interfered with the radiological analysis. At the same time, those interfering conditions reflect the everyday practice and help to evaluate the technique in a real clinical setting. Larger prospective controlled cohorts will probably be required before definitely supplanting DSA in the postoperative assessment of clipped aneurysms.

Conclusions

Availability and high spatial resolution make 64-MDCTA a valuable tool to assess intracranial aneurysms clipping. Due to its low complication rate and good acceptance, this technique might be more beneficial than DSA for the follow-up of asymptomatic aneurysm patients. In particular conditions, such as occlusion with cobalt-alloy or multiple clips, complex aneurysms or doubt on collateral branches patency, conventional DSA remains the most accurate postoperative radiological exam to evaluate the quality of the clipping.

Reference List

1. Agid R, Lee SK, Willinsky RA, Farb RI, terBrugge KG: Acute subarachnoid hemorrhage: using 64-slice multidetector CT angiography to "triage" patients' treatment. **Neuroradiology** 48:787-794, 2006.
2. Agid R, Willinsky RA, Lee SK, Terbrugge KG, Farb RI: Characterization of aneurysm remnants after endovascular treatment: contrast-enhanced MR angiography versus catheter digital subtraction angiography. **AJNR Am J Neuroradiol** 29:1570-1574, 2008.
3. Anxionnat R, Bracard S, Ducrocq X, Trousset Y, Launay L, Kerrien E, Braun M, Vaillant R, Scomazzoni F, Lebedinsky A, Picard L: Intracranial aneurysms: clinical value of 3D digital subtraction angiography in the therapeutic decision and endovascular treatment. **Radiology** 218:799-808, 2001.
4. Bahner ML, Bengel A, Brix G, Zuna I, Kauczor HU, Delorme S: Improved vascular opacification in cerebral computed tomography angiography with 80 kVp. **Invest Radiol** 40:229-234, 2005.
5. Byrne JV, Sohn MJ, Molyneux AJ, Chir B: Five-year experience in using coil embolization for ruptured intracranial aneurysms: outcomes and incidence of late rebleeding. **J Neurosurg** 90:656-663, 1999.
6. CARAT Investigators: Rates of delayed rebleeding from intracranial aneurysms are low after surgical and endovascular treatment. **Stroke** 37:1437-1442, 2006.
7. Chen W, Yang Y, Qiu J, Peng Y, Xing W: Sixteen-row multislice computerized tomography angiography in the postoperative evaluation of patients with intracranial aneurysms. **Br J Neurosurg** 22:63-70, 2008.
8. Coles DR, Smail MA, Negus IS, Wilde P, Oberhoff M, Karsch KR, Baumbach A: Comparison of radiation doses from multislice computed tomography coronary angiography and conventional diagnostic angiography. **J Am Coll Cardiol** 47:1840-1845, 2006.
9. Deetjen A, Mollmann S, Conradi G, Rolf A, Schmermund A, Hamm CW, Dill T: Use of automatic exposure control in multislice computed tomography of the coronaries: comparison of 16-slice and 64-slice scanner data with conventional coronary angiography. **Heart** 93:1040-1043, 2007.
10. Dehdashti AR, Binaghi S, Uske A, Regli L: Comparison of multislice computerized tomography angiography and digital subtraction angiography in the postoperative evaluation of patients with clipped aneurysms. **J Neurosurg** 104:395-403, 2006.
11. Dehdashti AR, Rufenacht DA, Delavelle J, Reverdin A, de TN: Therapeutic decision and management of aneurysmal subarachnoid haemorrhage based on computed tomographic angiography. **Br J Neurosurg** 17:46-53, 2003.
12. Ferre JC, Carsin-Nicol B, Morandi X, Carsin M, de Kersaint-Gilly A, Gauvrit JY, Desal HA: Time-of-flight MR angiography at 3T versus digital subtraction angiography in the imaging follow-up of 51 intracranial aneurysms treated with coils. **Eur J Radiol** 2008.
13. Feuerberg I, Lindquist C, Lindqvist M, Steiner L: Natural history of postoperative aneurysm rests. **J Neurosurg** 66:30-34, 1987.
14. Gauvrit JY, Leclerc X, Caron S, Taschner CA, Lejeune JP, Pruvo JP: Intracranial aneurysms treated with Guglielmi detachable coils: imaging follow-up with contrast-enhanced MR angiography. **Stroke** 37:1033-1037, 2006.
15. Gouliamos A, Gotsis E, Vlahos L, Samara C, Kapsalaki E, Rologis D, Kapsalakis Z, Papavasiliou C: Magnetic resonance angiography compared to intra-arterial digital subtraction angiography in patients with subarachnoid haemorrhage. **Neuroradiology** 35:46-49, 1992.
16. Harrison MJ, Johnson BA, Gardner GM, Welling BG: Preliminary results on the management of unruptured intracranial aneurysms with magnetic resonance angiography and computed tomographic angiography. **Neurosurgery** 40:947-955, 1997.
17. Hausleiter J, Meyer T, Hadamitzky M, Huber E, Zankl M, Martinoff S, Kastrati A, Schomig A: Radiation dose estimates from cardiac multislice computed tomography in daily practice: impact of different scanning protocols on effective dose estimates. **Circulation** 113:1305-1310, 2006.
18. Heiserman JE, Dean BL, Hodak JA, Flom RA, Bird CR, Drayer BP, Fram EK: Neurologic complications of cerebral angiography. **AJNR Am J Neuroradiol** 15:1401-1407, 1994.
19. Hochmuth A, Spetzger U, Schumacher M: Comparison of three-dimensional rotational angiography with digital subtraction angiography in the assessment of ruptured cerebral aneurysms. **AJNR Am J Neuroradiol** 23:1199-1205, 2002.
20. Hoh BL, Cheung AC, Rabinov JD, Pryor JC, Carter BS, Ogilvy CS: Results of a prospective protocol of computed tomographic angiography in place of catheter angiography as the only diagnostic and pretreatment planning study for cerebral aneurysms by a combined neurovascular team. **Neurosurgery** 54:1329-1340, 2004.
21. Kang HS, Han MH, Kwon BJ, Jung SI, Oh CW, Han DH, Chang KH: Postoperative 3D angiography in intracranial aneurysms. **AJNR Am J Neuroradiol** 25:1463-1469, 2004.

22. Kaufmann TJ, Huston J, III, Mandrekar JN, Schleck CD, Thielen KR, Kallmes DF: Complications of diagnostic cerebral angiography: evaluation of 19,826 consecutive patients. **Radiology** 243:812-819, 2007.
23. Kivisaari RP, Porras M, Ohman J, Siironen J, Ishii K, Hernesniemi J: Routine cerebral angiography after surgery for saccular aneurysms: is it worth it? **Neurosurgery** 55:1015-1024, 2004.
24. Lin T, Fox AJ, Drake CG: Regrowth of aneurysm sacs from residual neck following aneurysm clipping. **J Neurosurg** 70:556-560, 1989.
25. Lubicz B, Neugroschl C, Collignon L, Francois O, Baleriaux D: Is digital substraction angiography still needed for the follow-up of intracranial aneurysms treated by embolisation with detachable coils? **Neuroradiology** 50:841-848, 2008.
26. Missler U, Hundt C, Wiesmann M, Mayer T, Bruckmann H: Three-dimensional reconstructed rotational digital subtraction angiography in planning treatment of intracranial aneurysms. **Eur Radiol** 10:564-568, 2000.
27. Murphy M, Bell D, Worth RD, Jehle KS, Critchley GR, Norris JS: Angiography postclipping and coiling of cerebral aneurysms. **Br J Neurosurg** 19:225-228, 2005.
28. Pechlivanis I, Koenen D, Engelhardt M, Scholz M, Koenig M, Heuser L, Harders A, Schmieder K: Computed tomographic angiography in the evaluation of clip placement for intracranial aneurysm. **Acta Neurochir (Wien)** 2008.
29. Pechlivanis I, Schmieder K, Scholz M, Konig M, Heuser L, Harders A: 3-Dimensional computed tomographic angiography for use of surgery planning in patients with intracranial aneurysms. **Acta Neurochir (Wien)** 147:1045-1053, 2005.
30. Ramgren B, Siemund R, Cronqvist M, Undren P, Nilsson OG, Holtas S, Larsson EM: Follow-up of intracranial aneurysms treated with detachable coils: comparison of 3D inflow MRA at 3T and 1.5T and contrast-enhanced MRA at 3T with DSA. **Neuroradiology** 50:947-954, 2008.
31. Rixe J, Achenbach S, Ropers D, Baum U, Kuettner A, Ropers U, Bautz W, Daniel WG, Anders K: Assessment of coronary artery stent restenosis by 64-slice multi-detector computed tomography. **Eur Heart J** 27:2567-2572, 2006.
32. Ropers D, Pohle FK, Kuettner A, Pflederer T, Anders K, Daniel WG, Bautz W, Baum U, Achenbach S: Diagnostic accuracy of noninvasive coronary angiography in patients after bypass surgery using 64-slice spiral computed tomography with 330-ms gantry rotation. **Circulation** 114:2334-2341, 2006.
33. Sakuma I, Tomura N, Kinouchi H, Takahashi S, Otani T, Watarai J, Mizoi K: Postoperative three-dimensional CT angiography after cerebral aneurysm clipping with titanium clips: detection with single detector CT. Comparison with intra-arterial digital subtraction angiography. **Clin Radiol** 61:505-512, 2006.
34. Sindou M, Acevedo JC, Turjman F: Aneurysmal remnants after microsurgical clipping: classification and results from a prospective angiographic study (in a consecutive series of 305 operated intracranial aneurysms). **Acta Neurochir (Wien)** 140:1153-1159, 1998.
35. Sluzewski M, van Rooij WJ: Early rebleeding after coiling of ruptured cerebral aneurysms: incidence, morbidity, and risk factors. **AJNR Am J Neuroradiol** 26:1739-1743, 2005.
36. Sluzewski M, van Rooij WJ, Beute GN, Nijssen PC: Late rebleeding of ruptured intracranial aneurysms treated with detachable coils. **AJNR Am J Neuroradiol** 26:2542-2549, 2005.
37. Sprengers ME, van Rooij WJ, Sluzewski M, Rinkel GJ, Velthuis BK, de Kort GA, Majoie CB: MR Angiography Follow-Up 5 Years after Coiling: Frequency of New Aneurysms and Enlargement of Untreated Aneurysms. **AJNR Am J Neuroradiol** 2008.
38. Sugahara T, Korogi Y, Nakashima K, Hamatake S, Honda S, Takahashi M: Comparison of 2D and 3D digital subtraction angiography in evaluation of intracranial aneurysms. **AJNR Am J Neuroradiol** 23:1545-1552, 2002.
39. Taschner CA, Thines L, Lernout M, Lejeune JP, Leclerc X: Treatment decision in ruptured intracranial aneurysms: comparison between multi-detector row CT angiography and digital subtraction angiography. **J Neuroradiol** 34:243-249, 2007.
40. Tu RK, Cohen WA, Maravilla KR, Bush WH, Patel NH, Eskridge J, Winn HR: Digital subtraction rotational angiography for aneurysms of the intracranial anterior circulation: injection method and optimization. **AJNR Am J Neuroradiol** 17:1127-1136, 1996.
41. Urbach H, Dorenbeck U, von FM, Wilhelm K, Willinek W, Schaller C, Flacke S: Three-dimensional time-of-flight MR angiography at 3 T compared to digital subtraction angiography in the follow-up of ruptured and coiled intracranial aneurysms: a prospective study. **Neuroradiology** 50:383-389, 2008.
42. van Loon JJ, Yousry TA, Fink U, Seelos KC, Reulen HJ, Steiger HJ: Postoperative spiral computed tomography and magnetic resonance angiography after aneurysm clipping with titanium clips. **Neurosurgery** 41:851-856, 1997.
43. van dS, I, van LM, Vlassenbroek A, Velthuis B: Minimizing clip artifacts in multi CT angiography of clipped patients. **AJNR Am J Neuroradiol** 27:60-66, 2006.
44. Vieco PT, Morin EE, III, Gross CE: CT angiography in the examination of patients with aneurysm clips. **AJNR Am J Neuroradiol** 17:455-457, 1996.
45. Villablanca JP, Hooshi P, Martin N, Jahan R, Duckwiler G, Lim S, Frazee J, Gobin YP, Sayre J, Bentson J, Vinuela F: Three-dimensional helical computerized tomography angiography in the diagnosis, characterization, and management of middle cerebral artery aneurysms: comparison with conventional angiography and intraoperative findings. **J Neurosurg** 97:1322-1332, 2002.
46. Waaijer A, Prokop M, Velthuis BK, Bakker CJ, de Kort GA, van Leeuwen MS: Circle of Willis at CT angiography: dose reduction and image quality--reducing tube voltage and increasing tube current settings. **Radiology** 242:832-839, 2007.

47. Watanabe Y, Kashiwagi N, Yamada N, Higashi M, Fukuda T, Morikawa S, Onishi Y, Iihara K, Miyamoto S, Naito H: Subtraction 3D CT angiography with the orbital synchronized helical scan technique for the evaluation of postoperative cerebral aneurysms treated with cobalt-alloy clips. **AJNR Am J Neuroradiol** 29:1071-1075, 2008.
48. Wermer MJ, Greebe P, Algra A, Rinkel GJ: Incidence of recurrent subarachnoid hemorrhage after clipping for ruptured intracranial aneurysms. **Stroke** 36:2394-2399, 2005.
49. Wermer MJ, Rinkel GJ, Greebe P, Albrecht KW, Dirven CM, Tulleken CA: Late recurrence of subarachnoid hemorrhage after treatment for ruptured aneurysms: patient characteristics and outcomes. **Neurosurgery** 56:197-204, 2005.
50. Wermer MJ, van dS, I, Velthuis BK, Algra A, Buskens E, Rinkel GJ: Follow-up screening after subarachnoid haemorrhage: frequency and determinants of new aneurysms and enlargement of existing aneurysms. **Brain** 128:2421-2429, 2005.
51. Yang CY, Chen YF, Lee CW, Huang A, Shen Y, Wei C, Liu HM: Multiphase CT Angiography versus Single-Phase CT Angiography: Comparison of Image Quality and Radiation Dose. **AJNR Am J Neuroradiol** 2008.

Tables

Table 1 –Aneurysms characteristics, DSA and 64-MDCTA results

Aneurysm characteristics				DSA Results							64-MDCTA Results				
N°	Location	Nb clip(s)	Global Alloy Type	Quality	3D-recons	Clip artifacts on 3D	Remnant			Patency collateral vessels	Quality	Clip artifacts	Remnant	Patency collateral vessels	
							Presence	Size	only on 3D	Parent artery / Collaterals				Parent artery	Collaterals
1	R, CO	2	C	g	y	a	a			p / p	g	p	a	p	p
2	AcoA	3	C	g	y	s	p	1.5 mm	y	p / p	g	s	a	p	p
3	AcoA	2	C	g	y	a	p	2.5mm	y	p / p	g	s	p	p	p
4	L, MCA	3	C	g	y	p	a			p / p	g	s	a	p	p
5	L, MCA	2	C	g	y	s	a			p / p	g	p	a	p	p
6	R, PICA	1	C	g	n	na	a			p / a (distal PICA)	g	p	a	p	p
7	AcoA	1	C	g	y	s	p	3 mm	y	p / p	g	p	a	p	p
8	R, MCA	2	T	g	y	s	p	5 mm	y	p / p	g	a	p	p	p
9	AcoA	1	C	g	n	na	a			p / p	g	s	a	p	p
10	PC	1	C	g	y	a	a			p / p	g	p	a	p	p
11	PC	1	T	g	y	a	a			p / p	g	a	a	p	p
12	AcoA	2	T	g	y	a	a			a (AcoA) / p	g	a	a	a	p
13	L, MCA	1	C	g	n	na	a			p / p	g	s	a	p	p
14	R, ICA term	2	C	g	y	p	a			p / p	g	p	a	p	p
15	AcoA	1	T	g	n	na	a			p / p	g	a	a	p	p
16	L, SCA	1	T	g	n	na	p	1mm	n	p / p	g	a	a	p	p
17	AcoA	1	C	g	y	a	p	3 mm	y	p / p	g	p	a	p	p
18	AcoA	1	C	g	y	s	a			p / p	g	p	a	p	p
19	L, CO	2	C	g	y	a	a			p / p	g	a	a	p	p
20	R, Pcom	3	T	g	n	na	a			p / p	g	a	a	p	p
21	BT	1	C	g	n	na	p	4 mm	n	p / p	g	a	p	p	p
22	L, ICA term	1	T	g	y	a	p	4mm	n	p / p	g	a	p	p	p
23	L, MCA prox	1	T	g	y	s	a			p / p	g	a	a	p	p
24	L, MCA dist	1	T	g	y	p	a			p / p	g	a	a	p	p
25	R, MCA	1	T	g	y	a	a			p / p	g	a	a	p	p
26	R, PICA	1	C	g	y	a	a			p / p	g	a	a	p	p
27	L, MCA	1	C	g	y	p	p	1mm	y	p / p	g	p	p	p	p
28	R, AchoA	1	T	g	y	a	a			p / p	b	a	a	p	p
29	R, ICA term	1	T	g	y	a	p	1.5 mm	y	p / p	b	a	a	p	p
30	R, MCA	1	T	g	y	a	a			p / p	b	a	a	p	p
31	R, Pcom	1	T	g	y	a	a			p / p	g	a	a	p	p
32	R, ICA term	1	T	g	y	a	a			p / p	g	a	a	p	p
33	L, PICA	1	T	g	y	a	p	2.5mm	y	p / p	g	a	a	p	p
34	PC	1	T	g	n	na	a			p / p	g	a	a	p	p
35	PC	1	C	b	n	na	a			p / p	g	a	a	p	p
36	AcoA	2	C	g	n	na	a			p / p	g	a	a	p	p
37	L, MCA	2	C	g	y	a	a			p / p	g	a	a	p	p
38	R, CO	1	T	g	y	a	p	4.5 mm	n	p / p	g	a	p	p	p

R: right, L: left, CO: carotido-ophthalmic, AcoA: anterior communicating artery, MCA: middle cerebral artery, PC: pericallosal artery,
ICA term: internal carotid artery termination, SCA: superior cerebellar artery, Pcom: posterior communicating artery, BT: basilar artery tip,
prox: proximal, dist: distal, PICA: posterior inferior cerebellar artery, C: cobalt-alloy clip, T: titanium-alloy clip, g: good, b: bad, y: yes, n: no, na: non applicable, p: present, a: absent, s: significant,

Table 2 – Characteristics of missed remnants

	Missed Remnants						
	Size	**Location**	**Clip type**	**Nb clip**	**Clip shape**	**Size (mm)**	**Artifacts**
2	1.5 mm	AcoA	C	3	Straight	5.0, 7.0, 9.0	++
7	3 mm	AcoA	C	1	Fen. right angle	5.0 / 4.9	+
16	1 mm	L, SCA	T	1	Straight	7.0	-
17	3 mm	AcoA	C	1	Straight	5.0	+
29	1.5 mm	R, ICA term	T	1	Straight	5.0	-
33	2.5 mm	L, PICA	T	1	Straight	7.0	-

R: right, L: left, AcoA: anterior communicating artery, SCA: superior cerebellar artery, ICA term: internal carotid artery termination,
PICA: posterior inferior cerebellar artery, C: cobalt-alloy clip, T: titanium-alloy clip, ++ : important, +: present, -: absent

Table 3 – Post-clipping assessment algorithm according to the different conditions that might be encountered: (+) is for the technique that should be used in first instance

Conditions	**64-MDCTA**	**DSA**
anterior circulation	+	-
posterior circulation	+	-
cobalt-alloy clips	-	+
titanium-alloy clips	+	-
single or multiple clipping = 2	+	-
multiple clipping > 2	-	+
vasospasm	-	+
complex aneurysm	-	+
collateral branch occlusion	-	+

Figure legends

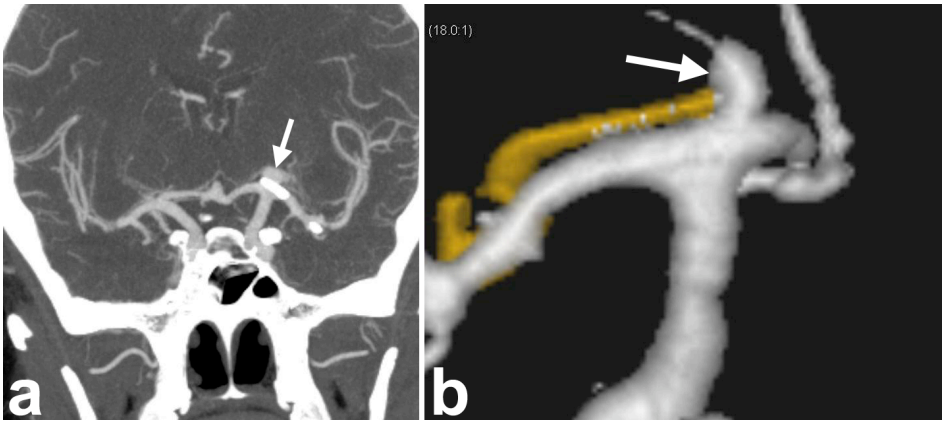

Figure 1- Aneurysm 22.
a: postoperative MIP view from 64-MDCTA showing a remnant above the clip (arrow) at the level of a left carotid termination aneurysm; b: postoperative 3D-reconstruction from the angiography finding the same remnant (arrow). Note that the residual sac is now partially thrombosed.

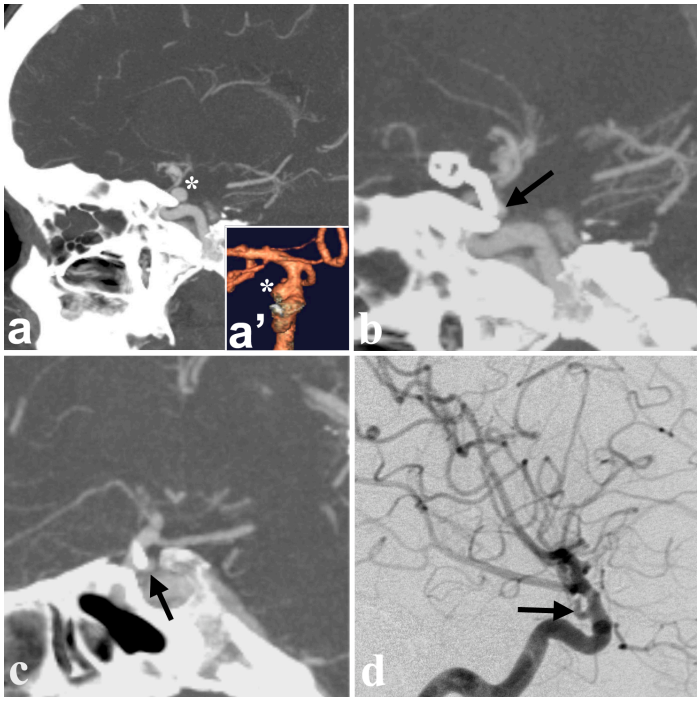

Figure 2- Aneurysm 38
a, a' : preoperative sagittal MIP view from 64-MDCTA and 3D reconstruction from angiography showing a right carotido-ophthalmic aneurysm projecting laterally (*); b,c: postoperative sagittal MIP view from 64-MDCTA showing a small residual at the tip of the clip (arrow); d: postoperative spin angiogram of the right ICA showing the residual aneurysm (arrow).

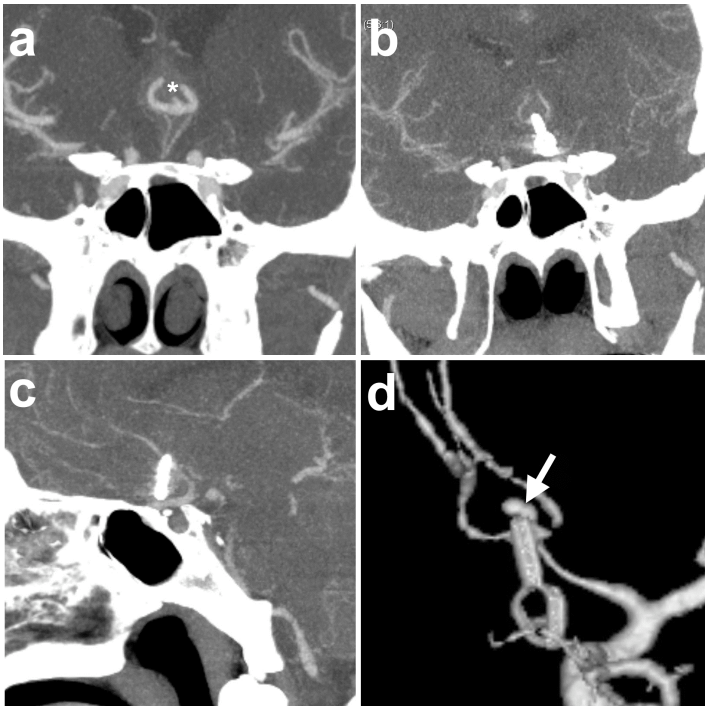

Figure 3- Aneurysm 17.
a: preoperative coronal MIP view from 64-MDCTA showing an anterior communicating aneurysm (*); b, c: postoperative coronal and sagittal MIP views from 64-MDCTA finding no residual aneurysm (same features were seen on axial). Note the vasospam on this early CTA; d: postoperative 3D reconstruction from angiography diagnosing a missed residual (arrow) at the tip of the clip (note a similar vasospasm as on CTA).

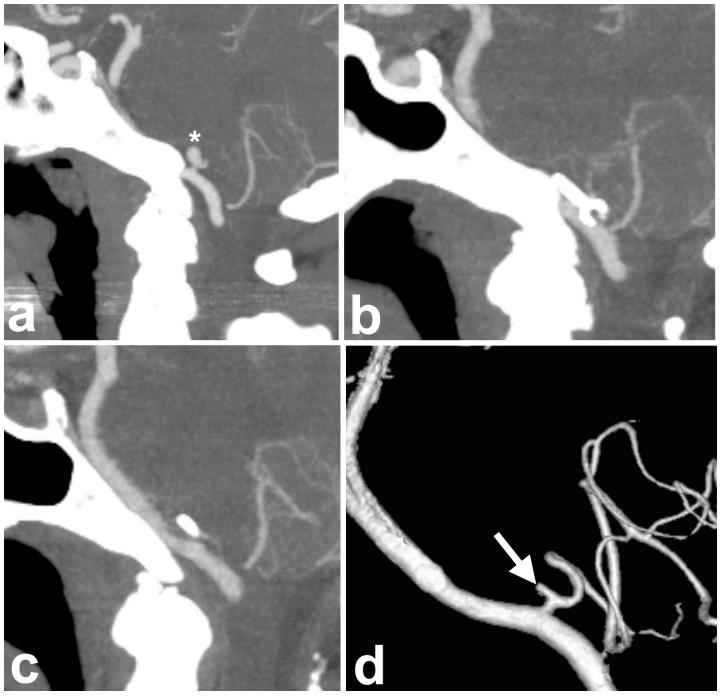

Figure 4- Aneurysm 33.
a: preoperative sagittal MIP view from 64-MDCTA showing a left PICA aneurysm (*); b, c: postoperative sagittal MIP views from 64-MDCTA finding no residual aneurysm (same features were seen on axial and coronal); d: postoperative 3D reconstruction from angiography diagnosing a small residual (arrow) behind the clip (subtracted on this view).

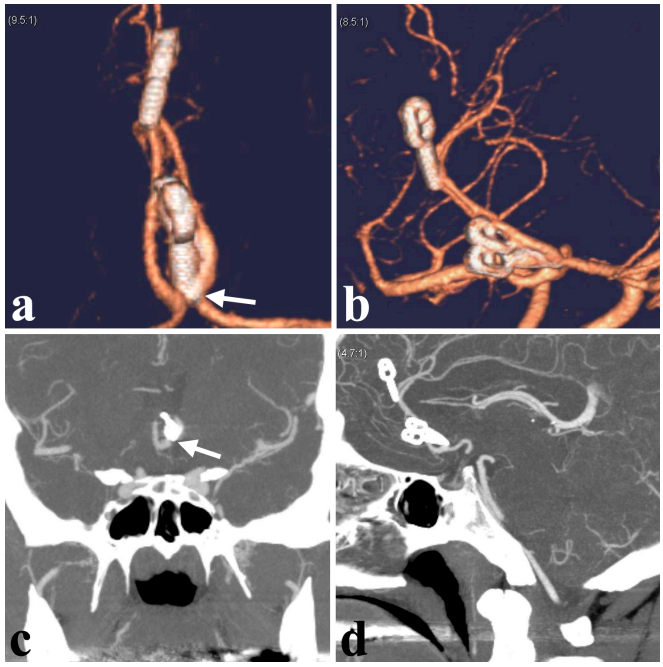

Figure 5- Aneurysms 11 (pericallosal) and 12 (anterior communicating):
Postoperative 3D reconstructions (a, b) and coronal-sagittal MIP views (c,d) from the 64-MDCTA showing perfect images of the 3 clips without any artifacts (titanium-alloy clips) and the absence of any remnant. Note that the anterior communicating artery (arrow) was occluded laterally during the procedure because of a tearing at the neck of the aneurysm.

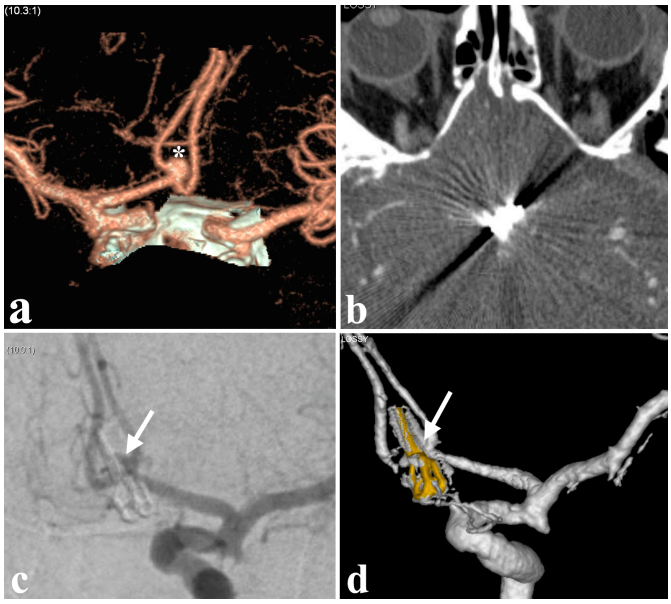

Figure 6- Aneurysm 4
a: preoperative 64-MDCTA showing an anterior communicating artery aneurysm (*); b: postoperative axial MIP view from 64-MDCTA showing important artifacts on 3 cobalt-alloy clips precluding from seeing the remnant; c: postoperative left ICA spin angiogram showing the residual aneurysms (arrow); d: postoperative 3D reconstruction from angiography, note the clips motion artifacts and the difficulties to see the remnant on this view.

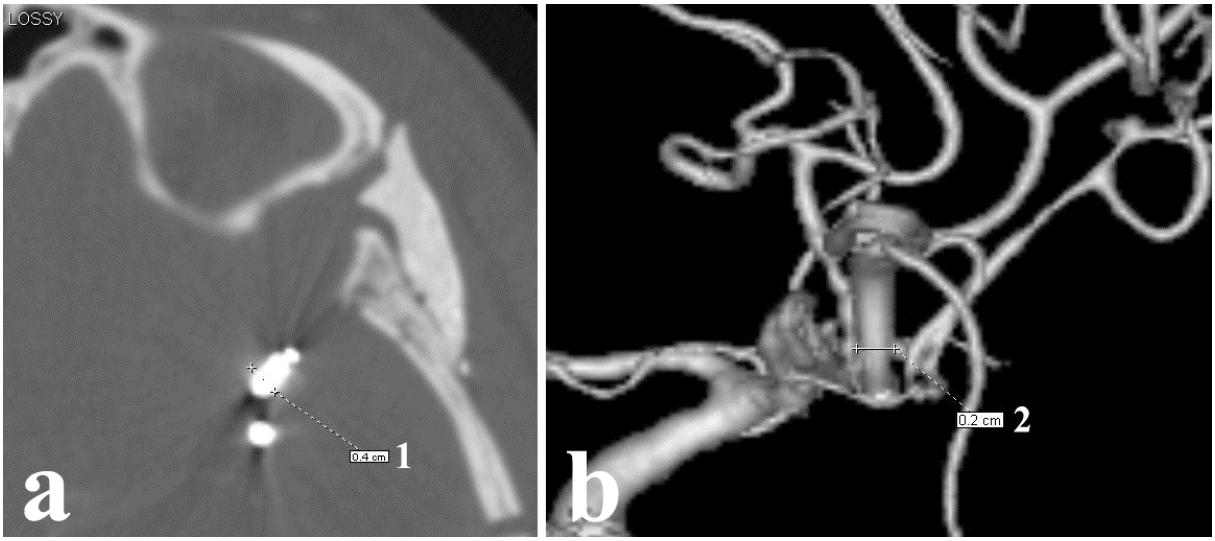

Figure 7- Aneurysm 2: postoperative 64-MDCTA (a) and 3D-angiography (b) of the left internal carotid artery evidencing the magnification phenomenon on the CTA; measurement 1 = 4 mm, measurement 2 = 2 mm.

Journal of Neurosurgery (submitted)

Assessment of extracranial-intracranial bypass patency with 64-slice multi-detector computerized tomography angiography

LAURENT THINES [1,2,4], MD., RONIT AGID [3,4], MD., AMIR R. DEHDASHTI [2,4], MD., LEODANTE DA COSTA [3,4], MD., M. CHRISTOPHER WALLACE [2,4], MD, MSc., KAREL G. TERBRUGGE [3,4], MD., MICHAEL TYMIANSKI [2,4], MD., PhD

[1] Department of Neurosurgery, Lille University Hospital, Lille, France
[2] Division of Neurosurgery and Department of Surgery, Toronto Western Hospital, Toronto, Ontario, Canada
[3] Division of Neuroradiology, Department of Medical Imaging, Toronto Western Hospital, Ontario, Canada
[4] University of Toronto Brain Vascular Malformation Study Group, Toronto Western Hospital, Toronto, Ontario, Canada

Running title: 64-MDCTA for EC-IC bypass

Keywords: bypass patency, cerebral revascularization, computed tomography angiography, extracranial-intracranial bypass, multi-detector computed tomography

Corresponding author: Dr. Michael Tymianski
Toronto Western Hospital, Division of Neurosurgery, 4W-435, 399 Bathurst Street, Toronto, ON, M5T-2S8, Canada
Tel: 416-603-5896 Fax: 416-603-5298 Email: mike.tymianski@uhn.on.ca

Object: Extracranial-intracranial (EC/IC) bypass is a useful procedure for the treatment of cerebral vascular insufficiency or complex aneurysms. We explored the role of multi-detector computed tomography angiography (MDCTA), instead of digital subtraction angiography (DSA), for the postoperative assessment of EC/IC bypass patency.

Methods: We retrospectively analysed a consecutive series of 21 MDCTAs from 17 patients that underwent 25 direct or indirect EC/IC bypass procedures between April 2003 and November 2007. Conventional DSA were available for comparison in 13 cases. MDCTA used a 64-slice MDCT scanner (Aquilion 64, Toshiba). The proximal and distal patencies were analyzed independently on MDCTA and DSA by a neuroradiologist and a neurosurgeon. The bypass was considered patent when the entire donor vessel was opacified without discontinuity from proximal to distal ends and was visibly in contact with the recipient vessel.

Results: MDCTA depicted the patency status in every patient. Bypasses were patent in 22 cases, stenosed in one and occluded in two. DSA always confirmed the results of the MDCTA (sensitivity = 100%, 95% CI = 0.655-1.0; specificity 100%, 95% CI = 0.05-1.0).

Conclusions: MDCTA is a non-invasive and accurate exam to assess the postoperative EC/IC bypass patency and could replace conventional DSA in routine follow-up.

Keywords: bypass patency, cerebral revascularization, computed tomography angiography, extracranial-intracranial bypass, multi-detector computed tomography

Introduction

Extracranial-intracranial (EC/IC) bypass surgery remains a useful option when flow augmentation is needed for the treatment of non-atherosclerotic cerebral ischemic disease (Moya-moya), for selected occlusive ischemic disorders, or when flow replacement is required for the exclusion of complex unclippable aneurysms or resection of skull base tumours.[6, 8, 26, 28, 29, 31, 36, 37, 51] The technique is continuously evolving, and is the subject of ongoing studies pertaining to its indications,[15] and its techniques.[5, 12, 38] Postoperatively, bypass patency has traditionally been assessed using digital subtraction angiography (DSA), and this has remained the gold standard for this purpose. Recent advances in non-invasive imaging technologies have raised the possibility of replacing DSA in order to reduce risks associated with this technique. [49] For example, computerized tomography angiography (CTA) and magnetic resonance angiography (MRA) are now commonplace in the diagnosis and follow-up of brain aneurysms. [1, 2, 10, 11, 14, 18, 30, 35, 42, 47] However, due to the small size of vessels involved in certain microvascular anastomoses, non-invasive imaging techniques are not yet in routine use in assessing the patency of EC/IC bypasses. Nevertheless, with the advent of 64-slice multi-detector computerized tomography (MDCT) scanners, CT angiograms have begun to reliably depict even the most distal branches of the intracranial arterial tree. This has led us to evaluate the accuracy of 64-slice MDCTA for the assessment of EC/IC bypass patency.

Clinical Material and Methods

Study population

This study was approved by the Research Ethics Board of our institution. We retrospectively analysed a consecutive series of patients who underwent a direct or an indirect EC/IC bypass with a postoperative multi-detector computerized tomography angiogram (MDCTA) between April 2003 and November 2007.

EC/IC bypass

The indications for EC/IC bypass are summarized in Table 1. Patients harbouring large or giant internal carotid artery (ICA) aneurysms requiring treatment by ICA occlusion and who failed a balloon test occlusion (BTO), underwent a high-flow bypass (HFBP) using a radial artery or a saphenous vein graft from the external carotid artery (ECA) or the extracranial ICA to the intracranial ICA or middle cerebral artery (MCA). Patients with intracranial narrowing or occlusion of cerebral arteries (e.g.: Moya-moya syndrome) usually underwent a low-flow bypass (LFBP) between the superficial temporal artery (STA) and the MCA. Occasionally, an indirect bypass was performed in instances where a direct bypass was not feasible due to the small size of recipient arteries or in conjunction with a direct bypass in order to further augment the revascularization.

CT angiogram (MDCTA)

All patients underwent a MDCTA from the aortic arch to the vertex using a 64-slice MDCT scanner (Aquilion 64, Toshiba Co., Tochigi-ken, Japan). MDCTA images were acquired following an intravenous timed injection of contrast (Visipaque 270, Amersham Health) using an auto-triggered injector. The injection parameters were: injection rate of 4ml/sec to a total volume of 40cc of contrast followed by the immediate injection of 20cc of normal saline. The scanning parameters were: 300 mAs, 120 kV, Matrix 512x512, FOV 28-32 cm, slice thickness 0.5 mm, Pitch 1.0, isotropic voxel size = 0.5 mm, acquisition time 11-16 seconds. The image processing consisted of standarized axial, coronal and sagittal multi-planar volume reformatted (MPVR) images, maximum intensity projections (MIP) images as well as three-dimensional (3D) Volume-Rendered (VR) reconstructions. Post-processing of

the source images was done using a dedicated workstation (Advantage Windows version 4.2 workstation, GE medical systems).

Digital subtraction angiography

Conventional intra-arterial cerebral angiography was performed with a biplane angiography unit (LUA or LCN; GE Medical Systems, France). Anteroposterior and lateral views of the vessels of interest were acquired. The diagnostic catheter used was a 4 or 5-F Berenstein catheter (Angiodynamics, Queensbury, NY) with the help of an angled 0.35-inch radiofocus guide wire (Terumo, Meditech, Watertown, MA). Intermittent flushing techniques with heparinized saline were used to prevent clots from developing in the catheter. The contrast media used for injections was nonionic (Omnipaque 300, Nycomed, Oslo, Norway). Injections were performed with a power injector (Mark V, Medrad, Indianola, Pa). Standard injection rates and volumes were as follows: 4–6 mL/sec for 8–12 mL for common carotid artery, 4–5 mL/sec for 8–10 mL for internal carotid artery, 2–3 mL/sec for 5 mL for external carotid artery.

Radiological analysis

Both MDCTA and conventional DSA were analysed independently by both an experienced neuroradiologist (A.R) and a neurosurgeon (L.T). Interobserver agreement was assessed with the kappa coefficient. The donor artery or graft (artery or vein) was followed from its extracranial origin (in the neck for HFBP or in the temporal region for LFBP), through the cranial opening and then intracranially to its anastomosis with the recipient artery. For each bypass, the donor vessels, the proximal and the distal anastomoses were considered patent if both extremities (proximal and distal) were filled with contrast and if the donor vessel or graft was identifiable throughout its entire course.

Results

Patient demographics and surgical indications

The demographic characteristics and bypass types are described in Table 1. In brief, between April 2003 and November 2007, MDCTAs were performed in 17 patients after a bypass procedure. The male: female ratio was 8:9. The average age of the patients was 44 years (range 25-67). Some of the patients had bilateral or multiple anastomoses on the same hemisphere and, in total, 25 direct or indirect EC/IC bypasses were available for analysis. Ten bypasses were performed for the treatment of giant intracranial aneurysms that could not be directly treated by microsurgical clipping, or by endovascular coiling, thus requiring a trapping or proximal occlusion. All such patients underwent prior evaluation using a BTO, and were found to be intolerant of parent artery occlusion. Fifteen bypasses were performed in order to treat intracranial occlusive disease presenting with ischemic symptoms. Eleven patients had Moya-moya syndrome, and 4 patients had other symptomatic intracranial occlusions.

Case Examples

Case Example 1: Long vein and radial artery - external carotid artery – middle cerebral artery bilateral bypasses (Fig.1)

Patient n°1, a 67 year-old woman, presented with a symptomatic right cavernous sinus syndrome with 6th nerve palsy and retro-orbital pain. The tortuosity of the brachiocephalic vessels precluded selective injections of the cervical arteries on DSA, particularly on the right hand side. DSA and MRI scans confirmed bilateral cavernous sinus aneurysms with a larger aneurysm on the right side (Fig. 1a). Because of the difficult vascular access (Fig. 1h), only an arch aortogram could be performed and the BTO, done by manual compression, showed good cross flow from the left ICA. The decision to treat the aneurysm using a right ICA occlusion

was made but because of the uncertainty of the BTO result and the presence of the contralateral aneurysm, a saphenous vein bypass was added from the right superficial temporal artery origin to an MCA branch (Fig. 1d, e). The patient partially recovered from her oculomotor palsy as the right cavernous aneurysm thrombosed and shrank (Fig. 1b, c). However, 3 years later she presented with a gradual onset of a new left 6th nerve palsy related to the growth of the left intracavernous aneurysm (Fig. 1b, c). This was treated by performing a radial artery ECA-MCA bypass. DSA was only feasible on the right side due to difficulties with vascular access (Fig. 1e). This showed patency of the bypass and filling of the MCA territory. MDCTA was able to demonstrate obvious patency of both bypasses (Fig. 1 f, g, h)

Case Example 2: Superficial temporal artery – middle cerebral artery bypass (Fig.2)
Patient n°7, a 46 year-old man, presented with three episodes of transient ischemic symptoms including right motor deficit, in-coordination and dysphasia. A severe stenosis at the origin of the left MCA was diagnosed at MRA and DSA with Moya-moya like collateral revascularization to the left hemisphere (Fig. 2b). The patient underwent mapping of his cerebrovascular reactivity (CVR) using blood oxygen level-dependent magnetic resonance imaging [25] (Fig. 2a). This CVR study revealed a severe loss of cerebral vascular reactivity in the left hemisphere. The patient underwent revascularization with a left STA-MCA EC/IC bypass (Fig. 2c). A postoperative DSA (Fig. 2d) and MDCTA (Fig.2e, f, g) both revealed patency of the bypass. This correlated nicely with a resolution of the patient's symptoms and normalization of the CVR map (Fig. 2h).

Case Example 3: Occipital artery-posterior inferior cerebellar artery bypasses (Fig.3)
Patient n°9, a 55 year-old male, suffered a childhood injury consisting of an axial cranial impact from a heavy falling object. He presented with an 18 month history of frequent vertebro-basilar transient ischemic episodes including vertigo, diplopia, ataxia, transient left side weakness and/or numbness, and a single episode of loss of consciousness lasting 45 min. A DSA revealed complete bilateral occlusions of the extracranial vertebral arteries at their horizontal segment between the occiput and C1, and poor retrograde filling of the distal basilar tree through small or non-existent posterior communicating arteries. In order to augment his vertebro-basilar flow, the patient underwent bilateral occipital artery to PICA bypasses. Post-operatively, the DSA revealed that both bypasses were patent with a good retrograde flow to the basilar artery from the left side (Fig. 3a, c). Despite the small size of the vessels involved and the posterior fossa location, an MDCTA also showed the patency of both bypasses (Fig. 3b, d, e, f). The presence of vascular clips applied along the distal occipital arteries did not interfere with the radiological MDCTA analysis.

Analysis of bypass patency

The mean time interval between the surgery and the MDCTA was 18 weeks. Eighteen of the MDCTAs were performed in the immediate postoperative period. Conventional DSA was available for comparison in 13 cases and the mean interval from surgery was 2 weeks. Both proximal and distal patency of the bypasses could be assessed with MDCTA in every patient (Table 2). In every instance, there was agreement between the two observers ($\kappa = 1$), attesting to the quality of both MDCTA and DSA in this study. The bypass was found to be fully patent in 22 of 25 cases. In two cases, the bypass was found to be occluded on post-operative MDCTA. In one (case 3), the venous graft was identified on MDCTA but appeared completely thrombosed which was confirmed at an early surgical revision. In the other case (case 4), the venous graft was not seen and was thus assumed to be thrombosed, a finding confirmed by the immediate postoperative DSA. In one case (case 3), a moderate stenosis was identified at the origin of the venous graft.

Thirteen cases had post operative DSA, permitting a comparison of both techniques. Based on these cases, and on the assumption that DSA remains the gold standard, the sensitivity of 64-MDCTA was 100% (95% CI = 0.655, 1.0) and its specificity was 100% (95% CI = 0.05, 1.0). Although these results are representative of a small sample of cases, they strongly suggest that 64-MDCTA, in appropriately selected cases, may be useful in assessing EC/IC bypass patency.

Discussion

EC/IC bypass follow-up

DSA has been the gold standard for the preoperative diagnosis of cerebral ischemic disease (i.e. Moya-moya [40]) and is still the primary exam for patients undergoing evaluation of complex aneurysms. Due to the resolution afforded by DSA, it has been the traditional means to assess the technical success of an EC/IC bypass. [36, 50] DSA allows the clear depiction of both extracranial and intracranial vessels and the selective catheterization of the bypassing segment provide a picture of the vascular bed supplied by the bypass. In addition, the application of DSA in the long term follow-up, and particularly in Moya-moya disease, helps to quantify the extent of the revascularization or neovascularization of the brain cortex. [24, 41] DSA is also a useful intraoperative adjunct to document intraoperative bypass patency. [4] Despite all those advantages, cerebral angiography can produce patient discomfort and is also associated with the following risks: groin haematoma (4%), transitory neurological symptoms (1-2%) and possible permanent neurological deficits (0.14-0.5%). [17, 20] Also, DSA can be technically challenging in elderly patients because of atherosclerotic arterial changes that may limit vascular access, and impose a higher risk of embolic events.

For this reason, some have opted for less invasive techniques for the preoperative management and the routine follow-up of patients undergoing EC/IC bypass surgery. In the diagnosis of Moya-moya disease, particularly in children, MRA can sometimes replace the cerebral angiography (guidelines from the Ministry of Health and Welfare of Japan [13]). For postoperative assessment, some authors have recommended the use of physical examination and doppler ultrasonography to assess the patency of bypass grafts. [39] A disadvantage of this approach may be the uncertainty of whether the correct vessel is tested. Progress in Doppler imaging now permits not only the visualization and confirmation of bypass patency of the bypass but also the extent of neovascularization after direct or indirect bypass which is an important factor in patients follow-up. [32] Similarly, developments in MR imaging now allow for the postoperative visualization of EC/IC bypasses. Good results were initially described with the use of three-dimensional (3D) time-of-flight (TOF) MR angiography (MRA) in the depiction of the patency of EC/IC bypasses. [22] More recently, phase-contrast MRA [23, 53] has been deemed superior to TOF-MRA and quantitative MRA may give further information regarding patency compared to conventional angiogram by measuring the intra-bypass flow itself. [19, 27] Unfortunately, despite its efficacy, this quantitative MRA protocol is not available in every institution.

64-MDCTA

Development of multidetector computerized tomography enabled the acquisition of thin overlapping images in a short scanning time thus increasing the spatial resolution of 2D source images and 3D reconstructions. 64-MDCTA has already been validated by cardiovascular teams for the postoperative follow-up of coronary stents and bypasses [33, 34] with high sensitivity (100%) and specificity (94%). Because of its low probability of complication, MDCTA is now worldwide used by cerebrovascular teams as a primary diagnostic method for the treatment planning of intracranial aneurysms. [1, 2, 11, 18, 30, 42, 47] Some reports have also showed its interest in the postoperative evaluation of clipped aneurysms. [10,

[35, 45] A few studies have applied 4-slice MDCTAs to the postoperative evaluation of EC/IC bypasses. [21, 43, 44] The present study is the first using a 64-slice MDCT scan for this purpose. The advent of MDCTA has greatly increased the spatial resolution of CT images enabling the recognition of smaller and smaller structures. The source voxel dimension obtained with our 64-MDCTA is 0.30 mm^3 (0.781mm×0.781mm×0.5 mm) which is smaller than that used with MRA or 4-MDCTA (0.5mm^3), thus improving the diagnostic accuracy of this technique compared to the previous reports. As a result, a clear depiction of the donor and recipient vessels as well the assessment of the patency of the EC/IC bypass was obtained in every one of our cases. In each case where a comparison with DSA or surgical findings was available, the result of the 64-MDCTA was confirmed, leading to a specificity and sensitivity of 100%. Although it does not selectively show the arterial territory supplied by the bypass, the technique has also been found to be effective for the long term postoperative follow-up to demonstrate the amount of neovascularization that developed after the EC/IC bypass procedure. [21] The large field of view available with 64-MDCTA allowed, in high-flow bypasses, the simultaneous demonstration of the proximal anastomosis (at the neck) and the distal anastomosis (on the cortical branch), which is useful when the vascular access is difficult. Whereas DSA shows only the vessels, the precision of the 3D reconstructions obtained with 64-MDCTA are useful to depict the relationship between the bone flap and the graft which could be very helpful in case of re-do procedures to avoid any damage to the bypass during the approach. The visualization of the bypass, as in post-clipping studies, wasn't modified by titanium clips application along the venous graft because the artifacts are proven to be considerably reduced at 64-MDCTA. [46]

Limitations of 64-MDCTA

MDCTA has several limitations as compared with other techniques. Compared with MRA, MDCTA exposes the patient to the injection of a potentially nephrotoxic contrast agent and to radiation. Risks from contrast administration are inherent to both DSA and MDCTA. The potential increased radiation dose delivered to the patient [7, 16] accompanying the increase in spatial and temporal resolution with 64-MDCTAs can be reduced as needed and optimized by dose-saving algorithms or software. [3, 9, 48, 52] MDCTA also lacks a dynamic evaluation of the bypass, and does not demonstrate the direction nor does it provide quantification of the flow. This default is compensated by the availability and speed of the exam and its better spatial resolution. A dynamic analysis when needed could be provided by its association to a complimentary non invasive quantitative technique like quantitative MRA or Doppler.

Clinical implications

The purpose of this study was similar to those who led to the validation of MDCTA for the preoperative and postoperative management of clipped aneurysms: to reduce the inconvenience and morbidity related to the conventional DSA technique and to simplify the imaging protocol. The excellent results obtained with 64-MDCTA encouraged us to progressively modify our postoperative radiological algorithm for the control of EC/IC bypasses. If the bypass is clearly seen on CTA all along its course, no further imaging is done. If the bypass is not well visualized, a conventional DSA is scheduled to confirm the result. In our department, this algorithm resulted in a decreased discomfort for the patients and a reduction of the hospitalization time. The CTA can be done by a technician, and its availability and rapidity are really helpful in case of an immediate postoperative neurological deficit. It provides images of the brain itself and at the same time of the blood vessels, allowing to rule out an intracerebral complication and to assess the bypass patency. This enables the cerebrovascular team to quickly proceed with a revision procedure if necessary.

Limitations of the study

The first limitation of our study is the relatively small number of patients enrolled. This is explained not only by the rarity of the EC/IC surgical procedure itself but also because 64-slice MDCTA has only been available recently. Larger cohorts will probably be required before definitely supplanting DSA in this indication. Another limitation is that a comparison between 64-MDCTA and the gold standard DSA (13 bypasses) or surgical findings (1 bypass) was only available in 14 of the 25 cases. The reason for this is that with the excellent results of 64-MDCTA, we modified our postoperative protocol progressively shifting toward control with CTA-alone to avoid the inherent complications of DSA.

Conclusions

64-MDCTA is a very promising technique in the evaluation of patients post EC/IC bypass. Its availability and its high spatial resolution make 64-MDCTA a valuable tool to assess the graft patency in the immediate postoperative period as well as during the long term follow-up.

References

1. Agid R, Lee SK, Willinsky RA, Farb RI, terBrugge KG: Acute subarachnoid hemorrhage: using 64-slice multidetector CT angiography to "triage" patients' treatment. **Neuroradiology 48**:787-794, 2006
2. Anderson GB, Steinke DE, Petruk KC, Ashforth R, Findlay JM: Computed tomographic angiography versus digital subtraction angiography for the diagnosis and early treatment of ruptured intracranial aneurysms. **Neurosurgery 45**:1315-1320, 1999
3. Bahner ML, Bengel A, Brix G, Zuna,I, Kauczor HU, Delorme S: Improved vascular opacification in cerebral computed tomography angiography with 80 kVp. **Invest Radiol 40**:229-234, 2005
4. Barrow DL, Boyer KL, Joseph GJ: Intraoperative angiography in the management of neurovascular disorders. **Neurosurgery 30**:153-159, 1992
5. Bregy A, Alfieri A, Demertzis S, Mordasini P, Jetzer AK, Kuhlen D et al: Automated end-to-side anastomosis to the middle cerebral artery: a feasibility study. **J Neurosurg 108**:567-574, 2008
6. Charbel FT, Meglio G, min-Hanjani S: Superficial temporal artery-to-middle cerebral artery bypass. **Neurosurgery 56**:186-190, 2005
7. Coles DR, Smail MA, Negus IS, Wilde P, Oberhoff M, Karsch, Comparison of radiation doses from multislice computed tomography coronary angiography and conventional diagnostic angiography. **J Am Coll Cardiol 47**:1840-1845, 2006
8. Couldwell WT, Liu JK, Amini A, Kan P: Submandibular-infratemporal interpositional carotid artery bypass for cranial base tumors and giant aneurysms. **Neurosurgery 59**:ONS353-ONS359, 2006
9. Deetjen A, Mollmann S, Conradi G, Rolf A, Schmermund A, Hamm CW, et al: Use of automatic exposure control in multislice computed tomography of the coronaries: comparison of 16-slice and 64-slice scanner data with conventional coronary angiography. **Heart 93**:1040-1043, 2007
10. Dehdashti AR, Binaghi S, Uske A, Regli L: Comparison of multislice computerized tomography angiography and digital subtraction angiography in the postoperative evaluation of patients with clipped aneurysms. **J Neurosurg 104**:395-403, 2006
11. Dehdashti AR, Rufenacht DA, Delavelle J, Reverdin A, de Tribolet N: Therapeutic decision and management of aneurysmal subarachnoid haemorrhage based on computed tomographic angiography. **Br J Neurosurg 17**:46-53, 2003
12. Ferroli P, Biglioli F, Ciceri E, Addis A, Broggi G: Self-closing U-clips for intracranial microanastomoses in high-flow arterial bypass: technical case report. **Neurosurgery 60**:ONSE170, 2007
13. Fukui M: Guidelines for the diagnosis and treatment of spontaneous occlusion of the circle of Willis ('moyamoya' disease). Research Committee on Spontaneous Occlusion of the Circle of Willis (Moyamoya Disease) of the Ministry of Health and Welfare, Japan. **Clin Neurol Neurosurg 99 Suppl 2**:S238-S240, 1997
14. Gauvrit JY, Leclerc X, Caron S, Taschner CA, Lejeune JP, Pruvo JP: Intracranial aneurysms treated with Guglielmi detachable coils: imaging follow-up with contrast-enhanced MR angiography. **Stroke 37**:1033-1037, 2006
15. Grubb RL, Jr., Powers WJ, Derdeyn CP, Adams HP Jr, Clarke WR: The Carotid Occlusion Surgery Study. **Neurosurg Focus 14**:e9, 2003
16. Hausleiter J, Meyer T, Hadamitzky M, Hube E, Zankl M, Martinoff S, et al: Radiation dose estimates from cardiac multislice computed tomography in daily practice: impact of different scanning protocols on effective dose estimates. **Circulation 113**:1305-1310, 2006
17. Heiserman JE, Dean BL, Hodak JA, Flom RA, Bird CR, Drayer BP, et al: Neurologic complications of cerebral angiography. **AJNR Am J Neuroradiol 15**:1401-1407, 1994
18. Hoh BL, Cheung AC, Rabinov JD, Pryor JC, Carter BS, Ogilvy CS: Results of a prospective protocol of computed tomographic angiography in place of catheter angiography as the only diagnostic and pretreatment planning study for cerebral aneurysms by a combined neurovascular team. **Neurosurgery 54**:1329-1340, 2004

19. Horn P, Vajkoczy P, Schmiedek P, Neff W: Evaluation of extracranial-intracranial arterial bypass function with magnetic resonance angiography. **Neuroradiology 46**:723-729, 2004
20. Kaufmann TJ, Huston J, III, Mandrekar JN, Schleck CD Thielen KR, Kallmes DF: Complications of diagnostic cerebral angiography: evaluation of 19,826 consecutive patients. **Radiology 243**:812-819, 2007
21. Kikuchi M, Asato M, Sugahara S, Nakajima K, Sato M, Nagao K, et al: Evaluation of surgically formed collateral circulation in moyamoya disease with 3D-CT angiography: comparison with MR angiography and X-ray angiography. **Neuropediatrics 27**:45-49, 1996
22. Kodama T, Ueda T, Suzuki Y, Yano T, Watanabe K: MRA in the evaluation of EC-IC bypass patency. **J Comput Assist Tomogr 17**:922-926, 1993
23. Kodoma T, Suzuki Y, Yano T, Watanabe K, Ueda T, Asada K: Phase-contrast MRA in the evaluation of EC-IC bypass patency. **Clin Radiol 50**:459-465, 1995
24. Matsushima T, Inoue T, Suzuki SO, Fujii K, Fukui M, Hasuo K: Surgical treatment of moyamoya disease in pediatric patients--comparison between the results of indirect and direct revascularization procedures. **Neurosurgery 31**:401-405, 1992
25. Mikulis DJ, Krolczyk G, Desal H, Logan W, Deveber G, Dirks P, et al: Preoperative and postoperative mapping of cerebrovascular reactivity in Moyamoya disease by using blood oxygen level-dependent magnetic resonance imaging. **J Neurosurg 103**:347-355, 2005
26. min-Hanjani S, Butler WE, Ogilvy CS, Carter BS, Barker FG: Extracranial-intracranial bypass in the treatment of occlusive cerebrovascular disease and intracranial aneurysms in the United States between 1992 and 2001: a population-based study. **J Neurosurg 103**:794-804, 2005
27. min-Hanjani S, Shin JH, Zhao M, Du X, Charbel FT: Evaluation of extracranial-intracranial bypass using quantitative magnetic resonance angiography. **J Neurosurg 106**:291-298, 2007
28. Mohit AA, Sekhar LN, Natarajan SK, Britz GW, Ghodke B: High-flow bypass grafts in the management of complex intracranial aneurysms. **Neurosurgery 60**:ONS105-ONS122, 2007
29. Okada Y, Shima T, Nishida M, Yamane K, Yamada T, Yamanaka C: Effectiveness of superficial temporal artery-middle cerebral artery anastomosis in adult moyamoya disease: cerebral hemodynamics and clinical course in ischemic and hemorrhagic varieties. **Stroke 29**:625-630, 1998
30. Pechlivanis I, Schmieder K, Scholz M, Konig M, Heuser L, Harders A: 3-Dimensional computed tomographic angiography for use of surgery planning in patients with intracranial aneurysms. **Acta Neurochir (Wien) 147**:1045-1053, 2005
31. Peerless SJ, Ferguson GG, Drake CG: Extracranial-intracranial (EC/IC) bypass in the treatment of giant intracranial aneurysms. **Neurosurg Rev 5**:77-81, 1982
32. Perren F, Horn P, Vajkoczy P, Schmidek P, Meairs S: Power Doppler imaging in detection of surgically induced indirect neoangiogenesis in adult moyamoya disease. **J Neurosurg 103**:869-872, 2005
33. Rixe J, Achenbach S, Ropers D, Baum U, Kuettner A, Ropers U, et al: Assessment of coronary artery stent restenosis by 64-slice multi-detector computed tomography. **Eur Heart J 27**:2567-2572, 2006
34. Ropers D, Pohle FK, Kuettner A, Pflederer T, Anders K, Daniel WG, et al: Diagnostic accuracy of noninvasive coronary angiography in patients after bypass surgery using 64-slice spiral computed tomography with 330-ms gantry rotation. **Circulation 114**:2334-2341, 2006
35. Sakuma I, Tomura N, Kinouchi H, Takahashi S, Otani T, Watarai J, et al: Postoperative three-dimensional CT angiography after cerebral aneurysm clipping with titanium clips: detection with single detector CT. Comparison with intra-arterial digital subtraction angiography. **Clin Radiol 61**:505-512, 2006
36. Schmiedek P, Piepgras A, Leinsinger G, Kirsch CM, Einhupl K: Improvement of cerebrovascular reserve capacity by EC-IC arterial bypass surgery in patients with ICA occlusion and hemodynamic cerebral ischemia. **J Neurosurg 81**:236-244, 1994
37. Spetzler RF, Schuster H, Roski RA: Elective extracranial-intracranial arterial bypass in the treatment of inoperable giant aneurysms of the internal carotid artery. **J Neurosurg 53**:22-27, 1980
38. Streefkerk HJ, Kleinveld S, Koedam EL, Bulder MM, Meelduk HD, Verdaasdonk RM: Long-term reendothelialization of excimer laser-assisted nonocclusive anastomoses compared with conventionally sutured anastomoses in pigs. **J Neurosurg 103**:328-336, 2005
39. Sundt TM Jr., Whisnant JP, Fode NC, Piepgras G, Houser OW: Results, complications, and follow-up of 415 bypass operations for occlusive disease of the carotid system. **Mayo Clin Proc 60**:230-240, 1985
40. Suzuki J, Takaku A: Cerebrovascular "moyamoya" disease. Disease showing abnormal net-like vessels in base of brain. **Arch Neurol 20**:288-299, 1969
41. Suzuki Y, Negoro M, Shibuya M, Yoshida J, Negoro T, Watanabe K: Surgical treatment for pediatric moyamoya disease: use of the superficial temporal artery for both areas supplied by the anterior and middle cerebral arteries. **Neurosurgery 40**:324-329, 1997
42. Taschner CA, Thines L, Lernout M, Lejeune JP, Leclerc X: Treatment decision in ruptured intracranial aneurysms: comparison between multi-detector row CT angiography and digital subtraction angiography. **J Neuroradiol 34**:243-249, 2007
43. Teksam M, McKinney A, Truwit CL: Multi-slice CT angiography in evaluation of extracranial-intracranial bypass. **Eur J Radiol 52**:217-220, 2004
44. Tsuchiya K, Aoki C, Katase S, Hachiya J, Shiokawa Y: Visualization of extracranial-intracranial bypass using multidetector-row helical computed tomography angiography. **J Comput Assist Tomogr 27**:231-234, 2003
45. van Loon JJ, Yousry TA, Fink U, Seelos KC, Reulen HJ, Steiger HJ: Postoperative spiral computed tomography and magnetic resonance angiography after aneurysm clipping with titanium clips. **Neurosurgery 41**:851-856, 1997

46. van der Schaaf I, van Leeuwen M, Vlassenbroek A, Velthuis B: Minimizing clip artifacts in multi CT angiography of clipped patients. **AJNR Am J Neuroradiol 27**:60-66, 2006
47. Villablanca JP, Hooshi P, Martin N, Jahan R, Duckwiler G, Lim S: Three-dimensional helical computerized tomography angiography in the diagnosis, characterization, and management of middle cerebral artery aneurysms: comparison with conventional angiography and intraoperative findings. **J Neurosurg 97**:1322-1332, 2002
48. Waaijer A, Prokop M, Velthuis BK, Bakker CJ, de Kort GA, van Leeuwen MS: Circle of Willis at CT angiography: dose reduction and image quality--reducing tube voltage and increasing tube current settings. **Radiology 242**:832-839, 2007
49. Wanebo JE, min-Hanjani S, Boyd C, Peery T: Assessing success after cerebral revascularization for ischemia. **Skull Base 15**:215-227, 2005
50. Weinstein PR, Baena R, Chater NL: Results of extracranial-intracranial arterial bypass for intracranial internal carotid artery stenosis: review of 105 cases. **Neurosurgery 15**:787-794, 1984
51. Wolfe SQ, Tummala RP, Morcos JJ: Cerebral revascularization in skull base tumors. **Skull Base 15**:71-82, 2005
52. Yang CY, Chen YF, Lee CW, Huang A, Shen Y, Wei C, et al: Multiphase CT Angiography versus Single-Phase CT Angiography: Comparison of Image Quality and Radiation Dose. **AJNR Am J Neuroradiol** 2008
53. Zhao M, Charbel FT, Alperin N, Loth F, Clark ME: Improved phase-contrast flow quantification by three-dimensional vessel localization. **Magn Reson Imaging 18**:697-706, 2000

Table 1 - Patient demographics and surgical indications

Patient n°	Sex	Age	Bypass indication	Type	Nb MDCTA
1	F	67	Giant intracavernous ICA aneurysms (bilateral)	R, V/MCA L, RAD/MCA	1 1
2	M	23	Large posterior ICA aneurysm (left)	L, V/ICA	1
3	M	47	Giant intracavernous ICA aneurysm (right)	R, V/MCA R, V/MCA R, RAD/MCA	1 1
4	F	37	Giant intracavernous ICA aneurysm (left)	L, V/MCA	1
5	F	55	Giant VB junction aneurysm (midline)	R, STA/PCA	1
6	F	48	Intracranial ICA occlusion (right)	R, V/MCA	1
7	M	46	Moya-moya (left)	L, STA/MCA	1
8	M	47	Moya-moya (right)	R, STA/MCA	1
9	M	55	Vertebro-basilar insufficiency	R, Occ/PICA L, Occ/PICA	1
10	F	54	Giant paraclinoid ICA aneurysm (left)	L, V/MCA	1
11	F	36	Moya-moya (bilateral)	R, STA/MCA L, EDAS	1 1
12	M	41	Moya-moya (bilateral)	L, STA/MCA R, STA/MCA	1 1
13	F	63	Giant paraclinoid ICA aneurysm (left)	L, V/MCA	1
14	F	35	MCA occlusion (left)	L, STA/MCA	1
15	M	45	Moya-moya (left)	L, STA/MCA L, EDAS	1
16	M	25	Moya-moya (right)	R, STA/MCA R, EDAS	1
17	F	25	Moya-moya (left)	L, STA/MCA	1
				N = 25	*N = 21*

F: female, M: male, ICA: internal carotid artery, VB; vertebrobasilar, MCA: middle cerebral artery, R: right, L: left, V: venous graft, RAD: radial artery graft, STA: superficial temporal artery, PCA: posterior cerebral artery, Occ: occipital artery, PICA: posterior inferior cerebellar artery, EDAS: encephalo-duro-arterio-synangiosis

Table 2 - Analysis of bypass patency

Patient n°	MDCTA results		DSA results	
	PP	DP	PP	DP
1	Y	Y	Y	Y
	Y	Y	no dsa	no dsa
2	Y	Y	Y	Y
3	N / thrombus	N / thrombus	no dsa ‡	no dsa ‡
	Y	Y	no dsa	no dsa
	Y / stenosis	Y	no dsa	no dsa
4	N	N	N	N
5	Y	Y	Y	Y
6	Y	Y	no dsa	no dsa
7	Y	Y	Y	Y
8	Y	Y	Y	Y
9	Y	Y	Y	Y
	Y	Y	Y	Y
10	Y	Y	Y	Y
11	Y	Y	Y	Y
	Y	Y	Y	Y
12	Y	Y	Y	Y
	Y	Y	no dsa	no dsa
13	Y	Y	Y	Y
14	Y	Y	no dsa	no dsa
15	Y	Y	no dsa	no dsa
	Y	Y	no dsa	no dsa
16	Y	Y	no dsa	no dsa
	Y	Y	no dsa	no dsa
17	Y	Y	no dsa	no dsa

PP: proximal patency, DP: distal patency, Y: bypass patent, N: bypass occluded, ‡: surgical confirmation

Figure legends:

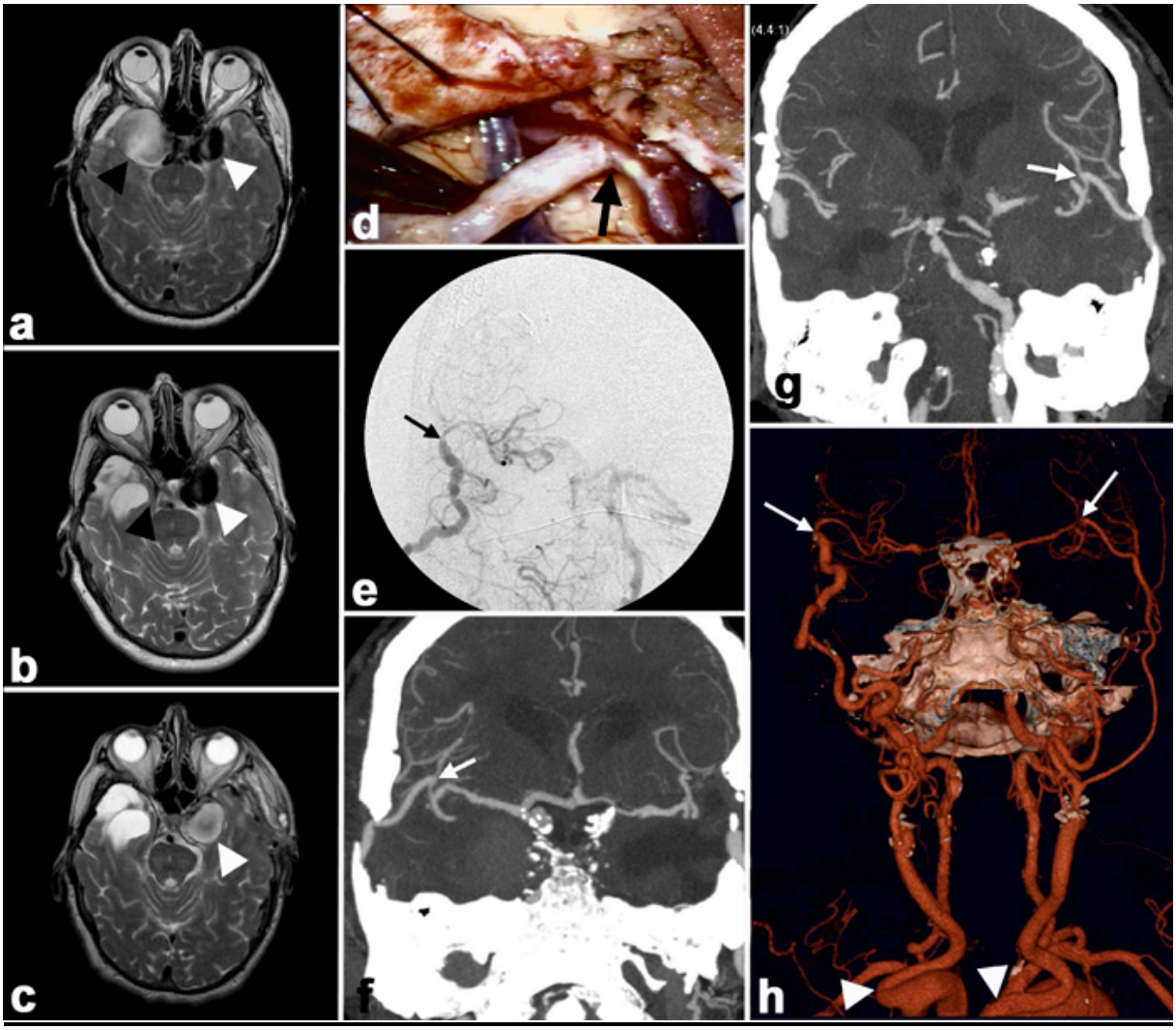

Figure 1- Case example 1- a: initial axial T2 weighted MRI showing bilateral intracavernous aneurysms, the right was initially larger and symptomatic (black arrowhead) and the left was asymptomatic (white arrowhead); b: axial T2 weighted MRI 3 years after a right ICA occlusion and long vein EC/IC bypass showing a shrunken right intracavernous aneurysm (black arrowhead) and an enlarged now symptomatic left intracavernous aneurysm (white arrowhead); c: final axial T2 weighted MRI after a left ICA occlusion and radial artery – MCA EC/IC bypass showing the shrinking of the left intracavernous aneurysm (white arrowhead); d: intraoperative picture of the right long vein EC/IC bypass (black arrow); e: right selective postoperative DSA (anterior view) of the venous graft showing a patent right EC/IC bypass (black arrow); f, g: coronal postoperative 64-MDCTAs evidencing the patency of the right and left EC/IC bypasses (white arrows); h: anterior view of postoperative 3D-reconstructions from 64-MDCTA showing both EC/IC bypasses (white arrows), note the tortuosity of both common carotid artery origin (white arrowheads).

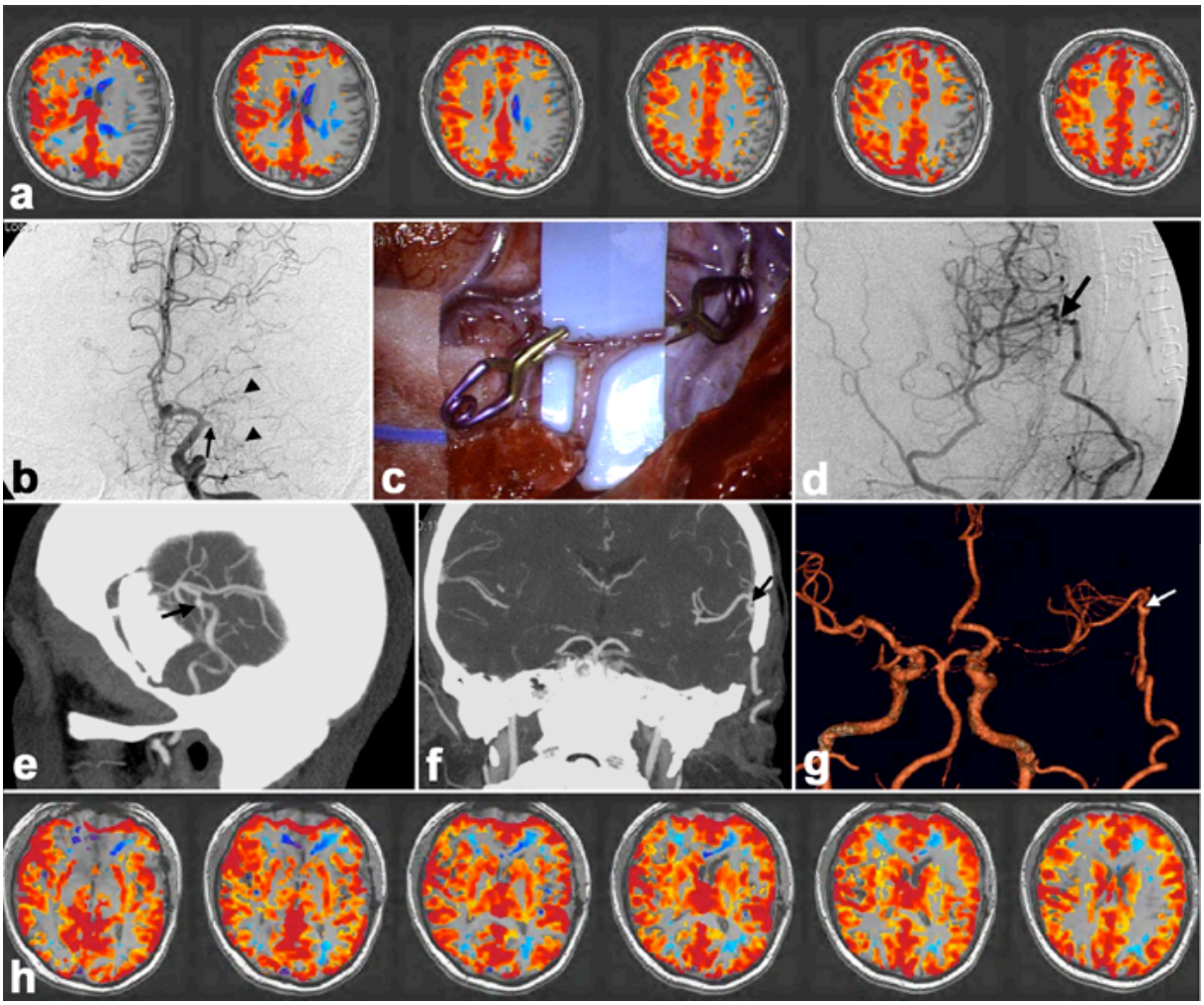

Figure 2- Case example 2 – a: cerebrovascular reactivity MR map showing a large and severe vascular reactivity defect in the left hemisphere; b: left internal carotid DSA (anterior view) showing a proximal occlusion of the left MCA (black arrow) and the Moya-moya like collaterals (black arrowheads); c: intraoperative picture of the left STA-MCA EC/IC bypass; d: postoperative DSA (anterior view) showing a patent left STA-MCA EC/IC bypass (black arrow); e, f: sagittal and coronal postoperative 64-MDCTAs evidencing the patency of the left STA-MCA EC/IC bypass (black arrows); g: anterior view of postoperative 3D-reconstructions from 64-MDCTA showing the left STA-MCA EC/IC bypass (white arrow); h: normalization of the 1-year postoperative cerebrovascular reactivity MR map in the left hemisphere.

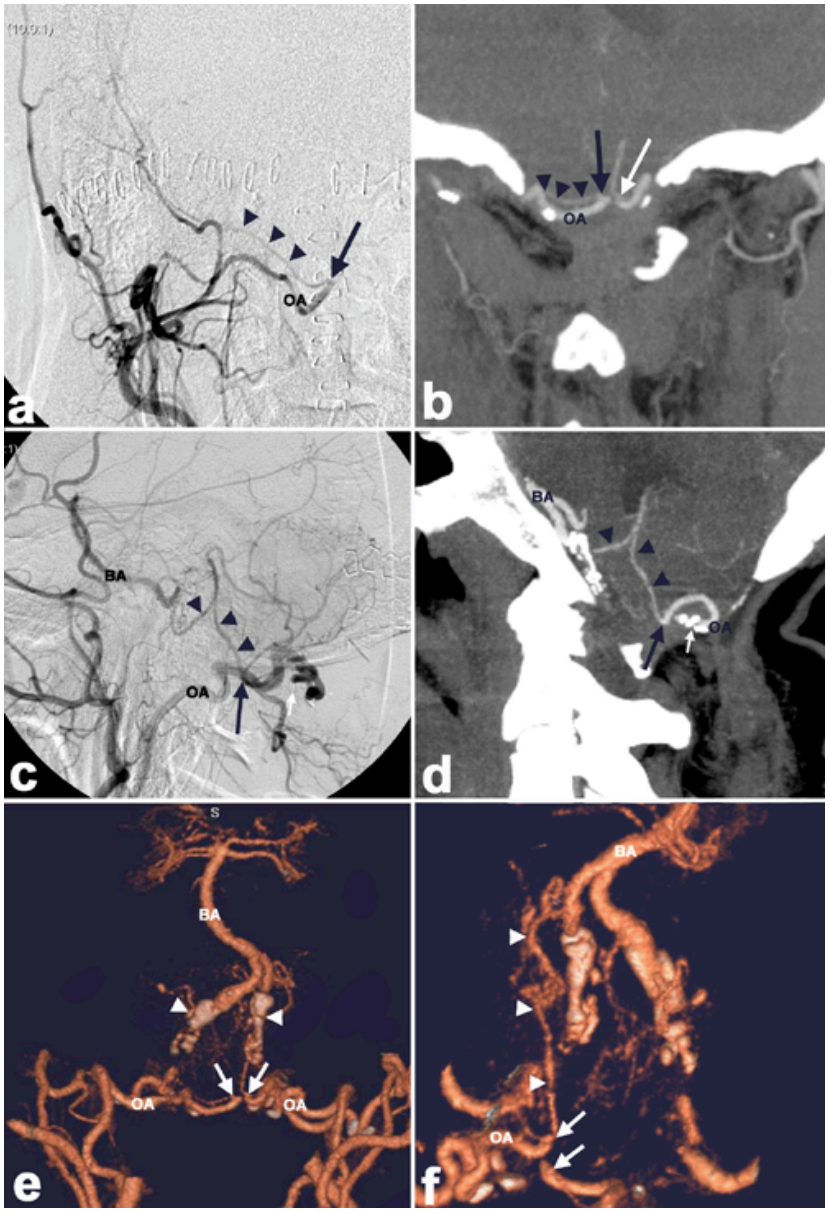

Figure 3- Case example 3 – a: anterior view of the postoperative right external carotid artery DSA showing a patent right occipital artery (OA) – PICA EC/IC bypass (black arrow), and the feeling of the distal territory of the right PICA on this side (black arrowheads); b: coronal postoperative 64-MDCTA evidencing the patency of both right (black arrow) and left (white arrow) occipital artery (OA)-PICA EC/IC bypasses and the feeling of the distal territory of the right PICA (black arrowheads); c, d: postoperative left external carotid artery DSA (lateral view) and sagittal 64-MDCTA showing a patent left occipital artery (OA) – PICA EC/IC bypass (black arrows), and the retrograde feeling of the left PICA (black arrowheads) to the basilar artery (BA), note the absence of artifacts related to the vascular clips (white arrows); e: anterior view of postoperative 3D-reconstructions from 64-MDCTA showing both occipital artery (OA) – PICA EC/IC bypasses (white arrows), note the occlusion of both vertebral arteries (white arrowheads), BA = basilar artery; f: right postero-lateral view of postoperative 3D-reconstructions from 64-MDCTA showing both occipital artery (OA) – PICA EC/IC bypasses (white arrows) and the retrograde feeling of the left PICA (white arrowheads) to the basilar artery (BA).